Game-theoretic Control of Autonomous Power Grids

Politecnico di Bari

Paolo Scarabaggio

Game-theoretic Control of Autonomous Power Grids

Thesis submitted for the degree of Philosophiae Doctor

Department of Electrical and Information Engineering
Politecnico di Bari

Tutors
Prof. Engr. *Mariagrazia Dotoli*
Dr. Engr. *Raffaele Carli*

2022

La borsa di dottorato è stata cofinanziata con risorse del
Programma Operativo Nazionale Ricerca e Innovazione 2014-2020 (CCI 2014IT16M2OP005),
Fondo Sociale Europeo, Azione I.1 "Dottorati Innovativi con caratterizzazione Industriale"

Dissertation submitted for the degree of *Philosophiae Doctor* in Electrical and Information Engineering (XXXV cycle)

Title:
Game-theoretic Control of Autonomous Power Grids

Ph.D Candidate:
Paolo Scarabaggio, Politecnico di Bari (Bari, Italy)

Tutors:
Prof. Engr. *Mariagrazia Dotoli*, Politecnico di Bari (Bari, Italy)
Dr. Engr. *Raffaele Carli*, Politecnico di Bari (Bari, Italy)

Coordinator:
Prof. Engr. *Mario Carpentieri*, Politecnico di Bari (Bari, Italy)

External Reviewers:
Prof. Engr. *Michela Robba*, Università di Genova (Genova, Italy)
Prof. Engr. *Carlos Ocampo-Martinez*, Universitat Politècnica de Catalunya - BarcelonaTech (Barcelona, Spain).

Last version:
October 20, 2022

Abstract

Power systems are currently undergoing a period of unprecedented transformations. Environmental and sustainability concerns lead to the replacement of centralized generation, based on conventional fossil fuel-based power plants, with distributed generation from renewable energy sources. In addition, a variety of new autonomous entities able to adjust their load demand or provide ancillary services to the grid are increasing the complexity of energy systems, requiring a decentralization of the control structures.

In this context, autonomous power grids have been proposed as a necessary paradigm to capture the need for distributed operation of power grids. Nevertheless, the existing control and optimization techniques are inadequate to reach this goal while ensuring the efficiency and security of power systems. Due to its capacity to capture interactions among interdependent decision-making entities, game theory offers a promising way to implement and control autonomous power grids. Nonetheless, several technical issues must be solved in order to fully implement this new paradigm. As a result, this thesis is dedicated to solving two of the most important research challenges in designing and operating game-theoretical control for autonomous power grids.

In the first part, this thesis deals with the development of optimization tools devoted to closing the gap between variable generation and adjustable load demand. The increasing penetration of renewable energy sources poses significant challenges to the existing power systems due to the difficulty in coping with their inherent time-varying nature. To this aim, a series of stochastic techniques for energy system optimization are proposed to accommodate uncertainty in autonomous power grids operation. Consequently, game-theoretical frameworks are defined with the aim of increasing the flexibility of the grid through the active participation of autonomous entities.

The second part of this thesis is further focused on coordinating autonomous entities in game-theoretical frameworks. The coordination of these entities is not straightforward due to the fact that they are interconnected through power lines and therefore must respect the so-called power flow constraints. The nonconvexity of the resulting control problem thus makes difficult to use traditional mathematical tools. To solve this problem, a novel mathematical theory for game-theoretical frameworks with nonconvex coupling constraints is developed and applied to ensure the quality and feasibility of autonomous power grid operation.

Gutta cavat lapidem non bis sed saepe cadendo:
sic homo fit sapiens bis non, sed saepe legendo
Giordano Bruno

Contents

Preface

This thesis is submitted in partial fulfillment of the requirements for the degree of *Philosophiae Doctor* in Electrical and Information Engineering at the *Politecnico di Bari*. This work was supported by the Italian Ministry of Research through the *Programma Operativo Nazionale (PON) Ricerca e Innovazione 2014-2020*.

The research presented in this dissertation was conducted at the *Decision and Control Laboratory* of Politecnico di Bari under the supervision of Professors **Mariagrazia Dotoli** and **Raffaele Carli**, between November 2019 and October 2022.

This work is to the best of my knowledge original, except where acknowledgments and references are made to previous work. Most part of this thesis has been published during these three years in different scientific publications where I am one of the authors. The papers are preceded by an introductory chapter (Chapter 1), that relates them to each other and provides background information and motivation for the work. A version of Chapters 2, 5, 6 and 7 have been presented in International Journals [1]–[4] while Chapters 3 and 4 have been published in the proceedings of International Conferences [13], [14]. A concluding chapter (Chapter 8) summarizes the main outcomes and findings for future developments, while in Appendix A, some theoretical preliminaries are reported.

Professors **Mariagrazia Dotoli** and **Raffaele Carli** were involved in the early stages of concept formation, as well as data collection, numerical implementation, analysis of experiments, and composition of the above-mentioned manuscripts.

Data collection, numerical implementation, analysis of experiments, and preparation of the original version of Chapter 2 was done primarily by Engr. **Nicola Mignoni** while I contributed mostly in the early stages of concept formation and during the manuscript composition. Chapters 3 and 4 were part of international research collaborations with Professor **Alessandra Parisio**, *Univerity of Manchester*, and Professor **Jan Jantzen**, *University of the Aegean*, respectively. Both were involved in the early stages of concept formation, numerical implementation, analysis of experiments, and composition of the above-mentioned manuscripts. The dataset used for the experiment in Chapter 3 was created by Professor **Jan Jantzen**. Chapters 5 and 6 were part of an extended international collaboration with Professor **Sergio Grammatico** from the *Technical University of Delft*, who was involved in the early stages of concept formation, as well as data collection, numerical implementation, analysis of experiments, and composition of the above-mentioned manuscripts.

In addition to the works presented in this thesis, I am one of the authors of further manuscripts on the control of autonomous power grids and energy systems that were not included in this thesis for lack of space. In particular, these papers cover the optimal control of complex energy systems [11], [15], the game-theoretic control of power grids and energy communities [16]–[19], the integration of energy storage in power grids [5], and the optimal charging of electric vehicles for the frequency regulation support [6]. Moreover, the use of machine learning techniques was employed to forecast failures in power distribution networks in works [7], [20] and to forecast the load demand variation and its correlation with the level of social mobility in works [12], [21].

Finally, during these three years, I also had the opportunity to follow additional research directions leading to the publication of several scientific papers. More in detail, I further focused on multi-agent systems in the context of influence maximization in social networks [8], [22] and distributed control of unmanned aerial vehicles [23]. Lastly, pushed by the urging need for social-based solutions to tackle the Covid-19 emergency, I worked on the control of pandemics through nonpharmaceutical policies [9], [10].

The full list of papers written by the author is reported hereafter.

List of Papers Written by the Author

International Journal Articles

[1] Mignoni, N., Scarabaggio, P., Carli, R., and Dotoli, M., "Control frameworks for transactive energy storage services in energy communities," *Control Engineering Practice*, vol. 130, p. 105 364, 2023. DOI: 10.1016/j.conengprac.2022.105364.

[2] Scarabaggio, P., Grammatico, S., Carli, R., and Dotoli, M., "Distributed Demand Side Management With Stochastic Wind Power Forecasting," *IEEE Transactions on Control Systems Technology*, vol. 30, no. 1, pp. 97–112, 2022. DOI: 10.1109/TCST.2021.3056751.

[3] Scarabaggio, P., Grammatico, S., Carli, R., and Dotoli, M., "Clarke's Local Equilibria in Nash Games with Nonconvex Coupling Constraints," *IEEE Transactions on Automatic Control* ***(under review)***, 2023. DOI: 10.36227/techrxiv.20079959.

[4] Scarabaggio, P., Carli, R., and Dotoli, M., "Noncooperative Equilibrium Seeking in Distributed Energy Systems Under AC Power Flow Nonlinear Constraints," *IEEE Transactions on Control of Network Systems*, 2022. DOI: 10.1109/TCNS.2022.3181527.

[5] Nasiri, F., Ooka, R., Haghighat, F., *et al.*, "Data Analytics and Information Technologies for Smart Energy Storage Systems: A State-of-the-Art Review," *Sustainable Cities and Society*, p. 104 004, 2022. DOI: 10.1016/j.scs.2022.104004.

[6] Scarabaggio, P., Carli, R., Cavone, G., and Dotoli, M., "Smart Control Strategies for Primary Frequency Regulation through Electric Vehicles: A Battery Degradation Perspective," *Energies*, vol. 13, no. 17, p. 4586, 2020. DOI: 10.3390/en13174586.

[7] Atrigna, M., Buonanno, A., Carli, R., *et al.*, "Power Distribution Grids Condition Monitoring under Heatwaves: a Machine Learning Approach to Fault Prediction," *IEEE Transactions on Industry Applications* ***(under review)***, 2023.

[8] Scarabaggio, P., Carli, R., and Dotoli, M., "On Fast and Effective Influence Spread Maximization in Social Networks," *IEEE Transactions on Systems, Man, and Cybernetics: Systems* ***(under review)***, 2023. DOI: 10.36227/techrxiv.13153139.

[9] Carli, R., Cavone, G., Epicoco, N., Scarabaggio, P., and Dotoli, M., "Model Predictive Control to Mitigate the COVID-19 Outbreak in a Multi-region Scenario," *Annual Reviews in Control*, vol. 50, pp. 373–393, 2020. DOI: 10.1016/j.arcontrol.2020.09.005.

[10] Scarabaggio, P., Carli, R., Cavone, G., Epicoco, N., and Dotoli, M., "Nonpharmaceutical Stochastic Optimal Control Strategies to Mitigate the COVID-19 Spread," *IEEE Transaction on Automation Science and Engineering*, vol. 19, no. 2, pp. 560–575, 2022. DOI: 10.1109/TASE.2021.3111338.

Italian Journal Articles

[11] Carli, R., Cavone, G., Dotoli, M., Jantzen, J., Kristensen, M., and Scarabaggio, P., *Controllo predittivo per lo sviluppo di energy Community flessibili ed efficienti*, *Tekneco.it* - Lecce (Italy) (in Italian) ISSN (ISSN-L): 2038-9302. Online: https://bit.ly/3nqB6L2 [Accessed: 2022-06-28], 2020.

[12] Scarabaggio, P., La Scala, M., Carli, R., and Dotoli, M., *Analisi degli effetti della pandemia da COVID-19 sulla domanda di energia elettrica: il caso del Nord Italia*, *L'Energia Elettrica* (in Italian) ISSN (ISSN-L): 0013-7308. Online: https://bit.ly/3Nu1Kxg [Accessed: 2022-06-28], 2020.

International Conference Proceedings

[13] Scarabaggio, P., Carli, R., Parisio, A., and Dotoli, M., "On Controlling Battery Degradation in Vehicle-to-Grid Energy Markets," in *2022 IEEE 18th International Conference on Automation Science and Engineering (CASE)*, IEEE, 2022, pp. 1206–1211. DOI: 10.1109/CASE49997.2022.9926729.

[14] Scarabaggio, P., Carli, R., Jantzen, J., and Dotoli, M., "Stochastic Model Predictive Control of Community Energy Storage under High Renewable Penetration," in *2021 29th Mediterranean Conference on Control and Automation (MED)*, IEEE, 2021, pp. 973–978. DOI: 10.1109/MED51440.2021.9480353.

[15] Carli, R., Cavone, G., Dotoli, M., Epicoco, N., and Scarabaggio, P., "Model predictive control for thermal comfort optimization in building energy management systems," in *2019 IEEE International Conference on Systems, Man and Cybernetics (SMC)*, 2019, pp. 2608–2613. DOI: 10.1109/SMC.2019.8914489.

[16] Scarabaggio, P., Carli, R., and Dotoli, M., "A game-theoretic control approach for the optimal energy storage under power flow constraints in distribution networks," in *2020 IEEE 16th International Conference on Automation Science and Engineering (CASE)*, 2020, pp. 1281–1286. DOI: 10.1109/CASE48305.2020.9216800.

[17] Mignoni, N., Scarabaggio, P., Carli, R., and Dotoli, M., "Game Theoretical Control Frameworks for Multiple Energy Storage Services in Energy Communities," in *2022 8th International Conference on Control, Decision and Information Technologies (CoDIT)*, IEEE, vol. 1, 2022, pp. 1580–1585. DOI: 10.1109/CoDIT55151.2022.9804087.

[18] Calefati, M., Proia, S., Scarabaggio, P., Carli, R., and Dotoli, M., "A Decentralized Noncooperative Control Approach for Sharing Energy Storage Systems in Energy Communities," in *2021 IEEE International Conference on Systems, Man, and Cybernetics (SMC)*, IEEE, 2021, pp. 1430–1435. DOI: 10.1109/SMC52423.2021.9658851.

[19] Scarabaggio, P., Grammatico, S., Carli, R., and Dotoli, M., "A distributed, rolling-horizon demand side management algorithm under wind power uncertainty," in *IFAC 2020, 21st IFAC World Congress 2020*, vol. 53, Elsevier, 2020, pp. 12 620–12 625. DOI: 10.1016/j.ifacol.2020.12.1830.

[20] Atrigna, M., Buonanno, A., Carli, R., *et al.*, "Effects of Heatwaves on the Failure of Power Distribution Grids: a Fault Prediction System Based on Machine Learning," in *2021 IEEE International Conference on Environment and Electrical Engineering and 2021 IEEE Industrial and Commercial Power Systems Europe (EEEIC / I CPS Europe)*, 2021, pp. 1–5. DOI: 10.1109/EEEIC/ICPSEurope51590.2021.9584751.

[21] Scarabaggio, P., La Scala, M., Carli, R., and Dotoli, M., "Analyzing the Effects of COVID-19 Pandemic on the Energy Demand: the Case of Northern Italy," in *2020 AEIT International Annual Conference (AEIT)*, 2020, pp. 1–6. DOI: 10.23919/AEIT50178.2020.9241136.

[22] Scarabaggio, P., Carli, R., and Dotoli, M., "A fast and effective algorithm for influence maximization in large-scale independent cascade networks," in *2020 7th International Conference on Control, Decision and Information Technologies (CoDIT)*, vol. 1, 2020, pp. 639–644. DOI: 10.1109/CoDIT49905.2020.9263914.

[23] Carli, R., Cavone, G., Epicoco, N., Di Ferdinando, M., Scarabaggio, P., and Dotoli, M., "Consensus-Based Algorithms for Controlling Swarms of Unmanned Aerial Vehicles," in *International Conference on Ad-Hoc Networks and Wireless*, Springer International Publishing, 2020, pp. 84–99. DOI: 10.1007/978-3-030-61746-2_7.

Acknowledgements

Undertaking this Ph.D. has been a truly life-changing experience for me and surely I would have quit many times without the support and guidance that I received from many people.

First and foremost, I would like to thank Prof. Mariagrazia Dotoli for being my primary supervisor during my studies. For every question I had, she either knew the answer or could point me in the right direction. Thank you for helping me grow professionally and teaching me how to be a good researcher (and person). Next, I would like to thank Prof. Raffaele Carli for all the patience he had in supervising me. He always had suggestions on what to do next and, even if things did not go as planned, he managed to motivate me.

I thoroughly enjoyed the cooperation with Prof. Sergio Grammatico, Jan Jantzen, and Alessandra Parisio. Their suggestions were always helpful and allowed me to have a wider spectrum of scientific practice.

I would also like to thank the research group of the D&C Lab. I always enjoyed coming to work, going to conferences, and joining other group activities with you.

Without the support of my parents, this would have not been possible. Thank you for believing in me and enabling me to come this far. To my many friends, you should know that your support and encouragement was worth more than I can express on paper. I would like to thank those who are fare from me, for enduring me, having my back, motivating me, and all the other countless things that made me not give up or go insane.

Finally, as Snoop said once: *Last but not least, I wanna thank me for tryna do more right than wrong.*

Acronyms

ALM *augmented Lagrangian method*. 22

APGs *autonomous power grids*. 4, 134

CESS *cloud energy storage systems*. 16

CL-GNE *Clarke's local generalized Nash equilibrium*. 91, 92, 94, 124

CL-GNEP *Clarke's local generalized Nash equilibrium problem*. 94, 124

CLs *controllable loads*. 50

DC *direct current*. 92

DCOPF *direct current optimal power flow*. 117

DERs *distributed energy resources*. 2

DG *distributed generation*. 1, 64, 116

DR *demand response*. 1

DS *distributed storage*. 65, 116

DSM *demand side management*. 1, 64

DSO *distribution system operator*. 118

ECLs *energy-based controllable loads*. 53

EHs *electrical heaters*. 1

EM *energy manager*. 52

ESSs *energy storage systems*. 3, 14, 50, 104

EVs *electrical vehicles*. 1, 35

FR *frequency regulation*. 36

G2V *grid-to-vehicle*. 3

GNE *generalized Nash equilibrium*. 22, 91, 123, 142

GNEP *generalized Nash equilibrium problem*. 22, 92, 123, 141, 142

HV *high voltage*. 117, 118

ICTs *information and communication technologies*. 1

IID *independent and identically distributed*. 56

JC *jointly convex*. 92

KKT *Karush–Kuhn–Tucker*. 94, 143

LV *low voltage*. 116

MPC *model predictive control*. 8, 37, 50
MV *medium voltage*. 116

NCLs *non-controllable loads*. 50
NE *Nash equilibrium*. 43, 91, 141
NEP *Nash equilibrium problem*. 43, 92, 141

OPF *optimal power flow*. 92, 104, 117

P2P *peer-to-peer*. 3, 15
PAR *peak-to-average ratio*. 36
PDF *probability density function*. 56, 64, 65
PNEP *penalized Nash equilibrium problem*. 125
PV *photovoltaic*. 2, 37

QVE *quasi-variational equilibrium*. 96
QVI *quasi-variational inequalities*. 92, 96, 124

RESs *renewable energy sources*. 1, 36, 50, 65, 104, 116

SAA *sample average approximation*. 56, 66
SE *sharing economy*. 16
SoC *state of charge*. 36

TCLs *thermal controllable loads*. 53
TOU *time to use*. 36

V2G *vehicle-to-grid*. 3, 36
vCL-GNE *variational Clarke's local generalized Nash equilibrium*. 96, 124
VESS *virtual energy storage systems*. 16
vGNE *variational generalized Nash equilibrium*. 92, 124, 143
VI *variational inequality*. 22, 92, 139, 142
VIP *variational inequality problem*. 95, 124
VPP *virtual power plant*. 16

Chapter 1

Introduction

Since the dawn of the industrial age, the ability to use different forms of energy has transformed living conditions for billions of people, enabling them to reach a level of comfort and mobility that is exceptional in human history [1]. On September 4, 1882, Thomas Edison launched the first commercial power plant at 257 Pearl Street, New York City [2]. From this first power plant, which supplied only a one-quarter square mile (0.65 square km) area, to a sprawling network of power lines, connecting distant power plants generating electricity and numerous points of use, significant progress has been made in power system technology concerning efficiency, quality, safety, and reliability [3].

For most of the last two centuries, the steady growth in energy consumption has been closely tied to rising levels of prosperity and economic opportunity. Nevertheless, it has become clear that current patterns of energy consumption are environmentally unsustainable [4]. In particular, the overwhelming reliance on fossil fuels may change the Earth's climate to an extent that could have grave consequences for the integrity of both natural systems and vital human systems [5]. New approaches and paradigms are urgently needed to develop a more sustainable energy system [6], [7]. Indeed, governmental efforts are aimed at changing the power system generation portfolios to reduce the reliance of our societies on conventional fossil-based power generation in favor of *renewable energy sources* (RESs) [8]–[10]. However, changing the energy sector without compromising the safety and reliability standards of conventional power systems is difficult, since this implies integrating a significant amount of RESs with limited (or no) inertia, the adoption of energy storage solutions, and the expansion of transmission and distribution networks.

The transformation of the energy sector will likely be made more challenging by the increasing trends in load demand caused by the adoption of *electrical heaters* (EHs) and *electrical vehicles* (EVs), as customers in both heat and transport sectors are moving away from fossil fuels [11]. Hence, end-users are expected to play a positive role in addressing these challenges, namely through the so-called *demand response* (DR) and *demand side management* (DSM) [12]–[14]. Achieving these goals becomes more feasible with the developments of *information and communication technologies* (ICTs) since they enable bidirectional communications between grid operators and end-users, namely to relay dynamic electricity prices, the availability of local generation resources, the requests for load flexibility, and also greatly facilitating load scheduling and the integration of *distributed generation* (DG) [5], [15]. Therefore, these technologies allow the provision of additional ancillary services, which could contribute to maintaining or improving the quality of the service. On the other hand, this opportunity raises several concerns about privacy, potential intrusions, and resiliency to communication failures, which need to be addressed [16].

1.1 Future Trends and Challenges for the Energy Sector

Based on the above discussions, several trends can be identified in the energy sector mainly directed by the need of finding efficient and effective solutions for resilient and sustainable power systems. Nevertheless, these trends may enhance several challenging issues that the power industry must address to promise a bright future for our societies. In this section, some of the most relevant trends and challenges encountered by the industry to move toward resilient and sustainable power systems are outlined.

1.1.1 Energy Crisis and Climate Change

Secure and price-consistent sources of primary energies are critical prerequisites for modern societies. The main primary energy sources are fossil fuels (coal, oil, and natural gas), which have been the key drivers of the twenty-first-century economic growth from an energy perspective [17]. However, fossil fuel reserves are not uniformly distributed over the Earth and they will not last forever, even according to the most optimistic forecasts [18]. Relying on the over-availability and efficiency of fossil fuels has been demonstrated to be a phenomenal mistake, since countries with inadequate reserves are nowadays facing serious concerns about energy production.

In addition, the heavy use of fossil fuels has created some severe environmental issues since the start of the industrial revolution, including global warming, photochemical smog and catastrophic air pollution, many of which are widely documented in the scientific literature [17], [19]. Alleviating climate changes and environmental concerns are the most challenging issues which are encountered by the power industry. Employing alternative and sustainable energy sources is therefore mandatory to avoid consequential effects on human society and economy in the near future.

1.1.2 Exploitation of Renewable Energy Sources

To tackle the energy crisis and climate change we should progressively decarbonize power systems, shifting to a fully renewable energy portfolio. However, RESs such as wind and solar are also known as *not dispatchable* sources because they cannot be controlled on demand, being fundamentally different from conventional generation sources. Moreover, power produced from these sources is *intermittent*, as it exhibits large fluctuations over time while it cannot be precisely forecasted in advance due to the *uncertain* nature of these sources [20]. We can use the term *variability* to encompass these three characteristics. Variability is the most important obstacle in integrating renewable generation into the electric energy system at deep penetration levels [21]. Even if aggregation over large areas tends to reduce the variability of renewable generation, the significant variability of RESs makes difficult an efficient operation of power systems [22].

The massive ongoing penetration of RESs within the power system likewise deteriorates its stability. The traditional power system has relied on a large number of synchronous generators to provide natural voltage and frequency control [23]. Conversely, the new form of renewable energy, which is rapidly increasing in power systems, cannot naturally provide active frequency and voltage regulation. Modern commercially available solid-state inverters are capable of supplying (capacitive as well as inductive) reactive power [24]. At the same time, fast communications of voltage measurements across the distribution network may allow for coordinated control actions. Power electronics interface converters should provide active contributions with frequency containment reserve services or the provision of synthetic inertia in order for the system to operate in a robust and secure manner [25].

1.1.3 Increasing Number of Distributed Energy Resources

Electric power system operations are designed to accommodate the natural variability of RESs as well as planned and unplanned contingencies. This is done at different time scales through load-frequency control, operational reserves, scheduling and unit commitment, demand response, and load shedding [21], [26]. Nevertheless, at deep penetration levels of RESs, reconfiguring these existing mechanisms to handle the increased variability is necessary with significant cost issues and operational challenges [27]. Future power grids should have a set of new features that will be necessary to satisfy the needs of the grid operators and the consumers, aiming at increasing the flexibility and resilience of power grids [27], [28]. These are represented by the so-called *distributed energy resources* (DERs) which are emerging technologies, such as solar *photovoltaic* (PV), fuel cells, dynamic response from loads, LED lighting, smart appliances, electric heat pumps, microgeneration

systems and *energy storage systems* (ESSs) [29] that are gradually changing the dynamics of power distribution systems making them more efficient and flexible, yet causing bidirectional power flows and voltage fluctuations that can impact optimal control and system operation [30]. Additionally, EVs can also be considered as DERs as they can positively increase the flexibility of the grid through *grid-to-vehicle* (G2V) and *vehicle-to-grid* (V2G) operation modes [31], [32]. Sales of EVs are expected to increase significantly in the near future and this growth places new and important challenges [33]. Besides the mentioned factors, the proliferation of EVs will increase significantly the overall load demand changing the load patterns (frequency, magnitude, and duration) which ultimately modify the concept of conventional loads and resultant load modeling [34]. This change, if not managed effectively, may degrade the reliability of power systems. With the integration of these emerging technologies, all of them establishing (unidirectional or bidirectional) communication with the power grid, a reliable control strategy is required to manage the power transactions and the network control in real-time, especially considering the dynamic and distributed integration of electric mobility systems and DR programs.

1.1.4 Outdated Electricity Markets

Electricity has physical constraints on transmission, generation, scheduling, and storage, economic constraints on generation costs and system infrastructure, and quality of service constraints. As a result, traditional commodity market structures are not suitable for electricity [35]. In fact, a certain level of centralized coordination and control is necessary to ensure a safe, economic, and reliable operation. Nevertheless, in the context of deep penetration of renewable energy, many new questions arise regarding new market mechanisms and structures. In particular, there is increasing competition and decentralization in generation and retail distribution, while new end-user-centric approaches are expected to be developed to ensure the dynamic involvement of consumers along with the awareness of the needs of the power grid [28], [36]. For such a purpose, the development of increasingly efficient, autonomous, and resilient technological solutions is required, as well as communication systems enabling end-user involvement in a dynamic way. These communication systems will allow defining periods of utilization for the electrical appliances according to power grid operators and end-users convenience, also integrating monitoring systems, to know in real-time the energy transactions and minimize the inefficient and unnecessary use of the electrical appliances. Moreover, it will be possible to define control strategies to optimize consumption patterns to better match demand and supply, i.e., within a DR paradigm [37]. Additionally, the expected empowerment of the so-called prosumers and emerging blockchain and distributed optimization technologies, local *peer-to-peer* (P2P) energy transactions will be necessary to boost energy flexibility and create new market opportunities [38].

1.1.5 Increasing Volumes and Sources of Data

Large amounts of data are being generated in different parts of the power sector as it is transformed by the ongoing digital revolution [39]. These data have a potential value for power companies, grid operators, and end-users, and can be exploited using big data algorithms for different purposes such as power supply and demand forecasting, state estimation, and grid control [39], [40]. The knowledge extracted from these data is thus expected to positively impact indicators relating to operation and maintenance costs, investment postponement, and quality of service. Furthermore, big data processing and mining are prompting the emergence of new business models (e.g., trading companies exploiting large datasets to better understand the behavior of their clients) and boosting the offer of new customized energy services to consumers [41].

In the future, a significant part of the electrical appliances will have access in real-time to some variables of the network. In addition to the necessary control of the electrical appliances, such parameters can be useful for supervision algorithms to evaluate if the control signals are consistent with the real operation of the grids. While modern

communication, control, and computing technologies are tremendous opportunities to improve electric power system response and resilience to failure, they also render the grid vulnerable to intentional attacks from internal or external parties [42]. This in fact increases the risk of compromising reliable and secure power system operation [42], [43]. The definition of mechanisms and supervision algorithms will be extremely important to prevent damages in the operation of the systems in case of failures in the command and management systems or in cases of attack or intrusion in the communication networks, having as the main objective the efficient and sustainable utilization of electrical energy, both for consumers and grid operators.

1.1.6 Resilience Against Increasing Unexpected Events

A large number of components in the existing power systems have been designed and installed decades ago. As a matter of fact, the higher failure rates of these components have increased significantly degrading the ability of the grid to handle unexpected events. As mentioned above, power systems have been designed and operated to withstand a great majority of disturbances while being able to supply to customers. However, when unexpected abnormal and/or catastrophic events occur, significant service interruptions are likely to threaten the security and functionality of the system [44], [45]. In addition, the interconnected nature of the system increases the probability of fault propagation, which can interrupt the service to a large number of customers [44]. Resilience is therefore an ever-increasing requirement that goes further than N-1 security. This involves the capability of islanding operation of parts of the distribution grid and the development of more effective emergency procedures that exploit bottom-up strategies using DER control capabilities [46].

1.2 Autonomous Power Grids: a New Paradigm to Tackle the Challenges of the Energy Sector

Traditional power systems distribute electricity primarily in one direction, flowing from large power plants to customer loads; however, increasing amounts of variable generation, DERs, distributed energy storage, and new loads are being added to electric grids causing bidirectional power flows and voltage fluctuations that impact the optimal control and system operations. In addition, due to the increased numbers and types of sensors, massive amounts of new data are being collected on energy grid conditions. This is increasing the complexity of energy systems to a point at which existing techniques to monitor, control, and optimize power systems will be inadequate. For example, existing techniques might not offer decision-making capabilities that are consistent with the form and function of future large-scale systems, which will be governed by faster dynamics, include heterogeneous energy assets that are controllable at different temporal resolutions, and accommodate a variety of deregulated energy markets.

The *National Renewable Energy Laboratory* has proposed a new operational and control paradigm named *autonomous power grids* (APGs) that may enable the secure, resilient and economic operations of future energy systems [47], [48]. Similar to autonomous vehicles –which do not require a physical driver and can make decisions on how to most effectively transport a person from one place to another– APGs do not require physical operators, can be extremely secure and resilient (self-healing), and can self-optimize in real time to ensure economic and reliable performance while integrating energy in all forms [48]. Key features of APGs include:

- *Autonomous*: capable of making decisions and operations without humans in the loop;
- *Scalable*: architecture able to control hundreds of millions of devices across many physical scales (distribution to transmission systems);

- *Resilient*: can self-reconfigure (grid-connected and islanded operations) and operate with and without communications;
- *Secure*: incorporate cybersecurity and physical security against threats;
- *Reliable and affordable*: ensure reliable and economic operations;
- *Operate in real-time*: controls, optimization, and data processing use algorithms that are fast enough to make real-time decisions;
- *Allow asynchronous communications*: able to pass information messages between asynchronous sources;
- *Robust*: deals with the uncertainty of stochastic resources and forecasts;
- *Flexible*: must be able to control and optimize across multi-physics energy flows and deal with variable resources.

Nevertheless, the existing control and optimization techniques are inadequate for handling the complexity of APGs. These conventional techniques are primarily centralized, and because of underlying computational complexity limits, they do not offer decision-making capabilities that are consistent with future energy systems that are governed by faster dynamics and complex market mechanisms; therefore, they cannot guarantee reliable, resilient, and efficient system operations. Extensive work has been done on the detailed modeling of complex individual systems or applications, the research defined single modeling paradigms to focus on single issues; however, studying the interactions among multiple systems or applications is still in the early stages. Although this has worked well historically, these modeling efforts will need to operate in an integrated fashion to realize the goal of APGs. Another aspect that increases complexity is that power grids include all energy domains as well as other domains that influence how energy is generated, distributed, converted, and used. The connections among these domains create interdependencies that challenge overall system design, planning, control, and optimization. Historically, little attention has been paid to the overlap among these areas, but APGs will need to be able to account for these interdependencies because of the increasing impacts that each energy and infrastructure domain has on one another. This detailed real-time information sharing is currently not the norm for the majority of power system operations and planning processes, wherein information is often segregated based on the traditional utility boundaries between transmission and distribution, load and generation, and planning and operations. This integration of modeling information becomes even more critical as additional energy systems become increasingly intertwined with the electric grid structure. A further challenge is understanding the need for information that must be shared by actors in the system while maintaining user privacy and system security. This is critical for distributed optimization and control of autonomous systems that do not have centralized structures. New modeling tools that allow for the expression of complex system interactions in novel manners are also necessary, and the development of these tools should allow for the use of multiple formalisms to accurately model disparate subsystems that are critical for multi-energy systems and thus should be able to be natively represented in such a framework.

1.3 Game Theory to Design, Implement and Control Autonomous Power Grids

The APGs paradigm can therefore be a solution for the arising challenges of the future energy sector due to its ability to deal with various stakeholders, conflicting optimization targets, and uncertainties. APGs are power networks composed of intelligent nodes that can operate, communicate, and interact autonomously to efficiently deliver power and electricity to their consumers. This heterogeneous nature motivates the adoption of advanced techniques for overcoming the various technical challenges at different levels

such as design, control, and implementation. Nevertheless, the complexity of future energy systems and APGs will render existing control and optimization techniques inadequate.

The proliferation of advanced technologies and services in power grids implies that disciplines such as game theory will naturally become prominent tools in the design and analysis of APGs. In particular, there is a need to deploy novel models and algorithms that can capture the need for distributed operation of APGs nodes for communication and control purposes. In addition, due to the heterogeneous nature of APGs, which are typically composed of a variety of nodes each having different capabilities and objectives, it is necessary to have low-complexity distributed algorithms that can efficiently represent competitive or collaborative scenarios between the various entities of APGs. In this context, game theory constitutes a robust framework that can address many of these challenges. Within the context of APGs, the applications of noncooperative games and learning algorithms are numerous. On the one hand, noncooperative games can be used to perform distributed demand-side management and real-time monitoring or to deploy and control power grids. On the other hand, economical factors such as markets and dynamic pricing are an essential part of APGs. In this respect, noncooperative games provide several frameworks, ranging from classical noncooperative Nash games to advanced dynamic games that enable designers to optimize and devise pricing strategies that adapt to the nature of the grid. In APGs, with the deployment of advanced networking technologies, it may be possible to enable a limited form of communication between the nodes that paves the way for introducing cooperative game-theoretic approaches. In fact, the integration of power, communication, and networking technologies in future grids opens up the door for several prospective applications in which smart nodes can cooperate so as to improve the robustness and efficiency of the grid. To make this idea a reality, control algorithms for APGs will need to be developed and implemented with the following characteristics:

- *Operate in real-time*: Control algorithms must operate fast enough to ensure real-time operations in electric grids that balance load and generation every second.
- *Handle asynchronous data and control actions*: Data need to be used from a variety of asynchronous measurements and sources, whereas distributed decision-making leads to asynchronous control actions.
- *Be robust*: This covers both reliability and resilience, where reliability is fault tolerance, and resilience is the ability to come back from a failed state. These control systems also must be robust to communications failures, prolonged communications outages, and large-scale disturbances.
- *Be scalable*: Control algorithms must operate in a scalable fashion to ensure control of hundreds of millions of devices.

1.4 Positioning of the Thesis with Respect to the Related Literature and Scientific Contributions

Due to its capability of capturing interactions among interdependent decision-making problems, game theory has been the canonical and prevailing paradigm adopted in power market studies. Clearly, game-theoretic approaches are a promising tool for the deployment of APGs. Nonetheless, the advantages of applying distributed game-theoretic techniques in modeling and controlling power networks are accompanied by several technical challenges that must be solved in order to fully implement the APGs paradigm.

As a result, since significant attention and effort need to be dedicated to designing game-theoretical control algorithms for APGs, this thesis follows two main research directions.

1. The first research direction investigates all the approaches that are able to increase the penetration of RESs thus reducing the gap between their increasing variable generation and the adjustable load demand. To this aim, this research studies the

operational and economic aspects of the application of stochastic programming to energy system optimization. Starting with control policies design to accommodate uncertainty in energy networks, we develop game-theoretical control designs with robust properties.

2. The second research direction focuses on coordinating selfish entities in APGs while ensuring feasible grid operations. In this context, we develop a novel mathematical theory that is able to ensure the fulfillment of nonconvex coupling constraints when decentralized and distributed game-theoretical frameworks are used.

This thesis presents the results of research conducted and published in a series of conference and journal papers by the author. The thesis is structured in two main parts –anticipated by the present Introduction– as described in the sequel.

1.4.1 Closing the Gap Between Variable Distributed Generation and Adjustable Demand in Autonomous Power Grids

The power systems of many countries have been able to accommodate rising shares of RESs. However, this trend poses significant challenges to the existing power systems, due to the difficulty in coping with the inherent time-varying nature of RESs. Among other technical challenges, frequency and voltage control can be impacted by RES-prompted mismatches between supply and demand. The transition to a zero-emissions energy system, based on high shares of volatile RESs, depends strongly on the ability to increase the flexibility of energy demand to avoid large imbalances between energy generation and consumption. In general, a positive correlation exists between the share of variable power sources and the power system flexibility needs. Flexibility, in this setting, concerns the extent to which such systems are able to manage unpredicted operating conditions, namely those induced by the variability of load and RESs [40]. In other words, without adequate flexibility mechanisms, it becomes increasingly harder to cope with mismatches between generation and demand stemming from their natural variations in real-time as the share of RES increases [49]. In addition, grid operators must overcome an ever-growing number of distributed energy resources being connected to the grid. Because of the soaring number of grid-tied devices, operators will no longer be able to use centralized control schemes. To this end, it is natural to investigate the application of distributed coordination techniques in APGs operation and control.

As a result, the first contribution of this thesis is to propose decentralized and distributed control schemes for controlling such a huge number of devices. In **Chapter 2** we define innovative game-theoretic control frameworks for energy communities equipped with independent service-oriented energy storage systems. The addressed control problem consists in optimally scheduling the energy activities of a group of prosumers, characterized by their own demand and renewable generation, and a group of energy storage service providers, able to store the prosumers' energy surplus and, subsequently, release it upon a fee payment. The two proposed approaches are validated through several numerical simulations on realistic scenarios.

The electrification of transport is expected to accentuate the challenges of balancing supply and demand. This is particularly the case for the (local) electricity distribution grid, where distributed energy devices, such as electric vehicles will strain grid infrastructure unevenly, creating instability and local bottlenecks in the grid. Nevertheless, as power grids are facing a reduced total system inertia as traditional generators are phased out in favor of RESs, this massive number of EVs represents a significant capacity of distributed energy storage that can be an alternative to large-scale storage devices, thus providing ancillary services back to the power grid. The influence of a single EV on the network is low; nevertheless, the aggregate impact becomes relevant when they are properly coordinated. Hence, in **Chapter 3** we design a game-theoretic approach for APGs where the flexibility and predictability of the system are increased thanks to the adoption of smart energy pricing mechanisms. In particular, we consider the frequent case of a group of EVs connected to a parking lot with a photovoltaic facility. We propose a novel strategy

to optimally control their batteries during the parking session, which is able to satisfy their requirements and energy constraints. The effectiveness of the proposed method is validated through numerical experiments based on a real scenario.

Flexibility can alleviate the impact of the inherent variability of RESs. Nevertheless, appropriate prediction, control, and precise representation of renewable energy systems play an important role to ensure a stable and uninterrupted energy supply. Stochastic optimization techniques can represent well the uncertainties, probabilities, and fluctuating behaviors of renewable energy systems and thus allow to evaluate their influence on the output of the system. To this aim, in **Chapter 4** we focus on the robust optimal on-line scheduling of a grid-connected smart energy system, where users are equipped with an adjustable load demand (e.g., (non-)controllable loads and ESSs). Leveraging on the pricing signals gathered from the power distribution grid and the predicted values for local production and demand, the energy activities inside the smart energy system are optimally scheduled. Differently from literature contributions, to cope with the uncertainty that affects the forecast of the inflexible demand profile and the renewable production curve, we propose a Stochastic *model predictive control* (MPC) approach aimed at minimizing the overall energy costs. The effectiveness of the method is validated through numerical experiments on the marina of Ballen, Samsø (Denmark), where a smart energy system with shared photovoltaic panels and a battery energy storage system supplies the local harbor community.

DSM is an essential practice to increase the flexibility of power grids providing opportunities to smooth the load profile over time by shaving peaks and filling valleys. Provided with financial incentives, customers would like to reduce part of their energy consumption or shift electricity usage during peak hours. As the last contribution to this research direction, we focus on increasing the RESs penetration by employing both the flexibility given by a DSM scheme and a series of stochastic techniques to better represent the uncertain nature of RESs. In particular, in **Chapter 5** we propose a distributed DSM approach for smart grids taking into account uncertainty in wind power forecasting. The smart grid comprehends traditional users as well as active users (prosumers). Through a rolling-horizon approach, prosumers participate in a DSM program, aiming at minimizing their cost in the presence of uncertain wind power generation. We assume that each user selfishly formulates its grid optimization problem as a noncooperative game and we define an approach to cope with the uncertainty in wind power availability by adopting a stochastic approximated framework. Numerical simulations on a real dataset show that the proposed stochastic strategy generates lower individual costs compared to the standard expected value approach.

1.4.2 Ensuring Quality and Feasibility of Autonomous Power Grids Operation

The traditional energy sector has been created to distribute the electrical energy produced by a few large power stations, to several consumers [50]. Therefore, traditional power distribution networks were designed for unidirectional, radial, and weakly meshed power flows. Nevertheless, the deregulation of energy markets and RESs are inducing a new model of energy production and distribution that has changed the way of delivering power to electricity customers [15]. New autonomous entities (e.g., prosumers and prosumagers) can inject energy back into the power grid, compromising power distribution networks that are now massively stressed by an incessant swap in the direction and magnitude of power flows compromising their stability [51].

The cooperation of such independent entities is challenging: on the one hand, they act selfishly; on the other hand, they must cooperate to ensure safe and secure grid operations. To this aim, in the second part of this thesis, we focus on coordinating these autonomous entities in game-theoretical frameworks.

These entities are physically interconnected through power lines; hence control frameworks must respect the so-called power flow constraints whose nonconvexity makes the use of traditional mathematical tools difficult. Facing this challenge, we develop a

novel mathematical theory for game-theoretical frameworks with nonconvex coupling constraints and apply it to ensure the quality and feasibility of autonomous power grid operation.

In particular, in **Chapter 6** we consider a class of Nash games with nonconvex coupling constraints where we leverage the theory of tangent cones to define a novel notion of local equilibrium: Clarke's local generalized Nash equilibrium (CL-GNE). Our first technical contribution is to show the stability of these equilibria on a specific local subset of the original feasible set. As a second contribution, we show that the proposed notion of local equilibrium can be equivalently formulated as the solution of a quasi-variational inequality, remarkably, with equal Lagrange multipliers. Next, we define conditions for the existence and uniqueness of the CL-GNE. To compute such an equilibrium, we propose two discrete-time distributed dynamics or fixed-point iterations. Our third technical contribution is to prove convergence under (strongly) monotone assumptions on the pseudo-gradient mapping of the game.

Having defined a theory to handle game-theoretical problems with nonconvex constraints, in **Chapter 7** we propose a novel noncooperative control mechanism for optimally regulating the operation of power distribution networks equipped with traditional loads, distributed generation, and active users. Active users participate in a noncooperative liberalized market designed to increase the penetration of renewable generation. The novelty of our game-theoretical approach consists in incorporating economic factors as well as physical constraints and grid stability aspects. Lastly, by integrating the proposed framework into a rolling-horizon approach, we show its effectiveness and resiliency through numerical experiments.

References

[1] Barca, S., "Energy, property, and the industrial revolution narrative," *Ecological Economics*, vol. 70, no. 7, pp. 1309–1315, 2011.

[2] Sulzberger, C., "Thomas edison's 1882 pearl street generating station," *IEEE Global History Network*, 2010.

[3] Hughes, T. P., *Networks of power: electrification in Western society, 1880-1930*. JHU press, 1993.

[4] Omer, A. M., "Energy, environment and sustainable development," *Renewable and sustainable energy reviews*, vol. 12, no. 9, pp. 2265–2300, 2008.

[5] Strbac, G., "Demand side management: Benefits and challenges," *Energy policy*, vol. 36, no. 12, pp. 4419–4426, 2008.

[6] Su, Y., "Smart energy for smart built environment: A review for combined objectives of affordable sustainable green," *Sustainable Cities and Society*, vol. 53, p. 101 954, 2020.

[7] Silva, B. N., Khan, M., and Han, K., "Towards sustainable smart cities: A review of trends, architectures, components, and open challenges in smart cities," *Sustainable Cities and Society*, vol. 38, pp. 697–713, 2018.

[8] Hosseini, S. M., Carli, R., and Dotoli, M., "Robust optimal energy management of a residential microgrid under uncertainties on demand and renewable power generation," *IEEE Trans. Autom. Sci. Eng.*, vol. 18, no. 2, pp. 618–637, 2021.

[9] Das, B. K., Hoque, N., Mandal, S., Pal, T. K., and Raihan, M. A., "A techno-economic feasibility of a stand-alone hybrid power generation for remote area application in bangladesh," *Energy*, vol. 134, pp. 775–788, 2017.

[10] Foley, A. and Olabi, A. G., *Renewable energy technology developments, trends and policy implications that can underpin the drive for global climate change*, 2017.

[11] Heinen, S., Mancarella, P., O'dwyer, C., and O'malley, M., "Heat electrification: The latest research in europe," *IEEE Power and Energy Magazine*, vol. 16, no. 4, pp. 69–78, 2018.

[12] Garcia, C. E., Prett, D. M., and Morari, M., "Model predictive control: Theory and practice—a survey," *Automatica*, vol. 25, no. 3, pp. 335–348, 1989.

[13] Lotfi, M., Monteiro, C., Shafie-Khah, M., and Catalão, J. P., "Evolution of demand response: A historical analysis of legislation and research trends," in *2018 twentieth international middle east power systems conference (MEPCON)*, IEEE, 2018, pp. 968–973.

[14] Eto, J., "The past, present, and future of us utility demand-side management programs," 1996.

[15] Siano, P., "Demand response and smart grids—a survey," *Renewable and sustainable energy reviews*, vol. 30, pp. 461–478, 2014.

[16] Deng, R., Yang, Z., Chow, M.-Y., and Chen, J., "A survey on demand response in smart grids: Mathematical models and approaches," *IEEE Transactions on Industrial Informatics*, vol. 11, no. 3, pp. 570–582, 2015.

[17] Singh, S., "Energy crisis and climate change: Global concerns and their solutions," *Energy: Crises, Challenges and Solutions*, pp. 1–17, 2021.

[18] Arutyunov, V. S. and Lisichkin, G. V., "Energy resources of the 21st century: Problems and forecasts. can renewable energy sources replace fossil fuels," *Russian Chemical Reviews*, vol. 86, no. 8, p. 777, 2017.

[19] Zou, C., Zhao, Q., Zhang, G., and Xiong, B., "Energy revolution: From a fossil energy era to a new energy era," *Natural Gas Industry B*, vol. 3, no. 1, pp. 1–11, 2016.

[20] Mahmood, D., Javaid, N., Ahmed, G., Khan, S., and Monteiro, V., "A review on optimization strategies integrating renewable energy sources focusing uncertainty factor–paving path to eco-friendly smart cities," *Sustainable Computing: Informatics and Systems*, vol. 30, p. 100 559, 2021.

[21] Bitar, E., Khargonekar, P. P., and Poolla, K., "Systems and control opportunities in the integration of renewable energy into the smart grid," *IFAC Proceedings Volumes*, vol. 44, no. 1, pp. 4927–4932, 2011.

[22] Iizaka, T., Jintsugawa, T., Kondo, H., Nakanishi, Y., Fukuyama, Y., and Mori, H., "A wind power forecasting method and its confidence interval estimation," *Electrical Engineering in Japan*, vol. 186, no. 2, pp. 52–60, 2014.

[23] Hirase, Y., Abe, K., Sugimoto, K., Sakimoto, K., Bevrani, H., and Ise, T., "A novel control approach for virtual synchronous generators to suppress frequency and voltage fluctuations in microgrids," *Applied Energy*, vol. 210, pp. 699–710, 2018.

[24] She, X., Huang, A. Q., Wang, F., and Burgos, R., "Wind energy system with integrated functions of active power transfer, reactive power compensation, and voltage conversion," *IEEE transactions on industrial electronics*, vol. 60, no. 10, pp. 4512–4524, 2012.

[25] Ackermann, T., Prevost, T., Vittal, V., Roscoe, A. J., Matevosyan, J., and Miller, N., "Paving the way: A future without inertia is closer than you think," *IEEE Power and Energy Magazine*, vol. 15, no. 6, pp. 61–69, 2017.

[26] Bessa, R., Moreira, C., Silva, B., and Matos, M., "Handling renewable energy variability and uncertainty in power systems operation," *Wiley Interdisciplinary Reviews: Energy and Environment*, vol. 3, no. 2, pp. 156–178, 2014.

[27] Panteli, M., Trakas, D. N., Mancarella, P., and Hatziargyriou, N. D., "Power systems resilience assessment: Hardening and smart operational enhancement strategies," *Proceedings of the IEEE*, vol. 105, no. 7, pp. 1202–1213, 2017.

[28] Lopes, J. A. P., Madureira, A. G., Matos, M., *et al.*, "The future of power systems: Challenges, trends, and upcoming paradigms," *Wiley Interdisciplinary Reviews: Energy and Environment*, vol. 9, no. 3, e368, 2020.

[29] Khan, Z. A., Ahmed, S., Nawaz, R., Mahmood, A., and Razzaq, S., "Optimization based individual and cooperative dsm in smart grids: A review," *2015 Power Generation System and Renewable Energy Technologies (PGSRET)*, pp. 1–6, 2015.

[30] Loewenstern, Y., Katzir, L., and Shmilovitz, D., "The effect of system characteristics on very-short-term load forecasting," in *2015 International School on Nonsinusoidal Currents and Compensation (ISNCC)*, IEEE, 2015, pp. 1–6.

[31] Alsharif, A., Tan, C. W., Ayop, R., Dobi, A., and Lau, K. Y., "A comprehensive review of energy management strategy in vehicle-to-grid technology integrated with renewable energy sources," *Sustainable Energy Technologies and Assessments*, vol. 47, p. 101 439, 2021.

[32] Yu, H., Niu, S., Shang, Y., Shao, Z., Jia, Y., and Jian, L., "Electric vehicles integration and vehicle-to-grid operation in active distribution grids: A comprehensive review on power architectures, grid connection standards and typical applications," *Renewable and Sustainable Energy Reviews*, vol. 168, p. 112 812, 2022.

[33] Carrilero, I., Ansean, D., Viera, J. C., Fernandez, Y., Pereirinha, P. G., and González, M., "Impact of fast-charging and regenerative braking in lifepo4 batteries for electric bus applications," in *2017 IEEE vehicle power and propulsion conference (VPPC)*, IEEE, 2017, pp. 1–6.

[34] Jones, C. B., Vining, W., Lave, M., *et al.*, "Impact of electric vehicle customer response to time-of-use rates on distribution power grids," *Energy Reports*, vol. 8, pp. 8225–8235, 2022.

[35] Kirschen, D. S. and Strbac, G., *Fundamentals of power system economics*. John Wiley & Sons, 2018.

[36] Richter, M., "Utilities' business models for renewable energy: A review," *Renewable and Sustainable Energy Reviews*, vol. 16, no. 5, pp. 2483–2493, 2012.

[37] Talari, S., Shafie-Khah, M., Siano, P., Loia, V., Tommasetti, A., and Catalão, J. P., "A review of smart cities based on the internet of things concept," *Energies*, vol. 10, no. 4, p. 421, 2017.

[38] Parag, Y. and Sovacool, B. K., "Electricity market design for the prosumer era," *Nature energy*, vol. 1, no. 4, pp. 1–6, 2016.

[39] Ting, B., "Inclusive energy transitions: An analysis of the potential for a digital revolution in south africa's electricity system," *Leap 4.0. African Perspectives on the Fourth Industrial Revolution: African Perspectives on the Fourth Industrial Revolution*, p. 349, 2021.

[40] Bessa, R. J., "Future trends for big data application in power systems," in *Big data application in power systems*, Elsevier, 2018, pp. 223–242.

[41] Baesens, B., Bapna, R., Marsden, J. R., Vanthienen, J., and Zhao, J. L., "Transformational issues of big data and analytics in networked business," *MIS quarterly*, vol. 40, no. 4, pp. 807–818, 2016.

[42] Pandey, R. K. and Misra, M., "Cyber security threats—smart grid infrastructure," in *2016 National power systems conference (NPSC)*, IEEE, 2016, pp. 1–6.

[43] Yan, Y., Qian, Y., Sharif, H., and Tipper, D., "A survey on cyber security for smart grid communications," *IEEE communications surveys & tutorials*, vol. 14, no. 4, pp. 998–1010, 2012.

[44] Panteli, M. and Mancarella, P., "Modeling and evaluating the resilience of critical electrical power infrastructure to extreme weather events," *IEEE Systems Journal*, vol. 11, no. 3, pp. 1733–1742, 2015.

[45] Zio, E., "Challenges in the vulnerability and risk analysis of critical infrastructures," *Reliability Engineering & System Safety*, vol. 152, pp. 137–150, 2016.

[46] Moreira, C. L., Resende, F. O., and Lopes, J. P., "Using low voltage microgrids for service restoration," *IEEE Transactions on Power Systems*, vol. 22, no. 1, pp. 395–403, 2007.

[47] Kroposki, B. D., Dall-Anese, E., Bernstein, A., Zhang, Y., and Hodge, B. S., "Autonomous energy grids," National Renewable Energy Lab.(NREL), Golden, CO (United States), Tech. Rep., 2017.

[48] Kroposki, B., Bernstein, A., King, J., *et al.*, "Autonomous energy grids: Controlling the future grid with large amounts of distributed energy resources," *IEEE Power and Energy Magazine*, vol. 18, no. 6, pp. 37–46, 2020.

[49] Soares, T., Bessa, R. J., Pinson, P., and Morais, H., "Active distribution grid management based on robust ac optimal power flow," *IEEE Transactions on Smart Grid*, vol. 9, no. 6, pp. 6229–6241, 2017.

[50] Lezama, F., Soares, J., Hernandez-Leal, P., Kaisers, M., Pinto, T., and Vale, Z., "Local energy markets: Paving the path toward fully transactive energy systems," *IEEE Transactions on Power Systems*, vol. 34, no. 5, pp. 4081–4088, 2018.

[51] Bahrami, S., Amini, M. H., Shafie-Khah, M., and Catalao, J. P., "A decentralized renewable generation management and demand response in power distribution networks," *IEEE Trans. Sustain. Energy*, vol. 9, no. 4, pp. 1783–1797, 2018.

Part 1: Closing the Gap Between Variable Distributed Generation and Adjustable Demand in Autonomous Power Grids

Chapter 2

Game-theoretical Control Frameworks for Energy Scheduling

Abstract

Recently, the decreasing cost of storage technologies and the emergence of economy-driven mechanisms for energy exchange are contributing to the spread of energy communities. In this context, this paper aims at defining innovative game-theoretic control frameworks for energy communities equipped with independent service-oriented energy storage systems. The addressed control problem consists in optimally scheduling the energy activities of a group of prosumers, characterized by their own demand and renewable generation, and a group of energy storage service providers, able to store the prosumers' energy surplus and, subsequently, release it upon a fee payment. We propose two novel resolution algorithms based on a game theoretical control formulation, a coordinated and an uncoordinated one, which can be alternatively used depending on the underlying communication architecture of the grid. The two proposed approaches are validated through several numerical simulations on realistic scenarios. Results show that the use of a particular framework does not alter fairness, at least at the community level, i.e., no participant in the groups of prosumers or providers can enormously benefit from changing its strategy while compromising others' welfare. Lastly, the approaches are compared with a centralized control method showing better computational results.

Contents

2.1 Introduction

A powerful solution contributing to the green transformation of modern power systems is represented by the so-called *energy community* [1]. The term denotes a community of users (private, public, or mixed) located in a specific reference area, where all stakeholders – such as end-users (e.g., citizens, companies, etc.), market players (e.g., utilities, service providers), practitioners, planners, and policy-makers – actively cooperate in developing a 'smart' energy system. More specifically, these communities promote the optimal exploitation of renewable sources and the widespread use of distributed storage while enabling the application of measures oriented to cost-effectiveness, sustainability, and reliability [1]–[3]. In the last years, community action on using renewable energy has increased remarkably, pushed by several energy-efficiency initiatives as well as financial incentives [4], [5].

Fostered by the decreasing cost of storage technologies and emerging mechanisms of energy exchange and sharing, a viable solution to attain self-consumption of on-site production is represented by the use of *energy storage systems* (ESSs) that are valuable resources for the community at the local level [6]. The use of ESSs allows users to create

energy arbitrage by discharging during price peaks and charging during off-peak periods if a variable energy price is considered [7], [8]. In addition, ESSs contribute to the overall resilience of the energy community when facing systematic failures or natural disasters [9]. Moreover, ESSs guarantee stability and power quality when uncertain renewable energy sources, such as wind power and photovoltaic, highly influence the energy community [10], [11]. Nevertheless, the full penetration of ESSs presents various challenges. Due to economic and logistic reasons, the deployment of an individual ESS for each prosumer is not always a viable option. Conversely, sharing ESSs among prosumers or relying on energy storage services innovatively offered by providers is a widespread solution in energy communities [12], [13].

Among the most popular methods, game-theoretical control techniques are especially suitable to address the issues related to energy storage sharing in a sustainable and reliable fashion [14]. Indeed, these methods incorporate powerful economy-driven control mechanisms for effectively coordinating and trading energy flows among the actors of microgrids and energy communities [15]. Differently from *peer-to-peer* (P2P) energy trading, which suffers from sustainability issues (if a prosumer sells energy to another one, the former gains an economical bonus, but it is not guaranteed that the latter will be able to provide energy to the former when needed: in such a case, the prosumer lacking energy will be forced to resort to the retailer [16]), the deployment of energy storage services continuously guarantee that the amount of stored energy is available for future use, injecting back energy sourced from renewable means.

In this context, this chapter aims at defining innovative control frameworks to optimally manage and share energy within a community with multiple and independent service-oriented energy storage systems. In particular, the considered energy community comprises prosumers, characterized by their own demand and renewable generation, and energy storage service providers, able to store the prosumers' energy surplus and subsequently release it upon a fee payment. The addressed control problem consists in optimally scheduling the energy activities of prosumers and providers, relying on an economy-driven mechanism, in order to make the prosumers' energy supply more efficient, while creating a sustainable and profitable business model for storage providers. In order to guarantee a solution to the problem, an energy retailer, characterized by conventional power generation, allows prosumers to buy/sell energy from/to the main grid. The novel proposed resolution algorithms are based on a game-theoretical control formulation of the energy scheduling problem. In particular, a coordinated and an uncoordinated control scheme are defined, to be alternatively used depending on the underlying communication architecture. The two proposed approaches are validated through numerical simulations on realistic scenarios. Lastly, the approaches are compared with a centralized control method showing better computational results.

2.1.1 Literature review

The traditional approach in utilizing energy resources relies on the individual distributed framework, in which an individually-owned resource is installed for each user separately [17]. Due to the logistic and cost inefficiency of such a framework, and the spread of energy community initiatives, recent studies suggest the sharing strategy for the utilization of key components such as ESSs to fully exploit their potentials [18]. However, no unifying framework has been proposed in the face of several access schemes based on the paradigms of physical/financial rights and of resource capacity/energy sharing [19]. A comprehensive review of the design and application of shared ESSs is provided in [20]. In such a paper, authors provide an architectural classification of shared ESSs, categorized into *private*, *interconnected*, *common*, and *independent* ESS solutions. Private and interconnected ESSs, which contemplate the presence of one ESS per user, are a highly inefficient solution, due to high infrastructural and maintenance costs as well as the necessity of a dedicated physical space [20]. For these reasons, researchers are focusing on both the alternatives of common and independent ESSs. The former type of ESS consists of an ESS block that can be simultaneously accessed by multiple users. Control strategies for this architecture

include formulations as resource allocation problem [21] and aggregator-based management [22]. Conversely, in the independent ESS architecture, storage devices are independently managed by profit-driven operators. Thus, the necessity of designing an adequate market mechanism for handling the interactions between ESS operators and users is necessary. For instance, authors in [23] propose a market framework considering the ESS operator as a stand-alone agent that evaluates the optimal storage trading strategy. In [24], a Stackelberg game-based energy trading strategy is developed for minimizing the energy cost in a neighborhood area with an independent shared ESS.

Many of the common and independent ESS applications fall in the realm of the *sharing economy* (SE) business model (also known as *access economy*), which has been growing in popularity in the last decade. Companies such as Airbnb and Uber are just two of the numerous examples of this economic paradigm. In [25] the opportunities arising from adopting SE models in energy communities have been explored. In particular, the authors consider a collection of firms that invest in ESS to arbitrage against variable energy prices and share the surplus of their stored energy. Authors in [26] show that applications of SE paradigms in ESS are an economically attractive solution for both ESS operators as well as ESS investors. In [27] the potential of shared ESS for a neighborhood area is demonstrated, in which residents are able to dynamically optimize the energy load and the energy storage level to minimize their electricity costs. Regarding control schemes of SE applications of ESS, authors in [28] explore different market design options based on cooperative and noncooperative game-theoretic models, showing that SE reduces the cost volatility for most users while keeping the community operational costs unchanged. Among the different SE-based implementations of shared ESS, two promising concepts are the *virtual energy storage systems* (VESS) [29], [30] and the *cloud energy storage systems* (CESS) [31], [32]. The VESS is inspired by the *virtual power plant* (VPP) concept. VPPs work as aggregators of coordinated distributed energy sources, in order to optimize the energy supply. Similarly, the VESS concept is based on integrating different distributed ESSs, in order to create a virtual single storage system, able to serve users in the network. In [33], an agent-based ESS management system is proposed for allowing the integration of storage devices into a VESS. Authors in [34] investigate the value of merchant-owned ESS in the day-ahead electricity market, developing an offering strategy for operating and optimizing the virtual storage plant constructed by merging the merchant-owned ESS units. In [35], a two-stage optimization model for VESS sharing is studied, where, in the first phase, the investment and pricing for the storage capacity are determined by the aggregator, while the purchase of virtual capacity is performed by the users during the second phase. As for the CESS, the originating idea is borrowed from *cloud computing* in computer science, where distributed machines are coordinated to provide data storage and computational power efficiently and readily. CESS adopts the same concept for ESS, differing from VESS in terms of size since CESS applications are meant to reach grid-scale energy markets. In [31], the authors propose the concept of CESS which is constructed by centralizing ESS resources. The same authors also demonstrate the benefits of CESS by investigating the investment and operating decisions of both the CESS coordinator and the consumers [36]. Regarding the control mechanisms for CESS, peer-to-peer energy sharing and coordination mechanisms are designed in [32] in order to make the penetration of renewable energy sources more effective.

2.1.2 Chapter Contribution

From the above literature review, it follows that the majority of studies on multiple ESS sharing focus on the economy-driven control mechanisms that enable the interaction between the users and ESS operators. Despite the rich state of the art on energy storage services and management, very few research studies pay attention to crucial operational aspects of the adopted mechanism. In fact, in order to allow the large-scale deployment of VESSs or CESSs, challenges such as practical effectiveness, computational efficiency, scalability, and privacy are obviously of primary importance.

Differently from the reviewed works, the contributions of this chapter can be summarized as follows.

- We define an energy scheduling model, characterized by limited information sharing and scalable communication architecture, which includes two groups of participants, namely, the energy storage service providers and the energy community prosumers (intended as customers of the energy storage service). Thanks to its scalability, the proposed approach can be implemented more efficiently than contributions [23], [24], where only a single ESS can be handled. Moreover, differently from [32], where the ESS is considered ideal, in our work we employ a realistic model, which accounts for energy losses.
- Differently from most approaches, such as [27], [31], that consider only a central coordinator managing all the different aspects of the energy community, we also propose a non-coordinated and fully distributed control architecture. However, we do not employ cooperative frameworks, such as [32], that cannot fully capture the real market interactions or noncooperative ones that are computationally demanding [28]. In fact, we develop uncoordinated and coordinated distributed control frameworks, which reach an overall economic performance close to the optimal centralized global formulation, whose implementation is in turn impractical for service-based solutions and is unfeasible from a computational point of view.
- Moreover, we avoid straightforward investments analysis act to guarantee economic feasibility such as in [25], [26], but we fully analyze the proposed approach from an operational point of view, ensuring the feasibility of the underlying business model arising from the prosumer-provider interactions, by simulating the latter on real-case scenarios.
- Lastly, we compare the results of the optimal centralized global formulation, like in [35], with the ones of our frameworks. We show a considerable saving in the computational effort by our approaches, with minimal loss on the economic performance.

2.2 System Model

Let us introduce some basic notation used throughout the rest of the chapter. $\mathbb{R}$ and $\mathbb{R}^+$ denote the set of real and positive real numbers, respectively. $\mathbb{N}$ denotes the set of natural numbers. $A^\top$ denotes the transpose of matrix A. $\|\boldsymbol{a}\|$ is the 2-norm of vector $\boldsymbol{a}$. Moreover, for a set $\mathcal{N} := \{1, ..., i, ..., N\} \subset \mathbb{N}$ we have that $\boldsymbol{x} := (\boldsymbol{x}_i)_{i\in\mathcal{N}}$ is equal to $\boldsymbol{x} := (\text{vec}(\boldsymbol{x}_1)^\top, ..., \text{vec}(\boldsymbol{x}_n)^\top, ..., \text{vec}(\boldsymbol{x}_N)^\top)^\top$ where $\text{vec}(\cdot)$ is the vectorization operator.

In this section, we describe the proposed energy community model, shown in Fig. 2.1, which includes several independent actors. In particular, we formally define the set of energy community actors (or agents) $\mathcal{C} := \{1, ..., C\} \subset \mathbb{B}$ as the union of the group of *prosumers* $\mathcal{P} := \{1, ..., P\} \subset \mathbb{N}$ and the group of *energy storage providers* –briefly called *providers*– $\mathcal{S} := \{1, ..., S\} \subset \mathbb{N}$. Note that $\mathcal{C} = \mathcal{S} \cup \mathcal{P}$ while $\mathcal{S} \cap \mathcal{P} = \varnothing$ (consequently, $C = P + S$). Let us now define the topology related to the allowed economic transactions between active agents. In particular, we define the matrix $\mathcal{A}$ as a symmetric $P \times S$ binary matrix such that for each prosumer $i \in \mathcal{P}$ and provider $j \in \mathcal{S}$ the element $\mathcal{A}_{ij}$ is one if the two agents have an agreement for exchanging energy or is zero otherwise. Moreover, we indicate the set of the provider neighbors associated to the prosumer $i \in \mathcal{P}$ as $\mathcal{N}_i = \{j \in \mathcal{S} \mid \mathcal{A}_{ij} = 1\}$ with cardinality $N_i = |\mathcal{N}_i|$, and the set of the prosumer neighbors associated to the provider j as $\mathcal{M}_j = \{i \in \mathcal{P} \mid \mathcal{A}_{ij} = 1\}$ with cardinality $M_j = |\mathcal{M}_j|$.

The control frameworks proposed in this chapter are based on the well-known rolling horizon paradigm, therefore let us define a control horizon composed of T time intervals, with $\mathcal{T} := \{1, ..., T\} \in \mathbb{N}$ [37].

The proposed energy community model relies on the following standing assumptions that are typically employed in related papers, e.g. [38].

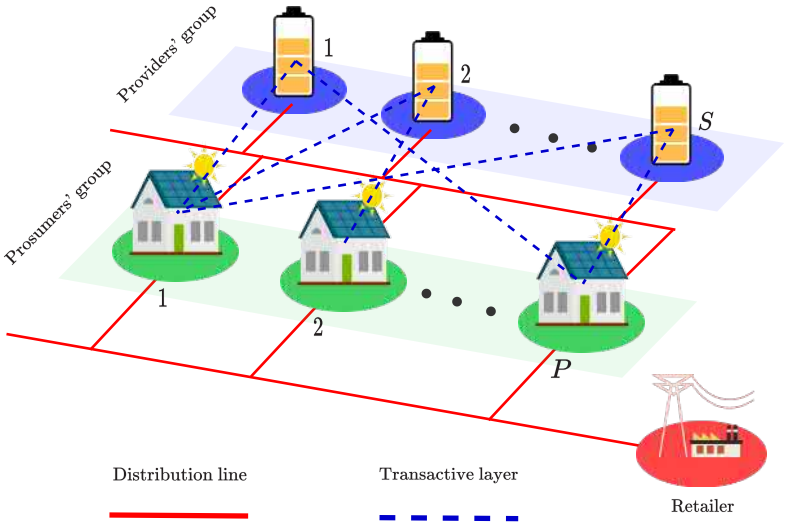

Figure 2.1: Energy community model. Dashed lines represent the economic transactions allowed between the involved actors. For instance, in the figure, prosumer 1 negotiates with providers 1, 2, and S (i.e., $\mathcal{A}_{11} = 1$, $\mathcal{A}_{12} = 1$, $\mathcal{A}_{1S} = 1$); prosumer 2 negotiates with providers 2 and S (i.e., $\mathcal{A}_{22} = 1$, $\mathcal{A}_{1S} = 1$); prosumer P negotiates with providers 1 and S (i.e., $\mathcal{A}_{P1} = 1$, $\mathcal{A}_{PS} = 1$).

- *Market structure*: the energy transactions between members of the same group cannot occur (e.g., a prosumer cannot exchange energy with another prosumer).
- *Energy retailer*: the energy community interacts with an external passive actor, required to guarantee the power balance in the community network. In particular, the *energy retailer* allows prosumers/sell energy from/to the main grid.
- *Perfect competition*: the profile of the energy storage pricing coefficient is equal for all providers.
- *Storage efficiencies*: the ESSs parameters, such as the leakage coefficient and the charging/discharging efficiencies, are constant for all providers.
- *Nonstochasticity*: the energy demand and the renewable energy production profiles are known for the entire time horizon and deterministic.

Having defined the structure of the energy community and the standing assumptions, we now describe in detail the model of the aforementioned independent actors.

2.2.1 Prosumers

These actors are characterized by variable load consumption and renewable energy production. They sell the surplus energy to or buy the deficit energy from the energy retailer in accordance with a time-variable pricing mechanism. As an alternative, they can store/withdraw energy in/from the ESSs owned by the storage providers, upon a renting fee.

For prosumer $i \in \mathcal{P}$, we indicate the energy demand and generation, at the generic time slot $t \in \mathcal{T}$, with D_{it} and G_{it}, respectively. The energy bought from the retailer at the time slot $t \in \mathcal{T}$ is $p^{\uparrow}_{it}$, while the energy sold to it is denoted by $p^{\downarrow}_{it}$. Moreover, the energy delivered to the storage provider $h \in \mathcal{N}_i$ at the time slot $t \in \mathcal{T}$ is $d^{\downarrow}_{iht}$, while the retrieved amount is $d^{\uparrow}_{iht}$. The portion of the charge level fraction dedicated to prosumer $i \in \mathcal{P}$ by provider $h \in \mathcal{N}_i$ is indicated with s_{iht}. We define vectors $\boldsymbol{p}^{\uparrow}_i = (p^{\uparrow}_{it})_{t\in\mathcal{T}}$, $\boldsymbol{p}^{\downarrow}_i = (p^{\downarrow}_{it})_{t\in\mathcal{T}}$, $\boldsymbol{d}^{\uparrow}_i = (\boldsymbol{d}^{\uparrow}_{it})_{t\in\mathcal{T}}$, $\boldsymbol{d}^{\downarrow}_i = (\boldsymbol{d}^{\downarrow}_{it})_{t\in\mathcal{T}}$, $\boldsymbol{s}_i = (s_{it})_{t\in\mathcal{T}}$ collecting all the aforementioned variables for the entire control horizon $\mathcal{T}$, where $\boldsymbol{d}^{\uparrow}_{it} = (d^{\uparrow}_{iht})_{h\in\mathcal{N}_i}$, $\boldsymbol{d}^{\downarrow}_{it} = (d^{\downarrow}_{iht})_{h\in\mathcal{N}_i}$, $\boldsymbol{s}_{it} = (s_{iht})_{h\in\mathcal{N}_i}$.

Accordingly, we define the control vector $\boldsymbol{v}_{\mathcal{P},i} = (\boldsymbol{p}_i^{\uparrow}, \boldsymbol{p}_i^{\downarrow}, \boldsymbol{d}_i^{\uparrow}, \boldsymbol{d}_i^{\downarrow}, \boldsymbol{s}_i)$ to collect all the decision variables for prosumer $i \in \mathcal{P}$.

Each prosumer $i \in \mathcal{P}$ aims at determining the optimal value of the control vector that minimizes the energy cost incurred throughout the entire time horizon $\mathcal{T}$, which can be formally defined as in (2.1):

$$J_{\mathcal{P},i}(\boldsymbol{v}_{\mathcal{P},i}) = \sum_{t\in\mathcal{T}} \Bigg[C_t p_{it}^{\uparrow} - R_t p_{it}^{\downarrow} + L_t \sum_{h\in\mathcal{N}_i} s_{iht} + \frac{1}{2}\xi_i \left(p_{it}^{\uparrow^2} + p_{it}^{\downarrow^2} + \sum_{h\in\mathcal{N}_i} \left(d_{iht}^{\uparrow^2} + d_{iht}^{\downarrow^2} \right) \right) \Bigg] \tag{2.1}$$

where $C_t \in \mathbb{R}^+$ and $R_t \in \mathbb{R}^+$ are the retailer's energy selling price and buying cost, respectively. Moreover, $L_t \in \mathbb{R}^+$ is the storage fee coefficient, which is equal for all providers, while $\xi_i \in \mathbb{R}^+$ represents the energy transmission cost coefficient for prosumer $i \in \mathcal{P}$. Note that the cost function (2.1) comprises two terms: the first contribution is composed of linear terms representing the cost/revenue due to energy exchanged with the retailer and the storage fee, while the second includes quadratic terms modeling the transmission costs.

Each i-th prosumer, $i \in \mathcal{P}$, is forced to respect the following constraints, for all $t \in \mathcal{T}$:

$$D_{it} - G_{it} = \sum_{h\in\mathcal{N}_i} \left(d_{iht}^{\uparrow} - d_{iht}^{\downarrow} \right) + p_{it}^{\uparrow} - p_{it}^{\downarrow}, \tag{2.2a}$$

$$s_{iht} = \alpha s_{ih,t-1} + \eta^{\uparrow} d_{iht}^{\downarrow} - \eta^{\downarrow} d_{iht}^{\uparrow}, \qquad \forall h \in \mathcal{N}_i \tag{2.2b}$$

$$s_{ih1} = s_{ihT}, \qquad \forall h \in \mathcal{N}_i \tag{2.2c}$$

$$d_{igt}^{\uparrow},\ d_{igt}^{\downarrow} = 0, \qquad \forall g \notin \mathcal{N}_i \tag{2.2d}$$

$$0 \leq\ d_{iht}^{\downarrow},\ d_{iht}^{\uparrow} \leq d_i^{\max}, \qquad \forall h \in \mathcal{N}_i \tag{2.2e}$$

$$0 \leq\ p_{it}^{\downarrow},\ p_{it}^{\uparrow} \leq p_i^{\max}, \tag{2.2f}$$

$$s_{iht} \geq 0, \qquad \forall h \in \mathcal{N}_i \tag{2.2g}$$

Constraints (2.2a) represent the energy balance equation over the whole control horizon. Constraints (2.2b) include the dynamical state equation for the charge level related to the ESS of each provider $h \in \mathcal{N}_i$, where α, $\eta^{\uparrow}$, and $\eta^{\downarrow}$ denote the leakage coefficient, and the charging and discharging efficiencies, respectively. Constraint (2.2c) ensures that the storage fraction held by prosumer $i \in \mathcal{P}$ in the ESS of provider $h \in \mathcal{N}_i$ is equal, at the end of time horizon, to the initial level. Constraints (2.2d) impose that the energy flow between prosumer i and any disconnected provider $g \notin \mathcal{N}_i$ is null. Equations (2.2e) and (2.2f) are technological constraints imposing the energy flows towards the ESS of each provider $h \in \mathcal{N}_i$ and towards the energy retailer to be non-negative and limited by the upper bounding values $d_i^{\max}$ and $p_i^{\max}$, respectively. Lastly, (2.2g) ensures the non-negativity of the i-th prosumer storage fraction. The resulting feasible set $\mathcal{K}_{\mathcal{P},i}$ for each prosumer $i \in \mathcal{P}$ is thus defined as:

$$\mathcal{K}_{\mathcal{P},i} = \left\{ \boldsymbol{v}_{\mathcal{P},i} \in \mathbb{R}^+_{2T+3TN_i} \mid (2.2a) - (2.2g)\ \text{hold} \right\}. \tag{2.3}$$

2.2.2 Energy storage providers

These actors are characterized by an energy storage capacity that can be used to store the prosumers' exceeding energy generation in return for a fee. In fact, energy storage is a key feature in energy communities, contributing to different services such as load shifting, frequency regulation, peak shaving, and energy arbitrage. Several energy storage technologies – such as electrochemical (batteries and fuel cells), electromechanical (flywheels and pump hydro), electrostatic (ultra-capacitors), and electromagnetic

(superconducting magnetic storage) types – are available. However, electrochemical batteries have recently been recognized as the game-changing technology in energy communities, due to their high applicability and low cost. Hence, in this work, we assume that each provider owns an electrochemical battery, whose model is detailed in the following.

For each provider $j \in \mathcal{S}$, we indicate the energy stored by and released to prosumer $k \in \mathcal{M}_j$ at the generic time slot $t \in \mathcal{T}$ with $q^{\uparrow}_{kjt}$ and $q^{\downarrow}_{kjt}$, respectively. The portion of the charge level reserved to prosumer $k \in \mathcal{M}_j$ by provider $j \in \mathcal{S}$ at time slot $t \in \mathcal{T}$ is indicated with b_{kjt}. We define vectors $\boldsymbol{q}^{\uparrow}_j = (\boldsymbol{q}^{\uparrow}_{jt})_{t\in\mathcal{T}}$, $\boldsymbol{q}^{\downarrow}_j = (\boldsymbol{q}^{\downarrow}_{jt})_{t\in\mathcal{T}}$, $\boldsymbol{b}_j = (\boldsymbol{b}_{jt})_{t\in\mathcal{T}}$ collecting all the aforementioned variables for the entire control horizon $\mathcal{T}$, where $\boldsymbol{q}^{\uparrow}_{jt} = (q^{\uparrow}_{kjt})_{k\in\mathcal{M}_j}$, $\boldsymbol{q}^{\downarrow}_{jt} = (q^{\downarrow}_{kjt})_{k\in\mathcal{M}_j}$ and $\boldsymbol{b}^{\downarrow}_{jt} = (b^{\downarrow}_{kjt})_{k\in\mathcal{M}_j}$. Accordingly, we define the control vector $\boldsymbol{v}_{\mathcal{S},j} = (\boldsymbol{q}^{\uparrow}_j, \boldsymbol{q}^{\downarrow}_j, \boldsymbol{b}_j)$ including all the decision variables for the j-th provider.

Each provider $j \in \mathcal{S}$ aims at determining the optimal value of the control vector that minimizes the energy storage service cost throughout the entire time horizon $\mathcal{T}$, which can be formally defined as:

$$J_{\mathcal{S},j}(\boldsymbol{v}_{\mathcal{S},j}) = \sum_{t\in\mathcal{T}} \sum_{k\in\mathcal{M}_j} \left[\frac{1}{2}\zeta_j (q^{\uparrow}_{kjt} + q^{\downarrow}_{kjt})^2 - L_t b_{kjt} \right] \tag{2.4}$$

where $L_t \in \mathbb{R}^+$ is the storage revenue coefficient that is the same for all providers and $\zeta_j \in \mathbb{R}^+$ is the ESS technological degradation coefficient. The cost function (2.4) comprises two terms: the first contribution is a quadratic term accounting for the degradation cost of the ESS (to be minimized), whilst the second represents the revenue obtained from the provided storage service (to be maximized).

Each j-th provider, $j \in \mathcal{S}$, is forced to respect the following constraints, for all $t \in \mathcal{T}$:

$$b_{kjt} = \alpha b_{kj,t-1} + \eta^{\uparrow} q^{\uparrow}_{kjt} - \eta^{\downarrow} q^{\downarrow}_{kjt}, \qquad \forall k \in \mathcal{M}_j \tag{2.5a}$$

$$b_{kj1} = b_{kjT}, \qquad \forall k \in \mathcal{M}_j \tag{2.5b}$$

$$q^{\uparrow}_{gjt},\ q^{\downarrow}_{gjt} = 0, \qquad \forall g \notin \mathcal{M}_j \tag{2.5c}$$

$$0 \leq\ q^{\uparrow}_{kjt},\ q^{\downarrow}_{kjt} \leq q^{\max}_j, \qquad \forall k \in \mathcal{M}_j \tag{2.5d}$$

$$\sum_{k\in\mathcal{M}_j} b_{kjt} \leq b^{\max}_j, \tag{2.5e}$$

$$b_{kjt} \geq 0, \qquad \forall k \in \mathcal{M}_j. \tag{2.5f}$$

Similarly to the prosumers case, constraints (2.5a) include the dynamical state equation for the portion of charge level reserved to each prosumer $k \in \mathcal{M}_j$. Constraint (2.5b) ensures that storage fraction held by provider $j \in \mathcal{S}$ for prosumer $k \in \mathcal{M}_j$ at the end of the time horizon is equal to the initial level. Constraints (2.5c) imposes that the energy flow between any provider $j \in \mathcal{S}$ and any disconnected prosumer $g \notin \mathcal{M}_j$ is null. Constraints (2.5d) impose that charging and discharging flows are non-negative and limited by the upper bound $q^{\max}_j$. Lastly, (2.5e) and (2.5f) impose that the cumulative charge level over all prosumers connected to provider $j \in \mathcal{S}$ is upper bounded by the maximum storage capacity $b^{\max}_j$ and that the charge level fraction reserved to each prosumer $k \in \mathcal{M}_j$ is non-negative. The constraints set $\mathcal{K}_{\mathcal{S},j}$ for each provider $j \in \mathcal{S}$ is thus defined as:

$$\mathcal{K}_{\mathcal{S},j} = \left\{ \boldsymbol{v}_{\mathcal{S},j} \in \mathbb{R}^+_{3TM_j} \mid (2.5a) - (2.5f) \text{ hold} \right\}. \tag{2.6}$$

Note that, despite the similarity of the two equations, (2.2) and (2.5) do not express in general the same dynamics. In fact, they represent the storage dynamics that prosumers and providers are *willing* to follow, respectively, but not necessarily agree upon. However, in order to work properly, we define a suitable mechanism that ensures that (2.2) and (2.5) converge to a common dynamics, as it will be shown in the following.

2.3 Energy Scheduling

The energy scheduling problem involving prosumers and providers in the considered energy community can be formulated in several ways. As a first approach, all the agents in $\mathcal{C}$ (i.e., all prosumers in $\mathcal{P}$ and providers in $\mathcal{S}$), constitute the grand coalition pursuing a common goal in order to guarantee the global community welfare. From a game-theoretical point of view, agents behave in a cooperative fashion, concurring to the minimization of a collective cost function, $J_{\mathcal{C}}$, defined as the sum of the individual cost functions:

$$J_{\mathcal{C}}(\boldsymbol{v}_{\mathcal{C}}) = \sum_{n \in \mathcal{C}} J_{\mathcal{C},n}(\boldsymbol{v}_{\mathcal{C},n}) \tag{2.7}$$

where, for the sake of compactness, we define $\boldsymbol{v}_{\mathcal{C}} = (\boldsymbol{v}_{\mathcal{C},n})_{n \in \mathcal{C}}$ as the concatenation of all the decision variable vectors for all players. Note that $\boldsymbol{v}_{\mathcal{C},n} = \boldsymbol{v}_{\mathcal{P},n}$, $\forall n \in \mathcal{P}$ and $\boldsymbol{v}_{\mathcal{C},n} = \boldsymbol{v}_{\mathcal{S},n}$, $\forall n \in \mathcal{S}$, while $J_{\mathcal{C},n} = J_{\mathcal{P},n}$, $\forall n \in \mathcal{P}$ and $J_{\mathcal{C},n} = J_{\mathcal{S},n}$, $\forall n \in \mathcal{S}$. As for the constraints sets, we indicate $\mathcal{K}_{\mathcal{C},n} = \mathcal{K}_{\mathcal{P},n}$, $\forall n \in \mathcal{P}$ and $\mathcal{K}_{\mathcal{C},n} = \mathcal{K}_{\mathcal{S},n}$, $\forall n \in \mathcal{S}$.

It is possible to prove that optimizing (2.7) provides a Pareto solution to all players [39], [40]. The function $J_{\mathcal{C}}$ is composed only of exogenous cost sources with respect to the coalition $\mathcal{C}$. In other words, the storage fees paid by the prosumers over the time horizon correspond to the total revenues earned by the providers for the storage service.

In addition to the local feasible sets $\mathcal{K}_{\mathcal{C},n}$, the coherence of the energy flow has to be ensured in accordance with the following *coupling constraints*:

$$d^{\uparrow}_{ijt} = q^{\downarrow}_{ijt}, \quad \forall i \in \mathcal{P}, \forall j \in \mathcal{S} \tag{2.8a}$$

$$d^{\downarrow}_{ijt} = q^{\uparrow}_{ijt}, \quad \forall i \in \mathcal{P}, \forall j \in \mathcal{S}. \tag{2.8b}$$

Therefore, we can define the global constraints set as:

$$\mathcal{K}_{\mathcal{C}} = \left\{ \boldsymbol{v}_{\mathcal{C}} \in \left(\bigcup_{n \in \mathcal{C}} \mathcal{K}_{\mathcal{C},n} \right) \mid (2.8a) - (2.8b) \text{ hold} \right\}. \tag{2.9}$$

Summing up, from the global perspective, the optimization problem is compactly written as:

$$\overline{\boldsymbol{v}}_{\mathcal{C}} = \underset{\boldsymbol{v}_{\mathcal{C}} \in \mathcal{K}_{\mathcal{C}}}{\arg\min}\, J_{\mathcal{C}}(\boldsymbol{v}_{\mathcal{C}}). \tag{2.10}$$

The above-formulated problem can be solved in a centralized fashion by a central unit that operates on behalf of all actors while scheduling and assigning resources. In particular, since (2.10) constitutes a quadratic programming problem, because of the quadratic terms in (2.1) and (2.4), the resolution of the global approach is straightforwardly achieved by using any convex optimization solver [41]. However, the global approach presents several drawbacks. First, such a formulation aims at minimizing the overall community cost, possibly penalizing some actors in the resulting control strategy. Furthermore, in the centralized architecture, privacy issues are not considered. In fact, the model is composed of heterogeneous agents for whom limiting the amount of shared information is highly recommended, if not requested. This is particularly relevant to providers, being independent companies for which data sharing could result in economic and security-related vulnerabilities. Finally, centralized solutions are prone to computational scalability concerns, when the number of agents becomes large, and low fault resiliency issues.

To overcome these drawbacks, let us introduce a reformulation of the energy scheduling problem, employing the noncooperative game theory, assuming that each player addresses its own individual energy scheduling problem. In this way, each player $n \in \mathcal{C}$ aims at minimizing its own objective function $J_{\mathcal{C},n}(\boldsymbol{v}_{\mathcal{C},n})$ by modifying its decision variable vector $\boldsymbol{v}_{\mathcal{C},n}$, given the choices of all the other players $\boldsymbol{v}_{\mathcal{C},-n}$, where $\boldsymbol{v}_{C,-n} = (\boldsymbol{v}_{\mathcal{C},1}, \cdots, \boldsymbol{v}_{\mathcal{C},n-1}\ \boldsymbol{v}_{\mathcal{C},n+1}\ \cdots\ \boldsymbol{v}_{\mathcal{C},C})^{\top}$. Hence, we have that each player solves an independent optimization problem:

$$\overline{\boldsymbol{v}}_{C,n} = \underset{\boldsymbol{v}_{C,n} \in \mathcal{K}_{\mathcal{C}}(\boldsymbol{v}_{C,-n})}{\arg\min} J_{\mathcal{C},n}(\boldsymbol{v}_{C,n}), \quad \forall n \in \mathcal{C}. \tag{2.11}$$

This formulation can be considered as a *generalized Nash equilibrium problem* (GNEP), since the decisions of the players are coupled through not only the cost functions but also a shared feasible set. The solution of the GNEP is the so-called *generalized Nash equilibrium* (GNE) hereafter formally defined.

Definition 2.3.1

A solution $\boldsymbol{v}_{\mathcal{C}}^{*} \in \mathcal{K}_{\mathcal{C}}$ *is a GNE if* $\forall n \in \mathcal{C}$

$$J_{\mathcal{C},n}(\boldsymbol{v}_{C,n}^{*}) \leq J_{\mathcal{C},n}(\boldsymbol{v}_{C,n}), \quad \forall \boldsymbol{v}_{C,n} \in \mathcal{K}_{\mathcal{C}}(\boldsymbol{v}_{C,-n}). \tag{2.12}$$

□

In other words, at a GNE no player can benefit from independently changing its own strategy, given that all the remaining players don't deviate from their own. In general, the existence of a GNE is not guaranteed; neither the uniqueness nor the convergence to an equilibrium is ensured.

In particular, the solution of a GNEP is a nontrivial problem, mainly due to the variability of the feasible sets. Several approaches to solve this problem are based on its reformulation through a *variational inequality* (VI). In fact, it can be proven that every solution of the VI is a solution for its corresponding GNEP, but the vice versa is, in general, not true [42]. The solutions of the GNEP that are also valid for the VI are called "variational solutions" and are usually referred to as economically fair. In fact, these points have a fair behavior between all the possible GNEs due to the equivalence of the Lagrangian multipliers (acting as penalizing coefficients) for all players' stationarity and primal feasibility conditions [41]. Moreover, variational solutions are preferred in several applications, due to their uniqueness when further assumptions hold [43].

The following section is focused on describing effective methods aimed at reaching the variational solution for the above-defined individual formulation (2.11).

2.4 Game-theoretical Control Frameworks

In this section, we focus on solving the individual formulation energy scheduling problem, since it grasps the competitiveness of the real-world energy market better than the global formulation. Several alternative algorithms have been proposed to solve the VI formulation of a GNEP [44].

In particular, two approaches are presented, namely the coordinated and the uncoordinated framework. In both cases, we leverage on a modified version of the classical *augmented Lagrangian method* (ALM) [45], where the quadratic penalty term of the Lagrangian $\mathcal{L}$ is substituted by a proximal regularizer, i.e.,

$$\mathcal{L}(\boldsymbol{v}_{\mathcal{C},n}, \boldsymbol{\pi}) = J_{\mathcal{C},n}(\boldsymbol{v}_{\mathcal{C},n}) + \boldsymbol{\pi} \cdot \boldsymbol{c}(\boldsymbol{v}_{\mathcal{C},n}) + \frac{\rho}{2} \left\| \boldsymbol{v}_{\mathcal{C},n} - \boldsymbol{v}_{\mathcal{C},n}^{(\tau-1)} \right\|^2 \tag{2.13}$$

with $\boldsymbol{c}(\boldsymbol{v}_{\mathcal{C},n})$ and $\boldsymbol{\pi}$ being, respectively, the vectors of the coupling constraints and related Lagrange multipliers vector. Note that in (2.13), and throughout the rest of the chapter, τ denotes the iteration step. The regularization coefficient $\rho = \kappa a^{C}$ in (2.13) is based on parameters $\kappa, a \in \mathbb{R}^{+}$, determined empirically. The update rule for $\boldsymbol{\pi}$ is based on the well-known gradient formula:

$$\boldsymbol{\pi}^{(\tau)} = \boldsymbol{\pi}^{(\tau-1)} + \chi \left(\boldsymbol{v}_{\mathcal{C},n}^{(\tau-1)} - \boldsymbol{c}\left(\boldsymbol{v}_{\mathcal{C},n}^{(\tau-1)} \right) \right) \tag{2.14}$$

where $\chi \in \mathbb{R}^{+}$ is the convergence step-size. In the following, we characterize each term of (2.13) for, respectively, the uncoordinated and coordinated frameworks.

2.4.1 Uncoordinated Framework

In the uncoordinated framework, agents in $\mathcal{P}$ and $\mathcal{S}$ are able to directly interact with each other. The communication layer for this framework is shown in Fig. 2.2, where each

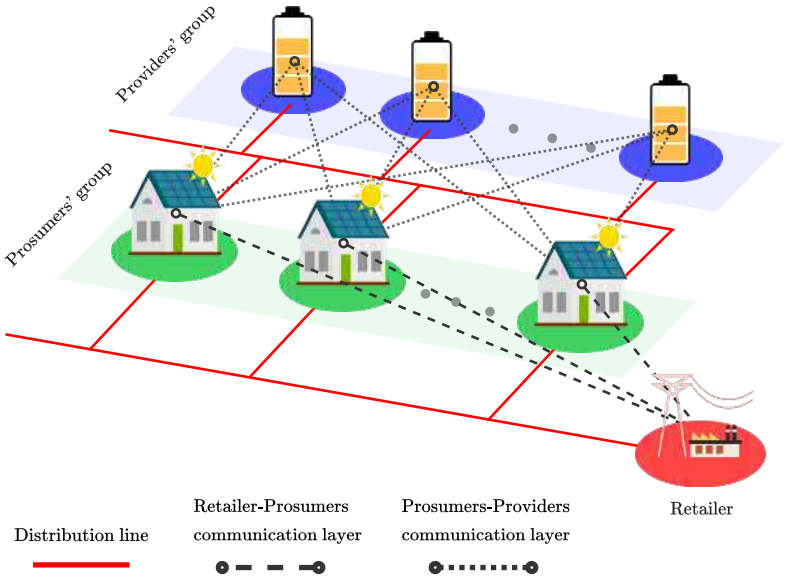

Figure 2.2: Energy community model: an overview of the communication layer in case of the uncoordinated control framework: any prosumer can exchange information with any provider; each prosumer communicates with the retailer.

prosumer communicates with the retailer and is allowed to communicate with all the providers. As regards the technological point of view, distributed ledger technologies have been proven to reliably support distributed communication and control in smart grids, in terms of cost-efficiency and privacy [46].

We now reformulate the Lagrangian formulation in (2.13) to solve the individual scheduling problem in (2.11) in the case of the uncoordinated architecture. To this aim, we define the Lagrange multipliers vectors $\lambda_{iht}^{(\tau)}$ and $\mu_{kjt}^{(\tau)}$ respectively associated to coupling constraints (2.8a)-(2.8b), whose update equations follow (2.14) for all $t \in \mathcal{T}$, i.e.,

$$\lambda_{iht}^{(\tau)} = \lambda_{iht}^{(\tau-1)} + \chi \left(d_{iht}^{\uparrow(\tau-1)} - q_{iht}^{\downarrow(\tau-1)} \right), \forall i \in \mathcal{P}, \forall h \in \mathcal{N}_i, \tag{2.15a}$$

$$\mu_{kjt}^{(\tau)} = \mu_{kjt}^{(\tau-1)} + \chi \left(d_{kjt}^{\downarrow(\tau-1)} - q_{kjt}^{\uparrow(\tau-1)} \right), \forall j \in \mathcal{S}, \forall k \in \mathcal{M}_j. \tag{2.15b}$$

Therefore, each prosumer and provider can calculate its penalty regularizers $\gamma_{\mathcal{P},i}^{(\tau)}$ and $\gamma_{\mathcal{S},j}^{(\tau)}$, defined, for all $i \in \mathcal{P}$ and $j \in \mathcal{S}$, as:

$$\gamma_{\mathcal{P},i}^{(\tau)} = \sum_{t\in\mathcal{T}} \sum_{h\in\mathcal{N}_i} \left(\lambda_{iht}^{(\tau)} \left(d_{iht}^{\uparrow} - q_{iht}^{\downarrow} \right) + \mu_{iht}^{(\tau)} \left(d_{iht}^{\downarrow} - q_{iht}^{\uparrow} \right) \right), \tag{2.16a}$$

$$\gamma_{\mathcal{S},j}^{(\tau)} = \sum_{t\in\mathcal{T}} \sum_{k\in\mathcal{M}_j} \left(\lambda_{kjt}^{(\tau)} \left(d_{kjt}^{\uparrow} - q_{kjt}^{\downarrow} \right) + \mu_{kjt}^{(\tau)} (d_{kjt}^{\downarrow} - q_{kjt}^{\uparrow}) \right). \tag{2.16b}$$

In order to guarantee convergence, proximal regularization terms $\theta_{\mathcal{P},i}^{(\tau)}$ and $\theta_{\mathcal{S},j}^{(\tau)}$ are added to prosumers' and the providers' objective functions respectively, i.e.,

$$\theta_{\mathcal{P},i}^{(\tau)} = \frac{\rho}{2} \left(\left\| \boldsymbol{d}_i^{\downarrow} - \boldsymbol{d}_i^{\downarrow(\tau-1)} \right\|^2 + \left\| \boldsymbol{d}_i^{\uparrow} - \boldsymbol{d}_i^{\uparrow(\tau-1)} \right\|^2 \right), \quad \forall i \in \mathcal{P} \tag{2.17a}$$

$$\theta_{\mathcal{S},j}^{(\tau)} = \frac{\rho}{2} \left(\left\| \boldsymbol{q}_j^{\downarrow} - \boldsymbol{q}_j^{\downarrow(\tau-1)} \right\|^2 + \left\| \boldsymbol{q}_j^{\uparrow} - \boldsymbol{q}_j^{\uparrow(\tau-1)} \right\|^2 \right), \quad \forall j \in \mathcal{S}. \tag{2.17b}$$

For the sake of compactness, we define $\gamma_{\mathcal{C},n}^{(\tau)} = \gamma_{\mathcal{P},n}^{(\tau)}$, $\forall n \in \mathcal{P}$ and $\gamma_{\mathcal{C},n}^{(\tau)} = \gamma_{\mathcal{S},n}^{(\tau)}$, $\forall n \in \mathcal{S}$, while $\theta_{\mathcal{C},n}^{(\tau)} = \theta_{\mathcal{P},n}^{(\tau)}$, $\forall n \in \mathcal{P}$ and $\theta_{\mathcal{C},n}^{(\tau)} = \theta_{\mathcal{S},n}^{(\tau)}$, $\forall n \in \mathcal{S}$. Therefore, we can write the

Algorithm 2.1 Uncoordinated ALM

1: $\tau \leftarrow 0$
2: **for** $i \in \mathcal{P}$, $j \in \mathcal{S}$, $t \in \mathcal{T}$ **do**
3: $\quad \lambda_{ijt}^{(\tau)} \leftarrow 0, \ \mu_{ijt}^{(\tau)} \leftarrow 0$
4: $\quad d_{ijt}^{(\tau)} \leftarrow 0, \ q_{ijt}^{(\tau)} \leftarrow 0$
5: **end for**
6: **while** stopping criterion is not reached **do**
7: $\quad \tau \leftarrow \tau + 1$
8: $\quad$ Agents in $\mathcal{C}$ solve (2.18);
9: $\quad$ Each prosumers $i \in \mathcal{P}$ communicates $d_{ijt}^{(\tau)}$ and $d_{ijt}^{(\tau)}$ to providers in $\mathcal{N}_i$;
10: $\quad$ Each provider $j \in \mathcal{S}$ communicates $q_{ijt}^{(\tau)}$ and $q_{ijt}^{(\tau)}$ to prosumers in $\mathcal{M}_j$;
11: $\quad$ Agents in $\mathcal{C}$ update the Lagrange multipliers by (2.15).
12: **end while**

Lagrangian form of the optimization problem for the uncoordinated framework as:

$$\boldsymbol{v}_{C,n}^{(\tau+1)} = \underset{\boldsymbol{v}_{C,n} \in \mathcal{K}_{\mathcal{C}_n}}{\arg\min} \left(J_{\mathcal{C},n}(\boldsymbol{v}_{C,n}) + \gamma_{\mathcal{C},n}^{(\tau)} + \theta_{\mathcal{C},n}^{(\tau)} \right), \quad \forall n \in \mathcal{C}. \tag{2.18}$$

The corresponding uncoordinated algorithm is summarized in Algorithm 2.1, and is described in detail in the sequel. First, all agents initialize the penalty factors and flow variables (lines 2-5). The noncooperative solution is reached in an uncoordinated manner through an iterative process until a termination criterion is not reached (lines 6-12). In detail, at each iteration τ, each agent independently solves its own optimization problem (line 8) and communicates the state of the energy flow variables to the corresponding neighbors (lines 9-10). Lastly, the Lagrange multipliers are updated (line 11).

2.4.2 Coordinated Framework

In the coordinated framework, agents in $\mathcal{P}$ and $\mathcal{S}$ do not directly interact, since a coordinator is present to gather the energy flow variables determined by the prosumers and providers, compute the Lagrange multipliers on behalf of all the agents, and sending back to prosumers and providers the updated Lagrange multipliers vectors. The coordinator is thus a non-profit actor that supports the selfish agents in the community in reaching an optimal solution to the energy management problem while ensuring that the energy balance coupling constraints are satisfied. The communication layer for the coordinated framework is shown in Fig. 2.3, where each prosumer communicates with the retailer, and all actors exchange information through the coordinator. This entity monitors and controls the energy activities in the community relying on an appropriate communication network (e.g., wireless radio connection, dial-up lines, Ethernet, and IP protocol). Wireless data communications are more convenient in comparison to wired communications since several advantages are available: cost-effective installation, fast placement, and remote applicability increase the attractiveness of these approaches. Particularly, Internet of Things solutions, combined with edge computing, are increasingly gaining attention [47].

We now reformulate the Lagrangian formulation in (2.13) to solve the individual scheduling problem in (2.11) in the case of the coordinated architecture. In such a case, the Lagrange multipliers are equal for all agents, for each time slot t, since the coordinator is in charge of ensuring the balance of the *aggregate energy flow*, in accordance with the following *coupling constraints*:

$$D_t^{\uparrow} = Q_t^{\downarrow}, \quad \forall t \in \mathcal{T} \tag{2.19a}$$

$$D_t^{\downarrow} = Q_t^{\uparrow}, \quad \forall t \in \mathcal{T} \tag{2.19b}$$

where $D_t^{\uparrow}$, $D_t^{\downarrow}$, $Q_t^{\uparrow}$ and $Q_t^{\downarrow}$ are introduced to denote the flow variables aggregates:

$$D_t^{\uparrow} = \sum_{i \in \mathcal{P}} \sum_{h \in \mathcal{N}_i} d_{iht}^{\uparrow}, \quad D_t^{\downarrow} = \sum_{i \in \mathcal{P}} \sum_{h \in \mathcal{N}_i} d_{iht}^{\downarrow}, \tag{2.20a}$$

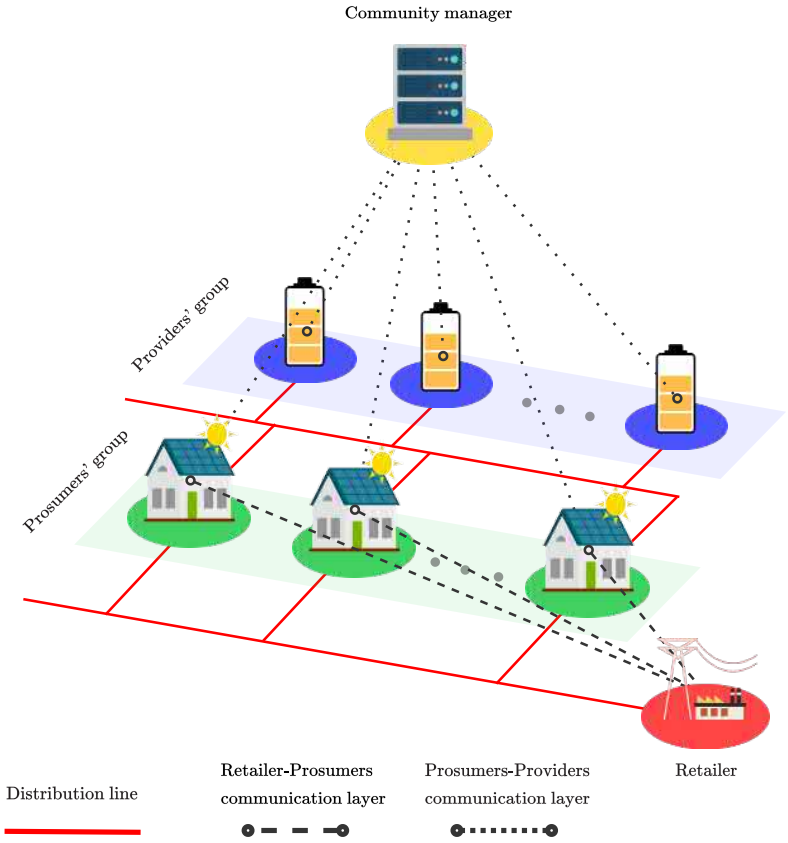

Figure 2.3: Energy community model: an overview of the communication layer in the case of coordinated control framework: the coordinator allows any prosumer to exchange information with providers and each prosumer communicates with the retailer.

$$Q_t^{\uparrow} = \sum_{j\in\mathcal{S}} \sum_{k\in\mathcal{M}_j} q_{kjt}^{\uparrow}, \quad Q_t^{\downarrow} = \sum_{j\in\mathcal{S}} \sum_{k\in\mathcal{M}_j} q_{kjt}^{\downarrow}. \tag{2.20b}$$

In particular, the Lagrange multipliers $\lambda_t^{(\tau)}$ and $\mu_t^{(\tau)}$ associated to constraints (2.19) are computed as follows:

$$\lambda_t^{(\tau)} = \lambda_t^{(\tau-1)} + \chi(D_t^{\uparrow} - Q_t^{\downarrow}), \quad \forall t \in \mathcal{T} \tag{2.21a}$$

$$\mu_t^{(\tau)} = \mu_t^{(\tau-1)} + \chi(D_t^{\downarrow} - Q_t^{\uparrow}), \quad \forall t \in \mathcal{T} \tag{2.21b}$$

so that the penalty regularizers of the coordinated framework, $\varphi_{\mathcal{P},i}^{(\tau)}$ and $\varphi_{\mathcal{S},j}^{(\tau)}$, can be defined, for all $i \in \mathcal{P}$, $j \in \mathcal{S}$, as:

$$\varphi_{\mathcal{P},i}^{(\tau)} = \varphi_{\mathcal{S},j}^{(\tau)} = \sum_{t\in\mathcal{T}} \left(\lambda_t^{(\tau)}(D_t^{\uparrow} - Q_t^{\downarrow}) + \mu_t^{(\tau)}(D_t^{\downarrow} - Q_t^{\uparrow}) \right). \tag{2.22}$$

Similarly to the previous case, we define $\varphi_{\mathcal{C},n}^{(\tau)} = \varphi_{\mathcal{P},n}^{(\tau)}, \forall n \in \mathcal{P}$ and $\varphi_{\mathcal{C},n}^{(\tau)} = \varphi_{\mathcal{S},n}^{(\tau)}, \forall n \in \mathcal{S}$, while $\theta_{\mathcal{C},n}^{(\tau)} = \theta_{\mathcal{P},n}^{(\tau)}$, $\forall n \in \mathcal{P}$ and $\theta_{\mathcal{C},n}^{(\tau)} = \theta_{\mathcal{S},n}^{(\tau)}$, $\forall n \in \mathcal{S}$. Therefore, the Lagrangian form of the optimization problem for the coordinated framework is written as follows:

$$\boldsymbol{v}_{C,n}^{(\tau+1)} = \underset{\boldsymbol{v}_{C,n}\in\mathcal{K}_{\mathcal{C}_n}}{\arg\min}\ J_{\mathcal{C},n}(\boldsymbol{v}_{C,n}) + \varphi_{\mathcal{C},n}^{(\tau)} + \theta_{\mathcal{C},n}^{(\tau)}, \quad \forall n \in \mathcal{C}. \tag{2.23}$$

The coordinated algorithm, summarized in Algorithm 2.2, is hereafter described in detail. Similarly to the uncoordinated algorithm, we initialize the common Lagrange

Algorithm 2.2 Coordinated ALM

1: $\tau \leftarrow 0$
2: **for** $i \in \mathcal{P}$, $j \in \mathcal{S}$, $t \in \mathcal{T}$ **do**
3: $\quad \lambda_t^{(\tau)} \leftarrow 0, \ \mu_t^{(\tau)} \leftarrow 0$
4: $\quad d_{ijt}^{(\tau)} \leftarrow 0, \ q_{ijt}^{(\tau)} \leftarrow 0$
5: **end for**
6: **while** stopping criterion is not reached **do**
7: $\quad \tau \leftarrow \tau + 1$
8: $\quad$ Agents in $\mathcal{C}$ solve (2.23);
9: $\quad$ Prosumers in $\mathcal{P}$ communicate flow variables $d_{ijt}^{(\tau)}$ and $d_{ijt}^{(\tau)}$ to the coordinator;
10: $\quad$ Providers in $\mathcal{S}$ communicate flow variables $q_{ijt}^{(\tau)}$ and $q_{ijt}^{(\tau)}$ to the coordinator;
11: $\quad$ The coordinator aggregates the energy flow by (2.20), updates the Lagrange multipliers by (2.21), and sends the updated back to all agents.
12: **end while**

multipliers vectors and the energy flow variables (lines 2-5). The noncooperative solution is reached in a coordinated fashion through an iterative process until a termination criterion is reached (lines 6-12). At each iteration τ, every agent computes its optimal energy schedule (line 8) and communicates the updated strategy to the coordinator (lines 9-10). Then, the coordinator calculates the flow variables aggregates $D_t^{\uparrow}$, $D_t^{\downarrow}$, $Q_t^{\uparrow}$, and $Q_t^{\downarrow}$, updates the Lagrange multipliers and sends the updated Lagrange multipliers back both to prosumers and providers (line 12).

2.5 Case Study

In this section, we assess the performance of the two proposed energy community control frameworks through numerical experiments on realistic scenarios. For the sake of providing a comparison with a reference method, the results obtained by the proposed uncoordinated and the coordinated distributed control framework is compared with those achieved by the optimal centralized framework.

All simulations are performed in MATLAB, using the Optimization Toolbox library, installed on a middle-end machine equipped with an Intel i5-7400, 3.00 GHz (4 cores) CPU, and 8 GB of RAM.

In particular, we consider a residential energy community equipped with distributed energy generation sources and service-based energy storage. The actors of the energy community include 10 prosumers and 8 providers. The control horizon corresponds to the entire day, equally subdivided into one-hour time slots.

Prosumers' energy generation and demand data are known parameters of the control frameworks, corresponding to the curves reported in Fig. 2.4. In particular, the reported data refer to a yearly report of energy consumption and production of an urban condominium. The renewable source considered in the experiments is a set of 27 PV panels (PEIMAR SG300M), each generating 300 Wp, and a three-phase inverter (SolarEdge SE8K), serving shared devices of the condominium, such as a heat generator, water pump, lighting, and elevator.

Energy buying and selling prices are defined over the time horizon and known by all agents in both the prosumers and providers groups. In particular, the considered energy cost is related to the Italian Enel "E-Light Bioraria" tariff [48]. This billing plan divides the day into two zones:

- *Orange*: Monday to Friday, from 8.00 to 19.00. The buying energy cost C_t is € 0.0774.
- *Blue*: Monday to Friday, from 19.00 to 8.00 and the entire day during weekends. The buying energy cost C_t is € 0.0574.

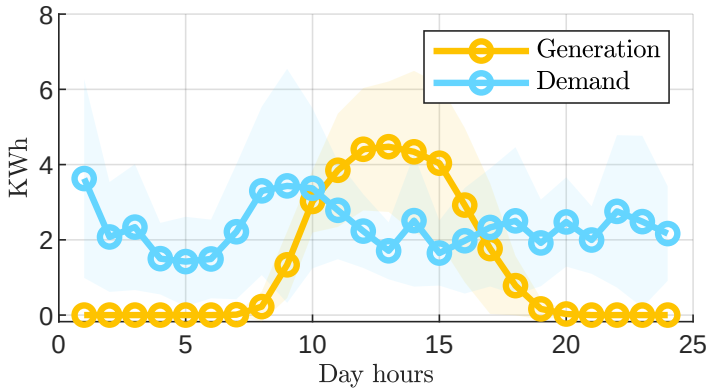

Figure 2.4: Prosumers' energy generation (yellow) and demand (cyan) curves. Lines correspond to the values averaged over the involved agents, while the shaded areas are the bounds of the standard deviation.

The relationship between the energy buying cost (i.e., C_t) and the energy selling price (i.e., R_t) for prosumers is the following:

$$R_t = \epsilon C_t, \quad \epsilon \in [0, 1] \tag{2.24}$$

where ϵ is the increment due to exogenous factors (e.g., taxes). As for the storage service pricing (i.e., L_t), for the sake of simplicity, a weighted average of the buying and selling price is considered:

$$L_t = \beta C_t + (1 - \beta) R_t \tag{2.25}$$

with $\beta \in [0, 1]$ being an arbitrary weight. By tuning the value of β, a large number of policies can be tested independently from the energy buying and selling price curves.

Finally, in Table 2.1 we report the tuning parameters of the proposed algorithms, as well as the technological parameters of the ESSs. In particular, the technological coefficients are sampled from normal distributions and the charge levels of ESSs are set to zero at the beginning of the day.

Since our work is focused on control frameworks for energy communities, for the sake of assessing the performance of the proposed methods in a comprehensive fashion, we adopt both economic (i.e., energy cost incurred by prosumers, revenue gained by providers, and revenue gained by the retailer), energy (i.e., prosumers' energy demand and generation as well as energy bought from and sold to the retailer, energy charged and discharged by the ESSs as well the storage state), and control/computational (i.e., residual of the coupling constraints for convergence and run time for scalability purpose) performance evaluation indicators.

Figure 2.5 reports the evolution of the energy flow variables over the control horizon. It is apparent that prosumers buy most of the energy during the early hours of the day, when the autonomous generation is at the lowest level, and sell the surplus during the middle hours of the day. It is worthwhile noting the effects of the storage service at the latest hours: the amount of bought energy is lower than the demand since prosumers start to retrieve the stored energy to compensate for the low autonomous production. As for the sold energy, the main volume is located, as expected, during the middle hours of the day. Furthermore, it can be noticed that the global amount of energy stored in the case of coordinated and uncoordinated frameworks is lower than in the centralized one. Moreover, its variance is narrower in the non-centralized frameworks, indicating that the storage service demand is uniformly distributed among providers.

Figures 2.6a, 2.6b, and 2.6c graphically summarize the costs and revenues sustained by each agent over the control horizon. Providers' revenues are negatively correlated with ζ, since such a coefficient indicates the tendency of ESSs to deteriorate. Some considerations related to the energy flow dynamics directly follow from the above-reported findings: the middle hours of the day are the less profitable ones for the retailer, which buys energy

Table 2.1: Parameters setup.

	Parameter	Value
Time horizon	T	24 (hours)
Group size	P	10
	S	8
Efficiencies	α	0.98
	$\eta^{\downarrow}$	1.03
	$\eta^{\uparrow}$	0.97
	σ	0.03
	$\overline{\zeta_j}$	0.005
	$\overline{\xi_j}$	0.0003
	ξ_j	$\sim N(\overline{\xi_i}, \sigma^2)$
	ζ_j	$\sim N(\overline{\zeta_i}, \sigma^2)$
Economical coefficients	ϵ	0.7
	β	0.5
Decision variables boundaries	$p^{\max}$	6 (kWh)
	$d^{\max}$	6 (kWh)
	$q^{\max}$	6 (kWh)
	$b^{\max}$	10 (kWh)
	b^{init}	0 (kWh)
	s^{init}	0 (kWh)
Convergence parameters	γ	0.098^{*} $0.98^{\dagger}$
	a	$1.04^{*,\dagger}$
	χ	0.01^{*} $0.7^{\dagger}$

* Coordinated
† Uncoordinated

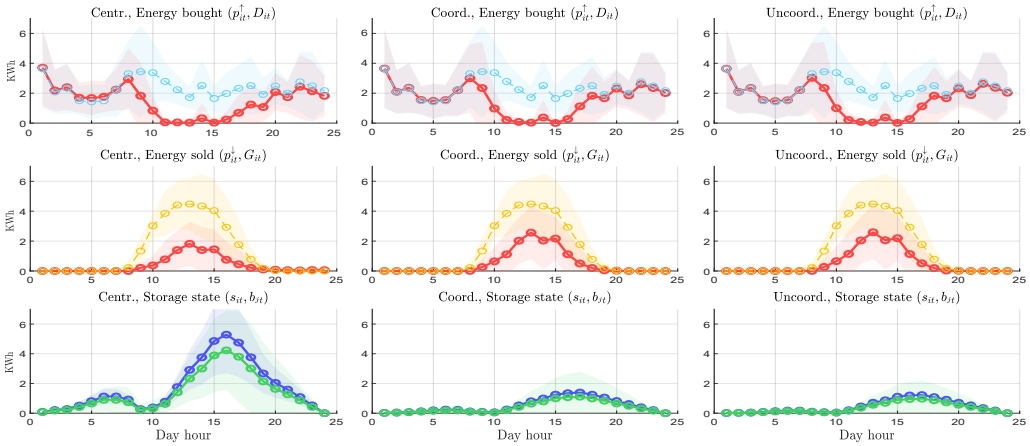

Figure 2.5: Energy transfer dynamics: the first, second, and third subplots column refers to the centralized, coordinated, and uncoordinated framework, respectively. The first row shows the profile of prosumers' demand D_{it} (cyan) and the profile of energy bought from the retailer $p^{\uparrow}_{it}$ (red). The second row represents the profile of prosumers generation G_{it} (yellow) and the profile of energy sold to the retailer $p^{\downarrow}_{it}$ (red). The third row shows the profile of prosumers' stored energy s_{iht} (green) and the profile of providers charge level b_{kjt} (blue). In all subplots Lines corresponds to the values averaged over the involved agents, while the corresponding shaded areas are the bounds of the standard deviation.

from the prosumer, instead of selling it. The retailer achieves the highest profit in the early morning when the solar generation is at the minimum level. During the latest hours of the day, revenues are still positive, although prosumers start using the stored surplus to satisfy the demand. An important aspect is that, for all the considered frameworks, the distribution of the economic curves follows the same trend. This implies that solving the optimization problem with a particular framework does not alter *fairness*, at least at the community level, i.e., no participant in the groups of prosumers or providers can strongly benefit from changing its strategy while compromising others' welfare. Also,

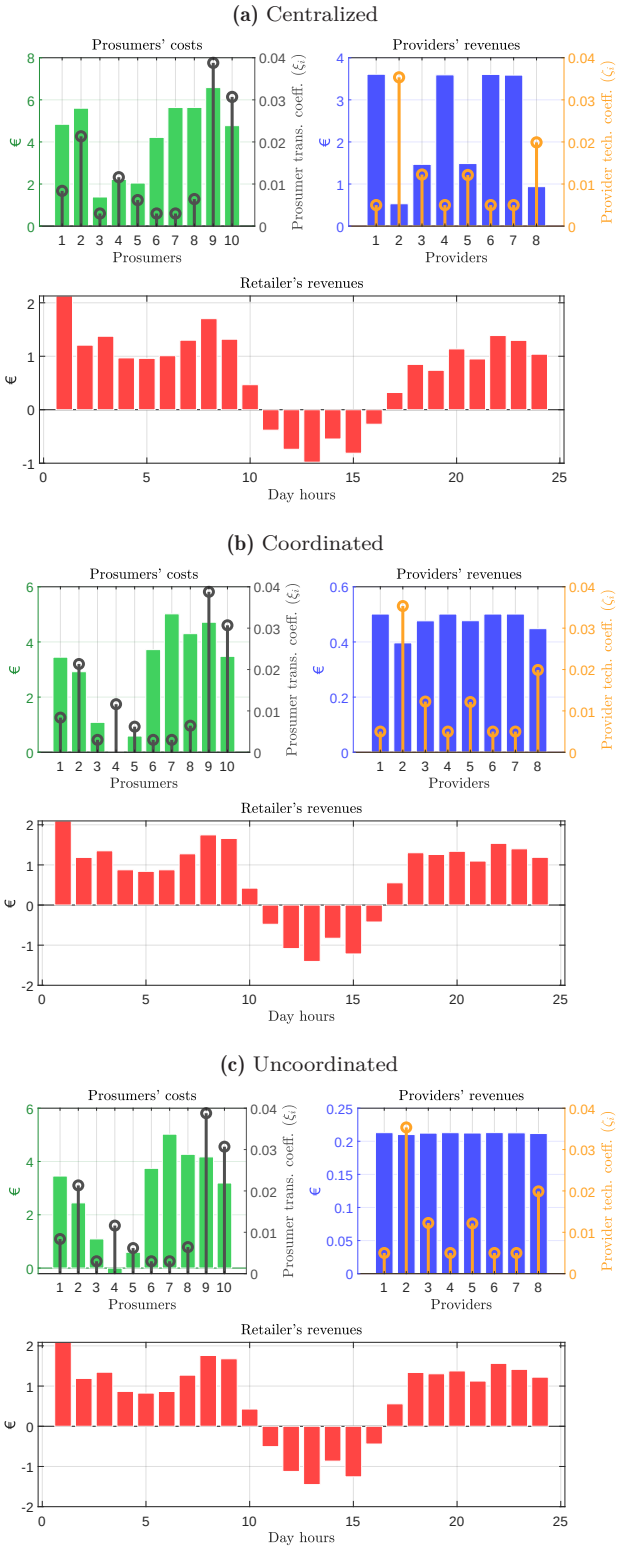

Figure 2.6: Economic results for the centralized (a), coordinated (b), and uncoordinated (c) framework. Total daily prosumers' costs (green bars) and providers' revenues (blue bars) are reported on a single-agent basis. Retailer revenues (red bars) are indicated on a time-slot basis. The brown and orange stems denote the values of the technological coefficients ξ_i and ζ_j over prosumers and providers, respectively.

it can be noticed that the distribution of the revenues for the providers becomes more homogeneous as we move from the centralized solution to the coordinated one, while the

largest uniformity is obtained in the uncoordinated case. This is a consequence of the perfect competition hypothesis and the noncooperative behavior of agents. Table 2.2 reports the revenues and the costs for the groups of prosumers and providers, as well as for the retailer. In particular, the "Total costs" column indicates the sum of the costs of

Table 2.2: Total costs and revenues for the group of prosumers, the groups of providers, and the retailer for each control framework.

		Cost of bought energy [€]	Revenues of sold energy [€]	Cost of storage service [€]	Cost of inefficiency* [€]	Community costs† [€]	Total costs§ [€]
Centralized	**Prosumers**	21.41	5.00	19.15	7.35	42.93	
	Providers	-	-	-19.15	0.34	-18.81	**7.70**
	Retailer	5.00	21.41	-	-	-16.42	
Decentralized	**Prosumers**	23.62	7.05	3.81	8.91	29.30	
	Providers	-	-	-3.81	0.014	-3.80	**8.93**
	Retailer	7.05	23.62	-	-	-16.57	
Distributed	**Prosumers**	23.83	7.31	1.70	9.51	27.77	
	Providers	-	-	-1.70	0.0035	-1.69	**9.51**
	Retailer	7.31	23.83	-	-	-16.57	

* Value related to the quadratic term in eq. (2.1) and eq. (2.4) for prosumers and providers, respectively.
† Value computed as: (Cost of bought energy) + (Cost of storage service) + (Cost of inefficiency) − (Revenues of sold energy).
§ Sum of the terms in the "Community cost" column.

all participants, including both the groups of prosumers and providers and the retailer. For the centralized case, it corresponds to the optimal value determined as a result of (2.7), whilst in the uncoordinated and coordinated cases, it is the sum of the optimal values determined as results of (2.11). It can be noticed that the total cost value increases moving from the centralized to the uncoordinated through the coordinated approach. From the prosumers' perspective, this means that the lowest total cost is achieved in the uncoordinated framework, whereas the lowest profit is made by providers. Retailer revenues are added for completeness's sake in Table 2.2, being itself part of the economic frame, even if we consider it as a passive agent.

Figures 2.7a and 2.7b report the residual value of the coupling constraints over iterations respectively for the coordinated and the uncoordinated algorithm, thus showing that convergence is ensured for both the proposed frameworks.

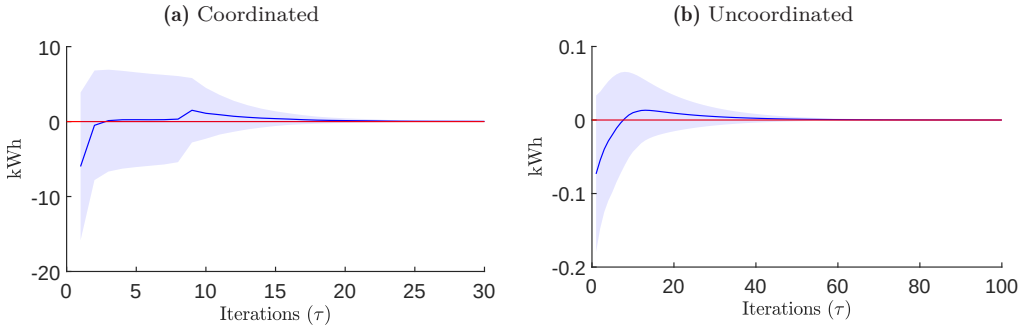

Figure 2.7: Convergence of the coordinated (a) and the uncoordinated (b) algorithm. The blue line indicates the average over the residual of (2.19) and (2.8) for the coordinated and the uncoordinated case, respectively. The shaded area is the bound of the standard deviation.

Finally, Fig. 2.8 reports the run time required by each framework. For the uncoordinated framework, the communication graph (Fig. 2.2) has been considered as *complete*, since it is the worst-case scenario from a computational perspective. For the non-centralized frameworks, simulation time T_{simul} is calculated as

$$T_{\text{simul}} = \max\left(T_{\mathcal{P}}, T_{\mathcal{S}}\right) \cdot N_{\text{iter}} \tag{2.26}$$

with $N_{\text{iter}} \approx 150$ being the number of iterations and $T_{\mathcal{P}}$ and $T_{\mathcal{S}}$ being the average simulation time for prosumers and providers, respectively. From Fig. 2.8 it is evident that T_{simul} approaches a sublinear trend $o(C)$ for the coordinated case and the uncoordinated

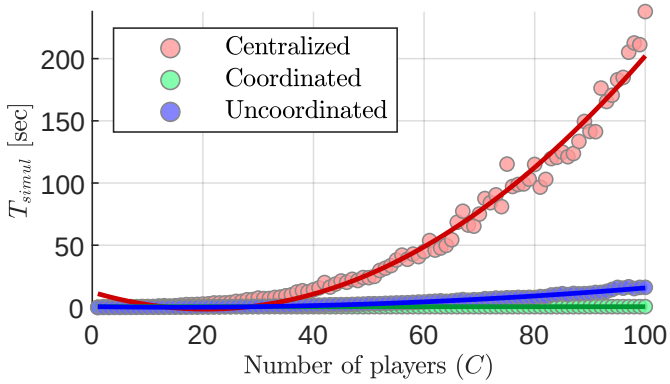

Figure 2.8: Run time versus the number of agents (up to 100) for each framework. Curves represent polynomial fitting.

case, while the centralized case shows the polynomial trend $\mathcal{O}(C^2)$. As a result, the inevitable economic performance loss occurring in the coordinated and uncoordinated frameworks comes with operational advantages from a computational point of view.

2.6 Conclusion

In the last decade, distributed energy generation and storage have significantly contributed to the spread of energy communities. This increasing trend makes it necessary to develop suitable control strategies, in order to efficiently exploit the generation and storage capabilities of the energy community. For the sake of satisfying such a need, in this chapter we propose two novel control schemes for energy communities –namely, the coordinated and the uncoordinated frameworks– with the following objectives:

- formulating of a scalable energy management architecture for communities equipped with multiple prosumers and independent ESS service providers;
- assessing the feasibility of the underlying client-service business model by simulating the frameworks on real-case scenarios;
- improving the computational effort with respect to the optimal centralized approach, while keeping the degree of information sharing at the minimum level and with minimal loss in the economic performance.

An additional merit of the presented approaches lies in their generalizability to address different service provisioning in energy communities, for instance, in the case of optimally trading local energy exchanges at peer-to-peer level and sharing common energy resources among the involved actors.

Nonetheless, this study is not without limitations, that need to be addressed in future developments. In particular, the energy generation and demand curves, as well as energy pricing profiles, are assumed to be deterministic, whilst the control frameworks are assumed to be not affected by modeling errors and non-idealities (e.g., latency, faults, etc.). Moreover, the individual objectives of involved actors could be enhanced to include wider sustainability payoffs beyond economic benefits. Lastly, the energy distribution network ignores the constraints flow constraints regarding active and reactive power. Therefore, future works will focus on these points, by effectively dealing with the presence of the uncertainty that affects the decision parameters, and integrating additional terms in the objective functions and realistic grid in the proposed frameworks.

References

[1] Gjorgievski, V. Z., Cundeva, S., and Georghiou, G. E., "Social arrangements, technical designs and impacts of energy communities: A review," *Renewable Energy*, 2021.

[2] Kim, B.-Y., Oh, K.-K., and Ahn, H.-S., "Coordination and control for energy distribution in distributed grid networks: Theory and application to power dispatch problem," *Control Engineering Practice*, vol. 43, pp. 21–38, 2015.

[3] Weaver, W. W., Robinett III, R. D., Parker, G. G., and Wilson, D. G., "Distributed control and energy storage requirements of networked dc microgrids," *Control Engineering Practice*, vol. 44, pp. 10–19, 2015.

[4] Soeiro, S. and Dias, M. F., "Community renewable energy: Benefits and drivers," *Energy Reports*, vol. 6, pp. 134–140, 2020.

[5] Hosseini, S. M., Carli, R., and Dotoli, M., "Robust optimal energy management of a residential microgrid under uncertainties on demand and renewable power generation," *IEEE Trans. Autom. Sci. Eng.*, vol. 18, no. 2, pp. 618–637, 2021.

[6] Bartolini, A., Carducci, F., Muñoz, C. B., and Comodi, G., "Energy storage and multi energy systems in local energy communities with high renewable energy penetration," *Renewable Energy*, vol. 159, pp. 595–609, 2020.

[7] Bradbury, K., Pratson, L., and Patiño-Echeverri, D., "Economic viability of energy storage systems based on price arbitrage potential in real-time us electricity markets," *Applied Energy*, vol. 114, pp. 512–519, 2014.

[8] Kolodziejczyk, W., Zoltowska, I., and Cichosz, P., "Real-time energy purchase optimization for a storage-integrated photovoltaic system by deep reinforcement learning," *Control Engineering Practice*, vol. 106, p. 104 598, 2021.

[9] Nguyen, H. T., Muhs, J. W., and Parvania, M., "Assessing impacts of energy storage on resilience of distribution systems against hurricanes," *Journal of Modern Power Systems and Clean Energy*, vol. 7, no. 4, pp. 731–740, 2019.

[10] Toledo, O. M., Oliveira Filho, D., and Diniz, A. S. A. C., "Distributed photovoltaic generation and energy storage systems: A review," *Renewable and Sustainable Energy Reviews*, vol. 14, no. 1, pp. 506–511, 2010.

[11] Iovine, A., Rigaut, T., Damm, G., De Santis, E., and Di Benedetto, M. D., "Power management for a dc microgrid integrating renewables and storages," *Control Engineering Practice*, vol. 85, pp. 59–79, 2019.

[12] Carli, R., Dotoli, M., Jantzen, J., Kristensen, M., and Othman, S. B., "Energy scheduling of a smart microgrid with shared photovoltaic panels and storage: The case of the ballen marina in samsø," *Energy*, vol. 198, p. 117 188, 2020.

[13] Scarabaggio, P., Carli, R., Jantzen, J., and Dotoli, M., "Stochastic Model Predictive Control of Community Energy Storage under High Renewable Penetration," in *2021 29th Mediterranean Conference on Control and Automation (MED)*, IEEE, 2021, pp. 973–978. DOI: 10.1109/MED51440.2021.9480353.

[14] Abrishambaf, O., Lezama, F., Faria, P., and Vale, Z., "Towards transactive energy systems: An analysis on current trends," *Energy Strategy Reviews*, vol. 26, p. 100 418, 2019.

[15] Akter, M. N., Mahmud, M. A., Haque, M. E., and Oo, A. M., "An optimal distributed energy management scheme for solving transactive energy sharing problems in residential microgrids," *Applied Energy*, vol. 270, p. 115 133, 2020.

[16] Soto, E. A., Bosman, L. B., Wollega, E., and Leon-Salas, W. D., "Peer-to-peer energy trading: A review of the literature," *Applied Energy*, vol. 283, p. 116 268, 2021.

[17] Sen, S. and Kumar, V., "Microgrid control: A comprehensive survey," *Annual Reviews in control*, vol. 45, pp. 118–151, 2018.

[18] Tucker, N. and Alizadeh, M., "An online scheduling algorithm for a community energy storage system," *arXiv preprint arXiv:2110.02396*, 2021.

[19] Parra, D., Swierczynski, M., Stroe, D. I., *et al.*, "An interdisciplinary review of energy storage for communities: Challenges and perspectives," *Renewable and Sustainable Energy Reviews*, vol. 79, pp. 730–749, 2017.

[20] Dai, R., Esmaeilbeigi, R., and Charkhgard, H., "The utilization of shared energy storage in energy systems: A comprehensive review," *IEEE Transactions on Smart Grid*, 2021.

[21] Wang, Z., Gu, C., Li, F., Bale, P., and Sun, H., "Active demand response using shared energy storage for household energy management," *IEEE Transactions on Smart Grid*, vol. 4, no. 4, pp. 1888–1897, 2013.

[22] Terlouw, T., AlSkaif, T., Bauer, C., and Van Sark, W., "Multi-objective optimization of energy arbitrage in community energy storage systems using different battery technologies," *Applied energy*, vol. 239, pp. 356–372, 2019.

[23] Szabó, D. Z., Duck, P., and Johnson, P., "Optimal trading of imbalance options for power systems using an energy storage device," *European Journal of Operational Research*, vol. 285, no. 1, pp. 3–22, 2020.

[24] Mediwaththe, C. P., Shaw, M., Halgamuge, S., Smith, D. B., and Scott, P., "An incentive-compatible energy trading framework for neighborhood area networks with shared energy storage," *IEEE Transactions on Sustainable Energy*, vol. 11, no. 1, pp. 467–476, 2019.

[25] Kalathil, D., Wu, C., Poolla, K., and Varaiya, P., "The sharing economy for the electricity storage," *IEEE Transactions on Smart Grid*, vol. 10, no. 1, pp. 556–567, 2017.

[26] Lombardi, P. and Schwabe, F., "Sharing economy as a new business model for energy storage systems," *Applied energy*, vol. 188, pp. 485–496, 2017.

[27] Le Cadre, H. and Mercier, D., "Is energy storage an economic opportunity for the eco-neighborhood?" *NETNOMICS: Economic Research and Electronic Networking*, vol. 13, no. 3, pp. 191–216, 2012.

[28] Vespermann, N., Hamacher, T., and Kazempour, J., "Access economy for storage in energy communities," *IEEE Transactions on Power Systems*, pp. 1–1, 2020. DOI: 10.1109/TPWRS.2020.3033999.

[29] Nikonowicz, L. B. and Milewski, J., "Virtual power plants-general review: Structure, application and optimization," *Journal of power technologies*, vol. 92, no. 3, p. 135, 2012.

[30] Ghavidel, S., Li, L., Aghaei, J., Yu, T., and Zhu, J., "A review on the virtual power plant: Components and operation systems," in *2016 IEEE International Conference on Power System Technology (POWERCON)*, IEEE, 2016, pp. 1–6.

[31] Liu, J., Zhang, N., Kang, C., Kirschen, D., and Xia, Q., "Cloud energy storage for residential and small commercial consumers: A business case study," *Applied energy*, vol. 188, pp. 226–236, 2017.

[32] Zhou, Y., Ci, S., Lin, N., Li, H., and Yang, Y., "Distributed energy management of p2p energy sharing in energy internet based on cloud energy storage," in *Proceedings of the Ninth International Conference on Future Energy Systems*, 2018, pp. 173–177.

[33] Unger, D. and Myrzik, J. M., "Agent based management of energy storage devices within a virtual energy storage," in *2013 IEEE Energytech*, IEEE, 2013, pp. 1–6.

[34] Pandžić, K., Pandžić, H., and Kuzle, I., "Virtual storage plant offering strategy in the day-ahead electricity market," *International Journal of Electrical Power & Energy Systems*, vol. 104, pp. 401–413, 2019.

[35] Zhao, D., Wang, H., Huang, J., and Lin, X., "Virtual energy storage sharing and capacity allocation," *IEEE transactions on smart grid*, vol. 11, no. 2, pp. 1112–1123, 2019.

[36] Liu, J., Zhang, N., Kang, C., Kirschen, D. S., and Xia, Q., "Decision-making models for the participants in cloud energy storage," *IEEE Transactions on Smart Grid*, vol. 9, no. 6, pp. 5512–5521, 2017.

[37] Koike, M., Ishizaki, T., Ramdani, N., and Imura, J.-i., "Optimal scheduling of battery storage systems and thermal power plants for supply–demand balance," *Control Engineering Practice*, vol. 77, pp. 213–224, 2018.

[38] Atzeni, I., Ordóñez, L. G., Scutari, G., Palomar, D. P., and Fonollosa, J. R., "Demand-side management via distributed energy generation and storage optimization," *IEEE Trans. Smart Grid*, vol. 4, no. 2, pp. 866–876, 2012.

[39] Zadeh, L., "Optimality and non-scalar-valued performance criteria," *IEEE Transactions on Automatic Control*, vol. 8, no. 1, pp. 59–60, 1963. DOI: 10.1109/TAC.1963.1105511.

[40] French, S., "Multi-objective decision analysis with engineering and business applications," *Journal of the Operational Research Society*, vol. 34, no. 5, pp. 449–450, 1983. DOI: 10.1057/jors.1983.105.

[41] Boyd, S., Boyd, S. P., and Vandenberghe, L., *Convex optimization*. Cambridge university press, 2004.

[42] Facchinei, F., Fischer, A., and Piccialli, V., "On generalized nash games and variational inequalities," *Operations Research Letters*, vol. 35, no. 2, pp. 159–164, 2007.

[43] Facchinei, F., Fischer, A., and Piccialli, V., "On generalized nash games and variational inequalities," *Operations Research Letters*, vol. 35, no. 2, pp. 159–164, 2007.

[44] Pang, J.-S., Scutari, G., Palomar, D. P., and Facchinei, F., "Design of cognitive radio systems under temperature-interference constraints: A variational inequality approach," *IEEE Transactions on Signal Processing*, vol. 58, no. 6, pp. 3251–3271, 2010.

[45] Chatzipanagiotis, N., Dentcheva, D., and Zavlanos, M. M., "An augmented lagrangian method for distributed optimization," *Mathematical Programming*, vol. 152, no. 1, pp. 405–434, 2015.

[46] Lombardi, F., Aniello, L., De Angelis, S., Margheri, A., and Sassone, V., "A blockchain-based infrastructure for reliable and cost-effective iot-aided smart grids," 2018.

[47] Chen, S., Wen, H., Wu, J., *et al.*, "Internet of things based smart grids supported by intelligent edge computing," *IEEE Access*, vol. 7, pp. 74 089–74 102, 2019.

[48] Enel, *E-light bioraria*, Accessed: [Online]. Available: https://www.enel.it/it/luce-e-gas/luce/offerte/e-light-bioraria (visited on 05/23/2021).

Chapter 3

Noncooperative Control for Energy Scheduling with Adjustable Load Demand

III

Abstract

Nowadays, power grids are facing reduced total system inertia as traditional generators are phased out in favor of renewable energy sources. Hence, new challenges came out concerning their operation and stability, in particular for frequency and voltage regulation. These problems are expected to deepen with the increasing penetration of *electrical vehicles* (EVs) connected to the power system. However, this massive number of EVs represents a significant capacity of distributed energy storage that can be an alternative to large-scale storage devices thus providing ancillary services back to the power grid. The influence of a single EV on the network is low; nevertheless, the aggregate impact becomes relevant when they are properly coordinated. In this context, we consider the frequent case of a group of EVs connected to a parking lot with a photovoltaic facility. We propose a novel strategy to optimally control their batteries during the parking session, which is able to satisfy their requirements and energy constraints. EVs participate in a noncooperative energy market based on a smart pricing mechanism that is designed in order to increase the predictability and flexibility of the aggregate parking load. Differently from the existing contributions, where the aim is to achieve the optimal charge level only, we employ an approach to minimize the degradation of batteries of EVs. The effectiveness of the proposed method is validated through numerical experiments based on a real scenario.

Contents

3.1 Introduction

Decarbonizing the transportation system, while improving its efficiency and sustainability, is a challenging strategic objective that is being stimulated worldwide by pressing climate change and environmental issues. To answer this need, a considerable proliferation of *electrical vehicles* (EVs) is spreading due to their potential in reducing greenhouse gas emissions. Moreover, EVs can also alleviate the uncertainty caused by highly fluctuating oil prices [1], [2].

Plug-in EVs can be recharged by simply connecting them to the electrical grid, which makes them more convenient than hybrid EVs [3]. Nevertheless, the expected massive deployment of charging stations, required by plug-in EVs, will increase issues of traditional power distribution systems leading to many new challenges and complications [4]. In conventional charging systems, EV charging is performed in a unidirectional mode: the

electricity only flows from the grid to the EV. This unidirectional charging could potentially lead to uncoordinated, unpredicted, and concentrated electricity demand. Hence, the most challenging issue is the coordination of EVs enforcing the stability of power grids under control while keeping the power quality at an acceptable level.

Despite these issues, EVs may generate potential benefits to the grid: for instance, they present a significant capacity of distributed energy storage that can provide ancillary services back to the power system. Indeed, EVs are mobile storage devices that can represent an alternative to larger-scale energy storage devices and are therefore become key elements in supporting grid operations [5], [6]. In particular, several research studies focus on the so-called *vehicle-to-grid* (V2G) concept, where batteries of EVs are employed as additional resources for the power grid [7]. In particular, in V2G applications, EVs can be beneficial for power grids through dynamic charge or bidirectional flow of electrical energy between vehicles and power grids. Nevertheless, as the impact of a single device is negligible, EVs should be aggregated and coordinated such that their contribution to the power system becomes significant. Considering these issues, efficient charging/discharging coordination schemes are necessary to maximize benefits for both grid operators and EVs owners [8].

3.1.1 Literature Review

Several approaches for smart charging and discharging of EVs have been proposed. We can classify these approaches in two categories.

The first category of approaches aims at either minimizing the charging cost or increasing the efficiency of charging strategies from the perspective of EVs. Each EV tries to minimize the energy cost taking into account the battery dynamics and the power grid operation. For instance, in [9] a fuzzy controller to manage the charging processes of EVs is proposed. Moreover, some works consider the concept of *time to use* (TOU) price as in [10], [11], where the authors study the charging/discharging scheme in V2G systems and obtained a state-dependent policy to minimize the charging cost for individual EVs. Other approaches focus on the service requirement for EVs' owners. For instance, [12] presents a novel charging scheduling scheme based on a Markov decision process to minimize the mean waiting time for EVs, whereas in [13] a mobility-aware charging strategy for EVs is proposed to address the range anxieties of individual EVs. However, few works consider the effects of degradation in batteries [14]. For example, in [15], the authors present a degradation model for EVs evaluating the impact of different charging strategies on the lifetime of the batteries. Lastly, in [16], a feasibility study of V2G frequency regulation under an economic and degradation perspective is suggested.

The second category comprehends all approaches focused on the operational efficiency of charging systems and the utilization of *renewable energy sources* (RESs). Here, the objective is to support the power grid operations while improving the power quality. For example, in [17] and [18] the authors propose a novel EVs charging mechanism such that the *peak-to-average ratio* (PAR) and the system peak load are reduced. In addition, several approaches focus on *frequency regulation* (FR) actions. For instance, the authors of [19] propose a novel decentralized control mechanism that allows EVs to participate in the FR. Moreover, in [20] the FR is ensured by controlling the *state of charge* (SoC) of batteries through a standard droop characteristic. To shift the peak loads in power systems due to the EVs deployment, there are two main approaches. One is to schedule the electricity demand by signing contracts between the utility company and EVs' owners [21]. This approach can be easily implemented; however, its flexibility is limited. Another approach is based on smart pricing mechanisms. Indeed, since the base load and charging demand are time-varying over a day, it is possible to adjust the electricity rate in different periods such that EVs' owners are willing to shift their charging time to off-peak time slots. Different pricing strategies can be applied, such as critical-peak pricing, real-time pricing, and TOU pricing. Nevertheless, game-theoretic approaches are ideal to address this issue, as they can reveal the relationship between the pricing and the charging strategy of owners. For instance, in [22], a game-theoretic approach is proposed to optimize the

charging schedule in a parking lot with a highly dynamic electricity price during the daytime, while in [23] a static noncooperative game for distributed charging of EVs is presented.

3.1.2 Chapter Contribution

The previous discussion shows that few works in the related literature consider simultaneously EVs charging requirements, while taking into account the impact of degradation and the effects of the aggregate power demand of EVs on the power system.

Differently from the available literature on the topic, this chapter aims at proposing a novel charging/discharging V2G control approach for a group of EVs connected to a parking lot with a *photovoltaic* (PV) rooftop. This control approach is based on *model predictive control* (MPC) and is able to optimally control batteries of EVs during their parking session. On the one hand, the proposed approach is able to increase the predictability and flexibility of the aggregate load of EVs connected to the parking lot, thus providing service provision to the power grid. This is accomplished through a novel smart pricing mechanism for electric energy based on the noncooperative game theory. On the other hand, the proposed control strategy allows different EVs to decide independently their charging/discharging profiles, while ensuring their charging requirement and personal preferences. In addition, differently from the majority of the relevant studies in the related literature, we propose a novel approach to minimize the degradation of batteries during the charging/discharging process. In particular, we propose a battery degradation model that estimates the number of cycles taking into account their depths. The effectiveness of the proposed method is validated through numerical experiments based on real data referring to a parking lot facility located in the United Kingdom. To better show the performance of the proposed mechanisms under the actual operating conditions, the comparison with a naïve reference strategy is presented.

3.2 System Model

In this section, we present the model of the proposed parking lot with solar rooftops. The parking lot is composed of $N \in \mathbb{N}$ charging piles connected to the power bus of the parking lot through an *energy manager*. The power bus is powered in a DC mode by the PV panels and by the main power grid through the AD/DC interface. We assume that EVs connected to charging piles accept to participate in an energy market based on a dynamic pricing mechanism. Hence, EVs can charge and discharge their batteries based on their personal preferences and the price of energy. Nevertheless, EVs cannot communicate with each other, in fact, each EV communicates only with the *energy manager*, whose responsibilities consist in broadcasting the dynamic energy price and steering energy flows. The energy market of the parking lot is based on a predictive control approach. Hence, let us discretize the time horizon in time slots with equal length Δ_t and indicate by $t \in \mathbb{N}$ the index of the generic time slot. The modeling of system components is shown in Fig. 3.1 and is discussed in detail as follows.

3.2.1 EVs Model

Let us now model the EVs connected to the charging pile during the parking phase. For a generic time slot $t \in \mathbb{N}$, we consider that a group of EVs $\mathcal{N}_t$ with cardinality $N_t \in \mathbb{N}$ is connected to the charging piles. Note that, at each time slot, the number of EVs in charge must be lower than the number of charging piles, i.e., $N_t \leq N$. Generally, we have different arrival A_i and departure times D_i for each EV, where the subscript i refers to a generic EV $i \in \mathcal{N}_t$. Note that we neglect the driving and waiting time in the parking lot; hence, the arrival and departure times refer only to the time on which the EV is connected to a charging pile.

Therefore, we model the operation of each EV by a shrinking horizon strategy, and for the generic time slot $t \in [A_i, D_i]$ we define the control horizon for EV $i \in \mathcal{N}_t$ as

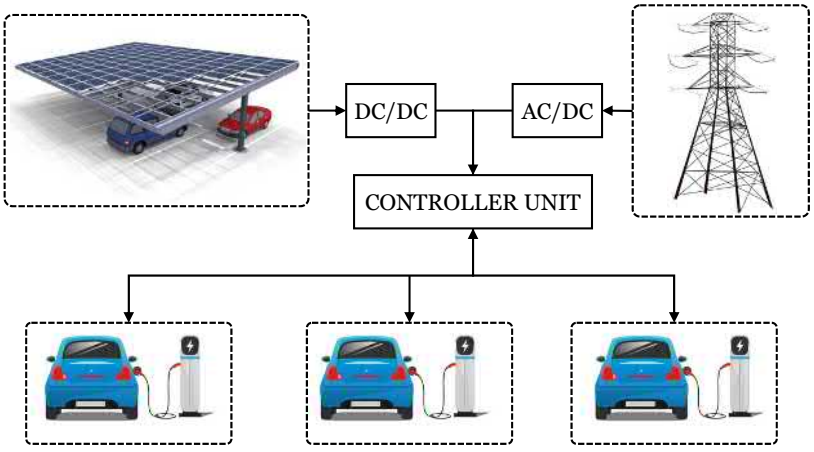

Figure 3.1: Scheme of the proposed smart EVs parking lot with solar rooftops.

$\mathcal{H}_{i,t} := \{t+1, ..., h, ..., D_i\}$, including $H_{i,t} = D_i - t$ time slots with equal length Δ_t. We remark that EVs have a control horizon with different lengths.

Assumption 3.2.1

We assume that, when an EV is parked, the owner sets a finite departure time, a minimum allowable SoC, and a minimum charging requirement for the end of the parking period. Therefore, we assume that if the owner leaves the parking earlier than the scheduled departure time, the minimum charging requirement cannot be fulfilled. However, the SoC of the battery at each time step of the charging session must always be greater than the minimum allowable SoC. □

To model the charging/discharging activities of the batteries, at each time step $t \in [A_i, D_i]$, we define vectors $\mathbf{c}_{i,t} := (c_i(h))^\top_{h\in\mathcal{H}_{i,t}}$ and $\mathbf{d}_{i,t} := (d_i(h))^\top_{h\in\mathcal{H}_{i,t}}$ collecting the profiles of energy stored/released in/from the battery of EV $i \in \mathcal{N}_t$, respectively. From the perspective of the system dynamics, without loss of generality, we can model EVs as first-order discrete-time systems. Hence, it is useful to define for each EV $i \in \mathcal{N}_t$: the leakage rate α_i, as well as the charging and discharging inefficiencies $0 < \beta_i^c \leq 1$ and $\beta_i^d \geq 1$ of the inverter. Even though these efficiencies vary over time, for the sake of simplicity, we assume them constant. The state of charge of the battery equals the charge level at the previous slot corrected by the energy charging and discharging profiles. Therefore, by defining vector $\mathbf{s}_{i,t} := (s_i(h))^\top_{h\in\mathcal{H}_{i,t}}$ collecting the state of charge profile, we can compute the dynamics of the battery for the generic time step $h \in \mathcal{H}_{i,t}$ as:

$$s_i(h) = \alpha_i s_i(h-1) + \beta_i^c c_i(h)\Delta_t - \frac{d_i(h)\Delta_t}{\beta_i^d}, \quad \forall h \in \mathcal{H}_{i,t}, \forall i \in \mathcal{N}_t. \tag{3.1}$$

Moreover, by denoting $\overline{c}_i$, $\underline{c}_i$, $\overline{d}_i$, and $\underline{d}_i$ the maximum and minimum charging and discharging rates, the following technical constraints must be satisfied:

$$\underline{c}_i \leq c_i(h) \leq \overline{c}_i, \quad \forall h \in \mathcal{H}_{i,t}, \forall i \in \mathcal{N}_t \tag{3.2}$$

$$\underline{d}_i \leq d_i(h) \leq \overline{d}_i, \quad \forall h \in \mathcal{H}_{i,t}, \forall i \in \mathcal{N}_t. \tag{3.3}$$

Lastly, as aforementioned in Assumption 3.2.1, the state of charge level is also bounded by the minimum allowable SoC ($\underline{s}_i$) and maximum capacity of the battery ($\overline{s}_i$) as follows:

$$\underline{s}_i \leq s_i(h) \leq \overline{s}_i, \quad \forall h \in \mathcal{H}_{i,t}, \forall i \in \mathcal{N}_t \tag{3.4}$$

while we assume that the SoC of the battery must respect the charging requirement imposed by the minimum SoC requirement at the end of the charging period (S_i) as follows:

$$s_i(D_i) \geq S_i, \quad \forall i \in \mathcal{N}_t \tag{3.5}$$

It should be noted that while all the others are technical parameters, $\underline{s}_i$ and S_i are parameters selected at each stopover by the owner of the EV following individual preferences.

Assumption 3.2.2

We assume that each owner can select a minimum charging requirement S_i that is technically feasible with respect to the leaving time, i.e., such that:

$$S_i \leq \alpha^{D_i - A_i} + \beta_i^c \, \overline{c}_i \sum_{j=1}^{D_i - A_i} \alpha^{D_i - A_i - j}. \tag{3.6}$$

□

Remark 3.2.1

It should be noted that, in general, the aforementioned storage model does not allows charging and discharging at the same time, i.e., $c_i(h)$ and $d_i(h)$ cannot be both strictly positive for the same time slot h. In fact, the proposed method is a common approach that permits to have two different coefficients without introducing a nonconvexity [24]. □

3.2.2 PV Model

The parking lot incorporates one or more PV panels on the rooftop, hence, as in [25] we model the PV system as a time-varying power source. We correlate the power output $r(h)$ at the generic time h to the global solar radiation $G(h)$ and the air temperature $T(h)$ through the following relation:

$$r(h) = \eta_1(1 - \eta_2(T(h) - T_{\mathrm{r}}))G(h) \tag{3.7}$$

where η_1 and η_2 are the characteristic efficiencies and T_r is the reference air temperature of the PV system.

Assumption 3.2.3

We assume that the solar energy collected by PV panels can only be used by the parking lot and it cannot be dispatched to the power grid. This assumption is reasonable since most of the power grid regulations do not allow the feedback injection of power due to stability and safety concerns. □

3.2.3 *Energy manager* Model

As mentioned above, EVs participate in an energy market managed by the *energy manager* of the parking lot. However, as EVs have different control horizons, at each generic time $t \in \mathbb{N}$ the *energy manager* should consider the horizon $\mathcal{H}_t := \{t+1, ..., h, ..., t+H\}$ including H_t time slots such that $H_t \geq H_i$ for all $i \in \mathcal{N}_t$.

First, the *energy manager* ensures that a demand-supply balance constraint is fulfilled. Indeed, at each time slot the *energy manager* may buy a certain amount of energy to satisfy the energy demand of the different EVs. Thus, for each time slot t, we define vector $\mathbf{r}_t := (r(h))_{h \in \mathcal{H}_t}^{\top}$ collecting the aggregated profile of energy produced by all PV panels. Accordingly, we have:

$$\sum_{i \in \mathcal{N}_t} (c_i(h) - d_i(h)) = g(h) + r(h) - r_l(h), \quad \forall h \in \mathcal{H}_t \tag{3.8}$$

where $r_l(h)$ is the amount of power loss due to Assumption 3.2.3.

Secondly, the *energy manager* broadcasts the energy price to all EVs. We preliminarily remark that, thanks to the high penetration of EVs and distributed generation in

distribution networks, the stability and predictability of power grids are dropping with respect to that of traditional grids. Therefore, we assume that the goal of the proposed smart pricing model is to increase the predictability and flexibility of the parking lot. More in detail, we assume that the *energy manager* receive a reference signal $\mathbf{g}_{\mathrm{r},t} := (g_{\mathrm{r}}(h))^{\top}_{h\in\mathcal{H}_t}$ representing the power that the parking lot agrees to follow. Hence, for each $h \in \mathcal{H}_t$ we define the mismatch as:

$$\Delta \mathrm{g}(h) = g_{\mathrm{r}}(h) - g(h). \tag{3.9}$$

We now suppose that the deviation (3.9) is dynamically regulated by the *energy manager* that encourages EVs to minimize the above-defined mismatch through a smart pricing mechanism. In particular, we consider a function C_i to model the unit cost of the energy bought from the distribution system. This function is the sum of a fixed energy price and a variable one based on (3.9), as:

$$C_i\left(\mathbf{c}_{i,t}, \mathbf{d}_{i,t}\right) = \sum_{h\in\mathcal{H}_{i,t}} k_i\left(h\right)\left(c_i\left(h\right) - d_i\left(h\right)\right) + v_i\left(h\right)\Delta \mathrm{g}\left(h\right)\left(c_i\left(h\right) - d_i\left(h\right)\right) \tag{3.10}$$

where $k_i(h) > 0$ and $v_i(h) > 0$ are the fixed and variable price coefficients at the h-th slot, respectively.

3.3 Peak-to-valley Degradation Approach

Degradation in terms of capacity decrease affects all battery technologies. The literature in this field is still limited.

On the one hand, the so-called calendar influencing factors refer to the natural degradation of devices, with temperature being the most important factor. Here, we ignore these degradation effects since they are not directly related to the control strategy. On the other hand, a large number of degradation effects are caused by operational factors [26]. In this context, an essential concept is the life cycle, which is defined as the maximum number of charge-discharge cycles until the capacity of the battery falls under a specific threshold. The maximum number of cycles of a specific battery is calculated by discharging and charging the battery from the maximum capacity to a specific state of charge [26]. We refer to this as a standard cycle, while the depth of discharge (DoD) is the difference between the maximum capacity and the specific state of charge. The nonlinear relation between DoD and the degradation associated with a specific cycle is the major stress factor of lithium-ion batteries –which are mainly used in EVs. However, in real applications, the charging and discharging profiles are different from the standard cycle. Despite these dynamics, most scientific works neglect this difference even if degradation is more severe with cycles performed at lower SoC levels. For instance, a cycle between 100%–70% of the SoC is equal to a cycle between 50%–20% [27].

3.3.1 Cycle Depth Degradation Function

In the related literature, only some studies model the relation between the DoD of each cycle and the capacity fade. Nevertheless, it is clearly essential to include degradation in any optimization model dealing with EVs. Therefore, by defining $u \in [0, 1]$ as the DoD of a generic cycle, let us define a cycle stress function $\phi(u) : [0, 1] \to \mathbb{R}_{\geq 0}$ to model the life loss from a single cycle measured in terms of changes in the capacity of the battery. This function indicates that, if a battery is repetitively discharged and charged with a DoD u, it can operate $1/\phi(u)$ cycles before reaching the end of life.

The cycle depth stress functions used in the literature for electrochemical batteries are either empirical or linearized models. These functions are generally chosen convex, as to exploit the convexity properties in the underlying optimization model. [28]–[31]. The two most common classes of degradation functions on which experimental data are usually fitted are:

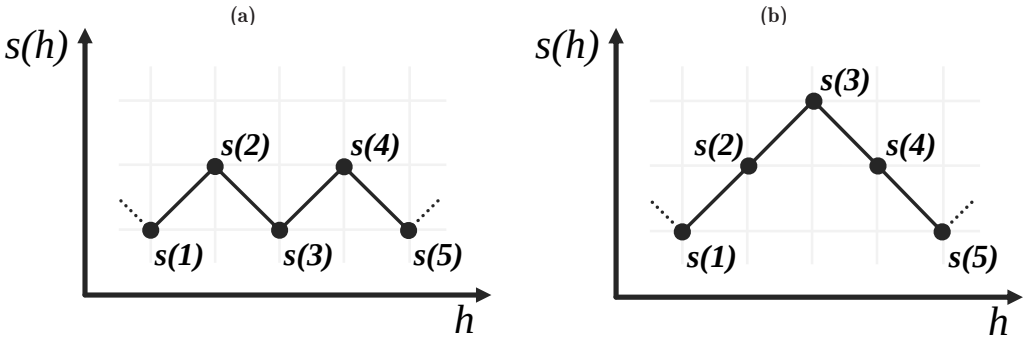

Figure 3.2: Example of two different SoC profiles.

1. exponential [31], [32]:
$$\phi(u) = \gamma_1 u e^{\gamma_2 u} \tag{3.11}$$
2. polynomial [30], [33]:
$$\phi(u) = \gamma_3 u^{\gamma_4} \tag{3.12}$$

where γ_1, γ_2, γ_3, and γ_4, are coefficients estimated with cycling aging experiments.

3.3.2 Cycle Counting Algorithm

Given the degradation dynamics of batteries, the degradation depends on the depth of each cycle. Nevertheless, the number and depth of each cycle depend on the SoC profile, which can be easily identified during experimental tests. However, in real applications, this task becomes challenging due to the irregularity of the SoC profile.

Starting from a SoC profile $\mathbf{s}$ over a control horizon $\mathcal{H}$, a widespread approach to estimate the number and depth of each cycle consists in defining the cycle depth as $(s(h) - s(h-1))^2$ for all $h \in \mathcal{H}$. Note that in this case the depths correspond to a half cycle, while their number equals the cardinality of the control horizon $\mathcal{H}$. Nevertheless, this approach is not able to discriminate between different SoC profiles. For instance, by analyzing the examples (a) and (b) in Fig. 3.2, it is evident that both SoC profiles have an equal charge/discharge depth $(s(h) - s(h-1))^2$ for each time step; however, due to the high nonlinear relation between cycle depth and degradation, the SoC profile (b) leads to a more significant total degradation, since the aggregate DoD is larger.

Given a SoC profile as an input, several approaches have been proposed to appropriately identify the number and depth of equivalent standard cycles. These methodologies make use of the so-called cycle counting methods to convert a continuous time series of irregular loads into a discrete number of standard cycles. One of the most used and noteworthy technique is the so-called *Rainflow* algorithm that identifies local extreme points and then counts the depth of all cycles based on the local extrema sequence [34].

Let us now propose a novel cycle counting approach to extrapolate the number of cycles employing a closed convex formulation that can be used by most optimization solvers. Our approach is inspired by the *Peak-to-valley* method used in mechanical fatigue analyses and described in the standard ASTM E1049-85(2017) [35]. In the first phase of the proposed *Peak-to-valley* counting approach, all SoC levels are ordered from the maximum to the minimum value. Then, the depth of the most damaging cycle is identified by computing the difference between the first value (i.e., the highest peak) and the lowest one (i.e., the deepest valley). Similarly, the second largest cycle is defined between the second higher peak and the second deepest valley, and so on until the contribution of all peaks/valleys is added to the depth count.

Algorithm 3.1 Naïve control algorithm

1: **for** $t = 1, \ldots$ **do**
2: **for** $i \in \mathcal{N}_t$ **do**
3: Set $c_i(t) \leftarrow \min\left\{\overline{c}_i, \max\left\{0, \frac{S_i - \alpha_i s_i(t-1)}{\beta_i^c \Delta_t}\right\}\right\}$
4: Set $d_i(t) \leftarrow \min\left\{\overline{d}_i, \max\left\{0, (\alpha_i s_i(t-1) - S_i)\, \beta_i^d \Delta_t\right\}\right\}$
5: Set $s_i(t) \leftarrow \alpha_i s_i(t-1) + \beta_i^c c_i(t) \Delta_t - \frac{d_i(t)\Delta_t}{\beta_i^d}$
6: **end for**
7: **end for**

3.3.3 EVs Degradation Cost Function

As mentioned above, we can directly relate the degradation to the control actions. More in detail, given the charging/discharging profiles we can obtain, employing the *Rainflow* or *Peak-to-valley* counting approaches, a set of cycles $\mathcal{R}$ and thus a cycle depths vector $\mathbf{u}(\mathbf{c}_{i,t}, \mathbf{d}_{i,t}) := (u_r)_{r \in \mathcal{R}}$. Thus, we define an aggregate cycle depth stress function as:

$$\Phi(\mathbf{u}(\mathbf{c}_{i,t}, \mathbf{d}_{i,t})) = \sum_{r \in \mathcal{R}} \phi(u_r). \tag{3.13}$$

Therefore, let us now design a battery degradation cost function for each vehicle $i \in \mathcal{N}^t$ by converting the life loss associated to a series of cycles into a cumulative cost as:

$$L_i(\mathbf{c}_{i,t}, \mathbf{d}_{i,t}) = \Phi_i(\mathbf{u}(\mathbf{c}_{i,t}, \mathbf{d}_{i,t}))E_i B_i \tag{3.14}$$

where B_i is the per capacity battery replacement cost and E_i is its capacity.

3.4 Energy Scheduling

In this section we formalize the solution algorithm to solve the optimization problem for the proposed parking lot in a decentralized fashion. However, for the sake of defining a baseline method, let us first describe a simple naïve strategy.

3.4.1 Naïve EVs Scheduling Strategy

Algorithm 3.1 defines a naïve charging strategy for determining the amount of energy to be charged/discharged into/from each EV at each time slot. This control strategy comprises the following logic. As soon as the SoC level in the battery is lower than the final required SoC level, the EV is charged at the maximum level (line 3). However, if the SoC level exceeds the final required SoC level, the EV charging is switched-off and the battery is discharged accordingly (line 4). Finally, the SoC level is updated (line 5), and the algorithm steps are repeated at each time slot and for each EV (lines 1–7).

3.4.2 Game-theoretic EVs Scheduling Strategy

The objective of the pricing model is to increase the predictability of the overall parking lot leveraging on a smart pricing mechanism. However, due to the formulation in (3.10), the cost of the energy for each EV depends on its strategy as well as on the strategies of other EVs. The resulting problem can be solved in a centralized fashion; however, in such a case, the controller unit must access all preferences and information from all EVs. Due to these privacy issues, a decentralized architecture is more appropriate. In particular, a natural framework to capture such a competitive and decentralized decision-making process relies on game theory. Let us define the components of the game-theoretic framework.

1. *Players:* the game comprehends a set of players represented by the EVs in N_t connected to the parking lot;

2. *Strategies:* each player can choose a strategy from a given set to improve the welfare. In our case, the strategy of each EV $i \in \mathcal{N}_t$ is defined as $\mathbf{x}_{i,t} := (\mathbf{c}_{i,t}^\top, \mathbf{d}_{i,t}^\top)^\top \in \mathbb{R}_{\geq 0}^{2H_{i,t}}$. We define for each EV i the vector $\mathbf{x}_{-i,t} := \mathrm{col}\,(\mathbf{x}_{1,t}, ..., \mathbf{x}_{i-1,t}, \mathbf{x}_{i+1,t}, ..., \mathbf{x}_{N,t})$ collecting the strategies of all EVs different from i, while $\mathbf{x} := \mathrm{col}\,(\mathbf{x}_1, ..., \mathbf{x}_{i,t}, ..., \mathbf{x}_N)$ collects the strategies of all EVs. Each EV $i \in \mathcal{N}_t$ can choose a strategy from the local feasible set defined as:

$$\Omega_{i,t} = \left\{ \mathbf{x}_{i,t} \in \mathbb{R}_{\geq 0}^{2H_{i,t}} \mid (3.1)\text{-}(3.5) \text{ hold} \right\}, \forall i \in \mathcal{N}_t. \tag{3.15}$$

3. *Cost functions:* each player of the game has a cost function J_i representing the welfare. The cost function for each EV $i \in \mathcal{N}_t$ is based on the pricing mechanism (3.10) and the degradation (3.14) as follows:

$$J_i\left(\mathbf{x}_{i,t}, \mathbf{x}_{-i,t}\right) = C_i\left(\mathbf{c}_{i,t}, \mathbf{d}_{i,t}\right) + L_i\left(\mathbf{c}_{i,t}, \mathbf{d}_{i,t}\right). \tag{3.16}$$

In the game, each EV $i \in \mathcal{N}_t$ tries to minimize its cost function $J_i\left(\mathbf{x}_{i,t}, \mathbf{x}_{-i,t}\right) : \mathbb{R}^{2H_{i,t}} \to \mathbb{R}$, by choosing a strategy in its local feasible set $\mathbf{x}_i \in \Omega_{i,t}$. However, the resulting N_t optimization problems are not independent and are defined as:

$$\forall i \in \mathcal{N}_t : \quad \underset{\mathbf{x}_{i,t} \in \Omega_{i,t}}{\operatorname{argmin}} \; J_i\left(\mathbf{x}_{i,t}, \mathbf{x}_{-i,t}\right). \tag{3.17}$$

The combination of these interdependent optimization problems is the so-called *Nash equilibrium problem* (NEP), whose solution is the *Nash equilibrium* (NE).

Definition 3.4.1 (*Nash equilibrium problem*)

Solving the NEP means computing a NE, which is a collective strategy profile such that no single player can benefit from a unilateral deviation if all the other players act according to the NE. More formally:

$$\forall i \in \mathcal{N}_t \colon J_i(\mathbf{x}_{i,t}^*, \mathbf{x}_{-i,t}^*) \leq \inf\left\{ J_i(\mathbf{x}_{i,t}, \mathbf{x}_{-i,t}^*) | \mathbf{x}_{i,t} \in \Omega_{i,t} \right\}. \tag{3.18}$$

□

Hence, the collection of interdependent optimization problems (3.17) defines a game $\mathcal{G}_t$ that has to be solved repeatedly at each time step $t \in \mathbb{N}$. In particular, at the generic time slot t, there are N_t EVs connected to the parking lot, each with a different control horizon that terminates at their leaving time. The proposed solution scheme is formally reported in Algorithm 3.2.

The algorithm is based on an iterative procedure (lines 1, 17). At each time step t, the *energy manager* obtains the PV forecasting $\mathbf{r}_t$ and the reference signal $\mathbf{g}_{\mathrm{r},t}$ (line 2). Consequently a new game $\mathcal{G}_t$ is defined with all EVs in N_t connected at the time slot t (line 3). Given the overall aggregated game $\mathcal{G}_t$ we employ the well-known best response mechanism to compute an equilibrium [36]. Such a mechanism is iterative (lines 7–14); hence, let us adopt the notation $\mathbf{x}_{i,t}\{k\}$ to represent the provisional strategy at the k-th iteration of the best response process. At each iteration, the *energy manager* broadcasts the mismatch $\Delta\mathbf{g}\{k\}$ and the price coefficients $\mathbf{k}_i$ and $\mathbf{v}_i$ to all EVs (lines 8–9). Consequently, every EV attempts to reduce its cost function, solving its optimization problem over its control horizon $\mathcal{H}_{i,t}$ (line 11). The central unit terminates the iterative process when all strategies converge to an equilibrium. The optimization problems are solved at every time slot for the whole control horizons; however, only the first step of the solution is implemented (line 16).

Remark 3.4.1

The central unit broadcasts to each EV $i \in \mathcal{N}_t$ vector $\Delta\mathbf{g}\{k\}$. This is directly related to the strategies of all the other users $\mathbf{x}_{-i,t}\{k\}$ and the reference signal $\mathbf{g}_{\mathrm{r},t}$. However, due to the aggregation made by the energy manager, this vector does not contain

Algorithm 3.2 MPC control algorithm

for $t = 1, \ldots$ **do**
  Energy manager obtains $\mathbf{r}_t$ and $\mathbf{g}_{\mathrm{r},t}$
  Consider the new game $\mathscr{G}_t$
  Set $k \leftarrow 0$
  Set $\mathbf{x}_{i,t}\{0\} \leftarrow \mathbf{x}_i^0$ for all $i \in \mathcal{N}_t$
  Energy manager broadcasts $\mathbf{k}_{i,t}$ and $\mathbf{v}_{i,t}$ for all $i \in \mathcal{N}_t$
  while A NE of $\mathscr{G}_t$ is reached **do**
    Energy manager computes $\Delta\mathbf{g}\{k\}$ with (3.8) and (3.9)
    Energy manager broadcasts $\Delta\mathbf{g}\{k\}$
    for $i \in \mathcal{N}_t$ **do**
      $\mathbf{x}_{i,t}\{k+1\} \leftarrow \mathrm{argmin}_{\mathbf{x}_{i,t} \in \Omega_{i,t}} J_i\left(\mathbf{x}_{i,t}, \mathbf{x}_{-i,t}\{k\}\right)$
    end for
    Set $k \leftarrow k + 1$
  end while
  Set $\mathbf{x}_{i,t} \leftarrow \mathbf{x}_{i,t}\{k+1\}$
  Apply $\mathbf{x}_{i,t}(t+1)$ for all $i \in \mathcal{N}_t$ and discard the rest
end for

any private information. Moreover, each EV sends to the energy manager only their charging schedule without communicating any information on its personal preferences, e.g., the degradation coefficients. □

3.5 Case Study

In this section we show the performance of the proposed noncooperative approach through several numerical experiments. In particular, we consider a real scenario to study the behavior of the charging game and the impact on the parking lot.

Simulations are based on a public dataset provided by the Cambridge City Council in the United Kingdom [37]. This dataset includes the usage of seven different parking lots in the city of Cambridge with the registered length of stay in hours of cars parked and is available at [38]. The car parking data are available from October 2018 to September 2019 and are formatted using entries and exits, durations, times, and dates. The arrival and leaving records are rounded to the nearest minute integer (i.e., the maximum error of these data is one minute). As a case study, we refer in particular to the Grafton East car park. The Grafton parking lot has three levels and comprises 874 car spaces, which are approximately $4.50 \times 2.30\mathrm{m}^2$ large.

In Fig. 3.3 we show the parking building on aerial photography. As shown in Fig. 3.3, The last level of the parking lot, with a capacity of 305 cars, is located on the rooftop, which does not have any protection for the cars. Therefore, we assume the installation of a solar carport structure and, considering the installation of the model in [39], we obtain approximately $1500\mathrm{m}^2$ of solar panels corresponding to a nominal power of 200kW. As for solar data, we obtain the historical global horizontal radiance and air temperature related to the car parking coordinates from [40]. These data are available with a maximum granularity of 5 minutes.

Let us now first analyze the dataset as shown in Fig.3.4. By analyzing the average arrival and leaving time we note that the maximum number of entrances each day is between the hours of 6:00 and 10:00 while the busiest day for the total car park entrances is Friday. Moreover, By analyzing the dataset, we have that the average duration of stay is lower than 200 minutes. Given these usage data and the available granularity of solar data, we assume a time step for the proposed MPC approach of 5 minutes. This choice is a good compromise between the need of reducing the total time steps, and consequently the computational complexity, and the choice of having an accurate control

Figure 3.3: Overview of the Grafton East car park, Cambridge (UK) [41].

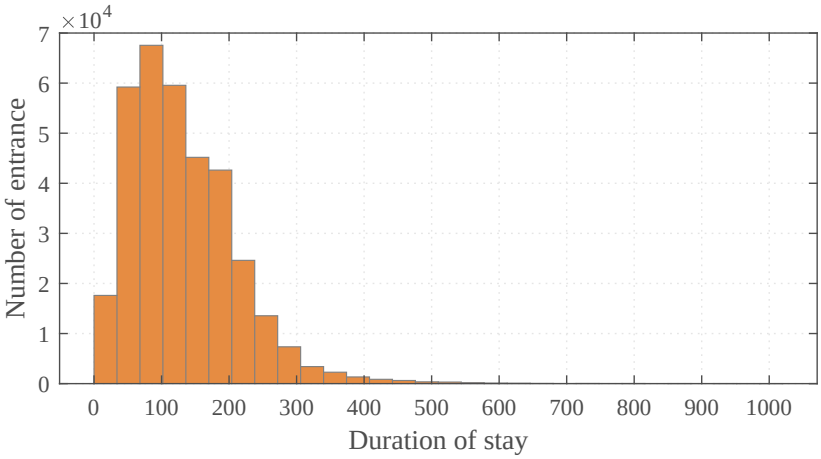

Figure 3.4: Distribution of the duration of stay in minute for the Grafton East car park.

Table 3.1: Simulation Parameters

Parameter	Min	Max	Unit
Max charging rate	10	20	kW
Max discharging rate	10	20	kW
Charging efficiency	0.95	0.99	%
Discharging efficiency	1.01	1.05	%
Leakage rate	0.97	0.99	%
Min battery level	0	10	kWh
Max battery level	40	70	kWh
Initial SoC	10	60	%
Final SoC	60	100	%

system. Consequently, we round the arrival and leaving times at the nearest 5-minutes slot, obtaining a total error of 6 minutes.

As regards the characteristic parameters for each EV, we assume a random sampling with the realistic boundaries reported in Table 3.1, which are obtained from the current technological level of EVs lithium-ion batteries. The final required SoC is sampled according to Assumption 3.2.2.

Computations for all users are done in parallel. We implement the scheduling problem in MATLAB R2020a on a desktop PC equipped with an Intel i7 core processor and 8 GB RAM. We perform the simulations considering three different scenarios:

- Scenario 1. We employ the naïve control approach through Algorithm 3.1.

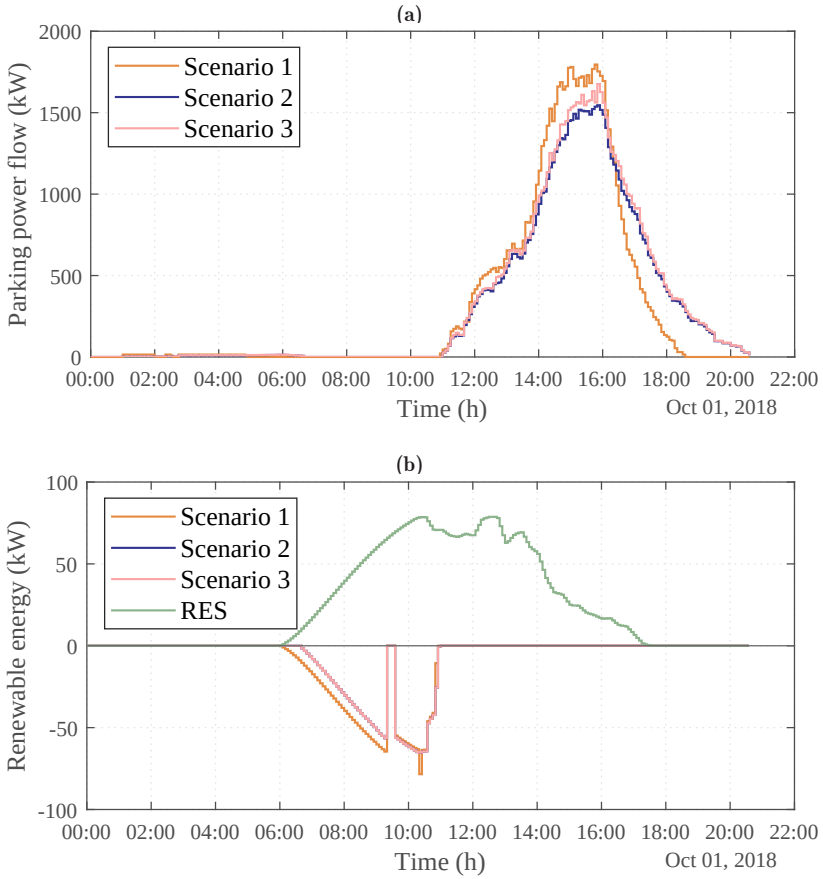

Figure 3.5: Daily inflow/outflow profile from/to the main grid in kWh/h.

- Scenario 2. We employ the novel MPC optimal control approach without considering the impact of degradation; hence, we employ Algorithm 3.2.
- Scenario 3. We employ the novel MPC optimal control approach considering the impact of degradation with the proposed *Peak-to-valley* method and a quadratic degradation function with coefficient $\gamma_1 = 0.1$; hence, we employ Algorithm 3.2.

We address the EVs scheduling for the whole simulation time. However, for the sake of space, we report here the detailed analysis considering only one day of simulation. Hence, in Fig. 3.5a we show the aggregate energy flow between the parking lot and the main grid, i.e., the energy bought from the main grid in each time slot. From the picture, it is apparent that the novel control strategy is able to reduce the energy peaks occurring when a standard charging approach is used. Furthermore, by analyzing Fig. 3.5b, where the total RES output and the RES loss is shown, it apparent that the novel approach is able also to reduce the energy loss from the PV production.

Having assessed the performance of the proposed approach to optimally control the system components over one day, let us now investigate the effects on the long term by using the following two indicators:

1) self-supply index - It is defined as the percentage of the RES lost to the energy totally produced:

$$\mathrm{EL}_T = \frac{\sum_{t=1}^{T} r_l(t)}{\sum_{t=1}^{T} r(t)} \tag{3.19}$$

2) total-mismatch index - It is defined as the sum of the total parking power mismatch:

$$\mathrm{TM}_T = \sum_{t=1}^{T} \Delta \mathrm{g}(t). \tag{3.20}$$

As regards the *self-supply* index we have a value of 0.29, 0.38, and 0.39 for Scenario 1, 2, and 3, respectively. By observing these results it is clear that the proposed approach takes advantage of the RES and consequently of the solar facility. Conversely, as regards the *total-mismatch* we obtain a value of 28.33, 25.02, and 24.94 GW in Scenario 1, 2, and 3, respectively. The best performance is thus achieved by the proposed control approach (i.e., Scenario 3) due to its ability to increase the predictability of the parking lot. Finally, it should be noted that, when the degradation is considered, the values of the two aforementioned indices are slightly poorer than those of Scenario 2.

3.6 Conclusion

The use of electric vehicles is being widespread mainly due to their potential in reducing greenhouse gas emissions. Coping with this issue, we propose a novel noncooperative energy market for battery charging, based on a smart pricing mechanism that is able to increase the predictability of the aggregate load from the distribution grid point of view, while minimizing the degradation wearing costs of batteries. The evidence from a yearly basis analysis conducted on a real scenario shows that the proposed approach achieves higher performance than a standard one.

Future work should focus on including additional terms in the objective function and technical constraints affecting the operations of system components.

References

[1] Oda, T., Aziz, M., Mitani, T., Watanabe, Y., and Kashiwagi, T., "Mitigation of congestion related to quick charging of electric vehicles based on waiting time and cost–benefit analyses: A japanese case study," *Sustainable cities and society*, vol. 36, pp. 99–106, 2018.

[2] Hosseini, S. M., Carli, R., and Dotoli, M., "Robust optimal energy management of a residential microgrid under uncertainties on demand and renewable power generation," *IEEE Trans. Autom. Sci. Eng.*, vol. 18, no. 2, pp. 618–637, 2021.

[3] Laha, A., Yin, B., Cheng, Y., Cai, L. X., and Wang, Y., "Game theory based charging solution for networked electric vehicles: A location-aware approach," *IEEE Transactions on Vehicular Technology*, vol. 68, no. 7, pp. 6352–6364, 2019.

[4] Das, H., Rahman, M., Li, S., and Tan, C., "Electric vehicles standards, charging infrastructure, and impact on grid integration: A technological review," *Renewable and Sustainable Energy Reviews*, vol. 120, p. 109 618, 2020.

[5] Aliu, A., Marjanovic, O., and Parisio, A., "Charge/discharge event model for electric vehicles with predictive control application," in *2021 29th Mediterranean Conference on Control and Automation (MED)*, IEEE, 2021, pp. 192–197.

[6] Bellocchi, S., Manno, M., Noussan, M., and Vellini, M., "Impact of grid-scale electricity storage and electric vehicles on renewable energy penetration: A case study for italy," *Energies*, vol. 12, no. 7, p. 1303, 2019.

[7] Thompson, A. W., "Economic implications of lithium ion battery degradation for vehicle-to-grid (v2x) services," *Journal of Power Sources*, vol. 396, pp. 691–709, 2018.

[8] Hosseini, S. S., Badri, A., and Parvania, M., "The plug-in electric vehicles for power system applications: The vehicle to grid (v2g) concept," in *2012 IEEE International Energy Conference and Exhibition (ENERGYCON)*, IEEE, 2012, pp. 1101–1106.

[9] Mohamed, A., Salehi, V., Ma, T., and Mohammed, O., "Real-time energy management algorithm for plug-in hybrid electric vehicle charging parks involving sustainable energy," *IEEE Transactions on Sustainable Energy*, vol. 5, no. 2, pp. 577–586, 2013.

[10] Liang, H., Choi, B. J., Zhuang, W., and Shen, X., "Optimizing the energy delivery via v2g systems based on stochastic inventory theory," *IEEE Transactions on Smart Grid*, vol. 4, no. 4, pp. 2230–2243, 2013.

[11] Wei, Z., Li, Y., Zhang, Y., and Cai, L., "Intelligent parking garage ev charging scheduling considering battery charging characteristic," *IEEE transactions on industrial electronics*, vol. 65, no. 3, pp. 2806–2816, 2017.

[12] Zhang, T., Chen, W., Han, Z., and Cao, Z., "Charging scheduling of electric vehicles with local renewable energy under uncertain electric vehicle arrival and grid power price," *IEEE Transactions on Vehicular Technology*, vol. 63, no. 6, pp. 2600–2612, 2013.

[13] Wang, M., Liang, H., Zhang, R., Deng, R., and Shen, X., "Mobility-aware coordinated charging for electric vehicles in vanet-enhanced smart grid," *IEEE Journal on Selected Areas in Communications*, vol. 32, no. 7, pp. 1344–1360, 2014.

[14] Baure, G. and Dubarry, M., "Durability and reliability of ev batteries under electric utility grid operations: Impact of frequency regulation usage on cell degradation," *Energies*, vol. 13, no. 10, p. 2494, 2020.

[15] Świerczyński, M., Stroe, D. I., Lærke, R., *et al.*, "Field experience from li-ion bess delivering primary frequency regulation in the danish energy market," *Ecs Transactions*, vol. 61, no. 37, p. 1, 2014.

[16] Han, S. and Han, S., "Economic feasibility of v2g frequency regulation in consideration of battery wear," *Energies*, vol. 6, no. 2, pp. 748–765, 2013.

[17] Wang, R., Wang, P., and Xiao, G., "Two-stage mechanism for massive electric vehicle charging involving renewable energy," *IEEE Transactions on Vehicular Technology*, vol. 65, no. 6, pp. 4159–4171, 2016.

[18] Liu, Y., Deng, R., and Liang, H., "Game-theoretic control of phev charging with power flow analysis," *AIMS Energy*, vol. 4, no. 2, pp. 379–396, 2016.

[19] Liu, H., Hu, Z., Song, Y., and Lin, J., "Decentralized vehicle-to-grid control for primary frequency regulation considering charging demands," *IEEE Transactions on Power Systems*, vol. 28, no. 3, pp. 3480–3489, 2013.

[20] Li, X., Huang, Y., Huang, J., *et al.*, "Modeling and control strategy of battery energy storage system for primary frequency regulation," in *2014 International Conference on Power System Technology*, IEEE, 2014, pp. 543–549.

[21] Ruiz, N., Cobelo, I., and Oyarzabal, J., "A direct load control model for virtual power plant management," *IEEE Transactions on Power Systems*, vol. 24, no. 2, pp. 959–966, 2009.

[22] Zhang, L. and Li, Y., "A game-theoretic approach to optimal scheduling of parking-lot electric vehicle charging," *IEEE Transactions on Vehicular Technology*, vol. 65, no. 6, pp. 4068–4078, 2015.

[23] Beaude, O., Lasaulce, S., and Hennebel, M., "Charging games in networks of electrical vehicles," in *2012 6th International Conference on Network Games, Control and Optimization (NetGCooP)*, IEEE, 2012, pp. 96–103.

[24] Darivianakis, G., Georghiou, A., Smith, R. S., and Lygeros, J., "The power of diversity: Data-driven robust predictive control for energy-efficient buildings and districts," *IEEE Transactions on Control Systems Technology*, vol. 27, no. 1, pp. 132–145, 2017.

[25] Charles Lawrence Kamuyu, W., Lim, J. R., Won, C. S., and Ahn, H. K., "Prediction model of photovoltaic module temperature for power performance of floating pvs," *Energies*, vol. 11, no. 2, p. 447, 2018.

[26] Scarabaggio, P., Carli, R., Cavone, G., and Dotoli, M., "Smart Control Strategies for Primary Frequency Regulation through Electric Vehicles: A Battery Degradation Perspective," *Energies*, vol. 13, no. 17, p. 4586, 2020. DOI: 10.3390/en13174586.

[27] Maheshwari, A., Paterakis, N. G., Santarelli, M., and Gibescu, M., "Optimizing the operation of energy storage using a non-linear lithium-ion battery degradation model," *Applied Energy*, vol. 261, p. 114 360, 2020.

[28] Shi, Y., Xu, B., Zhang, B., and Wang, D., "Leveraging energy storage to optimize data center electricity cost in emerging power markets," in *Proceedings of the Seventh International Conference on Future Energy Systems*, 2016, pp. 1–13.

[29] Xu, B., Oudalov, A., Ulbig, A., Andersson, G., and Kirschen, D. S., "Modeling of lithium-ion battery degradation for cell life assessment," *IEEE Transactions on Smart Grid*, vol. 9, no. 2, pp. 1131–1140, 2016.

[30] Koller, M., Borsche, T., Ulbig, A., and Andersson, G., "Defining a degradation cost function for optimal control of a battery energy storage system," in *2013 IEEE Grenoble Conference*, IEEE, 2013, pp. 1–6.

[31] Millner, A., "Modeling lithium ion battery degradation in electric vehicles," in *2010 IEEE Conference on Innovative Technologies for an Efficient and Reliable Electricity Supply*, IEEE, 2010, pp. 349–356.

[32] Ortega-Vazquez, M. A., "Optimal scheduling of electric vehicle charging and vehicle-to-grid services at household level including battery degradation and price uncertainty," *IET Generation, Transmission & Distribution*, vol. 8, no. 6, pp. 1007–1016, 2014.

[33] Laresgoiti, I., Käbitz, S., Ecker, M., and Sauer, D. U., "Modeling mechanical degradation in lithium ion batteries during cycling: Solid electrolyte interphase fracture," *Journal of Power Sources*, vol. 300, pp. 112–122, 2015.

[34] Rychlik, I., "A new definition of the rainflow cycle counting method," *International journal of fatigue*, vol. 9, no. 2, pp. 119–121, 1987.

[35] "Standard Practices for Cycle Counting in Fatigue Analysis," American Society for Testing and Materials, West Conshohocken, PA, USA, Standard, Jun. 2017.

[36] Parise, F., Gentile, B., Grammatico, S., and Lygeros, J., "Network aggregative games: Distributed convergence to nash equilibria," in *2015 54th IEEE Conference on Decision and Control (CDC)*, IEEE, 2015, pp. 2295–2300.

[37] *Grafton East car park*, [Online; accessed 25. Feb. 2022], 2022. [Online]. Available: https://www.cambridge.gov.uk/grafton-east-car-park.

[38] *Cambridge City Parking Data | Cambridgeshire Insight Open Data*, [Online; accessed 25. Feb. 2022], 2022. [Online]. Available: https://data.cambridgeshireinsight.org.uk/dataset/cambridge-city-parking-data.

[39] *Carport solar mounting system Details - CY Solar Technology Co., Ltd.* [Online; accessed 25. Feb. 2022], 2022. [Online]. Available: https://cysolarmounts.com/product/solar_carport_mounting_system.

[40] *Solcast - Solar Forecasting & Solar Irradiance Data*, [Online; accessed 25. Feb. 2022], 2022. [Online]. Available: https://solcast.com.

[41] *Google Earth*, [Online; accessed 25. Feb. 2022], 2021. [Online]. Available: https://www.google.it/intl/it/earth.

Chapter 4

Stochastic Control for Energy Scheduling with Variable Distributed Generation

Abstract

This chapter focuses on the robust optimal on-line scheduling of a grid-connected smart energy system, where users are equipped with *non-controllable loads* (NCLs) and *controllable loads* (CLs), shared *renewable energy sources* (RESs) and *energy storage systems* (ESSs). Leveraging on the pricing signals gathered from the power distribution grid and the predicted values for local production and demand, the energy activities inside the smart energy system are decided by an energy manager in terms of the charging/discharging strategies of the ESS as well as the consumption schedule of the CLs and the profile of the energy exchanged with the grid. Differently from literature contributions commonly focused on deterministic optimal control schemes, to cope with the uncertainty that affects the forecast of the inflexible demand profile and the renewable production curve, we propose a Stochastic *model predictive control* (MPC) approach aimed at minimizing the community energy costs. The effectiveness of the method is validated through numerical experiments on the marina of Ballen, Samsø (Denmark), where a smart energy system with shared photovoltaic panels and a battery energy storage system supplies the local harbor community. Finally, the comparison with a standard deterministic optimal control approach shows that the proposed stochastic MPC achieves higher performance in terms of minimized energy cost and maximized self-consumption of on-site production.

Contents

4.1 Introduction

Improving the efficiency, sustainability, and affordability of power systems with respect to the expected energy needs is nowadays a challenging strategic objective that is being spurred worldwide by pressing climate change and environmental issues [1]. A powerful solution contributing to the required green transformation is represented by the so-called *smart energy systems* [2]. This new paradigm of production and consumption indeed brings various potential benefits, both to the involved service operators and final users, ranging from the reduction of procurement costs to the optimization of the demand curve, from the improvement of the power quality and reliability to the high penetration of distributed generation and storage [3].

In particular, in last years the community action on the use of renewable energy has increased remarkably, spurred on by several energy efficiency initiatives as well as financial incentives [4].

Nevertheless, the full implementation of smart energy systems present various challenges. First, an organizational paradigm for the management of energy activities has to be defined. Different structures are envisioned; however, the commonly employed framework relies on the presence of a manager who is responsible of managing and trading energy activities among all the devices according to a predefined goal [5]. Independently from the implemented architecture, the success of smart energy systems relies on how the storage system is optimally dispatched. After all, final users inside the smart energy systems expect a tangible financial and sustainable benefit. As a consequence, the necessity of developing an effective optimal energy scheduling framework tackling such an expected objective is apparent.

4.1.1 Literature Review

Recently, smart energy systems receive increasing attention from researchers. A first class of studies deals with the day-ahead scheduling of smart energy systems comprising consumers, prosumers, shared renewable energy sources as well as connection to a distribution grid. For instance, Hossain *et al.* [6] present a day-ahead scheduling of the battery charging-discharging profile aimed at minimizing energy cost while considering its degradation effects. Marzband *et al.* [7] propose a day-ahead scheduling for a microgrid of residential users integrated with non-dispatchable and dispatchable energy resources and storage assets. Studies such as [6], [7] usefully investigate the potential role of storage systems in smart energy systems from an open-loop point of view. Nevertheless, the effective deployment of smart energy systems requires a suitable closed-loop control mechanism to utilize the most recent predicted information, thus making the smart energy systems actually attractive also from the operational perspective.

For this reason, another wide thread of research focus on the online control strategies for the smart energy systems management with shared generation and storage. Among the several explored techniques, MPC is recognized as particularly valuable for such a kind of application [8]. For instance, Pezeshki *et al.* [9] propose an MPC-based algorithm for optimally controlling a ESS in presence of high penetration of renewables. The control goal is twofold: minimizing the energy cost and smoothing the load profile, while the photovoltaic generation is predicted using a neural network. Similarly, in [10] an MPC for the optimal control of a microgrid comprising consumers, shared photovoltaic panels and a ESS under time-varying pricing is presented. Numerical experiments on a realistic scenario show that the MPC control allows exploiting the 90% of the photovoltaic production, while reducing the yearly energy cost and improving the self-supply respectively by 8.2% and 1.6% with respect to a rule-based control scheme. Further receding horizon schemes are developed in [11]–[13] aimed at scheduling the optimal operations of behind-the-meter. Despite the rich state of the art on the MPC techniques, very few research studies on on-line scheduling pay attention to properly tackle the errors on the forecasts and system actual operations. Since reaching an optimal solution is not yet guaranteed due to the presence of uncertainty, seeking robust solutions is still among the real research challenges in the on-line scheduling problem. For instance, Lv *et al.* [14] propose a robust MPC algorithm to adjust the optimal control strategies against the inaccuracies of local generation and load profile prediction. Differently, Hossain *et al.* [15] present a stochastic MPC approach also considering the uncertainty that affects the electricity prices.

Although the cited studies [14], [15] as well as further works on robust and stochastic MPC such as [16]–[18] define effective closed-loop control approaches, the corresponding performance are evaluated on a short time window of analysis, commonly set to one day, thus not providing a thorough assessment of the actual expected capabilities at long-term. In addition, only the economic aspect in terms of energy cost savings is commonly addressed, while self-reliance performance, such as yearly self-supply and energy independence indicators, are not explicitly assessed.

4.1.2 Chapter Contribution

To cope the above-mentioned gap, this chapter proposes a stochastic MPC to address the uncertainty affecting both measurements (i.e., inflexible demand profile) and models (renewable production) and thus robustify the resolution of the proposed smart energy system scheduling problem. Leveraging on the pricing signals gathered from the power grid and the predicted values for local production and demand, the energy activities inside the community are decided by an *energy manager* (EM) in terms of the charging/discharging strategies of the ESS as well as the consumption schedule of the CLs and the profile of the energy exchanged with the grid. The final goal aims at minimizing the community energy cost. The effectiveness of the proposed method is validated through numerical experiments on the scenario presented in [10]: the marina of Ballen, Samsø (Denmark), where a smart energy system with shared photovoltaic panels and a battery energy storage system supplies the local harbor community. The method is validated through numerical experiments conducted on a yearly basis analysis. In particular, the comparison with standard deterministic optimal control approaches shows that the proposed stochastic MPC achieves higher performances in terms of minimized energy cost and maximized self-consumption of on-site production.

4.2 System Model

In this section we present the model of the proposed smart energy systems that includes NCLs, CLs, shared RESs and a ESS. The energy activities inside the smart energy systems are decided by the EM, that optimally determines the charging/discharging strategies of the ESS, the operations of the CLs, and the profile of the energy exchanged with the grid. All decisions are based on the pricing signals acquired from the power grid and the forecast related to the overall demand of NCLs and the total generation of RESs. We assume that the EM is connected to all smart energy systems components through a digital communication infrastructure.

The EM applies a rolling horizon strategy, thus we consider a prediction and a control horizon. The value of a cost function computed over the time horizon is repetitively optimized at subsequent time slots, while only the control strategies corresponding to the first time step are applied according to the receding horizon concept [19]. At the generic time t, we consider an identical prediction and control horizon defined as $\mathcal{H}(t) := \{t{+}1, ..., t{+}h, ..., t{+}H\}$ including H discrete time slots with equal length Δh.

The modeling of system components is discussed in detail as follows.

4.2.1 Shared Renewable Energy Sources

First of all, we assume that the community incorporates one or more shared RES (e.g., a PV system). We define for each time slot t a vector $\mathbf{r}(t) := (r(t{+}1), ..., r(t{+}h), ..., r(t{+}H))^\top$ that collects the actual aggregated profile of energy produced by all the RESs in the time window $\mathcal{H}(t)$.

The EM cannot exactly predict the future output of RESs, since variations in weather conditions deeply impact their production. Consequently, we assume that the EM is able to forecast the RESs production for the time window $\mathcal{H}(t)$ using a prediction algorithm based on weather forecasting. For each time slot t, we thus define a vector $\tilde{\mathbf{r}}(t) := (\tilde{r}(t{+}1), ..., \tilde{r}(t{+}h), ..., \tilde{r}(t{+}H))^\top$ collecting the forecasted aggregated profile of energy produced by the RESs.

4.2.2 Non-Controllable Loads

We assume that the community-based microgrid includes several NCLs, i.e., inflexible loads with a demand profile that cannot be modulated. We define for each time slot t a vector $\mathbf{b}(t) := (b(t{+}1), ..., b(t{+}h), ..., b(t{+}H))^\top$ collecting the actual aggregated energy profile of NCLs consumption in the time window $\mathcal{H}(t)$.

Similarly to the RESs, this vector is unknown for the EM. Consequently, we assume that EM is able to forecast the aggregate NCLs profile using a prediction algorithm based on historical consumption data. For each time slot t, we thus define a vector $\tilde{\mathbf{b}}(t) := (\tilde{b}(t+1), ..., \tilde{b}(t+h), ..., \tilde{b}(t+H))^\top$ collecting the forecasted aggregated profile of energy required by the NCLs.

4.2.3 Energy Based Controllable Loads

Moreover, we consider a group of *energy-based controllable loads* (ECLs), i.e., flexible loads whose operation can be in some way modulated on a favorable schedule. Thanks to their inherent flexibility, the EM can control these loads in order to mitigate any eventual power imbalance in the microgrid. Without loss of generality, let us consider the modeling of one ECL. In particular, we define for each time slot t the ECL profile as $\mathbf{c}(t) := (c(t+1), ..., c(t+h), ..., c(t+H))^\top$. Note that this profile is directly controlled by the EM thus is not affected by uncertainty and forecasting errors. Vector $\mathbf{c}(t)$ has to be computed in accordance with the following constraint:

$$\underline{\mathbf{c}}(t) \leq \mathbf{c}(t) \leq \overline{\mathbf{c}}(t) \tag{4.1}$$

where $\underline{\mathbf{c}}(t) := (\underline{c}(t+1), ..., \underline{c}(t+h), ..., \underline{c}(t+H))^\top$ and $\overline{\mathbf{c}}(t) := (\overline{c}(t+1), ..., \overline{c}(t+h), ..., \overline{c}(t+H))^\top$ are vectors collecting the time-varying bounds. Lastly, we assume that for each time window $\mathcal{H}(t)$ the ECL must fulfill a predetermined time-varying quantity $\overline{C}(t)$ as:

$$\mathbf{c}(t)^\top \mathbf{1}_H = \overline{C}(t) \tag{4.2}$$

where $\mathbf{1}_H$ is a all-ones column vector of H entries.

4.2.4 Thermal Based Controllable Loads

We include in the smart energy system also a group of *thermal controllable loads* (TCLs), i.e., loads of heating and conditioning systems controlled by users' comfort. These loads take advantage of the thermal inertia of buildings or large-scale facilities (e.g., school, gym...) to smooth their impact on the energy demand of the overall community, while ensuring the occupants' well-being. Without loss of generality, let us consider the modeling of one TCL. In particular, we assume that a given facility employs an HVAC (heating, ventilation and air conditioning) heat pump to maintain the desired thermal comfort conditions. We use the discrete time model presented in [20] to represent the facility indoor temperature:

$$\begin{aligned} T(t+h) = e^{\frac{\Delta h}{\tau}} T(t+h-1) \\ + (1 - e^{\frac{\Delta h}{\tau}})(T^e(t+h) - \pi y(t+h)),\ h \in \mathcal{H}(t) \end{aligned} \tag{4.3}$$

where $T(t+h)$ and $T^e(t+h)$ are the indoor and outdoor temperature at time slot $t+h$, respectively, τ is the constant time of the first order dynamic of the facility zone temperature, and π is the temperature gain of the heat pump. Note that vector $\mathbf{T}^e(t) := (T^e(t+1), ..., T^e(t+h), ..., T^e(t+H))^\top$ collecting the outdoor temperature profile in the time window $\mathcal{H}(t)$ is an unknown input parameter. Similarly to RESs and NCLs, we assume that temperature forecasting are available for the time window as $\tilde{\mathbf{T}}^e(t) := (\tilde{T}^e(t+1), ..., \tilde{T}^e(t+h), ..., \tilde{T}^e(t+H))^\top$. Conversely, the vector $\mathbf{T}(t) := (T(t+1), ..., T(t+h), ..., T(t+H))^\top$ collects the indoor temperature profile is a control variable to be computed in accordance with the following constraint:

$$\underline{\mathbf{T}}(t) \leq \mathbf{T}(t) \leq \overline{\mathbf{T}}(t) \tag{4.4}$$

where $\underline{\mathbf{T}}(t) := (\underline{T}(t+1), ..., \underline{T}(t+h), ..., \underline{T}(t+H))^\top$ and $\overline{\mathbf{T}}(t) := (\overline{T}(t+1), ..., \overline{T}(t+h), ..., \overline{T}(t+H))^\top$ denote the vectors of lower and upper bounding of the indoor temperature that represent thermal comfort preferences. Lastly, vector $\mathbf{y}(t) := (y(t+1), ..., y(t+h), ..., y(t+$

$H))^\top$ collecting the heat pump energy consumption profile is a control variable to be computed in accordance with:

$$\mathbf{0}_H \leq \mathbf{y}(t) \leq \bar{y}\mathbf{1}_H \tag{4.5}$$

where $\bar{y}$ is the maximum energy that the heat pump can consume in one time slot and $\mathbf{0}_H$ is a column vector of H zero entries.

4.2.5 Energy Storage System

For the sake of providing flexibility to the community energy scheduling, the proposed microgrid model comprehends also a ESS. To model the charging/discharging activities of the ESS, at each time step t, we define vectors $\mathbf{s}_c(t) := (s_c(t+1), ..., s_c(t+h), ..., s_c(t+H))^\top$ and $\mathbf{s}_d(t) := (s_d(t+1), ..., s_d(t+h), ..., s_d(t+H))^\top$ collecting respectively the control variables representing the profiles of energy stored/released in/from the ESS. Moreover, we define the vector $\mathbf{L}(t) := (L(t+1), ..., L(t+h), ..., L(t+H))^\top$ collecting the charge level profile of the ESS. We assume that this profile follows the following discrete equation:

$$L(t+h) = L(t+h-1) + \eta_c s_c(t+h) - s_d(t+h)/\eta_d,\ h \in \mathcal{H}(t) \tag{4.6}$$

where we define η_c and η_d as the charging and discharging efficiencies, respectively. The maximum charge/discharge level is also bounded by the minimum and maximum ESS capacity $\underline{L}$ and $\overline{L}$ as follows:

$$\begin{aligned}\underline{L} - L(t+h-1) \leq \eta_c s_c(t+h) - s_d(t+h)/\eta_d \\ \leq \overline{L} - L(t+h-1),\ h \in \mathcal{H}(t).\end{aligned} \tag{4.7}$$

Lastly, by denoting $\overline{s}$ and $\underline{s}$ as the maximum charging and discharging rates, the following technical constraints must be satisfied:

$$\mathbf{0}_H \leq \mathbf{s}_c(t) \leq \overline{s}\mathbf{1}_H,\ \mathbf{0}_H \leq \mathbf{s}_d(t) \leq \underline{s}\mathbf{1}_H. \tag{4.8}$$

4.2.6 Grid Energy Flow and Energy Cost

Nevertheless, a demand-supply balance constraint should be fulfilled in the smart energy systems at each time slot h as:

$$\mathbf{b}(t) + \mathbf{c}(t) + \mathbf{y}(t) - \mathbf{r}(t) + \mathbf{s}_c(t) - \mathbf{s}_d(t) = \mathbf{g}_i(t) - \mathbf{g}_o(t) \tag{4.9}$$

where vectors $\mathbf{g}_i(t) := (g_i(t+1), ..., g_i(t+h), ..., g_i(t+H))^\top$ and $\mathbf{g}_o(t) := (g_o(t+1), ..., g_o(t+h), ..., g_o(t+H))^\top$ contains control variables representing the profile of energy received/transferred from/to the power grid, respectively. The EM can buy energy from the main grid with a time-varying price. Conversely, we assume that the EM cannot sell energy to the main grid but only give it away without any monetary exchange (e.g., as in the European energy markets). Therefore, we express the cost incurred by the community to exchange the energy profile $\mathbf{g}_i(t)$ with the power grid over the whole time window $\mathcal{H}(t)$ as:

$$\mathbf{J}(\mathbf{g}_i(t)) = \mathbf{k}(t)^\top \mathbf{g}_i(t) \tag{4.10}$$

where $\mathbf{k}(t) := (k(t+1), ..., k(t+h), ..., k(t+H))^\top$ collects the known time-varying buying cost coefficients.

4.3 Stochastic Energy Scheduling

Model Predictive Control is recognized as particularly valuable for the control of smart energy systems. In fact, MPC can use both predictions of future disturbances (e.g., demand fluctuations, weather, etc.) and given requirements (e.g., comfort ranges), to anticipate the energy needs of a system and optimize its operations. In fact, it relies on a dynamical model of the system, used to predict the system behavior. In particular,

an optimization problem, based on the dynamical model, is solved to optimize the performance of the system over the chosen control horizon. The optimization problem is solved over the time control horizon, however, only the first action is applied. Accordingly, the system is observed and the dynamical model is updated.

Having defined the dynamical model of the community-based microgrid and the pricing scheme, let us now define the optimal control strategy that allows the EM to compute its optimal operations aimed at minimizing of the community energy cost. In detail, we consider as objective function the cost as defined in (4.10); however, since the power flow with the main grid cannot be directly controllable by the EM, we redefine the cost function employing (4.9) as:

$$\mathbf{J}(\mathbf{u}(t), \mathbf{w}(t)) = \mathbf{k}(t)^\top (\mathbf{b}(t) + \mathbf{c}(t) + \mathbf{y}(t) - \mathbf{r}(t) + \mathbf{s}_c(t) - \mathbf{s}_d(t) + \mathbf{g}_o(t)) \quad (4.11)$$

where, for the sake of clarity, we collect the control variables in the vector $\mathbf{u}(t) = (\mathbf{c}(t), \mathbf{T}(t), \mathbf{y}(t), \mathbf{L}(t), \mathbf{s}_c(t), \mathbf{s}_d(t), \mathbf{g}_o(t))^\top$ and the uncertain parameters in the vector $\mathbf{w}(t) = (\mathbf{b}(t), \mathbf{r}(t), \mathbf{T}^e(t))^\top$. Note that we make explicit the dependence of the cost from the uncertain RESs production, NCLs demand, and outdoor temperature.

Nevertheless, by assuming a perfect knowledge of the future, i.e., to have a perfect forecasting system, we can define the optimal energy scheduling problem over the time window $\mathcal{H}(t)$ as:

$$\begin{aligned} \underset{\mathbf{u}(t)}{\text{minimize}} \quad & \mathbf{J}\left(\mathbf{u}(t), \mathbf{w}(t)\right) \\ \text{subject to} \quad & (4.1) - (4.9). \end{aligned} \quad (4.12)$$

Under the aforementioned assumption, (4.12) is a linear programming problem that consists in determining the $10H$ real decision variables $\mathbf{u}(t)$ which minimize the objective function in (4.11) and meet the $10H$ constraints in (4.1)-(4.9).

4.3.1 Expected Value Approach

In the proposed framework, the energy cost is a function of aleatory variables; therefore, the cost function is not only dependent on the decision variables. For instance, a wrong forecasting may lead to a wrong selection of the scheduling strategy and therefore to a higher cost than the expected one.

The most straightforward way to approach to solve this problem is to substitute the uncertain variables with their forecasting and therefore optimize the following deterministic cost function:

$$\tilde{\mathbf{J}}(\mathbf{u}(t), \tilde{\mathbf{w}}(t)) = \mathbf{k}(t)^\top \left(\tilde{\mathbf{b}}(t) + \mathbf{c}(t) + \mathbf{y}(t) - \tilde{\mathbf{r}}(t) + \mathbf{s}_c(t) - \mathbf{s}_d(t) + \mathbf{g}_o(t)\right) \quad (4.13)$$

where $\tilde{\mathbf{w}}(t) = (\tilde{\mathbf{b}}(t), \tilde{\mathbf{r}}(t), \tilde{\mathbf{T}}^e(t))^\top$.

It is worth pointing out that (4.11) defines the cost incurred by the community after the realization of the stochastic variables, while (4.13) indicates how much the community is presumed to pay employing the available forecasting. Therefore, we can define the an approximated optimal energy scheduling problem over the time window $\mathcal{H}(t)$ as:

$$\begin{aligned} \underset{\mathbf{u}(t)}{\text{minimize}} \quad & \tilde{\mathbf{J}}(\mathbf{u}(t), \tilde{\mathbf{w}}(t)) \\ \text{subject to} \quad & (4.1) - (4.9). \end{aligned} \quad (4.14)$$

4.3.2 Approximated Stochastic Approach

The main issue in employing the expected value approach is that the presence of a stochastic variable may lead to a non-optimal energy scheduling. To cope with this issue, several works make use of the Stochastic programming approach. This approach is based

Algorithm 4.1 Energy scheduling MPC algorithm

Input: $\tilde{\mathbf{w}}(t), \mathbf{k}(t), \mathbf{T}(0), \mathbf{L}(0), \underline{\mathbf{c}}(t), \overline{\mathbf{c}}(t), \overline{C}(t), \underline{\mathbf{T}}(t), \overline{\mathbf{T}}(t)$
1: **for** $t = 0, 1, 2, ...$ **do**
2: Get price coefficients $\mathbf{k}(t)$ from the main grid
3: Get users' preferences $\underline{\mathbf{c}}(t), \overline{\mathbf{c}}(t), \overline{C}(t), \underline{\mathbf{T}}(t)$ and $\overline{\mathbf{T}}(t)$
4: Generate $\tilde{\mathbf{b}}(t)$ based on historical data
5: Generate $\tilde{\mathbf{r}}(t)$ and $\tilde{\mathbf{T}}_e(t)$ based on weather data
6: Get initial state conditions $T(t)$ and $L(t)$
7: Solve the optimization problem (4.14)
8: Apply only $c(t+1), y(t+1), s_c(t+1)$ and $s_d(t+1)$
9: **end for**
Output: $\mathbf{c}(t), \mathbf{y}(t), \mathbf{s}_c(t), \mathbf{s}_d(t)$

on the assumption that even if the future values are not unknown, it is still possible to define a *probability density function* (PDF) able to describe in some way the random variable.

In fact, the cost function (4.13) is a stochastic variable itself [21], with the expected value defined as:

$$\mathbb{J}\left(\mathbf{u}(t), \mathbf{w}(t)\right) = \mathbb{E}[\mathbf{J}\left(\mathbf{u}(t), \mathbf{w}(t)\right)]\,. \tag{4.15}$$

However, determining the exact solution of (4.15) is possible only in a few cases. An alternative is to replace the random variable by a number of random samples and solve the resulting deterministic optimization problem [22]. This approach is usually called *sample average approximation* (SAA) and is based on having a PDF from which N *independent and identically distributed* (IID) random samples of the stochastic variable can be obtained.

In our case, we can obtain a vector of samples of the three variables from their respective PDFs defined as $\mathbf{r}_n(t) := (r_n(t+1), ..., r_n(t+h), ..., r_n(t+H))^\top$, $\mathbf{b}_n(t) := (b_n(t+1), ..., b_n(t+h), ..., b_n(t+H))^\top$ and $\mathbf{T}^e_n(t) := (T^e_n(t+1), ..., T^e_n(t+h), ..., T^e_n(t+H))^\top$ and then define an approximated stochastic cost function as:

$$\hat{\mathbb{J}}\left(\mathbf{u}(t), \hat{\mathbf{w}}(t)\right) = \frac{1}{N}\sum_{n=1}^{N} \mathbf{J}_n(\mathbf{u}(t), \mathbf{w}_n(t)) \tag{4.16}$$

where $\mathbf{w}_n(t) = (\mathbf{b}_n(t+h), \mathbf{r}_n(t+h), \mathbf{T}^e_n(t+h))^\top$ is a sample vector of the three stochastic variables, $\hat{\mathbf{w}}(t) = (\mathbf{w}_1(t), ..., \mathbf{w}_n(t), ..., \mathbf{w}_N(t))$ collects all the N samples and $\mathbf{J}_n(\cdot)$ is the cost function defined with the nth sample.

Hence, we can now define the approximated stochastic optimal control problem as:

$$\begin{aligned} \underset{\mathbf{u}(t)}{\text{minimize}} \quad & \hat{\mathbb{J}}\left(\mathbf{u}(t), \hat{\mathbf{w}}(t)\right) \\ \text{subject to} \quad & (4.1) - (4.9). \end{aligned} \tag{4.17}$$

4.3.3 Energy Scheduling MPC Algorithm under Uncertainty

Based on the two aforementioned approaches, we now define two algorithms for the community energy scheduling under uncertainty. In particular, we iteratively solve the two proposed optimal control problems (4.14) and (4.17) at each time slot t in accordance with the rolling horizon approach for the whole simulation period.

The first steps are the same for Algorithm 1 and Algorithm 2. At each time instant t, the following steps are repeated. Firstly, the EM receives the updated energy price coefficients from the main grid (line 2) and collects the users' preference in terms of controllable loads and indoor temperature (line 3). Then, the EM generates the NCLs' forecasting based on historical data (line 4) and generates the RESs forecasting based on weather data (line 5). Moreover, it updates the initial values of state variables for indoor temperature and storage charge level (line 6).

Algorithm 4.2 Stochastic energy scheduling MPC algorithm

Input: $\tilde{\mathbf{w}}(t), \mathbf{k}(t), \mathbf{T}(0), \mathbf{L}(0), \underline{\mathbf{c}}(t), \overline{\mathbf{c}}(t), \overline{C}(t), \underline{\mathbf{T}}(t), \overline{\mathbf{T}}(t)$
1: **for** $t = 0, 1, 2, ...$ **do**
2: Get price coefficients $\mathbf{k}(t)$ from the main grid
3: Get users' preferences $\underline{\mathbf{c}}(t), \overline{\mathbf{c}}(t), \overline{C}(t), \underline{\mathbf{T}}(t)$ and $\overline{\mathbf{T}}(t)$
4: Generate $\tilde{\mathbf{b}}(t)$ based on historical data
5: Generate $\tilde{\mathbf{r}}(t)$ and $\tilde{\mathbf{T}}_e(t)$ based on weather data
6: Get initial state conditions $T(t)$ and $L(t)$
7: Generate $3N$ PDFs based on $\tilde{\mathbf{b}}(t), \tilde{\mathbf{r}}(t)$ and $\tilde{\mathbf{T}}_e(t)$
8: Generate N IID samples $\mathbf{w}_n(t)$ from the PDFs
9: Solve the optimization problem (4.17)
10: Apply only $c(t+1), y(t+1), s_c(t+1)$ and $s_d(t+1)$
11: **end for**
Output: $\mathbf{c}(t), \mathbf{y}(t), \mathbf{s}_c(t), \mathbf{s}_d(t)$

After this common steps the two algorithms are different. In fact, Algorithm 1 describes the case where the expected value approach is used, while Algorithm 2 describe the case where the approximated stochastic approach is employed.

In particular, in Algorithm 1 the EM solves the online optimal control problem (4.14) that employs only the expected value for all uncertain parameters (line 7). Hence, control actions related to the first time step are extracted from the determined optimal decision variables and are applied to the system in a closed-loop control fashion (line 9).

Conversely, in Algorithm 2 the EM defines $3N$ PDFs based on the available forecasting and then generates N IID samples from the PDFs (line 7-8). The EM solves the online optimal control problem (4.17), and as for the previous algorithm, it applies the control actions related to the first time step in a closed-loop control fashion (line 9).

4.4 Case Study

In this section we show the performance of the proposed stochastic MPC algorithm through several numerical experiments. As a case study we refer to harbor community located in the Ballen marina, Samsø (Denmark), where a smart energy system is being installed and tested in the framework of the Horizon2020 European research project SMILE [23]. As shown in Fig. 4.1, the electric system of the community includes a PV plant [60 kWp], a ESS [237 kWh], inflexible demand from the harbor master's office, service buildings, and visiting boats [105,000 kWh/year] as well as demand for CLs. The system is connected to the public electricity supply.

Simulations are based on a public real data set [24] shown in Fig. 4.2. In particular, Fig. 4.2.a and Fig. 4.2.b show the NCLs electricity consumption and the PV production measured in 2016, respectively. The demand shows a large peak in the summer period, when many boats visit the marina, while during the rest of the year the load is moderate. This is partially counterbalanced by the PV panels, which start the highest production in May. However, the demand peak is so large that the PV panels are unable to fully cover the demand, implying the need of further energy coming from storage and/or the main grid. Moreover, the instability of the PV power production makes necessary the support of the main power grid. The price of electricity follows the spot price on the Nord Pool electricity market as shown in Fig. 4.2.c. Lastly, in Fig. 4.2.d we plot the outdoor temperature data used in the simulations. This last was measured 10 kilometers from the Ballen marina in 2016. Note that for the sake of clarity all the data in Fig. 4.2 are shown on a daily basis.

The PDFs used in the simulations are uniform distributions defined as $b(t) \sim \mathcal{U}(\max\{\tilde{b}(t) - \varepsilon_b, 0\}, \tilde{b}(t) + \varepsilon_b)$, $r(t) \sim \mathcal{U}(\max\{\tilde{r}(t) - \varepsilon_r, 0\}, \tilde{r}(t) + \varepsilon_r)$ and $T^e(t) \sim \mathcal{U}(\tilde{T}^e(t) - \varepsilon_e, \tilde{T}^e(t) + \varepsilon_e)$. The values of ε_b, ε_r and ε_e are set respectively equal to the 5% of the maximum value reachable by the three uncertain parameters.

Figure 4.1: Overview of the Ballen marina (DK) with its energy community components [23].

As regard the system components, the minimum and maximum allowed charging levels for the ESS are set respectively to $\underline{l} = 0$ and $\overline{l} = 237$kWh, the charging /discharging rates are limited by the inverter, thus are set to $\overline{s} = \underline{s} = 49$kWh, and the charging and discharging efficiencies are both equal to 97% (i.e, $\eta_c = \eta_d = 0.97$). The state of charge of the ESS is assumed to be empty at the beginning of the simulation time (i.e., $l(0) = 0$). The marina has a shared facility, which comprehends also the harbour master's office. This building is open from 7am to 16pm on working days during winter and every day during the other seasons. The energy consumption of the HVAC system only is optimally controlled in order to impose the thermal comfort in the range (18-22)°C. The electric consumption of the heat pump is 9kWh/day.

We implement the scheduling problem in MATLAB R2020a on a desktop PC equipped with an Intel i7 core processor and 8 GB RAM. We perform the simulations considering a sampling time of 1 hour and a period of analysis of one year ($t \in [0, T]$, with $T = 8760$) with a prediction horizon of $H = 24$ hours (i.e., $\mathcal{H}(t) = (t+1, t+24)$). In particular, we analyze three different scenarios:

- *Scenario 1*: The EM perfectly knows all future NCLs demands and the RESs generation; hence, the problem to be solved is deterministic. We refer this as the seer case. This scenario is an upper bound for any other approach.
- *Scenario 2*: The EM relies only on the available forecasting without applying any approach to cope with the uncertainty. In this scenario, we employ the expected value approach through Algorithm 1.
- *Scenario 3*: The EM employs the proposed stochastic approach by generating a set of IID sampling from several defined PDFs. Hence, we apply Algorithm 2.

We address the community energy scheduling of the presented case study by applying the above-described methods in eight different simulations, as reported in Table 4.1. The first two simulations (i.e., S10 and S20) are related to Scenario 1 and Scenario 2, respectively. Conversely, Simulations S30-S35 refer to Scenario 3 where we only change the number of samplings to be used.

For the sake of space, we report the detailed results of simulation S10 only; hence, Fig. 4.3 referring to the first scenario (where the EM knows exactly the future values of uncertain variables) shows the charging/discharging activities of the ESS and the relative state of charge on a daily basis. It is apparent that the charging/discharging profiles are almost symmetrical, this indicates that energy that is stored by the ESS is consumed within the same day. Moreover, in Fig. 4.4 we show the energy flow between the smart

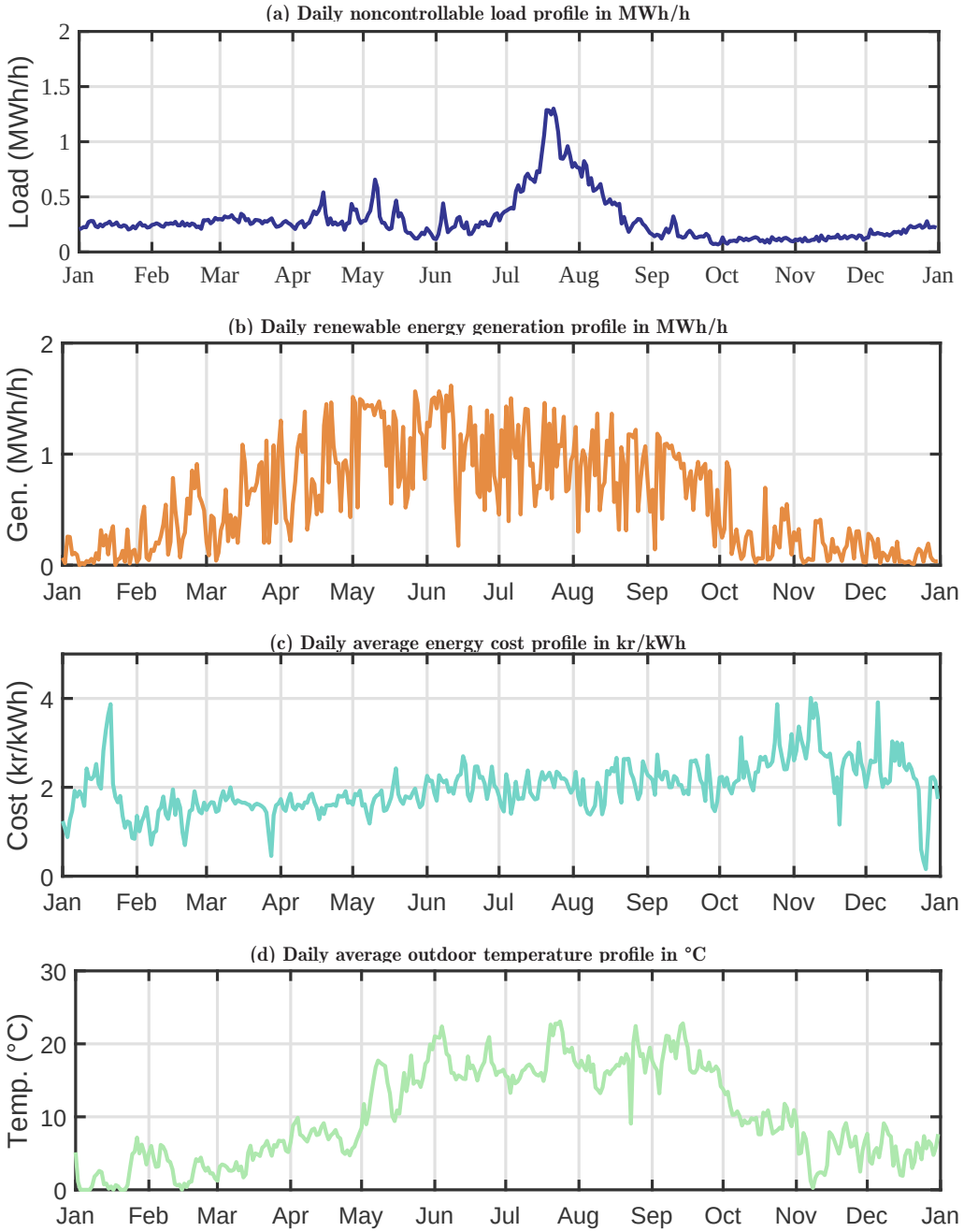

Figure 4.2: Data used for the numerical simulations shown on a daily basis: daily noncontrollable load demand in MWh/h (a), daily renewable energy generation in MWh/h (b), daily average energy cost in kr/kWh (c), daily average outdoor temperature in °C (d).

energy system and the main grid, i.e., the energy bought/transferred from/to the main grid in one day. From the picture, it is apparent that the smart energy system is not auto-sufficient and still needs to buy energy in the summer when the RESs production is not sufficient. Furthermore, the energy transferred to the main grid is on average higher in May-June when the PV production is relatively consistent with respect to the demand.

Having assessed the performance of the proposed approach to optimally control the system components, let us now investigate the effects of the different approaches to cope with the uncertainty by using three indicators:

Table 4.1: Simulations Results

Simulation		N	Time (s)	EC_T	ΔEC_T	SS_T	EI_T
S10	Seer	1	78	32159	13.6	0.41	0.80
S20	Exp. value	1	79	37208	0.0	0.40	0.78
S30	Stochastic	5	93	34182	8.1	0.41	0.79
S31	Stochastic	10	121	33475	10.0	0.41	0.79
S32	Stochastic	20	166	33123	11.0	0.41	0.80
S33	Stochastic	50	540	32966	11.4	0.41	0.80
S34	Stochastic	100	1830	32916	11.5	0.41	0.80
S35	Stochastic	150	3937	32871	11.7	0.41	0.80

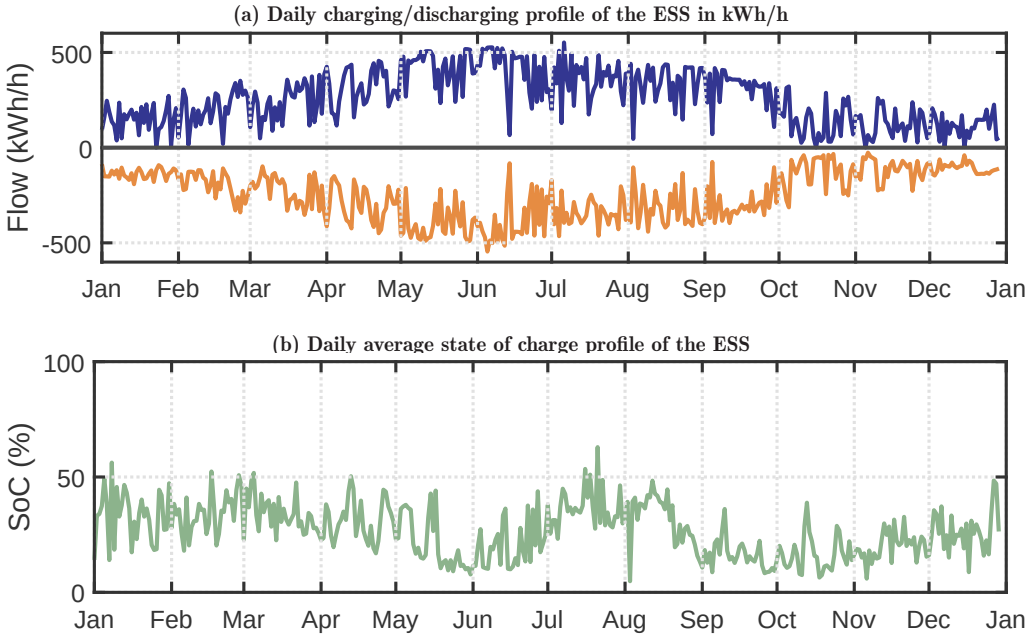

Figure 4.3: Daily inflow/outflow profile from/to the main grid in kWh/h.

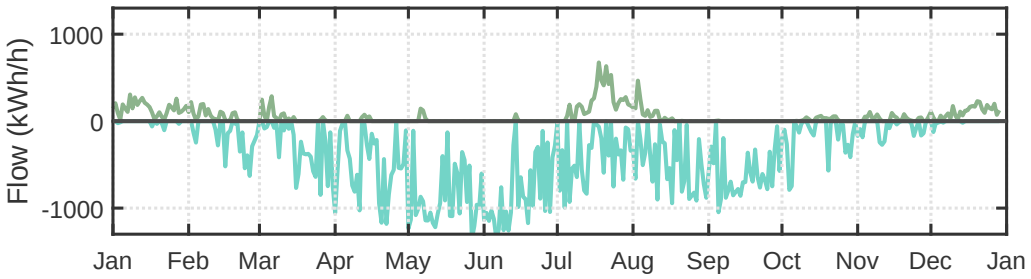

Figure 4.4: Daily inflow/outflow profile from/to the main grid in kWh/h.

1) The *total energy cost* concerns the business economy and is defined as:

$$EC_T = \sum_{t=1}^{T} k\,(t)\, x_i\,(t) \tag{4.18}$$

2) The *self-supply* indicates the percentage of the energy totally transferred to the main grid (and thus definitely lost) to the energy totally produced in the community, and it is thus defined as:

$$SS_T = 1 - \frac{\sum_{t=1}^{T} g_o(t)}{\sum_{t=1}^{T} r(t)} \tag{4.19}$$

3) The *energy-independence* indicates the percentage of energy totally bought from

the main grid to the energy totally consumed in the community, and it is defined as:

$$\mathrm{EI}_T = 1 - \frac{\sum_{t=1}^{T} g_i(t)}{\sum_{t=1}^{T} b(t) + c(t) + y(t)}. \tag{4.20}$$

Note that the EC_T should be as low as possible, whilst SS_T and EI_T have to maximized.

We report the main results of our simulations in Table 4.1, namely: the approach used in the simulation, the number of samplings (if a stochastic approach is used), the running time (in seconds), and the values of the aforementioned indicators EC_T, SS_T, and EI_T. Moreover, to better compare different approaches, we define also $\Delta\mathrm{EC}_T$ as the difference in percentage between EI_T obtained in a simulation with respect to the one obtained for S20, i.e., the expected value approach one. Doing so, we show the savings obtained with respect to the simplest approach.

In particular, observing the simulation results of the third scenario when a different number of samples N is performed (S30-35), it is clear that with any number of samples lead to a decrease in the total energy cost incurred by the community. In fact, even with a small number of samplings it is possible to save 8.1% of the total energy cost compared to the expected approach. Moreover, by increasing the number of samplings, we can improve the results up to 11.7% with 150 samples. It is worth to point out that this is incredibly high since the maximum result that is possible to obtain with the perfect knowledge of the future in S10 is 13.6%. However, the relative increase is lower when the number of samples increases, while the computational time increase exponentially.

Conversely, the self-reliance perspective does not significantly improve with a stochastic approach; in fact, the indicators SS_T and EI_T show approximately the same values in the latter simulations.

Summing up, it is apparent that the best performance is achieved by the approximated stochastic MPC algorithm due to its ability to take into account different outcomes of the uncertain values. The minimum energy cost is achieved by simulations with higher number of samplings, however, even with a small set of samples the savings are remarkable and the computational time that is comparable to the expected value one.

4.5 Conclusion

In this chapter, we present a stochastic model predictive control approach to effectively determine the robust cost-optimal energy scheduling of a grid-connected smart energy system, where users are equipped with non-controllable and controllable loads and share renewable energy sources and an energy storage system. The evidence from an a yearly basis analysis conducted in realistic situations shows that the proposed stochastic control achieves higher performances than a deterministic optimal control approach in terms of minimized energy cost and maximized self-consumption of on-site production.

Future work should focus on including other devices such as different kinds of controllable loads or individually owned energy sources, and integrating additional objective functions and technical constraints affecting the operations of system components. Finally, for the sake of improving the computational performance of the algorithm, distributed and decentralized resolution of the energy scheduling algorithm will be investigated.

References

[1] Carli, R. and Dotoli, M., "Decentralized control for residential energy management of a smart users' microgrid with renewable energy exchange," *IEEE/CAA Journal of Automatica Sinica*, vol. 6, no. 3, pp. 641–656, 2019.

[2] Gjorgievski, V. Z., Cundeva, S., and Georghiou, G. E., "Social arrangements, technical designs and impacts of energy communities: A review," *Renewable Energy*, 2021.

[3] Abada, I., Ehrenmann, A., and Lambin, X., "Unintended consequences: The snowball effect of energy communities," *Energy Policy*, vol. 143, p. 111 597, 2020.

[4] Soeiro, S. and Dias, M. F., "Community renewable energy: Benefits and drivers," *Energy Reports*, vol. 6, pp. 134–140, 2020.

[5] Abada, I., Ehrenmann, A., and Lambin, X., "On the viability of energy communities," *The Energy Journal*, vol. 41, no. 1, 2020.

[6] Hossain, M. A., Pota, H. R., Squartini, S., Zaman, F., and Guerrero, J. M., "Energy scheduling of community microgrid with battery cost using particle swarm optimisation," *Applied Energy*, vol. 254, p. 113 723, 2019.

[7] Marzband, M., Alavi, H., Ghazimirsaeid, S. S., Uppal, H., and Fernando, T., "Optimal energy management system based on stochastic approach for a home microgrid with integrated responsive load demand and energy storage," *Sustainable cities and society*, vol. 28, pp. 256–264, 2017.

[8] Pippia, T., Sijs, J., and De Schutter, B., "A single-level rule-based model predictive control approach for energy management of grid-connected microgrids," *IEEE Transactions on Control Systems Technology*, vol. 28, no. 6, pp. 2364–2376, 2019.

[9] Pezeshki, H., Wolfs, P., and Ledwich, G., "A model predictive approach for community battery energy storage system optimization," in *IEEE PES General Meeting| Conference & Exposition*, IEEE, 2014, pp. 1–5.

[10] Carli, R., Dotoli, M., Jantzen, J., Kristensen, M., and Othman, S. B., "Energy scheduling of a smart microgrid with shared photovoltaic panels and storage: The case of the ballen marina in samsø," *Energy*, vol. 198, p. 117 188, 2020.

[11] Arasteh, F. and Riahy, G. H., "Mpc-based approach for online demand side and storage system management in market based wind integrated power systems," *International Journal of Electrical Power & Energy Systems*, vol. 106, pp. 124–137, 2019.

[12] Batiyah, S., Sharma, R., Abdelwahed, S., and Zohrabi, N., "An mpc-based power management of standalone dc microgrid with energy storage," *International Journal of Electrical Power & Energy Systems*, vol. 120, p. 105 949, 2020.

[13] Pimm, A. J., Palczewski, J., Morris, R., Cockerill, T. T., and Taylor, P. G., "Community energy storage: A case study in the uk using a linear programming method," *Energy Conversion and Management*, vol. 205, p. 112 388, 2020.

[14] Lv, C., Yu, H., Li, P., *et al.*, "Model predictive control based robust scheduling of community integrated energy system with operational flexibility," *Applied energy*, vol. 243, pp. 250–265, 2019.

[15] Hossain, M. A., Chakrabortty, R. K., Ryan, M. J., and Pota, H. R., "Energy management of community energy storage in grid-connected microgrid under uncertain real-time prices," *Sustainable Cities and Society*, p. 102 658, 2020.

[16] Parisio, A., Rikos, E., and Glielmo, L., "Stochastic model predictive control for economic/environmental operation management of microgrids: An experimental case study," *Journal of Process Control*, vol. 43, pp. 24–37, 2016.

[17] Zhang, Y., Meng, F., Wang, R., Zhu, W., and Zeng, X.-J., "A stochastic mpc based approach to integrated energy management in microgrids," *Sustainable cities and society*, vol. 41, pp. 349–362, 2018.

[18] Zhang, Y., Fu, L., Zhu, W., Bao, X., and Liu, C., "Robust model predictive control for optimal energy management of island microgrids with uncertainties," *Energy*, vol. 164, pp. 1229–1241, 2018.

[19] Garcia, C. E., Prett, D. M., and Morari, M., "Model predictive control: Theory and practice—a survey," *Automatica*, vol. 25, no. 3, pp. 335–348, 1989.

[20] Ramanathan, B. and Vittal, V., "A framework for evaluation of advanced direct load control with minimum disruption," en, *IEEE Transactions on Power Systems*, vol. 23, no. 4, pp. 1681–1688, 2008.

[21] Shapiro, A., "Stochastic programming approach to optimization under uncertainty," *Mathematical Programming*, vol. 112, no. 1, pp. 183–220, 2008.

[22] Kim, S., Pasupathy, R., and Henderson, S. G., *A guide to sample average approximation*. Springer, 2015, pp. 207–243.

[23] Jantzen, J., "Requirements specification: Deliverable d3.4 [internet," en, *SMILE*, 2019, Available from: [Online]. Available: https://www.h2020smile.eu.

[24] Jantzen, J. and Kristensen, M., *The Ballen2016 Data Set*, http : / / arkiv . energiinstituttet.dk/643/, [Accessed on: 20-01-2020], 2019.

Chapter 5

Noncooperative Stochastic Control for Energy Scheduling under Variable Distributed Generation and Adjustable Load Demand

V

Abstract

In this chapter, we propose a distributed *demand side management* (DSM) approach for smart grids taking into account uncertainty in wind power forecasting. The smart grid comprehends traditional users as well as active users (prosumers). Through a rolling-horizon approach, prosumers participate in a DSM program, aiming at minimizing their cost in the presence of uncertain wind power generation by a game theory approach. We assume that each user selfishly formulates its grid optimization problem as a noncooperative game. The core challenge in this chapter is defining an approach to cope with the uncertainty in wind power availability. We tackle this issue from two different sides: by employing the expected value to define a deterministic counterpart for the problem and by adopting a stochastic approximated framework. In the latter case, we employ the sample average approximation technique, whose results are based on a *probability density function* (PDF) for the wind speed forecasts. We improve the PDF by using historical wind speed data, and by employing a control index that takes into account the weather condition stability. Numerical simulations on a real dataset show that the proposed stochastic strategy generates lower individual costs compared to the standard expected value approach.

Contents

5.1 Introduction

The contemporary energy landscape includes a limited number of industries that concentrate the electricity production in some fossil and nuclear power plants. Moreover, the electricity distribution system is still unidirectional and passive. This architecture makes it difficult to profitably coordinate supply and demand. Indeed, most of the time, suppliers have to operate expensive ancillary plants in order to satisfy the changing power demand, with a significant environmental impact. Moreover, the growing demand for energy drives the formulation of plans to expand and upgrade the contemporary electricity grids. However, energy sustainability is currently a worldwide concern, making it difficult to use old paradigms for these upgrades.

In this context, smart grids find their place in leading to new features in the management of the electricity network. Among the basic functionalities of smart grids, there are *demand side management* (DSM), *distributed generation* (DG), and

distributed storage (DS). As a result, smart grids allow balancing and coping with energy peaks, improving efficiency, security, and quality of the power distribution system [1]. Furthermore, one of the most important advantages of smart grids is their potential to efficiently integrate *renewable energy sources* (RESs) in the distribution system. In fact, in the traditional configuration system, this integration is difficult due to the highly intermittent and stochastic behavior of weather conditions.

5.1.1 Literature review

There is a considerable amount of scientific literature on smart grids, and various approaches have been proposed to implement DSM programs [2]–[5].

A growing body of literature studies the use of game theory in DSM. Advantages of such an approach are in its ability to straightforwardly model the selfish nature of users and in its capacity to model decentralized or distributed control strategies, which are particularly effective in the case of large-scale systems [6], [7]. For instance, in [6], the authors propose a Stackelberg game between the electricity provider and users: the model is able to maximize the profit of the distribution provider and the welfare of the users. However, the presented approach is developed only for the deterministic case and does not consider the presence of RESs. In [7], a pricing strategy encourages the optimal generation and storage by the users. The study focuses only on the day-ahead optimization problem, and unfortunately it does not include RESs. In addition, in [8] the authors present an optimization algorithm for the scheduling of electrical activities of a microgrid, where users are connected to a distributor and are allowed to exchange renewable energy produced by individually owned distributed resources. However, such a renewable energy production is modeled in a deterministic way, disregarding the presence of uncertainty.

Essentially, the uncertainty in renewable energy production makes it hard to choose the optimal scheduling strategy of a smart grid. Therefore, DSM techniques can help mitigating this variability. In the related literature two approaches are typically employed: updating the RES forecasts (e.g., using a rolling-horizon approach), or employing probability distributions. In the first class of approaches, we recall a noncooperative model that includes a wind power source presented in [9]. In the model, all the potential uncertain variables are supposed to be deterministic, and a shrinking-horizon approach is used to handle their possible variations during the day.

Within the second class of approaches, we recall [10], where the authors propose a stochastic optimization model for the day-ahead energy scheduling, which incorporates DSM for managing the variability of RES. The proposed stochastic day-ahead algorithm considers random outages of system components and forecast errors for the RES. A Monte Carlo simulation creates multiple scenarios for representing possible realizations of uncertainty, and a mixed-integer linear problem is employed to solve the resulting stochastic problem. In [11], a risk-averse strategy for islanded microgrids with a high share of RES is presented. A sampling-based Monte Carlo forecast is chosen to handle RES variability, generating a collection of independent scenarios with the same probability. Other models represent uncertainty in the wind power availability, where wind power prediction errors are typically assumed to follow a Gaussian probability distribution. On the other hand, a number of studies suggest the use of the Weibull and Rayleigh distribution to characterize the wind speed [12], [13]. In [14], a Weibull distribution is used to forecast the wind speed, and a nonlinear function is employed to transform it into a power *probability density function* (PDF) for the power output. The objective function considers the reserve cost for overestimation and penalty cost for underestimation of RES power availability. The same approach is used in [15], where the authors investigate the effects of renewable energy integration on the power system from a stochastic point of view. In [16], the authors implement a stochastic programming strategy, by using a historical curve for the wind speed scenarios, and by validating the results using the wind speed forecasts. However, approaches in [10]–[16] rely on a centralized framework, that is questionable in case of large scale systems. Other references [17], [18] propose the use of

a normal distribution aimed at considering the wind speed variability. For instance, in [19], a Monte Carlo simulation is employed to generate a scenario tree to predict wind power availability. Moreover, a stochastic planning approach based on a Monte Carlo method is proposed in [20] to model the uncertain wind behavior.

5.1.2 Chapter Contribution

In this chapter, we propose a smart grid model that comprises a central unit and several interconnected demand-side users with a wind turbine. Users can be merely energy consumers, or they can participate actively in the grid optimization process. We implement a DSM model where the central unit updates the energy price based on the aggregate load and the wind power availability. We assume that each active user acts selfishly, trying to minimize his total expense by updating his DG and DS strategies. However, choices have to be made by users respecting their local preference and the overall grid constraints. To take into account the selfish nature of users, we model the resulting energy scheduling problem as a Nash game, extending the approach originally developed in [7] for the day-ahead deterministic scheduling case and subsequently modified in [9] using a shrinking-horizon technique in a deterministic and semi-decentralized setting. More precisely, we present a novel receding-horizon DSM strategy in a stochastic and semi-decentralized setting.

In this context, we consider the uncertainty in wind power availability, and our policy to manage this significant issue is twofold. Firstly, we model the DSM model in a rolling-horizon fashion, considering updatable wind speed forecasts. Secondly, we propose a stochastic distributed optimization strategy. We propose a framework where each user could consider a Weibull distribution based on historical wind speed data and a Gaussian distribution to locally model the uncertainty in the wind speed forecasts. Furthermore, we firstly apply to the smart grid context an instability index that evaluates the overall atmospheric conditions and modifies the latter distribution. Consequently, each user could generate a PDF for the wind power availability by adopting an approximated nonlinear relation between wind speed and power. By merging the historical and forecast PDF, we address the cases where the wind speed forecasts are particularly uncertain. We obtain a number of samplings from the aforementioned PDFs and use the *sample average approximation* (SAA) to generate an averaged cost function that takes into account several different wind power availability scenarios. Finally, we show the effectiveness of the proposed mechanism on a realistic case study, using real forecasts and real historical measured data. In particular, we examine the advantage that a single user obtains by adopting the proposed stochastic approach with respect to other competitors that employ a deterministic counterpart for the problem.

Summing up, many attempts have been made to design DSM strategies for smart grid management [6], [7]. However, the majority of works focuses only on the day-ahead optimization problem, while considering the supply side exclusively. In our work, instead, we propose a model that includes a wind turbine, and we perform a long-term analysis employing real wind speed forecasts. Moreover, we validate the results with real on-site measured wind speed data.

Regarding the RES presence in the grid, the majority of the studies in the related literature, see for instance [3], [8], [9], considers the RES power availability as a deterministic variable, disregarding the stochastic nature of these sources. The few approaches considering uncertainty in wind power availability typically define a discrete PDF for the possible outcomes or to assume the wind power prediction errors to follow a Gaussian probability distribution [10], [11]. However, these approaches rely on a centralized framework which has evident computational and privacy limitation. In addition, one of the significant drawbacks of these methods is the incorrect representation of wind power uncertainty due to the nonlinearity in the wind power generation process. Hence, to overcome this issue, in this work we consider the wind power availability as a stochastic variable, and describe its uncertainty by defining a PDF based on real forecast

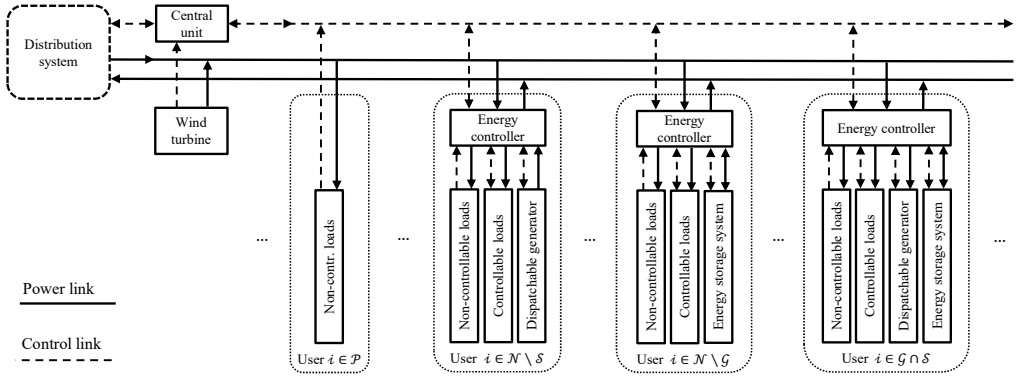

Figure 5.1: Scheme of energy flows and connections in the smart grid.

and real historical data, assessing all the parameters values. Moreover, we use this PDF to perform a stochastic programming approach and improve the performance of the model.

5.2 System Model

The focus of this section is to present the smart grid model, where we consider as a starting point the smart grid introduced in [7]. The model in [7] considers a day-ahead optimization process for a group of active users regulated by a central unit. The active users modify their energy scheduling profile aiming at decreasing their total cost by using some distributed energy sources or energy storage devices. A related approach is employed in [9], improving the model in [7] including a RES in the supply side and implementing a shrinking-horizon approach on a daily base to cope with the uncertainty in wind power availability. The model includes an algorithm to reach an equilibrium between the active users while respecting the overall grid constraints.

For the purpose of a long-time simulation, we modify the approaches presented in [7] and[9] considering a receding-horizon strategy on an hourly basis. We suppose that the control and the prediction horizon have a fixed length H, and they are moving ahead at every time slot (hence, eventually straddling two days). Moreover, we define the control horizon at the generic time slot k as $\mathcal{H} = \{k, ..., k + H - 1\}$.

The scheme of the considered smart grid is represented in Fig. 5.1. The smart grid is composed of a central unit, and several users that share a wind turbine. Users are also connected to the distribution system from/to which they can buy or sell electricity, and they are also connected to a central unit, which is able to keep the overall smart grid electricity consumption inside a fixed range. In our setting, the central unit broadcasts the hourly price coefficients and forecasts the wind speed for the wind turbine location. Each active user has an energy controller that decides a consumption, generation and storage strategy, based on its devices' status, the wind speed forecasts, and the aggregate grid load.

5.2.1 Flexible demand-side model

We consider a group of demand side users $\mathcal{D}$, divided into two subsets of passive $\mathcal{P}$ and active $\mathcal{N}$ users (prosumers), where $\mathcal{D} = \mathcal{P} \cup \mathcal{N}$ and $\mathcal{P} \cap \mathcal{N} = \varnothing$, with cardinality D, P and N respectively. Each user $i \in \mathcal{D}$ has a per-slot non-controllable energy consumption $e_i(h)$, $\forall, h \in \mathcal{H}$. Let us define the non-controllable energy consumption scheduling vector $\boldsymbol{e}_i = (e_i(h))_{h \in \mathcal{H}}$. Passive users $i \in \mathcal{P}$ are merely energy consumers, while active users $i \in \mathcal{N}$ participate in the grid optimization process by modifying their, controllable energy consumption, distributed production or storage strategies. We assume that each active user is connected bidirectionally to the power grid, and to a communication infrastructure that enables a two-way communication between the user's energy controller and the

central unit. In addition to the non-controllable energy consumption, all active users have a per-slot controllable energy consumption $d_i(h)$ for $h \in \mathcal{H}$ (e.g., a heating system or a boiler), that they can modify based on the market condition. We assume a first constraint on the controllable energy consumption as follows:

$$d_i^{\min} \leq d_i(h) \leq d_i^{\max}, \quad \forall h \in \mathcal{H}, \forall i \in \mathcal{N}\,. \tag{5.1}$$

Moreover, we assume that the controllable energy demand must be satisfied on a daily base, therefore, let us include an additional constraint on the daily energy demand. Since in our model the control horizon can straddle on two days, it is useful to define $\mathcal{H}_1$ as the set that comprehends the remaining time slots of the preceding day, and consequently, $\mathcal{H}_2$ the time slots of the subsequent day included in the control horizon. By naming $\bar{h}$ the last time slot of the preceding day, we can write more formally:

$$\mathcal{H}_1 = \left[k, \bar{h}\right] \cap \mathbb{Z}, \quad \mathcal{H}_2 = \left[\bar{h}+1, k+H-1\right] \cap \mathbb{Z} \tag{5.2}$$

$$\sum_{h \in \mathcal{H}_1} d_i(h) = \xi_{i,1}^{\text{left}}, \quad \sum_{h \in \mathcal{H}_2} d_i(h) = \xi_{i,2}, \quad \forall i \in \mathcal{N} \tag{5.3}$$

where $\xi_{i,2}$ is the controllable energy demand in the second day, and $\xi_{i,1}^{\text{left}}$ is the remaining controllable energy demand in the first day, i.e., the remaining part of the daily controllable energy demand of the first day that must be satisfied by the end of the day. Let us define for each prosumer $i \in \mathcal{N}$ the controllable energy consumption scheduling vector $\boldsymbol{d}_i = (d_i(h))_{h \in \mathcal{H}}$ and a set of feasible strategies:

$$\boldsymbol{\Omega}_{\boldsymbol{d}i} = \left\{\boldsymbol{d}_i \in \mathbb{R}^H_{\geq 0} \mid (5.1), (5.3) \text{ hold}\right\}, \quad \forall i \in \mathcal{N}. \tag{5.4}$$

Moreover, a prosumer can be either a dispatchable energy producer $i \in \mathcal{G}$ with a per-slot energy generation $g_i(h)$, and/or an energy storage user $i \in \mathcal{S}$ with per-slot energy storage profile $s_i(h)$. Note that in general $\mathcal{G} \cap \mathcal{S} \neq \varnothing$ and $\mathcal{G} \cup \mathcal{S} = \mathcal{N}$. The per-slot load profile $l_i(h)$, $\forall h \in \mathcal{H}$, $\forall i \in \mathcal{D}$ is hence:

$$l_i(h) = \begin{cases} e_i(h) & \text{if } i \in \mathcal{P} \\ e_i(h) + d_i(h) - g_i(h) + s_i(h) & \text{if } i \in \mathcal{N} \end{cases} \tag{5.5}$$

which expresses the energy flow between the grid and user $i \in \mathcal{D}$. For every user $i \in \mathcal{D}$ let us then define for the control horizon $\mathcal{H}$, the energy load scheduling vector $\boldsymbol{l}_i = (l_i(h))_{h \in \mathcal{H}}$. Obviously, for all the passive users $i \in \mathcal{P}$ it holds $\boldsymbol{l}_i = \boldsymbol{e}_i$.

5.2.2 Flexible energy generation model

Let us consider the group of prosumers $i \in \mathcal{G}$ equipped with dispatchable energy devices (e.g., internal combustion engines, gas turbines, or fuel cells). These active users can thus: produce energy to satisfy their demand, charge their battery, or sell to the grid during the peak time slots when the energy request is higher. We assume that each energy producer is subject to variable production costs (e.g., fuel cost, maintenance) and fixed cost. Let us define an energy production cost function $W_i(g_i(h))$ for all the users $i \in \mathcal{G}$, comprehending the variable production costs, i.e., the fuel and the maintenance costs. We assume that W_i is linear with a coefficient η_i, i.e., $W_i(g_i(h)) = \eta_i g_i(h)$. These prosumers are interested in optimizing their production strategies to obtain the highest advantage while respecting their local preferences. We assume so a first constraint in the generation capacity; besides a non-negative minimum, a maximum per-slot energy generation can take into account the devices' technological restrictions:

$$0 \leq g_i(h) \leq g_i^{\max}, \quad \forall h \in \mathcal{H}, \forall i \in \mathcal{G}\,. \tag{5.6}$$

In order to prevent the device's overuse, we include additional constraints on the maximum production over H consecutive time slots:

$$\sum_{z=h-H+1}^{h} g_i(z) \leq \psi_i, \quad \forall h \in \mathcal{H}, \forall i \in \mathcal{G} \tag{5.7}$$

where ψ_i is the maximum amount of energy that active user $i \in \mathcal{G}$ can generate in a period of H time slots. Note that, in (5.7) we also consider the energy generated in the time slots that precede the control horizon; therefore, these constraints depend on the previously implemented strategies.

Obviously, at each time slot h we have that $g_i(h) = 0$ for all the prosumers $i \notin \mathcal{G}$. Let us define for each producer $i \in \mathcal{G}$ an energy production scheduling vector $\boldsymbol{g}_i = (g_i(h))_{h\in\mathcal{H}}$ and a set of feasible strategies:

$$\boldsymbol{\Omega}_{\boldsymbol{g}_i} = \left\{\boldsymbol{g}_i \in \mathbb{R}^H_{\geq 0} \mid (5.6), (5.7) \text{ hold}\right\}, \quad \forall i \in \mathcal{G}. \tag{5.8}$$

5.2.3 Flexible energy storage model

Let us now model the group of energy storage devices (e.g., batteries, flywheels, fuel cells) owned by the prosumers $i \in \mathcal{S}$. Disregarding the actual different storage technology, without lack of generalization, we can characterize these devices by charging efficiency, discharging efficiency, leakage rate, maximum capacity, and maximum charging rate, as modeled in the sequel. Hence, for each user $i \in \mathcal{S}$, it is useful to define: the charging and discharging inefficiencies $0 < \beta_i^{(+)} \leq 1$ and $\beta_i^{(-)} \geq 1$, the leakage rate $0 < \alpha_i \leq 1$, the maximum capacity ζ_i, and the maximum hourly charging rate $s_i^{\max}$. The current charge level in the device equals the previous slot charge level decreased by the leakage rate and corrected by the energy storage profile. However, the latter is altered through the charging and discharging inefficiency. As in [7], we define it as:

$$q_i(h) = \alpha_i q_i(h-1) + \beta_i^\top s_i(h), \quad \forall i \in \mathcal{S} \tag{5.9}$$

where the vector $s_i(h) = [s_i^{(+)}(h), s_i^{(-)}(h)]^\top$ collects the battery charging and discharging profile at time slot h, and $\beta_i = [\beta_i^{(+)}, -\beta_i^{(-)}]^\top$ collects the charging and discharging inefficiencies. While in [7] and [9] the authors perform an isolated daily optimization process and consider a constraint on the charge level for the last time slot of one day, here we employ a rolling-horizon approach and introduce a minimum charge level $q_i^{\min}$ for each time slot, designed to prevent damages on the devices:

$$q_i^{\min} - \alpha_i q_i(h-1) \leq \beta_i^\top s_i(h) \leq \zeta_i - \alpha_i q_i(h-1), \quad \forall i \in \mathcal{S}. \tag{5.10}$$

Furthermore, the maximum charging and discharging rate must be respected [21], i.e.,

$$-s_i^{\max} \leq \beta_i^\top s_i(h) \leq s_i^{\max}, \quad \forall h \in \mathcal{H}, \forall i \in \mathcal{S}\,. \tag{5.11}$$

As for the distributed generation, at each time slot h we have that $s_i^{(+)}(h) = s_i^{(-)}(h) = 0$ for all the prosumers $i \notin \mathcal{S}$. Moreover, it is possible to define for each producer $i \in \mathcal{S}$ an energy storage scheduling vector $\boldsymbol{s}_i = ((s_i^{(+)}(h))_{h\in\mathcal{H}}, (s_i^{(-)}(h))_{h\in\mathcal{H}})$ and a set of feasible strategies:

$$\boldsymbol{\Omega}_{\boldsymbol{s}i} = \left\{\boldsymbol{s}_i \in \mathbb{R}^{2H}_{\geq 0} \mid (5.9), (5.10), (5.11) \text{ hold}\right\}, \quad \forall i \in \mathcal{S}. \tag{5.12}$$

5.2.4 Energy cost and pricing market

Let us now denote by $\omega(h)$ the power generated at time slot h by the wind turbine connected with the grid and $L(h)$ the total aggregate grid load for time slot h, with:

$$L(h) = \sum_{i\in\mathcal{D}} l_i(h), \quad \forall h \in \mathcal{H}. \tag{5.13}$$

As in [22], we consider a function C_h to model the cost per unit of energy bought from the distribution system as:

$$C_h(L(h), \omega(h)) = K_h(L(h) - \omega(h)), \quad \forall h \in \mathcal{H} \tag{5.14}$$

where $K_h > 0$ is the fixed price coefficient at the h-th slot (so that price results are time-varying). According to (5.14), the generic user $i \in \mathcal{D}$ per every time slot h pays to

the distribution system the amount $K_h(L(h) - \omega(h))l_i(h)$ to receive $l_i(h)$. Furthermore, as in [9], we include a global constraint on the aggregate per-slot energy load:

$$L_{\min} \leq L(h) \leq L_{\max}, \quad \forall h \in \mathcal{H} \tag{5.15}$$

where we define $L_{\max}$ as the maximum aggregate load that the grid can afford before a blackout occurs and $L_{\min}$ as a lower bound to prevent the turning off of some primary power plants.

We suppose that the central unit defines the global grid constraints taking into account its energy production facilities. Hence, we should include the availability of wind power; however, for the sake of simplicity, we assume that the wind power availability influences only the energy price and is not affecting the limitations on the aggregate load. Lastly, it is important to remark that (5.15) is a constraint that couples together all the prosumers' decisions.

In the following section we characterize the wind power availability.

5.3 Variable Generation Characterization

5.3.1 Wind speed and wind power generation

Wind power is one of the most important renewable energy sources, and it has been widely developed in recent years. The high fluctuations in the wind power output may lead to a mismatch between power production and electricity demand. The traditional approaches to cope with this issue rely on the hypothesis that the wind power forecasting error follows a normal distribution. However, this assumption neglects the nonlinear relation between wind speed and the generated power. Here, we consider the availability of wind power for the smart grid, under uncertainty on the wind speed, assuming that the relation between the generated power and the wind speed is nonlinear [23]. More precisely, the relation between the wind speed value v and the output power $\omega(v)$ in a conventional wind turbine is a function of several factors. In the turbine, if the wind speed is lower than a cut-in wind speed value v_{in}, the wind cannot defeat the mechanical friction in the system. After this threshold, the output power increases rapidly with the wind speed, following the Betz law until a rated wind speed value v_{rated} [24]. The turbines are equipped with a braking system, that after this value of rated wind speed, keeps the output equal to the turbine rated power ω_{rated}. Once the wind speed exceeds a safety cut-off value v_{out}, the turbine stops producing energy and is secured by completely stopping the rotor. A reliable yet simple piece-wise linear approximation for this relationship is the following [16]:

$$\omega(v) = \begin{cases} \omega_{\text{rated}} \frac{v - v_{\text{in}}}{v_{\text{rated}} - v_{\text{in}}} & \text{if} \quad v \in [v_{\text{in}}, v_{\text{rated}}] \\ 0 & \text{if} \quad v \in [0, v_{\text{in}}] \cup [v_{\text{out}}, \infty) \\ \omega_{\text{rated}} & \text{if} \quad v \in [v_{\text{rated}}, v_{\text{out}}]. \end{cases} \tag{5.16}$$

In Fig. 5.2 we show the reliability of the proposed approximate power curve (5.16), by comparing the power curve provided by the manufacturer and the proposed approximate power curve for a typical wind turbine. By using in (5.16) the expected value $\bar{v}(h)$ obtained by the central unit, it is possible to calculate the wind power production at the expected wind speed value $\bar{\omega}(h) = \omega(\bar{v}(h))$. As an alternative to the expected value approach described overhead, we can describe the behavior of the wind speed v with a PDF that reflects the expectation of the wind speed over a period of time and guides the wind power availability assessment. A PDF can adequately describe the wind speed, based on historical data or wind speed forecasts; the PDF can be either a single function or a combination of two or more functions. The Weibull distribution, Rayleigh distribution, and normal distribution are widely used distributions for modeling the wind speed. We refer to [25], for an extensive review of the PDFs used for wind speed assessment.

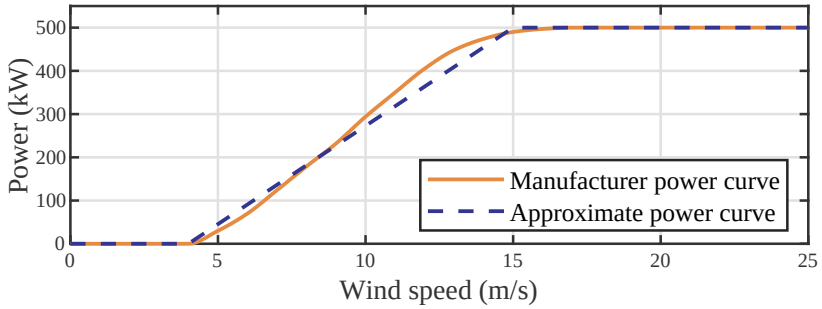

Figure 5.2: Manufacturer and approximate power curve for the NedWind-40 wind turbine [26]. The turbine power curve has characteristic parameters: $v_{\text{in}} = 4\text{m/s}$, $v_{\text{rated}} = 15\text{m/s}$, $v_{\text{out}} = 25\text{m/s}$ and $\omega_{\text{rated}} = 500\text{kW}$.

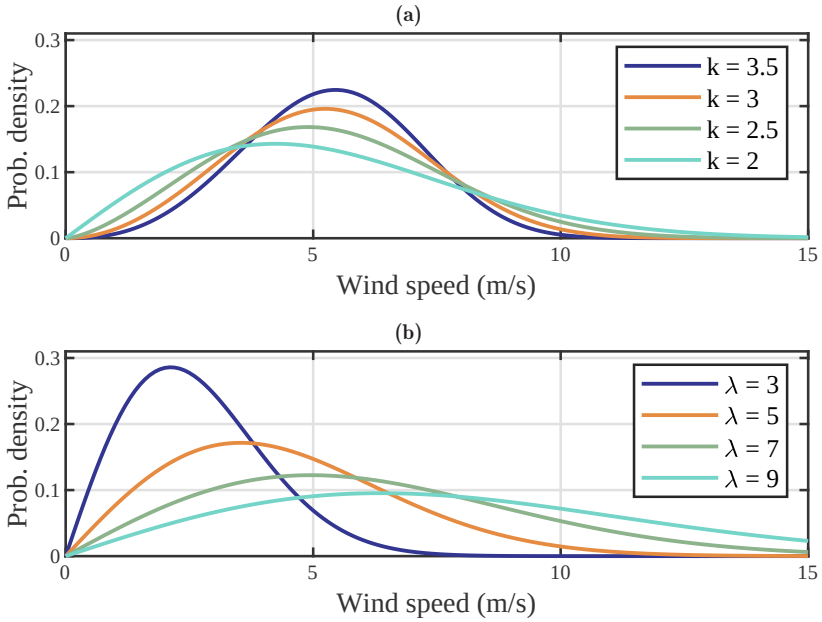

Figure 5.3: Weibull distributions with: (a) $\lambda_w = 6$ and different k_w values; (b) $k_w = 2$ and different λ_w values.

5.3.2 Historical distribution

The Weibull and Rayleigh distribution is believed to best describe the wind speed variations over a long term period. Therefore, we assume that the wind speed in a given location follows the Weibull distribution [27], with the λ_w scale and k_w shape parameters. Specifically, we assume that these parameters vary with the turbine location and the period in the year (e.g., for every month). By naming v the wind speed value, we may express, for some given scale and shape parameters, the Weibull wind speed PDF as:

$$f_W(v) = \begin{cases} \frac{k_w}{\lambda_w}\left(\frac{v}{\lambda_w}\right)^{k_w-1} \exp\left(-\left(\frac{v}{\lambda_w}\right)^{k_w}\right) & \text{if} \quad v \geq 0 \\ 0 & \text{if} \quad v < 0. \end{cases} \tag{5.17}$$

Figure 5.3 shows some examples of the Weibull distribution with different λ_w and k_w parameters. A high value of k_w, e.g. 3.5, indicates that the difference between the hourly mean wind speed (MWS) and the annual MWS is little. Viceversa, a low value of k_w, e.g. 2, means a high divergence from the annual MWS. The value of λ_w reflects the average wind speed of the wind farm. When a location has a high value of λ_w, it has a high average wind speed; however, this indicates also a significant variation from the annual MWS.

We now characterize the wind power PDF $f(\omega)$ by modifying the approach presented in [17]. Due to the turbine performance curve, the probability that the output power ω is null can be calculated considering the cumulative probability $F_v(v_{\text{in}})$ that $v < v_{\text{in}}$ and the cumulative probability $F_v(v_{\text{out}})$ that $v > v_{\text{out}}$, and is therefore:

$$f(0) = \mathbb{P}[\omega = 0] = F_v(v_{\text{in}}) + (1 - F_v(v_{\text{out}})). \tag{5.18}$$

Moreover, the probability that $\omega = \omega_{\text{rated}}$ can be calculated considering the cumulative probability that $v \in [v_{\text{rated}}, v_{\text{out}}]$, and is:

$$f(\omega_{\text{rated}}) = \mathbb{P}[\omega = \omega_{\text{rated}}] = F_v(v_{\text{out}}) - F_v(v_{\text{rated}}). \tag{5.19}$$

In the interval $[0, \omega_{\text{rated}}]$, the PDF of the generated power ω can be obtained via a one-to-one mapping with the wind speed [28]. By denoting $A = \left(\frac{v_{\text{rated}}}{v_{\text{in}}}\right) - 1$ and $C = \frac{v_{\text{in}}}{\omega_{\text{rated}}}$, we have that:

$$f(\omega) = \frac{k_w AC}{\lambda_w} \left(\frac{\left(1 + \frac{A\omega}{\omega_{\text{rated}}}\right) v_{\text{in}}}{\lambda_w} \right)^{k_w - 1} \exp\left(- \left(\frac{\left(1 + \frac{A\omega}{\omega_{\text{rated}}}\right) v_{\text{in}}}{\lambda_w} \right)^{k_w} \right). \tag{5.20}$$

Summing up, given the turbine parameters, the location, and the period in the year, we can define the historical PDF for the generated wind power as:

$$f(\omega) = \begin{cases} \left(1 - \exp\left(-\left(\frac{v_{\text{in}}}{\lambda_w}\right)^{k_w}\right) + \exp\left(-\left(\frac{v_{\text{out}}}{\lambda_w}\right)^{k_w}\right)\right) \delta(\omega) & \text{if } \omega = 0 \\ \frac{k_w AC}{\lambda_w} \left(\frac{\left(1 + \frac{A\omega}{\omega_{\text{rated}}}\right) v_{\text{in}}}{\lambda_w} \right)^{k_w - 1} & \\ \qquad \exp\left(- \left(\frac{\left(1 + \frac{A\omega}{\omega_{\text{rated}}}\right) v_{\text{in}}}{\lambda_w} \right)^{k_w} \right) & \text{if } \omega \in (0, \omega_{\text{rated}}) \\ \left(\exp\left(-\left(\frac{v_{\text{rated}}}{\lambda_w}\right)^{k_w}\right) - \exp\left(-\left(\frac{v_{\text{out}}}{\lambda_w}\right)^{k_w}\right)\right) \delta(\omega) & \text{if } \omega = \omega_{\text{rated}} \\ 0 & \text{if } \omega > \omega_{\text{rated}} \end{cases} \tag{5.21}$$

The scale λ_w and the shape k_w parameters of the Weibull distribution have a significant impact on the wind power historical PDF. Indeed, for a particular turbine, a different period of the year leads to different Weibull parameters λ_w and k_w, and consequently, to a different power PDF. In Fig. 5.4 we show two examples of the historical PDF with different values for the Weibull parameters.

5.3.3 Forecast distribution

The previous methodology to define a PDF for wind power is based on historical data, and therefore describes the uncertainty of wind speed in the long term. However, it neglects the availability of updatable wind speed forecasts, i.e., a series of forecasts which may be updated at each time shift of the predictive control horizon. Conversely, in this paper, we assume to have a series of wind speed forecasts for the whole control horizon and that the forecasting error is a random variable following a normal distribution [17]. In detail, we assume that to every forecasted wind speed value μ it is possible to assign a standard deviation σ based on the prediction reliability.

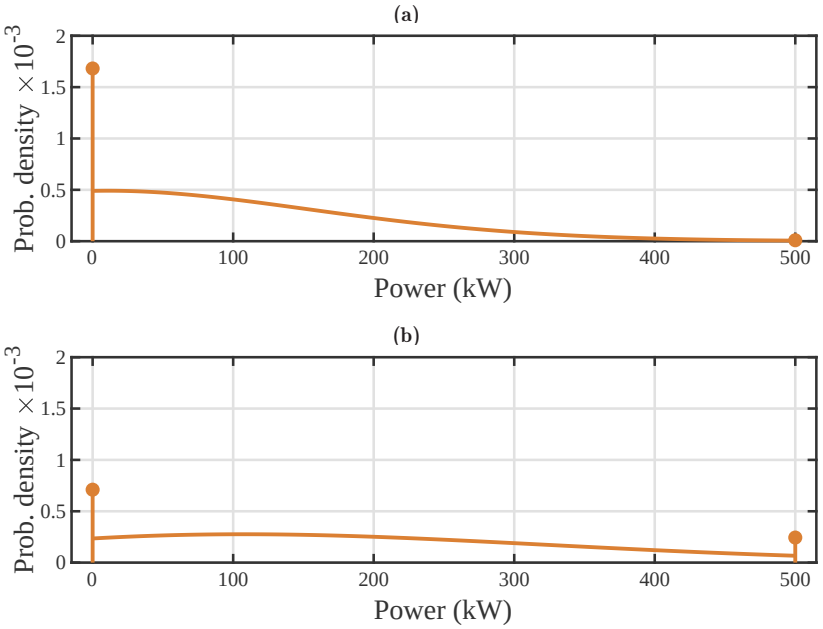

Figure 5.4: Wind power historical PDF (5.21) for different Weibull parameters, calculated for the NedWind-40, with v_{in}=4m/s, v_{rated}=15m/s, v_{out}=25m/s and $\omega_{\text{rated}} = 500$kW. (a) $\lambda_w = 6$ and $k_w = 2$. (b) $\lambda_w = 9$ and $k_w = 2$.

By following the aforementioned framework to compute the historical PDF, we calculate the probability that $\omega = 0$ by considering the cumulative probability that $v < v_{\text{in}}$ and that $v > v_{\text{out}}$, as in (5.18). Moreover, the probability that $\omega = \omega_{\text{rated}}$ can be calculated as in (5.19), considering the cumulative probability that $v \in [v_{\text{rated}}, v_{\text{out}}]$.

In the interval $[0, \omega_{\text{rated}}]$, the PDF of the generated power, by denoting again $A = \left(\frac{v_{\text{rated}}}{v_{\text{in}}}\right) - 1$ and $C = \frac{v_{\text{in}}}{\omega_{\text{rated}}}$, is:

$$f(\omega) = \frac{C}{\sqrt{2\pi\sigma^2}} \exp\left(-\frac{\left(\left(1 + \frac{A\,\omega}{\omega_{\text{rated}}}\right) v_{\text{in}} - \mu\right)^2}{2\sigma^2}\right) \tag{5.22}$$

Summarizing, let us define a forecast PDF for the generated power, given a forecasted wind speed value μ and a standard deviation σ, in (5.23).

$$f(\omega) = \begin{cases} \left(\frac{1}{\sqrt{2\pi\sigma^2}}\left(\int_{-\infty}^{v_{\text{in}}} \exp\left(-\frac{(v-\mu)^2}{2\sigma^2}\right) dv \right.\right. \\ \qquad \left.\left. + \int_{v_{\text{out}}}^{+\infty} \exp\left(-\frac{(v-\mu)^2}{2\sigma^2}\right) dv\right)\right) \delta(\omega) & \text{if } \omega = 0 \\ \frac{C}{\sqrt{2\pi\sigma^2}} \exp\left(-\frac{\left(\left(1 + \frac{A\,\omega}{\omega_{\text{r}}}\right) v_{\text{in}} - \mu\right)^2}{2\sigma^2}\right) & \text{if } \omega \in (0, \omega_{\text{rated}}) \\ \left(\frac{1}{\sqrt{2\pi\sigma^2}} \int_{v_{\text{r}}}^{v_{\text{out}}} \exp\left(-\frac{(v-\mu)^2}{2\sigma^2}\right) dv\right) \delta(\omega) & \text{if } \omega = \omega_{\text{rated}} \\ 0 & \text{if } \omega > \omega_{\text{rated}} \end{cases} \tag{5.23}$$

Figure 5.5 shows that the wind power forecast PDF cannot be expressed by the normal distribution due to the nonlinear relation between wind speed and wind power. Indeed,

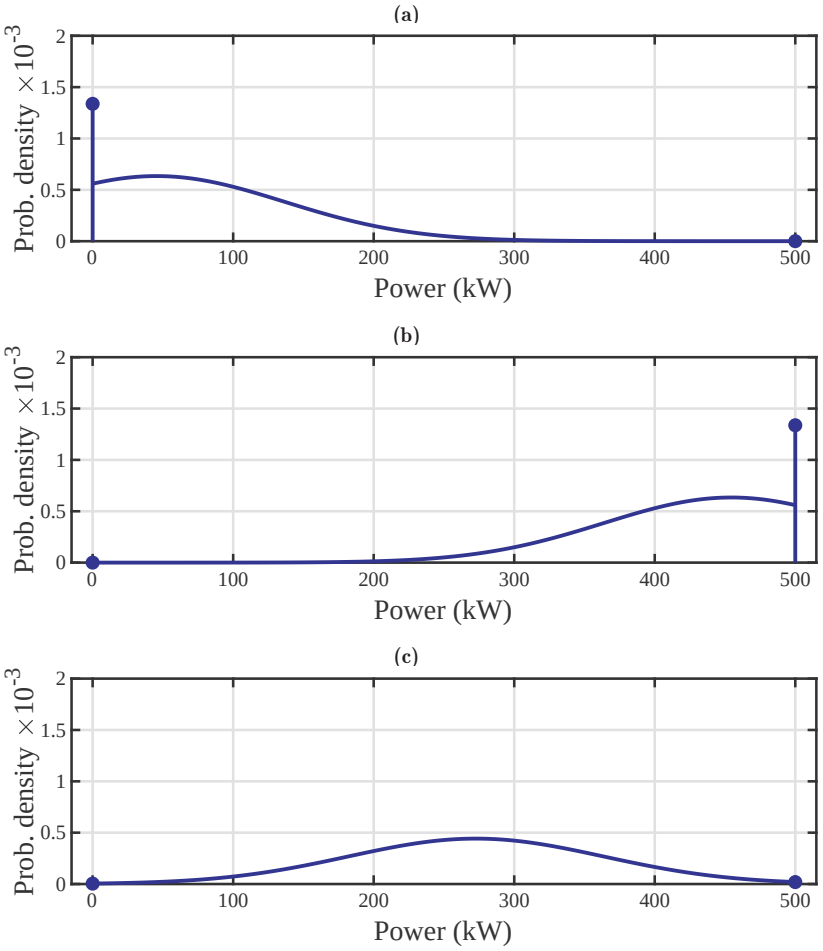

Figure 5.5: Wind power forecast PDF (5.23) for different wind speed values. Calculated for the NedWind-40, with $v_{\text{in}} = 4\text{m/s}$, $v_{\text{rated}} = 15\text{m/s}$, $v_{\text{out}} = 25\text{m/s}$ and $\omega_{\text{rated}} = 500\text{kW}$. (a) $\mu = 5\text{m/s}$ and $\sigma = 2\text{m/s}$. (b) $\mu = 14\text{m/s}$ and $\sigma = 2\text{m/s}$. (c) $\mu = 10\text{m/s}$ and $\sigma = 2\text{m/s}$.

the wind power forecast PDF has an asymmetric distribution, with different peak values.

The range for the wind power PDF varies from 0 to the rated power, consisting of a continuous part and two of impulse functions. When the wind speed is lower than the cut-in wind speed or higher than the cut-out wind speed, the PDF of the wind power concentrates at 0, with a higher impulse function (Fig. 5.5(a)). When the wind speed is between the rated wind speed and the cut-out wind speed, the wind power PDF focuses on the rated power, with a high impulse function (Fig. 5.5(b)). Lastly, when the wind speed is between the cut-in wind speed and the rated wind speed, the PDF of the wind power can be described by the normal distribution (Fig. 5.5(c)).

We remark here that in the wind power forecast PDF we assume that the wind speed forecasting errors follow the normal distribution. Nevertheless, an evaluation of the Gaussian parameter should be made to characterize the forecasts correctly. The standard deviation of a wind speed forecast can be calculated from the past forecasting error distributions. However, it is difficult to assess accurately these values in the range in which the wind speed is extremely high, because the number of sample data is limited. The literature shows that many factors contribute to the uncertainty in the wind speed forecast, the most important being:

- the uncertainty related to the weather prediction models;
- the wind farm location, since the weather prediction models are not performing with the same accuracy for all the locations;

- the wind farm geography and morphology;
- the forecasted wind speed value, since the uncertainty increases with this value. This relation is not linear, especially with high-speed value;
- the forecasting horizon, because a long term forecast has a higher uncertainty;
- the weather "stability", i.e., stable weather conditions have more reliable forecasts.

Reference [29] shows that uncertainty is strongly related to the wind speed value and the forecasting horizon. These relations, together with the uncertainty related to a specific weather prediction model and the wind farm location and geography, can be estimated using historical data.

5.3.4 Instability index

The weather conditions are not always the same; a more stable atmospheric situation empowers better forecasts, reducing uncertainty in the wind power forecast. To evaluate the weather condition, [30] introduces a methodology to assess the risk of short-term wind power forecasts by using a meteorological risk index. The index relies on the ensemble forecasting methodology. Instead of making a single prediction of the most likely weather, a set of forecasts is produced. The set aims at indicating the range of possible future states of the atmosphere. This is usually made by changing the initial condition of the model and observing how the results are perturbed. Differently from [30], we define an instability index obtained by evaluating the error made by forecasts of different time instances.

In detail, let us evaluate the stability of the weather conditions at the generic time slot k. Hence, we denote with v_r the registered wind speed at the previous time slot $k-1$, and v_t the forecasted wind speed value for time slot $k-1$ obtained at time slot $(k-1)-t$, i.e., the forecast made at the time slot $(k-1)-t$ for the time slot $k-1$. By collecting the previously recorded and forecasted data, each user calculates the instability index as:

$$n = \sum_{t=1}^{T} \tau_t \, |v_r - v_t| \tag{5.24}$$

where T is the number of previous forecasts employed to calculate the index, and τ_t are weights that give less importance to the error made by the older predictions, i.e., the error $|v_r - v_1|$ should has a stronger impact than $|v_r - v_T|$ in evaluating the index. Moreover, we assume that $\sum_{t=1}^{T} \tau_t = 1$.

As we show in the numerical experiments, the forecasting error increases linearly with the instability index. At every time slot k, we calculate the instability index employing the data related to the previous time slot $k-1$, and we modify the standard deviation for the subsequent forecasts. For instance, when the index is low, we assume that the forecast is accurate, and therefore, we reduce the standard deviation of the next time slots' forecasts. However, as the weather conditions typically change within a few hours, we do not employ the instability index to modify the standard deviation value for the forecast of the entire control horizon H.

5.3.5 Composed distribution

Highly uncertain forecasts are caused by high wind speed values, long prediction horizon, or unstable weather conditions. In some cases, uncertainty can be considerably high, leading to an overestimation in the forecast PDF. A combination of the information contained in the historical and the forecast PDFs can reduce this problem. The authors in [31] present several ways to combine PDFs. In particular, let us employ the logarithmic method:

$$f(\omega) = c f_1(\omega)^{w_1} f_2(\omega)^{w_2} \tag{5.25}$$

where $f_1(\omega)$ is the historical PDF, $f_2(\omega)$ the forecast PDF, w_1 and w_2 are weights with $w_1 + w_2 = 1$, and c a normalizing constant. It is worth pointing out that the weight

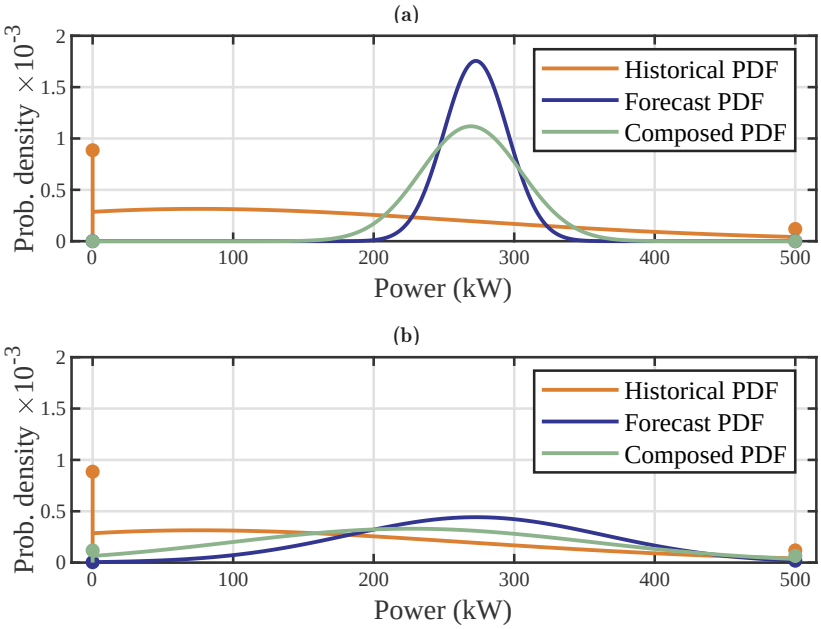

Figure 5.6: Composed wind power PDF (5.25) with different standard deviation values. Calculated for the NedWind-40, with $v_{\text{in}} = 4\text{m/s}$, $v_{\text{rated}} = 15\text{m/s}$, $v_{\text{out}} = 25\text{m/s}$, $\omega_{\text{rated}} = 500\text{kW}$, $\mu = 10\text{m/s}$, $\lambda_w = 8$ and $k_w = 2$. (a) $\sigma = 0.5\text{m/s}$. (b) $\sigma = 2\text{m/s}$.

indicates the PDF's influence. For the sake of simplicity, in the rest of the paper, we employ the same weight to all the PDFs, i.e., $w_1 = w_2 = 0.5$. In Fig. 5.6 we show an example of this methodology. In the first figure, the forecast PDF has a smaller standard deviation value, which indicates a more accurate and reliable prevision. The composed PDF, in this case, is comparable to the forecast PDF. On the other hand, in the second figure, the forecast has high uncertainty, and the composed PDF is corrected by the information contained in the historical PDF.

5.4 Noncooperative Stochastic Energy Scheduling

The objective of this section is to define the overall optimization problem for the smart grid model described in Section 5.2.

5.4.1 Game model

Game theory describes and analyzes scenarios with interactive decisions. Noncooperative game theory is a branch of game theory employed to solve conflicts between interacting players [32]. Considering our smart grid model, and bearing in mind the users' selfish behavior and the aforementioned cost function, for a generic user the price of energy depends on the other users' strategy. Hence, it is meaningful to model the optimization problem as a noncooperative game, as proposed in [7].

In the noncooperative game, each player behaves selfishly to optimize its own welfare, generally quantified through a cost function. A noncooperative game is usually defined by its three components:

- the players, that in our case are all the prosumers $i \in \mathcal{N}$ participating in the grid optimization process;
- a cost function J_i for each player;
- the strategy of each player $\boldsymbol{x}_i = (\boldsymbol{d}_i, \boldsymbol{g}_i, \boldsymbol{s}_i)^\top$, which corresponds to a specific consumption, generation and storage profile.

In the model, according to (5.14), the energy price at each time slot is a function of the aggregate load and the wind power generation; the latter is here regarded as a stochastic variable. Accordingly, for each active user $i \in \mathcal{N}$ we can define the cost function as the monetary exchange with the distribution system over the control horizon $\mathcal{H}$. Let us define the strategy vector for the generic prosumer $i \in \mathcal{N}$ at the generic time slot h as $x_i(h) = (d_i(h), g_i(h), s_i(h))^\top$, the strategy scheduling vector $\boldsymbol{x}_i = (\boldsymbol{d}_i, \boldsymbol{g}_i, \boldsymbol{s}_i)^\top$ and the local feasible strategy set that takes into account the individual user preferences as:

$$\Omega_{\boldsymbol{x}_i} = \left\{ \boldsymbol{x}_i \in \mathbb{R}^{4H} \,|\, \boldsymbol{d}_i \in \Omega_{\boldsymbol{d}_i}, \boldsymbol{g}_i \in \Omega_{\boldsymbol{g}_i}, \boldsymbol{s}_i \in \Omega_{\boldsymbol{s}_i} \right\}, \forall i \in \mathcal{N}. \tag{5.26}$$

Then, by using the pricing model in (5.14) and by naming with $\boldsymbol{x}_{-i}$ the collection of the strategy scheduling vectors $\boldsymbol{x}_j$ of all users $j \in \mathcal{D} \setminus \{i\}$, the total expense for a generic prosumer $i \in \mathcal{N}$ over the control horizon $\mathcal{H}$ is:

$$J_i(\boldsymbol{x}_i, \boldsymbol{x}_{-i}, \boldsymbol{\omega}) = \sum_{h \in \mathcal{H}} K_h(l_{-i}(h) + e_i(h) + \delta^\top x_i(h) - \omega(h)) \cdot \\ \cdot (e_i(h) + \delta^\top x_i(h)) + \sum_{h \in \mathcal{H}} W_i(\delta_g^T x_i(h)) \tag{5.27}$$

where $l_{-i}(h) = \sum_{i \in \mathcal{D} \setminus \{i\}} l_i(h)$ is the aggregate per-slot load of all the players $j \in \mathcal{D} \setminus \{i\}$, while $\delta = (1, -1, 1, -1)^\top$ and $\delta_g = (0, 1, 0, 0)^\top$ are auxiliary vectors. In our setting for the generic time slot h, the available wind power $\omega(h)$ is a stochastic variable that reveals its value ex-post. Therefore, users cannot calculate the exact value of J_i in advance.

Although each user acts selfishly, by choosing a strategy included in its local feasible set $\Omega_{\boldsymbol{x}_i}$, the global grid constraint in (5.15) must be respected. Hence, we should consider a noncooperative generalized game, where the coupling between the players occurs not only via the cost functions but additionally through a collective global feasible set. In our settings, the coupling constraints are introduced by an affine function, $\boldsymbol{x} \mapsto A\boldsymbol{x} - b$, where $A \in \mathbb{R}^{2H \times 4HN}$ and $b \in \mathbb{R}^{2H}$. In particular, let us define $b = [L_{\max} - L_P(k), ..., L_{\max} - L_P(k+H-1), L_P(k) - L_{\min}, ..., L_P(k+H-1) - L_{\min}]^\top$, with $L_P(h) = \sum_{i \in \mathcal{P}} l_i(h)$ the cumulative consumption of the passive user $i \in \mathcal{P}$, and $A = [A_1, ..., A_N] = \mathbf{1}_N \otimes \Delta$, being $\Delta = [I_H, -I_H, I_H, -I_H]$, $I_H \in \mathbb{R}^{H \times H}$ the identity matrix and $\otimes$ the Kronecker product. We remark that A_i outlines how the active user $i \in \mathcal{N}$ is involved in the global coupling constraints.

Thus we can now define the collective global feasible set $\mathcal{X}$ as the intersection between the collection of the local feasible sets of all the prosumers $\boldsymbol{\Omega} = \prod_{i=1}^N \Omega_{\boldsymbol{x}_i}$ and the coupling constraint. More formally, we have, therefore:

$$\mathcal{X} = \boldsymbol{\Omega} \cap \left\{ \boldsymbol{x} \in \mathbb{R}^{4HN} \mid A\boldsymbol{x} - b \leq \mathbf{0}_{2H} \right\}. \tag{5.28}$$

where $\boldsymbol{x} = (\boldsymbol{x}_i)_{i=1}^N$ is the collective strategy scheduling vector.

Overall, we obtain N inter-dependent optimization problems as in the following:

$$\forall i \in \mathcal{N} : \begin{cases} \underset{x_i \in \mathbb{R}^{4H}}{\operatorname{argmin}} \ \tilde{J}_i(\boldsymbol{x}_i, \boldsymbol{x}_{-i}, \boldsymbol{\omega}) \\ \quad \text{s.t. } (\boldsymbol{x}_i, \boldsymbol{x}_{-i}) \in \mathcal{X} \end{cases} \tag{5.29}$$

where $\tilde{J}_i$, is the assumption that each active user $i \in \mathcal{N}$ makes for the real cost function in (5.27), given the wind speed forecast provided by the central unit. We remark that (5.27) is a function of a stochastic variable, therefore, each user tries to define a function that reflects it as much as possible.

The formulation in (5.29) defines a generalized Nash equilibrium (GNE) problem that we can indicate in compact form as $\mathscr{G} = (\mathcal{X}, \tilde{\mathbf{J}})$, where $\mathcal{X}$ is the collective global feasible set as in (5.28) and $\tilde{\mathbf{J}} = (\tilde{J}_i(\boldsymbol{x}_i, \boldsymbol{x}_{-i}, \boldsymbol{\omega}))_{i=1}^{|\mathcal{N}|}$ is the collection of the active users' cost function. In the game theory solving the GNE problem in (5.29) means the computation of a GNE, which is a collective strategy profile $\boldsymbol{x}^* \in \mathcal{X}$ with the property that no single player can

Algorithm 5.1 Preconditioned forward backward (pFB)

Input: γ, A, b, $\tilde{\mathbf{J}}$, $\boldsymbol{\Omega}$
1: Set $\lambda = \mathbf{0}_{2H}$ and initialize $\boldsymbol{x}$
2: **while** An adequate termination criterion is reached **do**
3: **for** $i = 1, ..., N$ **do**
4: $x_i^+ = \text{proj}_{\Omega_{x_i}} \left[x_i - \gamma \left(\nabla_{\boldsymbol{x}_i} \tilde{J}_i(\boldsymbol{x}_i, \boldsymbol{x}_{-i}, \boldsymbol{\omega}) + A_i^\top \lambda\right)\right]$
5: **end for**
6: $\lambda^+ = \text{proj}_{\mathbb{R}^{2H}_{\geq 0}} \left[\lambda + \gamma \left(2A\boldsymbol{x}^+ - A\boldsymbol{x} - b\right)\right]$
7: **end while**
Output: $\boldsymbol{x}^*$

benefit from a unilateral deviation from $\boldsymbol{x}_i^*$, if all the other players act according [32]. More formally, we have:

$$J_i(\boldsymbol{x}_i^*, \boldsymbol{x}_{-i}^*) \leq \inf \left\{ J_i(\boldsymbol{x}_i, \boldsymbol{x}_{-i}^*) \mid (\boldsymbol{x}_i, \boldsymbol{x}_{-i}^*) \in \mathcal{X} \right\}. \tag{5.30}$$

In the rest of this Section, we introduce an algorithm to compute a GNE in a semi-decentralized fashion. Moreover, we present two variants of the cost function $\tilde{J}_i$, i.e., the guess made by the ith user given the stochasticity of the wind power availability.

5.4.2 Semi-decentralized equilibrium computation

Once we have defined the overall aggregated game $\mathcal{G} = (\mathcal{X}, \tilde{\mathbf{J}})$, let us now employ the preconditioned forward backward (pFB) algorithm presented in [33] to compute an equilibrium in a semi-decentralized fashion.

In Algorithm 5.1, at every time slot, the central unit broadcasts an initial value for the so-called incentive signal λ. At each iteration, every user attempts to reduce his cost function, given the current value for the grid coefficients, the wind forecast, and the aggregative load on the grid, taking a gradient step of length γ projected into the feasible local set. Next, the central unit collects all the users' strategies $\boldsymbol{x}$, then it calculates the incentive signal λ^+ for the subsequent iteration taking into account the expected constraint violation. Moreover, the central unit broadcasts to each prosumer $i \in \mathcal{N}$ the vector $\boldsymbol{l}_{-i} = (\sum_{i \in \mathcal{D} \setminus \{i\}} l_i(h))_{h \in \mathcal{H}}$. This is directly related to the strategies of all the other users $\boldsymbol{x}_{-i}$, however, due to the aggregation does not contain any private information. Finally, the central unit terminates the iterative process when an adequate termination criterion is reached, i.e., when all the strategies and the incentive signal λ converge. Note that the pFB algorithm guarantees the convergence to the unique *variational* GNE, therefore, all agents are penalized in the same way in order to satisfy the shared constraints. This approach is economically fair because the cost for fulfilling the common constraints is fairly shared, i.e., all agents are subject to the same dual variables ($\lambda_i = \lambda_j$, $\forall i, j$) [33].

5.4.3 Expected value formulation

In the proposed pricing scheme, the energy price is a function of an aleatory variable, such as the wind power availability. Moreover, we suppose that active users know the characteristic turbine parameters and that the central unit broadcasts at every time slot the wind speed forecast for the entire control horizon. Therefore, each active user decides how to manage the uncertainty in the wind speed forecasts. The most straightforward way to approach the problem is to consider the wind power availability as a deterministic variable by employing the expected value of the wind speed forecast $\bar{v}(h)$. By using (5.16), it is then possible to calculate the expected value for the wind power production $\bar{\omega}(h)$. Calling $\bar{\boldsymbol{\omega}} = (\bar{\omega}(h))_{h \in \mathcal{H}}$ the wind power expected production vector, we can now formally define the cost function for a generic active user that employs the expected value approach as:

$$\bar{J}_i(\boldsymbol{x}_i, \boldsymbol{x}_{-i}, \bar{\boldsymbol{\omega}}) = \sum_{h\in\mathcal{H}} K_h(l_{-i}(h) + e_i(h) + \delta^T x_i(h) - \bar{\omega}(h))\cdot \\ \cdot (e_i(h) + \delta^T x_i(h)) + \sum_{h\in\mathcal{H}} W_i(\delta_g^T x_i(h)). \quad (5.31)$$

It is worth pointing out that (5.27) determines how much a generic user actually pays to the grid after the realization of the stochastic variable (the so-called wait-and-see value), while (5.31) indicates how much the user is presuming to pay by employing this approach, which is different from the expected value of the cost function.

5.4.4 Approximated stochastic programming

The main issue in employing the expected value approach is that the presence of a stochastic variable may lead to a non-optimal energy schedule; this opens the door to a wealth of different approaches to cope with this problem. Stochastic programming is a framework used to solve models with uncertainty, taking advantage of the fact that the PDF ruling the random variable is known or can be in some way estimated. More specifically, we suppose that the cost function of a generic user is a stochastic variable itself [34], with expected value:

$$\mathbb{J}_i\left(\boldsymbol{x}_i, \boldsymbol{x}_{-i}, \boldsymbol{\omega}\right) = \mathbb{E}_\omega[J_i\left(\boldsymbol{x}_i, \boldsymbol{x}_{-i}, \boldsymbol{\omega}\right)]\,. \quad (5.32)$$

Determining the exact solution of (5.32) is complicated; an alternative solution methodology replaces the random variable by finite random samples and solves a resulting deterministic optimization problem [35]. This methodology is often called Sample Average Approximation (SAA). This technique is mainly based on having a prior known PDF, from which M independent and identically distributed (IID) random samples of the stochastic variable are obtained. In our case, by using M samples obtained through one of the aforementioned wind power PDFs, (5.21) or (5.23) or (5.25), we can define an approximated cost function for a generic active user $i \in \mathcal{N}$, as:

$$\hat{J}_i(\boldsymbol{x}_i, \boldsymbol{x}_{-i}, \hat{\boldsymbol{\omega}}_i) = \frac{1}{M_i}\sum_{m=1}^{M_i} J_i^m(x_i, \boldsymbol{x}_{-i}, \boldsymbol{\omega}_i^m) \quad (5.33)$$

where $\boldsymbol{\omega}_i^m$ is one of the samples for the wind power production vector, M_i is the number of samples that the generic user decides to perform, J_i^m is the cost function defined with the mth samples, and $\hat{\boldsymbol{\omega}}_i = (\boldsymbol{\omega}_i^m)_{m=1}^{M_i}$ is the collection of all the wind power production vector samples. Note that $\boldsymbol{\omega}_i^m = (\omega(h)_i^m)_{h\in\mathcal{H}}$ is one of the sampled scenarios for the whole control horizon; however, it should be noted that each $\omega(h)_i^m$ is sampled from a time slot specific PDF.

It is well known that under relatively mild conditions, the defined approximate stochastic solution converges to the "true" stochastic one, as the sample size M increases (the interested readers is referred to the discussion in [34] and [35] on this issue which is beyond the scope of this paper).

5.4.5 Rolling-horizon DSM algorithm

Let us now propose a novel procedure to continuously control prosumers by embedding Algorithm 5.1 into the receding horizon scheme of Algorithm 5.2. In particular, at each generic time slot k, prosumers participate in the optimization process to define the consumption, generation and storage strategies for the next control horizon $\{k, ..., k + H - 1\}$.

In the initialization phase of each time shift (line 2 of Algorithm 5.2), the central unit broadcasts the price coefficients $\boldsymbol{K}^k = (K_h)_{h=k}^{k+H-1}$ and the wind speed forecasts $\bar{\boldsymbol{v}}^k = (\bar{v}(h))_{h=k}^{k+H-1}$ for the entire control horizon.

Now for clarity, let us divide the active users set $\mathcal{N}$ into $\mathcal{N}_D$ and $\mathcal{N}_S$, where $\mathcal{N} = \mathcal{N}_D \cup \mathcal{N}_S$ and $\mathcal{N}_D \cap \mathcal{N}_S = \varnothing$. The first set comprehends the users that rely

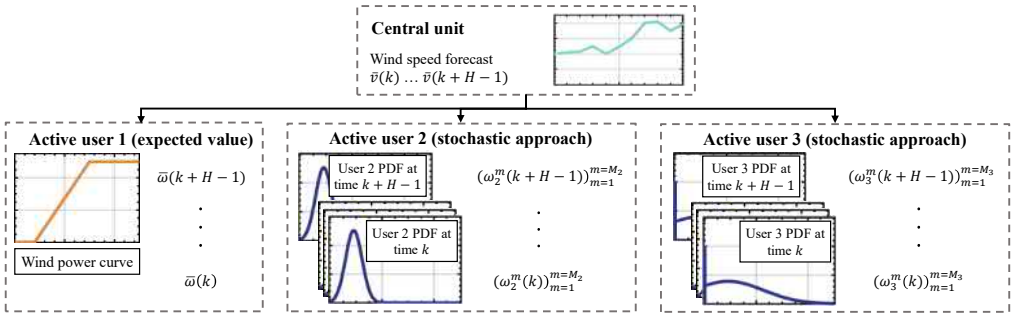

Figure 5.7: Illustration of the DSM scheme with three prosumers.

Algorithm 5.2 Rolling-horizon pFB algorithm

Input: $\bar{\boldsymbol{v}}$, $\boldsymbol{K}$,$\boldsymbol{\Omega}$, $L_{\min}$, $L_{\max}$
1: **for** $k = 1, ...$ **do**
2: Central unit broadcasts $\bar{\boldsymbol{v}}^k$ and $\boldsymbol{K}^k$
3: **for** $i = 1, ..., N$ **do**
4: **if** $i \in \mathcal{N}_{\mathcal{D}}$ **then**
5: Calculate $\bar{\boldsymbol{\omega}}^k$ with (5.16)
6: **else if** $i \in \mathcal{N}_{\mathcal{S}}$ **then**
7: Generate $\forall h \in \{k, ..., k+H-1\}$ a set of wind power PDF with (5.21) or (5.23) or (5.25)
8: Generate M_i IID samples $\forall h \in \{k, ..., k+H-1\}$ from the PDFs
9: **end if**
10: Set $\tilde{J}_i^k$ in accordance with (5.34)
11: **end for**
12: Calculate $L_P(h) = \sum_{i \in \mathcal{P}} l_i(h) \forall h \in \{k, ..., k+H-1\}$
13: Consider the new game $\mathscr{G}^k = (\mathcal{X}^k, \tilde{\mathbf{J}}^k)$
14: Compute GNE of $\mathscr{G}^k$, $\boldsymbol{x}^{*,k}$, with Algorithm 5.1
15: Apply $x_i^*(k)\ \forall i \in \mathcal{N}$
16: Update each user local feasible set $\boldsymbol{\Omega}^{k+1}$
17: **end for**
Output: $\boldsymbol{x}^*\{k\}$

on the information given by the central unit to calculate the expected value for the wind power forecast for the control horizon $\bar{\boldsymbol{\omega}}^k = (\bar{\omega}(h))_{h=k}^{k+H-1}$ (line 14). Conversely, the second set contains the users utilizing the SAA cost function (5.33): these users believe that the implementation of an approximated stochastic strategy will bring a profitable advantage. Latter users generate a different PDF for each time slot of the whole control horizon (line 7). The PDFs can be based only on the historical data (5.21), the wind speed forecast (5.23), or both (5.25). In the last two cases, users may also apply the instability index during the PDFs creation phase. Consequently, they are obtaining M IID samplings for every time slot of the control horizon from the PDFs (line 8). Therefore, each user defines its cost function (line 10) as:

$$\tilde{J}_i^k = \begin{cases} \bar{J}_i^k(\boldsymbol{x}_i^k, \boldsymbol{x}_{-i}^k, \bar{\boldsymbol{\omega}}^k) & \text{if } i \in \mathcal{N}_{\mathcal{D}} \\ \hat{J}_i^k(\boldsymbol{x}_i^k, \boldsymbol{x}_{-i}^k, \hat{\boldsymbol{\omega}}_i^k) & \text{if } i \in \mathcal{N}_{\mathcal{S}}. \end{cases} \tag{5.34}$$

We underline that the superscript k is used to indicate that the cost functions and the variables refer to the control horizon $\{k, ..., k+H-1\}$.

A new aggregated game is defined by considering the global feasible set $\mathcal{X}^k$ and the cost functions' collection $\tilde{\mathbf{J}}^k = (\tilde{J}_i^k)_{i=1}^{|\mathcal{N}|}$ (line 12-13). Moreover, the optimization problem is solved for the whole control horizon by calculating an equilibrium via Algorithm 5.1 (line 14).

The solution of the GNE problem is the optimal strategy $\boldsymbol{x}_i^{*,k}$ for each user $i \in \mathcal{N}$. However, following the receding horizon implementation, only the first step of the solution $x_i^*(k) = (g_i^*(k), s_i^*(k))^\top$ is implemented. Lastly, each user updates its local feasible set $\boldsymbol{\Omega}^{k+1}$ considering the implemented strategy.

5.5 Case Study

In this section, we present the results of the proposed methodology, obtained using real data from several offshore platforms in the North Sea. Each of these offshore drilling rigs includes a meteorological station that measures the wind speed, and other hourly averaged weather data. In particular, we chose eight platforms connected with the Meteorological Assimilation Data Ingest System (MADIS) [36], from which it is possible to obtain historical data and hourly current measured data. In Table 5.1 we show the platforms' coordinates; it is relevant to point out that several existing wind farms are present in the area (e.g., the Orsted Hornsea wind farm is located approximately at 53.880 N 1.790). We collect the forecasts employing a script that calls every hour within an API several different weather providers to obtain the next 24 hours wind speed forecasts for all the wind farms locations [37][38]. The employed wind speed forecasts data cover a period of 9 months. We underline that the forecasting models include the data of the offshore platforms through the MADIS.

5.5.1 Historical Weibull Parameters

As discussed earlier, the Weibull parameters have a significant impact on the historical wind power PDF. Therefore, to take into account this issue, we estimate the parameters for each platform and every day of the year. We calculate them by centering a 30-day window on a specific day and by getting all the available historical data for this window. For example, we estimate the Weibull parameters for August 21 by getting all the measured wind speed values in the interval between August 6 and September 5 for all the past available years (e.g., from 2009 to 2019). Table 5.2 shows the Weibull parameters calculated employing the data of the entire year and only for the month of May. The period of the year and the location cause the discrepancy between the parameters. For instance, the platforms closer to the coast hold a lower λ_w than the other platforms.

5.5.2 Forecast Standard Deviation

In our model, we assume that the wind speed forecasts' errors follow a normal distribution. Therefore, the only parameter to determine is the standard deviation σ. We obtain this parameter by performing an analysis of the weather providers' past forecasting errors. More in detail, for each weather provider and each station, we estimate through a linear regression procedure the standard deviation employing the forecasted value and the forecasting horizon. The results are comparable with the literature and show that some weather providers are more accurate than others. Moreover, the relation between the forecasting horizon, the forecasted wind speed value, and the standard deviation can have stronger or weaker importance. We employ the relations mentioned above to assign to each forecast a reasonable standard deviation value. In Fig. 5.8 we show these relations for one of the meteorological stations mentioned above.

5.5.3 Instability Index

In this work, we propose an instability index to evaluate the overall weather conditions. We calculate it by comparing the measured wind speed value in a time slot and the six past forecasts made for it. We calculate the relationship between the instability index and the standard deviation empirically. In particular, we bucket the index, and we calculate the standard deviation of the errors of the binned data.

Table 5.1: Offshore meteorological station location

Station code and name	Coordinates
Station 62121 - Carrack	53.500 N 2.700 E
Station 62127 - Cleeton	54.000 N 0.700 E
Station 62144 - Clipper	53.400 N 1.700 E
Station 62145 - North Sea	53.102 N 2.800 E
Station 62148 - Barque	53.600 N 1.500 E
Station 62149 - West Sole	53.700 N 1.100 E
Station 62150 - Amethyst	53.600 N 0.700 E
Station 62165 - Ravenspurn N.	54.000 N 1.100 E

Table 5.2: Weibull parameters for the considered stations

Station code	λ_w (Year)	k_w (Year)	λ_w (May)	k_w (May)
Station 62121	8.92797	2.24957	7.95649	2.61785
Station 62127	6.80654	1.95317	6.81277	1.76822
Station 62144	8.22549	2.09191	7.21183	2.45309
Station 62145	9.33593	2.15606	8.52988	2.48171
Station 62148	8.33172	2.13873	7.48135	2.59125
Station 62149	8.80511	2.17411	7.66658	2.53036
Station 62150	7.94109	2.12239	6.59681	2.38217
Station 62165	8.28173	2.18134	7.17359	2.63819

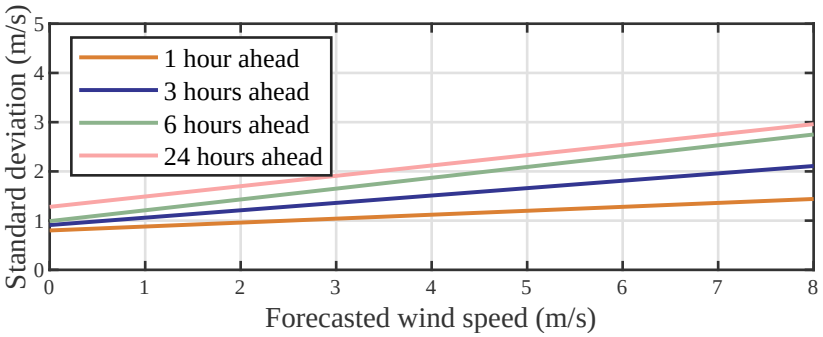

Figure 5.8: Correlation between the standard deviation of the prediction error, the predicted wind speed value, and the forecast horizon for the station 62121.

Figure 5.9(a) shows how the standard deviation changes compared with its mean value. The figure indicates approximately that for values of the index lower than one, the standard deviation is lower than the average value. Furthermore, Fig. 5.9(b) shows the relative frequency of the instability index. The index is mainly concentrated between 0.5 and 1; this indicates quite stable weather conditions, while higher values mean unstable conditions. Lastly, in Fig. 5.10 we show the instability index variability. The figure shows that the index is highly variable on a long term analysis, while it is relatively stable within a few hours.

At each time slot, we employ the index to increase or reduce the standard deviation of future forecasts. However, due to the index variability, we apply it to modify only the subsequent three slots of the control horizon.

5.5.4 Numerical case study

Once we have introduced the dataset, let us now define the smart grid model employed in the numerical simulations. The smart grid has 500 users, 50 of which are active.

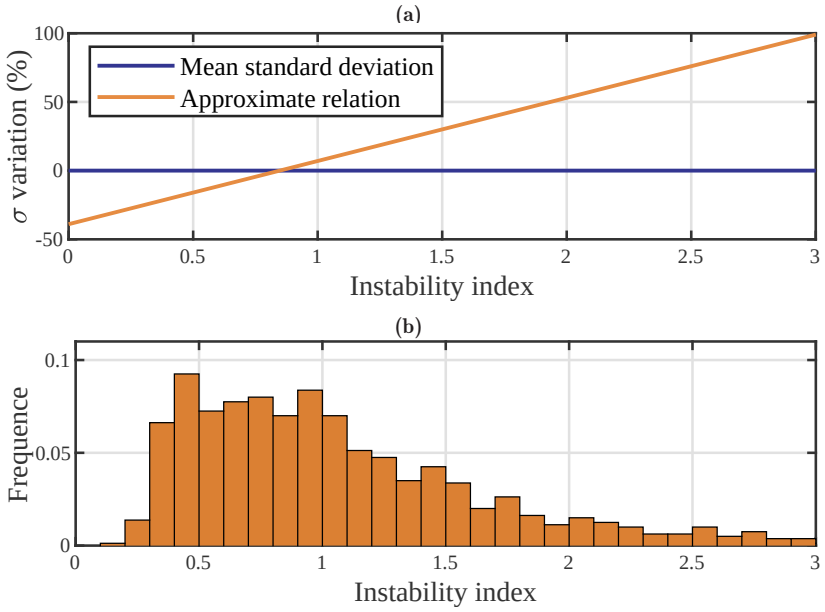

Figure 5.9: Instability index for the station 62121: (a) Relative percentage variation of the forecast standard deviation. (b) Relative frequency.

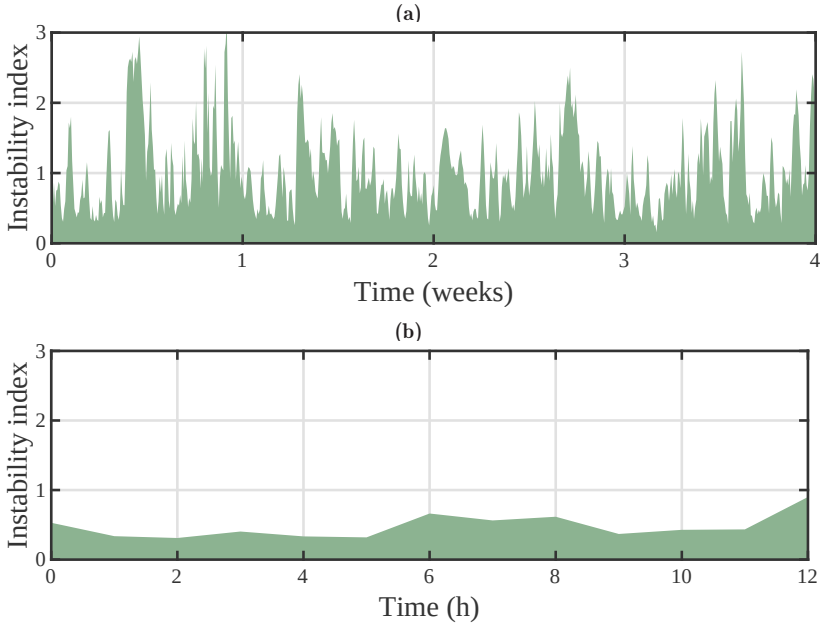

Figure 5.10: Instability index for the station 62121: (a) Variation in 4 weeks. (b) Variation in 12 hours.

We consider a total simulation time of 30 days and a control horizon of 24 hours. The wind turbine is a NedWind-40 with a rated power of $\omega_{\text{rated}} = 500\,kW$ and wind speed characteristic values $v_{\text{in}} = 4\,m/s$, $v_{\text{rated}} = 15\,m/s$, $v_{\text{out}} = 25\,m/s$. The prosumers have a consumption curve that follows the average load hourly curve for UK households (without electric heating) [39]. The load curve has a daily average of $\sum e_i(h) = 9.5kWh$ and presents a peak in the evening hours. The cost coefficient K_h is $0.20\,€/kWh$ for the daily hours (from 8:00 to 24:00) and $0.15\,€/kWh$ at night (00:00 to 08:00). For the sake of simplicity, the global constraints are proportional with the average aggregate load. For the sake of simplicity, we assume for each prosumer a null maximum controllable energy demand, i.e., $\xi_i = 0$, $\forall i \in \mathcal{N}$. The generation cost is supposed linear with a coefficient $\eta_i = 0.04\,€/kWh$; moreover, the maximum hourly dispatchable generation is

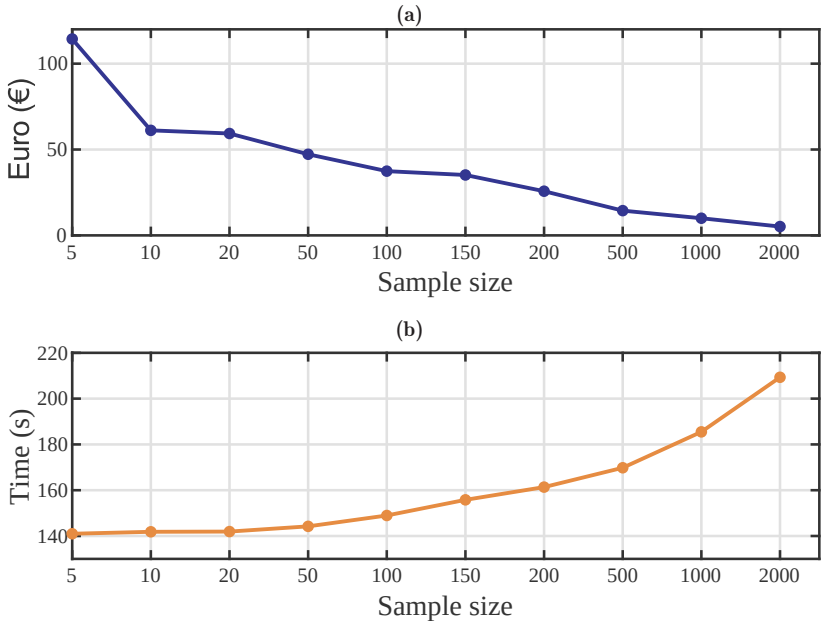

Figure 5.11: Results for station 62121 as a function of the number of samples. (a) Final cost standard deviation. (b) Computation time.

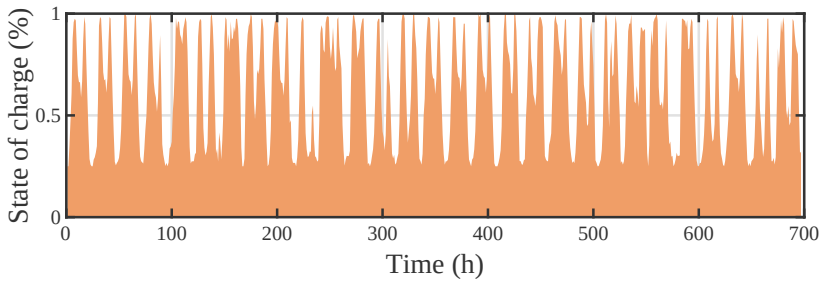

Figure 5.12: Results for station 62121: Mean state of charge of all batteries

$g_i^{\max}(h) = 0.1\,kWh$ while the maximum generation is $\psi_i = 0.8Hg_i^{\max}(h)$.

The storage devices are lithium-ion batteries, with a leakage rate $\alpha = 0.90$, charging and discharging inefficiency equal to $\beta_i^{(+)} = 0.99$ and $\beta_i^{(-)} = 1.01$, $c_i = 4kW$ the battery capacity, $s_i^{\max} = 0.5c_i\ KWh$ the maximum charging rate and $c_i^{\text{initial}} = q_i^{\min} = 0.25c_i$. Let us assume that all active users hold one dispatchable generation device and one energy storage device and that for the sake of simplicity, all the characteristics of these devices are identical. The computations for all the users are done in parallel. The gradient coefficient for Algorithm 1 is $\gamma = 0.1$ and the termination criterion is $\|\boldsymbol{x}^+ - \boldsymbol{x}\|_2^2 + \|\lambda^+ - \lambda\|_2^2 \leq 0.1$.

We added an additional day at the end of the simulation period with null energy demand and null wind power production. By adding this day, keeping energy in the battery would be a hidden cost for the prosumers. Therefore, we implicitly have that at the end of each simulation the state of charge of each battery equals the initial charge, thus, allowing us to compare fairly all the different set of simulations. In Fig. 5.12, we show the average state of charge for all active users $i \in \mathcal{S}$. From the figure, it is evident the highly cyclic pattern and that the state of charge at the end of the simulation period equal the initial one. Note that we also plotted the additional day to better show this behave.

Next, we perform an analysis from a stochastic point of view. Therefore, performing a single simulation for a defined set of data would not be significant. Hence, for each set of data, we repeat the simulation 50 times, which allows us to perform a more reliable analysis. In addition, in our analysis we aim at evaluating the savings obtained employing

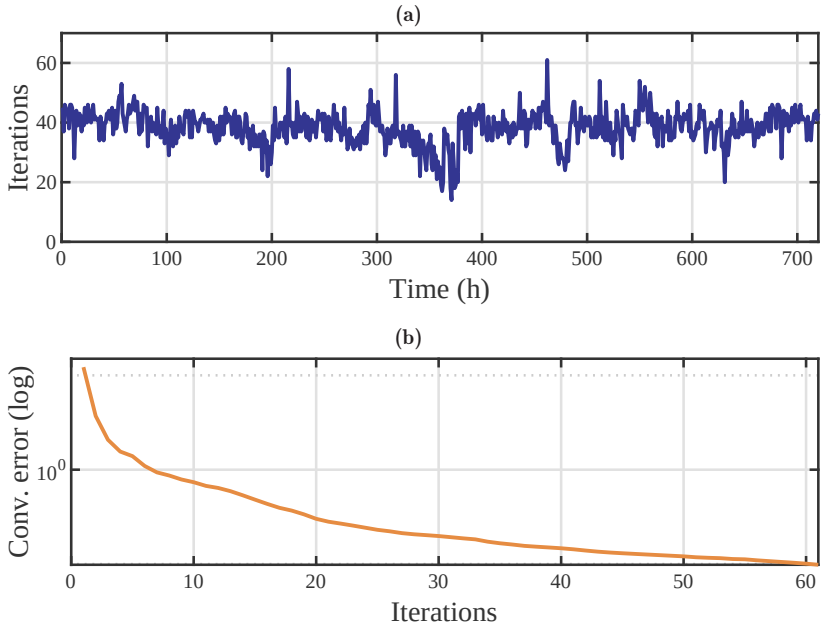

Figure 5.13: Computational results for station 62121. (a) Number of iterations required for each time shift. (b) Iterations vs convergence plot.

the proposed stochastic approach with respect to the standard expected value approach. However, before doing so, one could think of how big should the sampling size be to obtain an accurate approximate stochastic function. Hence, in the first case of analysis, we evaluate the results that a generic stochastic user obtains by increasing the number of samples. Let us remark that, for every sample size, we perform the simulation 50 times, and we evaluate the overall final results.

Figure 5.11(a) plots the standard deviation of the total costs that the stochastic user $i \in \mathcal{N}_{\mathcal{S}}$ pays to the grid. With the employed set of data, we obtain the convergence to the real stochastic value with approximately 200 samples; however, the total simulation time increases with the number of samples due to the increased complexity in the cost function.

Let us analyze the computational aspects of the proposed approach. Simulations are carried out in the MATLAB environment on a laptop equipped with a 1.3 GHz Intel Core i5 CPU and 8 GB RAM. By employing the aforementioned termination criterion, and analyzing the results of all the stations, Algorithm 1 required, on average, approximately 40 iterations to converge. Moreover, the algorithm did not require more than 92 iterations with all the tested settings. Concerning the simulation time, on the aforementioned machine, Algorithm 1 required, on average, 5.45 seconds to converge while the minimum and the maximum required time are 1.86 and 10.01 seconds, respectively. For instance, in Fig. 5.13 (a), we show the number of necessary iterations at each time shift of the simulation period, moreover, in Fig. 5.13 (b), we show the convergence to iteration plot for the time slot that required more iterations. Note that with 50 users, the chosen termination criterion is extremely severe.

The last case of analysis examines the performance of the proposed stochastic approach when different PDFs for the samples are employed. We analyze the results from the point of view of a single active user, named “test user”. In Table 5.3 we show a recap for the different strategies adopted by the active user in the different sets of data. We calculate a naive cost for the test user by using the strategy labeled Sim01; this is the cost that the test user pays where he employs the expected value approach, together with all its active competitors.

In Fig. 5.14(a), we employ a Boxplot graph to show the savings or the losses that the test user obtains by adopting a different strategy to handle the uncertainty in wind power

Table 5.3: Active users' strategy (test user)

Code	Test user strategy	Other users'
Sim01	Expected	49 Expected
Sim02	Historical PDF	49 Expected
Sim03	Forecast PDF	49 Expected
Sim04	Forecast PDF with inst. index	49 Expected
Sim05	Composed PDF	49 Expected
Sim06	Composed PDF with inst. index	49 Expected

Table 5.4: Active users' strategy (all prosumers)

Code	All users strategy
Sim12	Historical PDF
Sim13	Forecast PDF
Sim14	Forecast PDF with inst. index
Sim15	Composed PDF
Sim16	Composed PDF with inst. index

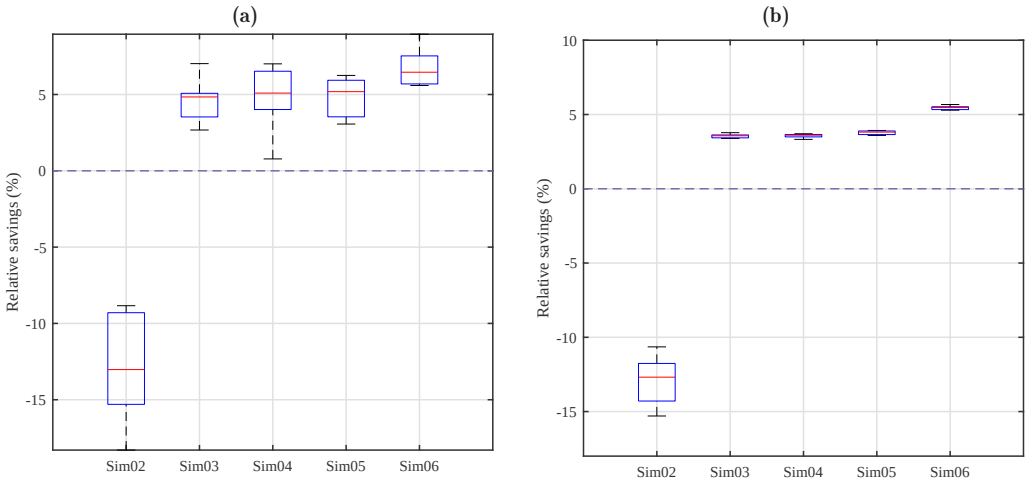

Figure 5.14: Results for station 62121: (a) Boxplot of the test user savings with respect to the expected value strategy. (b) Boxplot of the total grid savings by employing a stochastic approach.

availability. In particular, using the strategy labeled Sim02, we show the results obtained with the mere use of the historical PDF and by neglecting the use of updatable forecasts; in this case, we obtain a loss with respect to the use of the forecast expected value. In addition, by the strategies labeled Sim03, Sim04, Sim05, and Sim06 we show how much the test user can save on average by adopting the proposed stochastic strategy. The simulations results show that the use of a better PDF, made by employing the instability index and/or by creating a composed PDF, increases the proposed approach performance.

Lastly, in Fig. 5.14(b) we show the total grid cost (the so-called welfare) when all the users employ a stochastic strategy, see Table 5.4 for a recap of the strategies adopted by all the active user. The simulations show that, when all the active users consider a wind power PDF (i.e., in cases Sim13, Sim14, Sim15, Sim16), obviously the savings are lower than in case of a single stochastic user (i.e., in cases Sim03, Sim04, Sim05, Sim06), as showed by the comparison of Fig. 11 (a) with Fig. 11 (b). On the other hand, the results in Fig. 11 (b) confirm that there is a clear saving with respect to the expected value case. Finally, the higher savings are obtained in Sim16, i.e., when the composed PDF is used together with the instability index.

5.6 Conclusion

We presented a novel approach to implement demand side management in smart grids with uncertain wind power availability. The evidence from this study shows that in realistic situations, considering different wind power availability scenarios increases the advantage of individual users against the competitors. In addition, we show that by including historical data and by taking into account the weather conditions with the proposed instability index, it is possible to improve the results significantly. Besides, the proposed approach is also able to improve the overall grid welfare.

Future work should focus on including the wind power availability in the global grid constraint, for instance by employing a penalty function or chance constraints. Moreover, the model could be enhanced by including other devices such as different kinds of controllable loads or individually owned energy sources, and integrating additional objective functions and technical constraints affecting the operations of system components.

References

[1] Tuballa, M. L. and Abundo, M. L., "A review of the development of smart grid technologies," *Renew. Sust. Energ. Rev.*, vol. 59, pp. 710–725, 2016.

[2] Kakran, S. and Chanana, S., "Smart operations of smart grids integrated with distributed generation: A review," *Renew. Sust. Energ. Rev.*, vol. 81, pp. 524–535, 2018.

[3] Ouammi, A., Dagdougui, H., and Sacile, R., "Optimal control of power flows and energy local storages in a network of microgrids modeled as a system of systems," *IEEE Trans. Control Syst. Technol.*, vol. 23, no. 1, pp. 128–138, 2014.

[4] Carli, R., Dotoli, M., and Pellegrino, R., "A hierarchical decision-making strategy for the energy management of smart cities," *IEEE Trans. Autom. Sci. Eng.*, vol. 14, no. 2, pp. 505–523, 2016.

[5] Dörfler, F., Bolognani, S., Simpson-Porco, J. W., and Grammatico, S., "Distributed control and optimization for autonomous power grids," in *2019 18th European Control Conference (ECC)*, IEEE, 2019, pp. 2436–2453.

[6] Maharjan, S., Zhu, Q., Zhang, Y., Gjessing, S., and Başar, T., "Demand response management in the smart grid in a large population regime," *IEEE Trans. Smart Grid*, vol. 7, no. 1, pp. 189–199, 2015.

[7] Atzeni, I., Ordóñez, L. G., Scutari, G., Palomar, D. P., and Fonollosa, J. R., "Demand-side management via distributed energy generation and storage optimization," *IEEE Trans. Smart Grid*, vol. 4, no. 2, pp. 866–876, 2012.

[8] Carli, R. and Dotoli, M., "Decentralized control for residential energy management of a smart users' microgrid with renewable energy exchange," *IEEE/CAA Journal of Automatica Sinica*, vol. 6, no. 3, pp. 641–656, 2019.

[9] Estrella, R., Belgioioso, G., and Grammatico, S., "A shrinking-horizon, game-theoretic algorithm for distributed energy generation and storage in the smart grid with wind forecasting," *IFAC-PapersOnLine*, vol. 52, no. 3, pp. 126–131, 2019.

[10] Wu, H., Shahidehpour, M., and Al-Abdulwahab, A., "Hourly demand response in day-ahead scheduling for managing the variability of renewable energy," *IET Gener. Transm. Distrib.*, vol. 7, no. 3, pp. 226–234, 2013.

[11] Hans, C. A., Sopasakis, P., Raisch, J., Reincke-Collon, C., and Patrinos, P., "Risk-averse model predictive operation control of islanded microgrids," *IEEE Trans. Control Syst. Technol.*, 2019.

[12] Jabr, R. and Pal, B. C., "Intermittent wind generation in optimal power flow dispatching," *IET Gener. Transm. Distrib.*, vol. 3, no. 1, pp. 66–74, 2009.

[13] Yao, F., Dong, Z. Y., Meng, K., Xu, Z., Iu, H. H.-C., and Wong, K. P., "Quantum-inspired particle swarm optimization for power system operations considering wind power uncertainty and carbon tax in australia," *IEEE Trans. Ind. Informat.*, vol. 8, no. 4, pp. 880–888, 2012.

[14] Biswas, P. P., Suganthan, P., and Amaratunga, G. A., "Optimal power flow solutions incorporating stochastic wind and solar power," *Energy Convers. Manag.*, vol. 148, pp. 1194–1207, 2017.

[15] Quan, H., Yang, D., Khambadkone, A. M., and Srinivasan, D., "A stochastic power flow study to investigate the effects of renewable energy integration," in *2018 IEEE Innovative Smart Grid Technologies-Asia (ISGT Asia)*, IEEE, 2018, pp. 19–24.

[16] Aghajani, G., Shayanfar, H., and Shayeghi, H., "Demand side management in a smart micro-grid in the presence of renewable generation and demand response," *Energy*, vol. 126, pp. 622–637, 2017.

[17] Kun, Y., Zhang, K., Zheng, Y., Dawei, L., Ying, W., and Zhenglin, Y., "Irregular distribution of wind power prediction," *Journal of Modern Power Systems and Clean Energy*, vol. 6, no. 6, pp. 1172–1180, 2018.

[18] Ko, W., Hur, D., and Park, J.-K., "Correction of wind power forecasting by considering wind speed forecast error," *Journal of International Council on Electrical Engineering*, vol. 5, no. 1, pp. 47–50, 2015.

[19] Pazouki, S., Haghifam, M.-R., and Moser, A., "Uncertainty modeling in optimal operation of energy hub in presence of wind, storage and demand response," *International Journal of Electrical Power & Energy Systems*, vol. 61, pp. 335–345, 2014.

[20] Afshar, K. and Shokri Gazafroudi, A., "Application of stochastic programming to determine operating reserves with considering wind and load uncertainties," *Journal of Operation and Automation in Power Engineering*, vol. 1, no. 2, pp. 96–109, 2007.

[21] Zheng, Y., Li, S., and Tan, R., "Distributed model predictive control for on-connected microgrid power management," *IEEE Trans. Control Syst. Technol.*, vol. 26, no. 3, pp. 1028–1039, 2017.

[22] Mohsenian-Rad, A.-H., Wong, V., Jatskevich, J., Schober, R., and Leon-Garcia, A., "Autonomous demand side management based on game-theoretic energy consumption scheduling for the future smart grid," *IEEE Trans. Smart Grid*, vol. 1, no. 3, pp. 320–331, 2010.

[23] Gao, M. S. and Jiang, H., "A dispatch algorithm for smart grid with wind generation," in *Applied Mechanics and Materials*, Trans Tech Publ, vol. 704, 2015, pp. 186–189.

[24] Ghaffari, A., Krstić, M., and Seshagiri, S., "Power optimization and control in wind energy conversion systems using extremum seeking," *IEEE Trans. Control Syst. Technol.*, vol. 22, no. 5, pp. 1684–1695, 2014.

[25] Carta, J. A., Ramirez, P., and Velazquez, S., "A review of wind speed probability distributions used in wind energy analysis: Case studies in the canary islands," *Renew. Sust. Energ. Rev.*, vol. 13, no. 5, pp. 933–955, 2009.

[26] "Nedwind-40 technical data sheet," NedWind Rhenen bV. (), [Online]. Available: https://www.windsofchange.dk/downloads.php?a=66&t=1&f=Nedwind.pdf (visited on 12/12/2019).

[27] Hetzer, J., David, C. Y., and Bhattarai, K., "An economic dispatch model incorporating wind power," *IEEE Trans. on Energy Convers.*, vol. 23, no. 2, pp. 603–611, 2008.

[28] Schinazi, R. B., *Transformations of Random Variables and Random Vectors*. Springer, 2012, pp. 201–268.

[29] Iizaka, T., Jintsugawa, T., Kondo, H., Nakanishi, Y., Fukuyama, Y., and Mori, H., "A wind power forecasting method and its confidence interval estimation," *Electrical Engineering in Japan*, vol. 186, no. 2, pp. 52–60, 2014.

[30] Pinson, P. and Kariniotakis, G., "On-line assessment of prediction risk for wind power production forecasts," *Wind Energy: An International Journal for Progress and Applications in Wind Power Conversion Technology*, vol. 7, no. 2, pp. 119–132, 2004.

[31] Clemen, R. T. and Winkler, R. L., *Calibrating and combining precipitation probability forecasts*. Springer, 1987, pp. 97–110.

[32] Scutari, G., Palomar, D. P., Facchinei, F., and Pang, J.-s., "Convex optimization, game theory, and variational inequality theory," *IEEE Signal Process. Mag.*, vol. 27, no. 3, pp. 35–49, 2010.

[33] Belgioioso, G. and Grammatico, S., "Projected-gradient algorithms for generalized equilibrium seeking in aggregative games are preconditioned forward-backward methods," in *2018 European Control Conference (ECC)*, IEEE, 2018, pp. 2188–2193.

[34] Shapiro, A., "Stochastic programming approach to optimization under uncertainty," *Mathematical Programming*, vol. 112, no. 1, pp. 183–220, 2008.

[35] Kim, S., Pasupathy, R., and Henderson, S. G., *A guide to sample average approximation*. Springer, 2015, pp. 207–243.

[36] "Meteorological assimilation data ingest system," National Oceanic and Atmospheric Administration. (), [Online]. Available: www.madis.ncep.noaa.gov (visited on 12/12/2019).

[37] "Storm glass – the global weather forecast api," Människa Maskin AB. (), [Online]. Available: www.stormglass.io (visited on 12/12/2019).

[38] "Weather api - historical weather api," Weatherbit LCC. (), [Online]. Available: www.weatherbit.io/ (visited on 12/12/2019).

[39] "Household electricity survey," Department of Energy and Climate Change. (), [Online]. Available: www.gov.uk/government/publications/household-electricity-survey--2 (visited on 12/12/2019).

Part 2: Ensuring Quality and Feasibility of Autonomous Power Grids Operation

Chapter 6

Game-theoretic Control Frameworks of Networked Systems with Nonconvex Coupling Constraints

Abstract

We consider a class of Nash games with nonconvex coupling constraints where we leverage the theory of tangent cones to define a novel notion of local equilibrium: *Clarke's local generalized Nash equilibrium* (CL-GNE). Our first technical contribution is to show the stability of these equilibria on a specific local subset of the original feasible set. As a second contribution, we show that the proposed notion of local equilibrium can be equivalently formulated as the solution of a quasi-variational inequality, remarkably, with equal Lagrange multipliers. Next, we define conditions for the existence and uniqueness of the CL-GNE. To compute such an equilibrium, we propose two discrete-time distributed dynamics, or fixed-point iterations. Our third technical contribution is to prove convergence under (strongly) monotone assumptions on the pseudo-gradient mapping of the game. Finally, we apply our theoretical results to a competitive version of the optimal power flow control problem.

Contents

6.1 Introduction

In noncooperative games, a number of self-interested agents with their own individual dynamics and constraints aim at optimizing their objective functions, possibly in competition with each other, e.g. due to the scarcity of shared resources. In this context, one of the most important concepts is the *Nash equilibrium* (NE) [1], which represents the common way to define the solution of a noncooperative game in many practical applications, from electricity markets to mobile-edge computing [2], [3]. Nevertheless, in several applications, the strategy that an agent can select depends not only on their preferences but also on those adopted by the other agents. In this case, the concept of equilibrium among agents is extended to the so-called *generalized Nash equilibrium* (GNE), which is recently getting strong attention from researchers of different fields, since the presence of coupled feasible sets is widespread in real-world applications [4]–[8].

From a control-theoretic perspective, the objective is to develop a coordination mechanism, namely, a discrete-time dynamical system for updating the strategies of the

agents towards an equilibrium: this is the so-called *generalized Nash equilibrium problem* (GNEP). Solving this problem is difficult, since the objective function and the constraints of each agent are interdependent. While the NE of a game with compact local feasible sets and strongly monotone pseudogradient is unique, uniqueness is instead not guaranteed in games with shared constraints. Thus, most methods to reach an equilibrium rely on the *variational inequality* (VI) theory [9], which has the advantage of possibly selecting a particular solution named *normalized solution* or *variational generalized Nash equilibrium* (vGNE). This solution has special properties and is usually referred as "economically meaningful" [9] or "fair" [10].

Most of the related literature focuses on *jointly convex* (JC) games that have locally convex objective functions and convex feasible set [11]. These assumptions allow ensuring the existence of equilibria and global convergence to solution algorithms [12], [13]. Actually, thanks to convexity, the convergence of several classes of multi-agent dynamics (centralized, decentralized, and distributed) to a GNE can be guaranteed [10], [11], [14]–[16].

Nevertheless, in many applications, convexity does not hold and thus some alternative approaches have been proposed in the literature. Among the works considering nonconvex games, let us mention the equilibrium notions of weak NE [17], local NE [18], generalized equilibrium [19], and critical NE [12]. All these concepts focus on the *Nash equilibrium problem* (NEP) and are not applicable to games with coupling constraints. For instance, in [13] and [20], the authors develop an optimization-based theory for games with nonconvex objective functions and nonconvex side constraints. Specifically, the authors define the concept of quasi-Nash equilibrium, defined as the solution of the VI obtained by aggregating the first-order optimality conditions of the individual agents. This approach has been applied to nonconvex power allocation games in cognitive radio networks [20], [21].

In [22] the authors present a framework to characterize local Nash equilibria in continuous games with nonconvex local feasible sets. The approach relies on necessary and sufficient first- and second-order conditions to ensure optimality of the local equilibrium point, thanks to the local convexity of the solution space around the equilibrium point. The mentioned approaches typically require either local convexity or the satisfaction of some optimality conditions, while they focus on problems with nonconvex objective functions. Moreover, the existence and convergence to such an equilibrium are not guaranteed.

Differently from the state of the art, in this chapter we introduce a novel local equilibrium concept that we call *Clarke's local generalized Nash equilibrium* (CL-GNE), since it is based on Clarke's cones theory. In particular, we define this equilibrium over Clarke's tangent cone as a local subset, and we show that it satisfies the first-order optimality conditions of the optimization problems of the agents. By characterizing such equilibria, we leverage on the theory of *quasi-variational inequalities* (QVI) to define locally variational, and thus locally fair, equilibrium points. Then, we show their existence and uniqueness in a well-defined subset of the original nonconvex feasible set. To compute a variational CL-GNE, we design two discrete-time autonomous dynamics, or fixed-point iterations. We prove convergence of our proposed dynamics to an equilibrium under certain technical conditions, namely (strongly) monotone pseudo-gradient mapping of the game and proximally smooth feasible set.

Finally, we apply our theoretical results to power systems control. Specifically, we define a *direct current* (DC) microgrid model comprehending several prosumers owning dispatchable generators aiming at maximizing their profits in a liberalized noncooperative market. In our model, we include physical constraints, thus our approach can be seen as a noncooperative version of the *optimal power flow* (OPF) problem to determine the best operating point with respect to power losses and energy production costs. Several game-theoretic methods have been proposed for solving this problem [23], yet most disregard physical constraints due to their nonconvexity. Instead, we propose a noncooperative version of the OPF including the actual power flow equations, namely, a set of nonlinear nonconvex algebraic equations. The resulting noncooperative game with shared nonconvex constraints falls exactly in our proposed framework, thus allowing us

to analyze the proposed concept in one of the most important problems in power systems control.

Basic Notation

$\mathbb{R}^n$, $\mathbb{R}^n_{>0}$ and $\mathbb{R}^n_{\geq 0}$ denote the set of real, positive real, and non-negative real n-dimensional vectors, respectively. $\mathbb{N}$ denotes the set of natural numbers. $\mathbb{B}$ denotes the closed unit ball centered at zero. $A^\top$ denotes the transpose of A. $\|A\|$ is the square norm of A. $\mathbf{0}_n$ and $\mathbf{1}_n$ indicate the column vectors with n entries all equal to 0 and to 1, i.e., $\mathbf{0}_n := (0, ..., 0)^\top \in \mathbb{R}^n$ and $\mathbf{1}_n := (1, ..., 1)^\top \in \mathbb{R}^n$, respectively. Moreover, $\mathbf{x} := \text{col}(\mathbf{x}_1, ..., \mathbf{x}_n)$ is equal to $\mathbf{x} := (\mathbf{x}_1^\top, ..., \mathbf{x}_n^\top)^\top$. We define the mapping $\text{proj}_{\mathcal{X}}(\cdot) : \mathbb{R}^n \to \mathcal{X}$ as the projection into the generic closed non-empty set $\mathcal{X} \subseteq \mathbb{R}^n$, i.e., $\text{proj}_{\mathcal{X}}(\mathbf{y}) = \text{argmin}_{\mathbf{x}\in\mathcal{X}} \|\mathbf{x} - \mathbf{y}\|$. Moreover, we define the mapping $\text{dist}(\mathbf{x}, \mathbf{y}) := \|\mathbf{x} - \mathbf{y}\|$ as the distance operator between two points and $\text{dist}(\mathbf{y}, \mathcal{X}) := \min_{\mathbf{x}\in\mathcal{X}} \|\mathbf{x} - \mathbf{y}\|$ as the distance operator between a point and a set. For a generic closed non-empty set $\mathcal{X} \subseteq \mathbb{R}^n$, we define the topological closure $\text{cl}(\mathcal{X})$ and the boundary $\text{bd}(\mathcal{X})$. The mapping $F(\cdot) : \mathbb{R}^n \to \mathbb{R}^n$ is Lipschitz continuous with a constant $\ell \in \mathbb{R}_{>0}$ if $\|F(\mathbf{x}) - F(\mathbf{y})\| \leq \ell \|\mathbf{x} - \mathbf{y}\|$, $\forall \mathbf{x}, \mathbf{y} \in \mathbb{R}^n$. F is strongly monotone with a constant $\mu \in \mathbb{R}_{>0}$ if $(F(\mathbf{x}) - F(\mathbf{y}))^\top (\mathbf{x} - \mathbf{y})) \geq \mu \|\mathbf{x} - \mathbf{y}\|^2$, $\forall \mathbf{x}, \mathbf{y} \in \mathbb{R}^n$ while F is pseudo monotone if $F(\mathbf{y})^\top (\mathbf{x} - \mathbf{y})) \geq 0 \implies F(\mathbf{x})^\top (\mathbf{x} - \mathbf{y})) \geq 0$, $\forall \mathbf{x}, \mathbf{y} \in \mathbb{R}^n$. Lastly, we define $\bar{F}_{\mathcal{X}} := \sup_{\mathbf{x}\in\mathcal{X}} \|F(\mathbf{x})\|$.

6.2 Generalized Nash Equilibrium Problems

We consider a game composed by a set of N agents, indexed by $i \in \mathcal{N} := \{1, ..., N\} \subseteq \mathbb{N}$ each with decision variables $\mathbf{x}_i \in \mathbb{R}^n$. Moreover, we define vectors $\mathbf{x}_{-i} := \text{col}(\mathbf{x}_1, ..., \mathbf{x}_{i-1}, \mathbf{x}_{i+1}, ..., \mathbf{x}_N) \in \mathbb{R}^{(N-1)n}$ and $\mathbf{x} := \text{col}(\mathbf{x}_1, ..., \mathbf{x}_i, ..., \mathbf{x}_N) \in \mathbb{R}^{Nn}$, collecting the strategies of all agents different from i and the strategies of all agents, respectively. Each agent $i \in \mathcal{N}$ tries to minimize its cost function $f_i(\mathbf{x}_i, \mathbf{x}_{-i}) : \mathbb{R}^n \times \mathbb{R}^{(N-1)n} \to \mathbb{R}$ by choosing a strategy in its local feasible set $\mathbf{x}_i \in \Omega_i \subseteq \mathbb{R}^n$, hence, $\mathbf{x} \in \mathbf{\Omega} = \prod_{i=1}^N \mathbf{\Omega}_i$.

In addition, let us consider a finite number of constraints indexed by $m \in \mathcal{M} := \{1, ..., M\} \subseteq \mathbb{N}$, each denoted as $g_m(\mathbf{x}) \leq 0$, defining the coupled feasible set:

$$\mathcal{X} = \mathbf{\Omega} \cap \left\{\mathbf{x} \in \mathbb{R}^{Nn} \mid g(\mathbf{x}) \leq \mathbf{0}_M\right\}, \tag{6.1}$$

where $g(\mathbf{x}) := ((g_m(\mathbf{x}))_{m\in\mathcal{M}})$. By defining the set-valued mapping $\mathcal{X}_i(\mathbf{x}_{-i}) := \{\mathbf{y}_i \in \mathbb{R}^n \mid (\mathbf{y}_i, \mathbf{x}_{-i}) \in \mathcal{X}\}$ one can define the N interdependent optimization problems as follows:

$$\forall i \in \mathcal{N} : \quad \begin{cases} \min\limits_{\mathbf{x}_i} & f_i(\mathbf{x}_i, \mathbf{x}_{-i}) \\ \text{s.t.} & \mathbf{x}_i \in \mathcal{X}_i(\mathbf{x}_{-i}). \end{cases} \tag{6.2}$$

To make the notation easier to follow, in the rest of this chapter, we ignore the presence of local constraints. However, they can be included directly in the coupled feasible set or approximated via barrier functions in the objective function.

The latter problem is a GNEP whose solution is the GNE, formally defined as follows.

Definition 6.2.1 (*Generalized Nash equilibrium*)

A GNE is a collective strategy $\mathbf{x}^* \in \mathcal{X}$ such that for each $i \in \mathcal{N}$ it holds:

$$f_i(\mathbf{x}_i^*, \mathbf{x}_{-i}^*) \leq \inf\left\{f_i(\mathbf{x}_i, \mathbf{x}_{-i}^*) \,|\, \mathbf{x}_i \in \mathcal{X}_i(\mathbf{x}_{-i}^*)\right\}. \tag{6.3}$$

□

In other words, a GNE is a collective strategy profile satisfying the property that no single agent in the game can improve its objective function by unilaterally changing its strategy with another feasible one.

Properties such as stability, uniqueness, and optimality of the GNE have been studied under different standing assumptions. The convexity of the coupling feasible set $\mathcal{X}$ in

(6.1) is one of the most employed standing assumptions [24]. Due to the nature of several applications, this set may result to be nonconvex. Here, we aim at analyzing the particular case of nonconvex feasible sets. Let us first introduce some preliminary assumptions used in the rest of the chapter [10].

Assumption 6.2.1

For each $i \in \mathcal{N}$ and for every $\mathbf{x}_{-i}$, the function $f_i(\cdot, \mathbf{x}_{-i})$ in (6.2) is convex and continuously differentiable. □

Assumption 6.2.2

For each $m \in \mathcal{M}$ and for every $\mathbf{x}_{-i}$, the function $g_m(\cdot, \mathbf{x}_{-i})$ in (6.1) is continuously differentiable (possibly nonconvex). The coupled feasible set $\mathcal{X}$ in (6.1) is nonempty, compact and satisfies the Mangasarian–Fromovitz constraint qualification (MFCQ). □

6.3 Clarke's Local Generalized Nash Equilibria: Definition and Characterization

Let us search for weaker equilibrium conditions, following the approach –commonly used in nonconvex optimization– which consists in looking for a stationary (possibly locally optimal) solution. In particular, let us propose a novel concept, namely *Clarke's local generalized Nash equilibrium problem* (CL-GNEP) and let us search for its possible solution, i.e., the *Clarke's local generalized Nash equilibrium* (CL-GNE). Our approach relies on the definition of Clarke's tangent cone $T_{\mathrm{cl}}(\mathcal{X}, \mathbf{x})$ at a point $\mathbf{x}$ for the (nonconvex) set $\mathcal{X}$ in (6.1) (see Appendix 6.A for preliminaries on cones). We note that the tangent cone is convex even if $\mathcal{X}$ is not. For the sake of keeping the notation light, let us define $\tilde{\mathcal{X}}(\mathbf{x}) := \mathbf{x} + T_{\mathrm{cl}}(\mathcal{X}, \mathbf{x})$.

Definition 6.3.1 (*Clarke's local generalized Nash equilibrium*)

A CL-GNE is a collective strategy $\mathbf{x}^* \in \mathcal{X}$ such that for each $i \in \mathcal{N}$:

$$f_i(\mathbf{x}_i^*, \mathbf{x}_{-i}^*) \leq \inf\{f_i(\mathbf{y}, \mathbf{x}_{-i}^*) \,|\, \mathbf{y} \in \tilde{\mathcal{X}}_i(\mathbf{x}_{-i}^*)\} \tag{6.4}$$

where the set-valued mapping $\tilde{\mathcal{X}}_i(\mathbf{x}_{-i}) := \{\mathbf{y}_i \in \mathbb{R}^n \mid (\mathbf{y}_i, \mathbf{x}_{-i}) \in \tilde{\mathcal{X}}(\mathbf{x})\}$ is the tangent cone of the i-th agent. □

Note that $\tilde{\mathcal{X}}(\mathbf{x})$ is the overall tangent cone, i.e., $\tilde{\mathcal{X}}(\mathbf{x}) = \prod_{i=1}^{N} \tilde{\mathcal{X}}_i(\mathbf{x}_{-i})$.

In other words, a CL-GNE is a collective strategy profile with the property that no single agent can benefit by unilaterally changing its strategy with another feasible one contained in Clarke's tangent cone. Due to its definition, the set of CL-GNEs is a superset of that of GNEs since Clarke's tangent cone comprehends only a subset of the original coupled feasible set.

Remark 6.3.1

Whenever the feasible set $\mathcal{X}$ in (6.1) is convex, the CL-GNEP is equivalent to the GNEP, since the set of CL-GNEs is equal to that of GNEs. Indeed, Clarke's tangent cone of a convex set includes the convex set itself[25]. □

A first approach to characterize a CL-GNE $\mathbf{x}^* \in \mathcal{X}$ is based on employing Clarke's normal cone $N_{\mathrm{cl}}(\mathcal{X}, \mathbf{x}^*)$, see Appendix 6.A. For each agent $i \in \mathcal{N}$ the following optimality condition must be verified: $-\nabla f_i(\mathbf{x}_i^*, \mathbf{x}_{-i}^*) \in N_{\mathrm{cl}}(\mathcal{X}_i(\mathbf{x}_{-i}^*), \mathbf{x}_i^*)$. This version of the optimality conditions is however not useful enough, due to the difficulty of constructing the normal cone in the nonconvex case. Thus, let us characterize the CL-GNE by deriving the *Karush–Kuhn–Tucker* (KKT) conditions for each agent $i \in \mathcal{N}$. For a constrained nonlinear program with a differentiable objective function, stationarity is defined by the KKT conditions that are necessarily satisfied by a locally optimal solution under an

appropriate constraint qualification. More formally, the KKT conditions for each agent are:

$$\text{KKT}_i : \begin{cases} 0 \in \nabla_{\mathbf{x}_i} f_i(\mathbf{x}_i^*, \mathbf{x}_{-i}^*) + \nabla_{\mathbf{x}_i} g(\mathbf{x}_i^*, \mathbf{x}_{-i}^*)\boldsymbol{\lambda}_i \\ \mathbf{0}_M \leq \boldsymbol{\lambda}_i \perp g(\mathbf{x}_i^*, \mathbf{x}_{-i}^*) \leq \mathbf{0}_M \end{cases} \tag{6.5}$$

where we assume the existence of dual variables $\boldsymbol{\lambda}_i = \text{col}(\lambda_i^1, ..., \lambda_i^m, ..., \lambda_i^M) \in \mathbb{R}^M_{\geq 0}$ satisfying the KKT optimality conditions for each individual optimization problem in (6.2). Note that if a constraint g_m is not active at $\mathbf{x}$, then the corresponding Lagrangian multiplier λ_i^m is necessarily zero for all agents $i \in \mathcal{N}$. On the other hand, multipliers corresponding to the same active constraint can have different values among agents.

Before exploiting the aforementioned optimality conditions, let us report the following remark.

Remark 6.3.2

Under Assumption 6.2.2, Clarke's tangent cone equals the so-called linearised feasible directions set denoted as $\mathcal{F}(\mathcal{X}, \mathbf{x})$, i.e., $T_{cl}(\mathcal{X}, \mathbf{x}) = \mathcal{F}(\mathcal{X}, \mathbf{x})$, see Appendix 6.A for technical details. □

Theorem 6.3.1

Let Assumption 6.2.1 and 6.2.2 hold. Then, the following statements are equivalent:

(i) *$\mathbf{x}^* \in \mathcal{X}$ is a CL-GNE;*

(ii) *for each $i \in \mathcal{N}$, $-\nabla f_i(\mathbf{x}_i^*, \mathbf{x}_{-i}^*) \in N_{cl}(\mathcal{X}_i(\mathbf{x}_{-i}^*), \mathbf{x}_i^*)$;*

(iii) *for each $i \in \mathcal{N}$, there exists a vector $\boldsymbol{\lambda}_i = \text{col}(\lambda_i^1, ..., \lambda_i^m, ..., \lambda_i^M) \in \mathbb{R}^M_{\geq 0}$ satisfying the KKT conditions in (6.5).*

□

Proof 6.3.1

To prove (i) ⇔ (ii), we recall that Clarke's tangent cone comprehends only a subset of the original set; thus, we can write the following condition on the cost function of each agent:

$$f_i(\mathbf{y}, \mathbf{x}_{-i}^*) \geq f_i(\mathbf{x}_i^*, \mathbf{x}_{-i}^*) + \nabla f_i(\mathbf{x}_i^*, \mathbf{x}_{-i}^*)^\top (\mathbf{y} - \mathbf{x}_i^*), \ \forall \mathbf{y} \in \tilde{\mathcal{X}}_i(\mathbf{x}_{-i}^*). \tag{6.6}$$

Moreover, since $-\nabla f_i(\mathbf{x}_i^*, \mathbf{x}_{-i}^*) \in N_{cl}(\mathcal{X}_i(\mathbf{x}_{-i}^*), \mathbf{x}_i^*)$ and due to the definition of normal cone, we have:

$$\inf_{\mathbf{y} \in \tilde{\mathcal{X}}_i(\mathbf{x}_{-i}^*)} \nabla f_i(\mathbf{x}_i^*, \mathbf{x}_{-i}^*)^\top (\mathbf{y} - \mathbf{x}_i^*) \geq 0. \tag{6.7}$$

Then, it follows that $f_i(\mathbf{y}, \mathbf{x}_{-i}^*) \geq f_i(\mathbf{x}_i^*, \mathbf{x}_{-i}^*)$, $\forall \mathbf{y} \in \tilde{\mathcal{X}}_i(\mathbf{x}_{-i}^*)$. Hence, if this holds for all agents $i \in \mathcal{N}$, then $\mathbf{x}^*$ is a CL-GNE.

To prove (i) ⇔ (iii), we exploit Remark 6.3.2: for each active constraint, we have $\nabla_{\mathbf{x}_i} g(\mathbf{x}_i^*, \mathbf{x}_{-i}^*)^\top \mathbf{y} \leq 0$, $\forall \mathbf{y} \in T_{cl}(\mathcal{X}_i(\mathbf{x}_{-i}^*), \mathbf{x}_i^*)$. Furthermore, for a generic vector $\mathbf{v}$, under Assumption 6.2.1 and 6.2.2, we have that $\mathbf{v} \in N_{cl}(\mathcal{X}_i(\mathbf{x}_{-i}^*), \mathbf{x}_i^*)$, if and only if there exists a vector $\boldsymbol{\lambda}_i = \text{col}(\lambda_i^1, ..., \lambda_i^m, ..., \lambda_i^M) \in \mathbb{R}^M$ such that:

$$\begin{aligned} \mathbf{v} &\in \nabla_{\mathbf{x}_i} g(\mathbf{x}_i^*, \mathbf{x}_{-i}^*)\boldsymbol{\lambda}_i \\ \mathbf{0}_M \leq \boldsymbol{\lambda}_i &\perp g(\mathbf{x}_i^*, \mathbf{x}_{-i}^*) \leq \mathbf{0}_M. \end{aligned} \tag{6.8}$$

Thus, for each agent $i \in \mathcal{N}$ we can write the KKT conditions in (6.5) by setting $\mathbf{v} = -\nabla_{\mathbf{x}_i} f_i(\mathbf{x}_i^*, \mathbf{x}_{-i}^*)$. Finally, since $\nabla_{\mathbf{x}_i} f_i(\mathbf{x}_i^*, \mathbf{x}_{-i}^*)^\top \mathbf{y} \geq 0$, $\forall \mathbf{y} \in T_{cl}(\mathcal{X}_i(\mathbf{x}_{-i}^*), \mathbf{x}_i^*)$ we ensure the existence of a non-negative vector of Lagrange multipliers $\boldsymbol{\lambda}_i = \text{col}(\lambda_i^1, ..., \lambda_i^m, ..., \lambda_i^M) \in \mathbb{R}^M_{\geq 0}$ satisfying the KKT optimality conditions for each individual optimization problem in (6.2) if $\mathbf{x}^*$ is a CL-GNE. ■

In the related literature [26], JC games are usually solved by finding a solution to the associated *variational inequality problem* (VIP), since the resulting vGNE not only exists

but is also unique whenever the cost functions are strongly monotone [27]. By relaxing the convexity condition on the coupling feasible set $\mathcal{X}$ in (6.1), we can no longer rely on the existence and uniqueness of a vGNE. However, we can still obtain a first-order necessary condition for a local minimizer. To this aim, by introducing the pseudogradient mapping

$$F(\mathbf{x}) = \begin{bmatrix} \nabla_{\mathbf{x}_1} f_1(\mathbf{x}_1, \mathbf{x}_{-1}) \\ \vdots \\ \nabla_{\mathbf{x}_N} f_N(\mathbf{x}_N, \mathbf{x}_{-N}) \end{bmatrix} \tag{6.9}$$

we consider the following *quasi-variational inequalities* (QVI) associated with the CL-GNEP in (6.2).

Definition 6.3.2 (*Quasi-variational inequality [28]*)

Given the tangent cone $\tilde{\mathcal{X}}(\mathbf{x})$ and the mapping F in (6.9), the quasi-variational inequality problem QVIP$(\tilde{\mathcal{X}}, F)$ consists in finding a vector $\mathbf{x}^* \in \tilde{\mathcal{X}}(\mathbf{x}^*)$, the so-called quasi-variational equilibrium (QVE), such that:

$$\inf_{\mathbf{y} \in \tilde{\mathcal{X}}(\mathbf{x}^*)} (\mathbf{y} - \mathbf{x}^*)^\top F(\mathbf{x}^*) \geq 0. \tag{6.10}$$

□

Having defined the concept of CL-GNE of a nonconvex game, we can now define the *variational Clarke's local generalized Nash equilibrium* (vCL-GNE)

Definition 6.3.3 (*variational CL-GNE*)

A vCL-GNE is a CL-GNE in (6.4) that satisfies the QVIP in (6.10). □

Note that, similarly to the relation between GNEP and VIP, not all solutions of the CL-GNEP are a solution of the QVIP; viceversa, a solution of the QVIP is always a solution of the original CL-GNEP.

Furthermore, if we consider the KKT conditions of the corresponding QVIP$(\tilde{\mathcal{X}}(\mathbf{x}), F(\mathbf{x}))$, we have that:

$$\begin{cases} 0 \in \boldsymbol{F}(\mathbf{x}) + \nabla_{\mathbf{x}} g(\mathbf{x}) \boldsymbol{\lambda} \\ \boldsymbol{\lambda} \geq 0 \quad \perp \quad g(\mathbf{x}) \leq 0 \end{cases} \tag{6.11}$$

where the solutions of the CL-GNEP that are preserved passing to the QVIP are exactly those for which all agents have the same multipliers for the respective constraints, thus, the following results can be proven.

Theorem 6.3.2

Let Assumptions 6.2.1 and 6.2.2 hold.

(i) *Let $\mathbf{x}^*$ be a solution of the CL-GNEP in (6.2), where the KKT conditions in (6.5) for all agents hold with the same Lagrangian multipliers $\boldsymbol{\lambda} = \boldsymbol{\lambda}_i$, $\forall i \in \mathcal{N}$. Then, $\mathbf{x}^*$ is a solution of the QVI in (6.10) and thus it is a vCL-GNE.*

(ii) *Viceversa, let $\mathbf{x}^*$ be a solution of the QVI in (6.10) and thus be a vCL-GNE. Then, $\mathbf{x}^*$ is a solution of the CL-GNEP in (6.2) at which the KKT conditions in (6.5) hold with the same Lagrangian multipliers, $\boldsymbol{\lambda} = \boldsymbol{\lambda}_i$, $\forall i \in \mathcal{N}$.* □

Proof 6.3.2

Under Assumptions 6.2.1 and 6.2.2, we note that the set $\tilde{\mathcal{X}}(\mathbf{x}^*)$ where we compute the KKT conditions in (6.5) for the CL-GNEP is convex. Thus, we can employ Theorem 3.1 in [11] to conclude the proof. ■

In other words, at a vCL-GNE, we have that in a local subset of $\mathcal{X}$ in (6.1) each agent cannot unilaterally minimize their own function while keeping the strategies of the other agents fixed. Moreover, when at this point the common optimal multiplier for all the agents associated with the individual constraints are the same, $\boldsymbol{\lambda} = \boldsymbol{\lambda}_i$, $\forall i \in \mathcal{N}$, then the point is a QVE, and thus a locally fair equilibrium point [10].

We can also characterize a vCL-GNE by employing Clarke's tangent cone. By Theorem 6.3.1 we have that in a CL-GNE $-\nabla f_i(\mathbf{x}_i^*, \mathbf{x}_{-i}^*) \in N_{\text{cl}}(\mathcal{X}_i(\mathbf{x}_{-i}^*), \mathbf{x}_i^*)$, $\forall i \in \mathcal{N}$. Thus, by leveraging on Theorem 6.3.2 we can prove the following corollary.

Corollary 6.3.1

Let Assumptions 6.2.1 and 6.2.2 hold. $\mathbf{x}^*$ is a vCL-GNE if and only if:

$$-\boldsymbol{F}(\mathbf{x}^*) \in N_{cl}(\mathcal{X}, \mathbf{x}^*). \tag{6.12}$$

with F as in (6.9) and $\mathcal{X}$ as in (6.1). □

To illustrate the proposed concept of vCL-GNE, let us present the following examples.

Example 6.3.1

Let us consider two agents, with strategies $\mathbf{x}_1 \in \mathbb{R}$ and $\mathbf{x}_2 \in \mathbb{R}$ with the same cost function. Both agents must respect the global constraint $\mathbf{x}_1^2 + \mathbf{x}_2^2 \geq 1$, represented in Fig. 6.1 (a) by the set $\mathcal{X}$ of points outside the unit circle, which is clearly nonconvex. Moreover, we include a further constraints $-2 \leq \mathbf{x}_i \leq 2$ ($\forall i = 1, 2$) to ensure the compactness of the set. Thus, we can formally define the game as:

$$\forall i \in \{1,2\} : \begin{cases} \min\limits_{-2 \leq \mathbf{x}_i \leq 2} & f_i(\mathbf{x}_i) = \mathbf{x}_i^2 \\ s.t. & \mathbf{x}_1^2 + \mathbf{x}_2^2 \geq 1. \end{cases} \tag{6.13}$$

The cost functions of the agents are decoupled and strictly convex, while the coupling constraint is nonconvex. The game has an infinite number of CL-GNEs. Moreover, by studying the KKT conditions we get:

$$\forall i \in \{1,2\} : \begin{cases} 2\mathbf{x}_i - \lambda_i 2\mathbf{x}_i = 0 \\ \lambda_i \geq 0 \perp \mathbf{x}_1^2 + \mathbf{x}_2^2 \geq 1. \end{cases} \tag{6.14}$$

From (6.14), we have for all points on the unitary circumference $\lambda_1 = \lambda_2 = 1$; hence, all these points are also vCL-GNE. In this example, the analysis of local equilibrium points is still useful since we can ensure the uniqueness of each vCL-GNE in their respective Clarke's tangent cone (indicated in light gray in Fig. 6.1). □

Example 6.3.2

Let us now consider a modified version of the game described in Example 1. In particular, we modify the coupling constraint as shown in Fig. 6.1 (b), thus formulating the following game:

$$\forall i \in \{1,2\}: \begin{cases} \min\limits_{-2 \leq \mathbf{x}_i \leq 2} & f_i(\mathbf{x}_i) = \mathbf{x}_i^2 \\ s.t. & (\mathbf{x}_1 - 1/4)^2 + (\mathbf{x}_2 - 1/4)^2 \geq 1. \end{cases} \tag{6.15}$$

Here the KKT conditions are:

$$\forall i \in \{1,2\}: \begin{cases} 2\mathbf{x}_i - \lambda_i(2\mathbf{x}_i - 1/2) = 0 \\ \lambda_i \geq 0 \perp 1 - (\mathbf{x}_1 - 1/4)^2 - (\mathbf{x}_2 - 1/4)^2 \leq 0. \end{cases} \tag{6.16}$$

From (6.16), we have that not all points on the circumference are CL-GNE; moreover, only two vCL-GNE exist that are $\mathbf{x}_1 = \mathbf{x}_2 = 1/4 + \sqrt{2}/2$ and $\mathbf{x}_1 = \mathbf{x}_2 = 1/4 - \sqrt{2}/2$. However, even if in these two vCL-GNEs the agents are fairly penalized (i.e., same

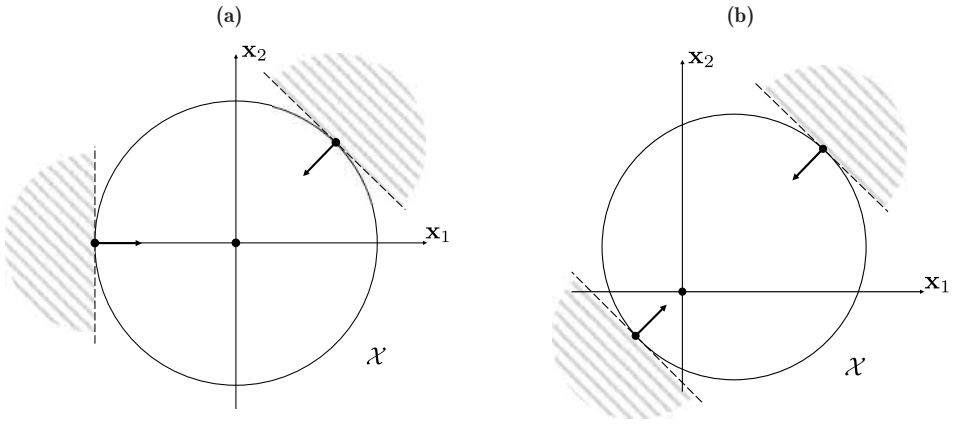

Figure 6.1: Illustration of CL-GNE points in Example 1 (a) and Example 2 (b).

value for the Lagrange multiplier), the corresponding characteristics are different. The vCL-GNE in quadrant I $(+;+)$ is not stable with respect to the coupling set, since the agents' strategies can jump into other quadrants improving the respective objectives. However, this equilibrium is stable within its Clarke's tangent cone. Conversely, the vCL-GNE in quadrant III $(-;-)$ is not only a vCL-GNE but also a vGNE. The difference between these two points can be seen also analyzing the respective multipliers. Indeed, we have $\lambda_1 = \lambda_2 = \sqrt{2}/4 + 1$ in the first case (quadrant I) while $\lambda_1 = \lambda_2 = 1 - \sqrt{2}/4$ in the second one (quadrant III). □

6.4 Existence and Uniqueness

Since the projection onto a nonconvex set is not a nonexpansive operator, classical existence and convergence proofs based on projected gradient approaches do not apply to our setting.

Let us thus focus on a particular class of nonconvex sets, namely *proximally smooth sets* firstly proposed by *Federer* in [29]; this concept is present in the literature with different but equivalent definitions [30], [31]. In fact, the concept of proximal smoothness can be related with the *p-convexity* [32], *$\mathcal{O}(2)$-convexity* [33], *weak convexity* [34], and *proximal regularity* [35].

Definition 6.4.1

A set $\mathcal{X} \subseteq \mathbb{R}^n$ is said to be proximally smooth if there exists $r > 0$ such that the distance function $\operatorname{dist}(\cdot, \mathcal{X})$ is continuously differentiable on the r-enlargement $U(\mathcal{X}, r) := \mathcal{X} + r\mathbb{B}$. □

Proximally smooth sets include several classes of nonconvex sets and also convex sets as special case (for any $r > 0$) [31], [35]. Let us recall the following properties of proximally smooth sets.

Lemma 6.4.1 (*Clarke et al. 1995 [31]*)

Let $\mathcal{X} \subseteq \mathbb{R}^n$ be a nonempty closed set. If $\mathcal{X}$ in (6.1) is r-proximally smooth, then the following properties hold for any $r' \in (0, r)$:

(i) $\operatorname{proj}_{\mathcal{X}}(\mathbf{x}) \neq \varnothing$ *for all* $\mathbf{x} \in U(\mathcal{X}, r')$;

(ii) $\operatorname{proj}_{\mathcal{X}}(\mathbf{x})$ *is a singleton for all* $\mathbf{x} \in U(\mathcal{X}, r')$;

(iii) $\operatorname{proj}_{\mathcal{X}}(\cdot)$ *is p-Lipschitz continuous on $U(\mathcal{X}, r')$, where $p = r/(r - r')$;*

(iv) *the proximal normal cone $N_{px}(\mathcal{X}, \cdot)$ is closed as a set-valued mapping;*

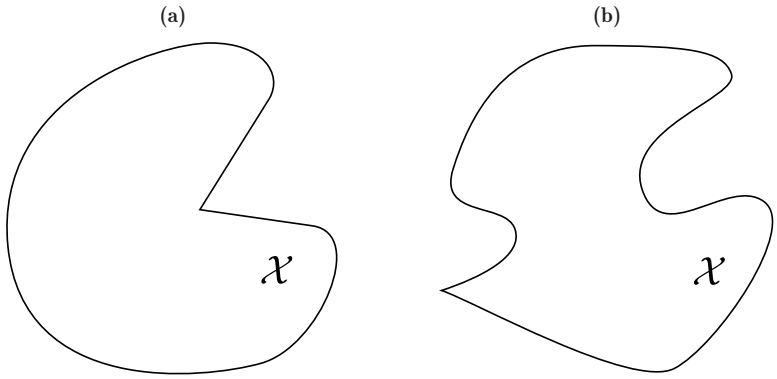

Figure 6.2: Example of a nonproximally smooth set (a) and of a proximally smooth set (b).

(v) *the proximal normal cone and Clarke's normal cone are equivalent (see Appendix 6.A).*

□

Informally speaking, a set is proximally smooth when the local nonconvexities are counterbalanced with the smoothness of constraints [36], [37]. For instance, the set in Fig. 6.2(a) is nonproximally smooth since it is nonsmooth in its nonconvex area. Nevertheless, as shown in Fig. 6.2(b) even with the presence of a "sharp point" the set is proximally smooth since it is locally convex around that point.

When the feasible set is defined by a single constraint, the only requirement for the set to be proximally smooth is the continuous differentiability of the constraint. However, this propriety is unfortunately not preserved under intersection without additional conditions [36], [38].

Let us ensure the existence of a vCL-GNE employing the weaker properties of the projection operator recalled in Lemma 6.4.1 and let us prove that a vCL-GNE is equivalent to a fixed point of the forward-backward mapping.

Lemma 6.4.2

Let Assumptions 6.2.1 and 6.2.2 hold and let the set $\mathcal{X}$ in (6.1) be r-proximally smooth. For any $\gamma \in (0, \frac{r'}{1+\bar{F}_{U(\mathcal{X},r)}})$ with $r' \in (0, r)$, the following statements are equivalent:

(i) $\mathbf{x}^* \in \mathcal{X}$ *is a vCL-GNE;*

(ii) $\mathbf{x}^* = \mathrm{proj}_{\mathcal{X}}(\mathbf{x}^* - \gamma F(\mathbf{x}^*))$, *i.e.,* $\mathbf{x}^* \in \mathit{fix}(\mathrm{proj}_{\mathcal{X}}(Id - \gamma F(\cdot)))$.

□

Proof 6.4.1

Since Assumption 6.2.2 holds, $U(\mathcal{X}, r)$ is compact and thus $\bar{F}_{U(\mathcal{X},r)}$ is limited. If $\mathbf{x}^* \in \mathcal{X}$, then we have that:

$$\begin{aligned} \mathrm{dist}(\mathbf{x}^* - \gamma F(\mathbf{x}^*), \mathcal{X}) &= \min_{\mathbf{y} \in \mathcal{X}} \|\mathbf{x}^* - \gamma F(\mathbf{x}^*) - \mathbf{y}\| \\ &\leq \|\mathbf{x}^* - \gamma F(\mathbf{x}^*) - \mathbf{x}^*\| = \gamma \|F(\mathbf{x}^*)\| \\ &\leq \gamma \bar{F}_{U(\mathcal{X},r)} < \frac{r'}{1 + \bar{F}_{U(\mathcal{X},r)}} \bar{F}_{U(\mathcal{X},r)} < r' \end{aligned} \quad (6.17)$$

hence $\mathbf{x}^* - \gamma F(\mathbf{x}^*) \in U(\mathcal{X}, r')$. Due to Lemma 6.4.1, $\mathrm{proj}_{\mathcal{X}}(\mathbf{x})$ is a singleton and $N_{px}(\mathcal{X}, \mathbf{x}^*) = N_{cl}(\mathcal{X}, \mathbf{x}^*)$, therefore we can recall Corollary 6.3.1 to conclude the proof. ■

Thanks to Lemma 6.4.2, we show the existence of a vCL-GNE when no assumptions are made on the pseudo-gradient mapping F in (6.9).

Proposition 6.4.1 (*Existence*)

Let Assumptions 6.2.1 and 6.2.2 hold and let the set $\mathcal{X}$ in (6.1) be r-proximally smooth and simply connected. Then, the CL-GNEP in (6.2) has at least one vCL-GNE. □

Proof 6.4.2

From Lemma 6.4.2 we have that any fixed point of the forward-backward mapping with $\gamma \in (0, \frac{r'}{1+\bar{F}_{U(\mathcal{X},r)}})$ is a vCL-GNE. Since Assumptions 6.2.1 and 6.2.2 hold and since the set is simply connected, we can employ the Lefschetz fixed-point theorem to prove that there exists at least one fixed point [39], [40]. ■

An alternative way to ensure the existence of the QVI in (6.10), and thus of a vCL-GNE, is presented in [28] by defining a convex set $\mathcal{T}$ such that for every $\mathbf{x} \in \mathcal{T}$, $\tilde{\mathcal{X}}(\mathbf{x})$ is a nonempty, closed, convex subset of $\mathcal{T}$. Note that in [28] the smoothness property is refereed as *continuity*.

Regarding uniqueness, we cannot ensure that a vCL-GNE is globally unique, nevertheless, with an additional assumption on the mapping F in in (6.9), local uniqueness holds in Clarke's tangent cone.

Remark 6.4.1 (*Local Uniqueness*)

Under Assumptions 6.2.1 and 6.2.2, if the mapping F in (6.9) is strictly monotone, then the strict inequality holds in (6.10) and thus any vCL-GNE $\mathbf{x}^* \in \mathcal{X}$ is unique in its Clarke's tangent cone $\tilde{\mathcal{X}}(\mathbf{x}^*)$. This statement can be derived from Proposition 12.11 in [41] as $\tilde{\mathcal{X}}(\mathbf{x}^*)$ is a convex set. □

6.5 Equilibrium Computation

Differently from convex sets, that are necessarily connected, requiring a nonconvex set to be simply connected is a rather strong assumption. In order to relax it, we strengthen assumptions on the pseudo-gradient mapping. In this section, we propose two algorithms for seeking a vCL-GNE when the pseudo-gradient mapping is strongly monotone and when it is merely monotone, respectively.

6.5.1 Existence and Convergence to a vCL-GNE under Strongly Monotone Pseudo-gradient Mappings

A popular algorithm for solving VIs with strongly monotone mappings is the projected pseudo-gradient method described in Algorithm 6.1, which generates, given a starting point $\mathbf{x}^0 \in \mathcal{X}$ (line-1) and a step size $\gamma > 0$, a sequence that approaches the solution set. In particular, at each iteration k, a gradient step of length γ is projected onto the feasible set $\mathcal{X}$ (line 3).

To prove that Algorithm 6.1 can be used to solve the QVI in (6.10), and thus the convergence to a vCL-GNE, let us recast this algorithm as a discrete-time system:

$$\mathbf{x}^{k+1} = \text{proj}_{\mathcal{X}}(\mathbf{x}^k - \gamma F(\mathbf{x}^k)). \tag{6.18}$$

We can prove the following result.

Lemma 6.5.1

Let Assumptions 6.2.1 and 6.2.2 hold and let $\gamma \in (0, \frac{r'}{1+\bar{F}_{U(\mathcal{X},r)}})$ with $r' \in (0, r)$. If $\mathbf{x}^*$ is a quasi-asymptotically stable (QAS) equilibrium point for (6.18), then $\mathbf{x}^*$ is a fixed point and it is a vCL-GNE. □

Algorithm 6.1 Projected pseudo-gradient algorithm

Input: $\gamma, \mathbf{x}^0$

Set $\mathbf{x} \leftarrow \mathbf{x}^0$
while An adequate termination criterion is reached **do**
  $\mathbf{x}^{k+1} \leftarrow \text{proj}_{\mathcal{X}}(\mathbf{x}^k - \gamma F(\mathbf{x}^k))$
end while

Output: $\mathbf{x}^*$

Proof 6.5.1

First, we note that, from its definition, $\mathbf{x}^* \in \mathcal{X}$ is a QAS equilibrium point if and only if there exists a basin of attraction $B(\mathbf{x}^*)$ such that for all $\mathbf{x}^0 \in B(\mathbf{x}^*)$ we have $\lim_{k\to\infty} \left\|\mathbf{x}^k - \mathbf{x}^*\right\| = 0$. Hence, any QAS equilibrium point is a fixed point of the dynamical system's evolution of (6.18) [42]. By Lemma 6.4.2, any fixed point of (6.18) is a vCL-GNE. ■

Therefore, to prove the convergence to a vCL-GNE we can analyze the autonomous evolution of the discrete-time system in (6.18) and search for possible QAS equilibrium points. By introducing a technical assumption, let us show the following convergence result.

Assumption 6.5.1

The set $\mathcal{X}$ in (6.1) is r-proximally smooth. The mapping F in (6.9) is strongly monotone with constant $\mu > 0$ and Lipschitz continuous with constant $\ell > 0$. □

Theorem 6.5.1

Let Assumptions 6.2.1–6.5.1 hold and let $\gamma \in (0, \min\{\frac{\sqrt{\ell^2+p^2(\mu^2-\ell^2)}+\mu p}{\ell^2 p}, \frac{r'}{1+\bar{F}_{U(\mathcal{X},r)}}\})$, such that $\mu \geq \ell$ and $r' \in (0, r)$. Then:

(i) *The CL-GNEP in (6.2) has at least one vCL-GNE;*

(ii) *The sequence generated by Algorithm 6.1 converges to a vCL-GNE.* □

Proof 6.5.2

In order to preserve the properties of Lemma 6.4.1, let us assume that $\mathbf{x}^0 \in \mathcal{X}$. Consequently, since at each iteration $\mathbf{x}^k \in \mathcal{X}$ and due to Lemma 6.4.2, we have that $\mathbf{x}^k - \gamma F(\mathbf{x}^k) \in U(\mathcal{X}, r')$ and thus Lemma 6.4.1 holds. Therefore, we have that:

$$\begin{aligned}
&\left\|\mathbf{x}^{k+1} - \mathbf{x}^*\right\|^2 = \\
&= \left\|\text{proj}_{\mathcal{X}}(\mathbf{x} - \gamma F(\mathbf{x})) - \text{proj}_{\mathcal{X}}(\mathbf{x}^* - \gamma F(\mathbf{x}^*))\right\|^2 \\
&\leq p^2 \left\|(\mathbf{x}^k - \gamma F(\mathbf{x}^k)) - (\mathbf{x}^* - \gamma F(\mathbf{x}^*))\right\|^2 \\
&= p^2 \left\|(\mathbf{x}^k - \mathbf{x}^*) - \gamma(F(\mathbf{x}^k) - F(\mathbf{x}^*))\right\|^2 \\
&= p^2 (\left\|\mathbf{x}^k - \mathbf{x}^*\right\|^2 + \gamma^2 \left\|F(\mathbf{x}^k) - F(\mathbf{x}^*)\right\|^2 \\
&\qquad - 2\gamma (F(\mathbf{x}^k) - F(\mathbf{x}^*))^\top (\mathbf{x}^k - \mathbf{x}^*)) \\
&\leq p^2 (1 - 2\gamma\mu + \gamma^2 \ell^2) \left\|\mathbf{x}^k - \mathbf{x}^*\right\|^2
\end{aligned} \tag{6.19}$$

where the first inequality holds since for a generic (possibly nonconvex) proximally smooth set the projection is Lipschitz continuous with constant $p = r/r-r'$, while for the last one we use the strong monotonicity and the Lipschitz continuity of the mapping F. Next we note that, if $\gamma < \frac{\sqrt{\ell^2+p^2(\mu^2-\ell^2)}+\mu p}{\ell^2 p}$ with $\mu \geq \ell$, we have that $p^2(1-2\gamma\mu+\gamma^2\ell^2) < 1$. Consequently, $\lim_{k\to\infty} \left\|\mathbf{x}^{k+1} - \mathbf{x}^*\right\|^2 = 0$ and thus the evolution of the discrete-time autonomous system (6.18) converges to a QAS equilibrium point

Algorithm 6.2 Tangent-cone-projected extra-gradient algorithm

Input: $\gamma, \mathbf{x}^0$

1: Set $\mathbf{x} \leftarrow \mathbf{x}^0$
2: **while** An adequate termination criterion is reached **do**
3: $\quad \mathbf{y}^k \leftarrow \text{proj}_{\mathcal{X}}(\mathbf{x}^k - \gamma F(\mathbf{x}^k))$
4: $\quad \mathbf{x}^{k+1} \leftarrow \text{proj}_{\tilde{\mathcal{X}}(\mathbf{y}^k)}(\mathbf{x}^k - \gamma F(\mathbf{y}^k))$
5: **end while**

Output: $\mathbf{x}^*$

that exists [42]. To conclude the proof we recall Lemma 6.5.1. ■

6.5.2 Existence and Convergence to a vCL-GNE under Monotone Pseudo-gradient Mappings

Let us now consider a weaker requirement for the pseudo-gradient mapping. Inspired by the classical Korpelevich's method [43], let us propose a novel algorithm for computing a vCL-GNE.

Our method is described in Algorithm 6.2 and generates from a starting point $\mathbf{x}^0 \in \mathcal{X}$ (line-1) a sequence approaching the solution set. In particular, at each iteration k, the algorithm requires two consecutive steps. Starting from $\mathbf{x}^k \in \mathcal{X}$, a temporary point $\mathbf{y}^k$ is computed by a gradient step of length γ projected onto the feasible set $\mathcal{X}$ (line 3). Next, the point for the subsequent iteration $\mathbf{x}^{k+1}$ is computed by taking a gradient step of length γ, with the gradient of the mapping calculated in $\mathbf{y}^k$, and projecting it onto the tangent cone computed at the same point $\tilde{\mathcal{X}}(\mathbf{y}^k)$ (line 4).

As for Algorithm 6.1, let us recast this algorithm as a discrete-time dynamical system and introduce a technical assumption to demonstrate the convergence to a vCL-GNE:

$$\begin{cases} \mathbf{y}^k = \text{proj}_{\mathcal{X}}(\mathbf{x}^k - \gamma F(\mathbf{x}^k)) \\ \mathbf{x}^{k+1} = \text{proj}_{\tilde{\mathcal{X}}(\mathbf{y}^k)}(\mathbf{x}^k - \gamma F(\mathbf{y}^k) \end{cases} \tag{6.20}$$

Assumption 6.5.2

The set $\mathcal{X}$ in (6.1) is r-proximally smooth. The mapping F in (6.9) is monotone and Lipschitz continuous with constant $\ell > 0$. □

Lemma 6.5.2

Let Assumptions 6.2.1,6.2.2 and 6.5.2 hold and let $\gamma \in (0, \frac{r}{1+\bar{F}_{U(\mathcal{X},r)}})$ with $r' \in (0, r)$. If the sequence generated by Algorithm 6.2 reaches $\mathbf{y}^k = \mathbf{x}^k$, then $\mathbf{x}^k$ is a QAS equilibrium point for (6.20). □

Proof 6.5.3

The proof follows directly from Lemma 6.5.1. ■

Lemma 6.5.3

Let Assumptions 6.2.1,6.2.2 and 6.5.2 hold and let $\gamma \in (0, \frac{r}{1+\bar{F}_{U(\mathcal{X},r)}})$ with $r' \in (0, r)$. If $\mathbf{x}^*$ is a QAS equilibrium point for (6.20), then $\mathbf{x}^*$ is a fixed point and it is a vCL-GNE. □

Proof 6.5.4

The proof follows directly from Lemma 6.5.1. ■

Theorem 6.5.2

Let Assumptions 6.2.1, 6.2.2 and 6.5.2 hold and let $\gamma \in (0, \min\{\frac{1}{\ell}, \frac{r}{4(1+\bar{F}_{U(\mathcal{X},r)})}\})$ with

$r' \in (0, r)$. *Then:*

(i) *The CL-GNEP in* (6.2) *has at least one vCL-GNE;*

(ii) *The sequence generated by Algorithm 6.2 converges to a vCL-GNE.* □

Proof 6.5.5

In order to preserve the smoothness properties of Lemma 6.4.1, we need to ensure that each iteration is contained in $U(\mathcal{X}, r')$. *First, by setting* $\gamma \in (0, \frac{r'}{4(1+\bar{F}_{U(\mathcal{X},r)})})$ *we note that:*

$$\begin{aligned}\operatorname{dist}(\mathbf{y}^k, \mathbf{x}^{k+1}) &\leq \left\|\mathbf{x}^k - \gamma F(\mathbf{x}^k) - \mathbf{x}^k + \gamma F(\mathbf{y}^k)\right\| \\ &\leq \gamma \left\|F(\mathbf{x}^k)\right\| + \gamma \left\|F(\mathbf{y}^k)\right\| \leq 2\gamma \bar{F}_{U(\mathcal{X},r)} \\ &< \frac{2r'}{4(1+\bar{F}_{U(\mathcal{X},r)})} \bar{F}_{U(\mathcal{X},r)} < \frac{r'}{2} \quad (6.21)\end{aligned}$$

where the first inequality holds since the tangent cone is convex. Hence, assuming that $\mathbf{x}^0 \in \mathcal{X}$ *and since* $\mathbf{y}^k \in \mathcal{X}$ *we ensure that each point* $\mathbf{x}^k$ *is contained in* $U(\mathcal{X}, r'/2)$. *Similarly, we have that* $\operatorname{dist}(\mathbf{x}^k, \mathbf{x}^k - \gamma F(\mathbf{x}^k)) \leq \gamma \bar{F}_{U(\mathcal{X},r)} \leq r'/2$ *and thus, by induction,* $\mathbf{x}^k - \gamma F(\mathbf{x}^k)$ *is contained in* $U(\mathcal{X}, r')$. *The same argument applies to* $\mathbf{x}^k - \gamma F(\mathbf{y}^k)$.

Next, by defining $\mathbf{z}^k = \mathbf{x}^k - \gamma F(\mathbf{y}^k)$ *and* $\mathbf{x}^{*k} = \operatorname{proj}_{\tilde{\mathcal{X}}(\mathbf{y}^k)}(\mathbf{x}^*)$ *we have that:*

$$\begin{aligned}\left\|\mathbf{x}^{k+1} - \mathbf{x}^{*k}\right\|^2 &= (\mathbf{x}^{k+1} - \mathbf{z}^k + \mathbf{z}^k - \mathbf{x}^{*k})^\top (\mathbf{x}^{k+1} - \mathbf{z}^k + \mathbf{z}^k - \mathbf{x}^{*k}) \\ &= \left\|\mathbf{z}^k - \mathbf{x}^{*k}\right\|^2 + \left\|\mathbf{z}^k - \mathbf{x}^{k+1}\right\|^2 + 2(\mathbf{x}^{k+1} - \mathbf{z}^k)^\top (\mathbf{z}^k - \mathbf{x}^{*k}). \quad (6.22)\end{aligned}$$

Moreover, since $\tilde{\mathcal{X}}(\mathbf{y}^k)$ *is convex and* $\mathbf{x}^{k+1} = \operatorname{proj}_{\tilde{\mathcal{X}}(\mathbf{y}^k)}(\mathbf{z}^k)$, *we have that* $2\|\mathbf{z}^k - \mathbf{x}^{k+1}\|^2 + 2(\mathbf{x}^{k+1} - \mathbf{z}^k)^\top (\mathbf{z}^k - \mathbf{x}^{*k}) = 2(\mathbf{z}^k - \mathbf{x}^{k+1})^\top (\mathbf{x}^{*k} - \mathbf{x}^{k+1}) \leq 0$. *Hence, we rewrite* (6.22) *as:*

$$\begin{aligned}\left\|\mathbf{x}^{k+1} - \mathbf{x}^{*k}\right\|^2 &\leq \left\|\mathbf{z}^k - \mathbf{x}^{*k}\right\|^2 - \left\|\mathbf{z}^k - \mathbf{x}^{k+1}\right\|^2 \\ &\leq \left\|\mathbf{x}^k - \mathbf{x}^{*k}\right\|^2 - \left\|\mathbf{x}^k - \mathbf{x}^{k+1}\right\|^2 + 2\gamma(\mathbf{y}^k - \mathbf{x}^{k+1})^\top F(\mathbf{y}^k) \quad (6.23)\end{aligned}$$

where for the last inequality we employ the monotonicity of F. *Since* $\tilde{\mathcal{X}}(\mathbf{y}^k)$ *is convex and* $\mathbf{x}^{k+1} \in \tilde{\mathcal{X}}(\mathbf{y}^k)$, *we have that* $(\mathbf{x}^{k+1} - \mathbf{y}^k)^\top ((\mathbf{x}^k - \gamma F(\mathbf{x}^k)) - \mathbf{y}^k) \leq 0$ *and therefore* $(\mathbf{x}^{k+1} - \mathbf{y}^k)^\top (\mathbf{x}^k - \gamma F(\mathbf{y}^k) - \mathbf{y}^k) = (\mathbf{x}^{k+1} - \mathbf{y}^k)^\top (\mathbf{x}^k - \gamma F(\mathbf{x}^k) - \mathbf{y}^k) + \gamma(\mathbf{x}^{k+1} - \mathbf{y}^k)^\top (F(\mathbf{x}^k) - F(\mathbf{y}^k)) \leq \gamma(\mathbf{x}^{k+1} - \mathbf{y}^k)^\top (F(\mathbf{x}^k) - F(\mathbf{y}^k))$. *Thus, we can rewrite* (6.23) *as:*

$$\begin{aligned}\left\|\mathbf{x}^{k+1} - \mathbf{x}^{*k}\right\|^2 &\leq \left\|\mathbf{x}^k - \mathbf{x}^{*k}\right\|^2 - \left\|\mathbf{x}^k - \mathbf{y}^k\right\|^2 \\ &\quad - \left\|\mathbf{y}^k - \mathbf{x}^{k+1}\right\|^2 + 2\gamma(\mathbf{x}^{k+1} - \mathbf{y}^k)^\top (F(\mathbf{x}^k) - F(\mathbf{y}^k)) \quad (6.24)\end{aligned}$$

Furthermore, by employing the Cauchy-Schwarz inequality and the Lipschitz propriety of F, *we have that* $2\gamma(\mathbf{x}^{k+1} - \mathbf{y}^k)^\top (F(\mathbf{x}^k) - F(\mathbf{y}^k)) \leq 2\gamma\ell \left\|\mathbf{x}^{k+1} - \mathbf{y}^k\right\| \left\|\mathbf{x}^k - \mathbf{y}^k\right\|$ *and thus:*

$$\begin{aligned}\left\|\mathbf{x}^{k+1} - \mathbf{x}^{*k}\right\|^2 &\leq \left\|\mathbf{x}^k - \mathbf{x}^{*k}\right\|^2 - \left\|\mathbf{x}^k - \mathbf{y}^k\right\|^2 - \left\|\mathbf{y}^k - \mathbf{x}^{k+1}\right\|^2 \\ &\quad + 2\gamma\ell \left\|\mathbf{x}^{k+1} - \mathbf{y}^k\right\| \left\|\mathbf{x}^k - \mathbf{y}^k\right\| \leq \left\|\mathbf{x}^k - \mathbf{x}^{*k}\right\|^2 - \left\|\mathbf{x}^k - \mathbf{y}^k\right\|^2 \\ &\quad - \left\|\mathbf{y}^k - \mathbf{x}^{k+1}\right\|^2 + \gamma^2\ell^2 \left\|\mathbf{x}^k - \mathbf{y}^k\right\|^2 + \left\|\mathbf{y}^k - \mathbf{x}^{k+1}\right\|^2 \quad (6.25)\end{aligned}$$

where in the last inequality we use that $(\gamma\ell \left\|\mathbf{x}^k - \mathbf{y}^k\right\| - \left\|\mathbf{y}^k - \mathbf{x}^{k+1}\right\|)^2 \geq 0$. *Therefore, we have that:*

$$\begin{aligned}(1 - \gamma^2\ell^2) \left\|\mathbf{x}^k - \mathbf{y}^k\right\|^2 &\leq \left\|\mathbf{x}^k - \mathbf{x}^{*k}\right\|^2 - \left\|\mathbf{x}^{k+1} - \mathbf{x}^{*k}\right\|^2 \\ &\leq \left\|\mathbf{x}^k\right\|^2 + \left\|\mathbf{x}^{*k}\right\|^2 - \left\|\mathbf{x}^{k+1}\right\|^2 - \left\|\mathbf{x}^{*k}\right\|^2 \quad (6.26)\end{aligned}$$

Since the sequence $(\mathbf{x}^k)_{k=0}^{\infty}$ *is bounded, by summing up for all integer* $K \geq 0$*, we get:*

$$(1-\gamma^2\ell^2)\sum_{k=0}^{K}\left\|\mathbf{x}^k-\mathbf{y}^k\right\|^2 \leq \left\|\mathbf{x}^0\right\|^2 \tag{6.27}$$

where the sequence $(\sum_{k=0}^{K}\left\|\mathbf{x}^k-\mathbf{y}^k\right\|^2)_{K\in\mathbb{N}}$ *is monotonically increasing and bounded. Therefore, if* $\gamma < 1/\ell$*, we have that* $\lim_{k\to\infty}\left\|\mathbf{x}^k-\mathbf{y}^k\right\|^2 = 0$ *and by Lemma 6.5.2 we have that the evolution of the discrete-time autonomous system* (6.20) *converges to a QAS equilibrium (existence follows by [42]). To conclude the proof, we invoke Lemma 6.5.3.* ■

6.5.3 Discussion on the Convergence Properties

Algorithms 6.1 and 6.2 are designed to reach the so-called "minimum potential" of the game. Indeed, since Assumptions 6.2.1, 6.5.1 and 6.5.2 hold, the pseudo-gradient mapping can be expressed as the gradient of a "potential function" and the variational reformulation can be seen as a generalization of potential games introduced in [44]. In this case, the set of variational equilibria corresponds to the set of minima and saddle points of this potential function (See Lemma 1 in [45]). However, for both algorithms, the convergence is ensured only to a generic vCL-GNE, which depends on the initial condition.

Let us illustrate this fact by analyzing the convergence of the proposed algorithms for Examples 1 and 2. We first note that these two sets are r-proximally smooth with $r < 1/2$ and thus both algorithms can be employed for instance with a step size $\gamma = 0.1$.

In Fig. 6.3 we show two phase plane plots for Examples 1 and 2. In particular, Fig. 6.3(a) refers to Example 1, while Figs. 6.3(b) refers to Example 2. These plots are constructed by exploring the trajectories of the agents' dynamics from different initial conditions. In the first example (Fig. 6.3(a)), as all the points of the circumference are vCL-GNE, both algorithms converge to a different point based on the initial values. Conversely, the second example has only two vCL-GNE. Nevertheless, both algorithms converge to the lower vCL-GNE with almost the whole initial conditions (Fig. 6.3(b)) since this has the minimum potential and thus smaller lower Lagrangian multipliers.

Moreover, in Fig. 6.4 we show the difference between the two algorithms in terms of iterations required to converge to a vCL-GNE. In order to perform this analysis, we select 10^5 initial conditions equally outdistanced and we analyze the agents' dynamics by showing the distance between $\mathbf{x}^k$ and the set $\mathcal{X}^*$ that collects all the vCL-GNEs of the games. In particular, we show the mean value of $\text{dist}(\mathbf{x}^k, \mathcal{X}^*)$ in blue together with the upper and lower boundaries in light blue. As expected, the distance with respect to a vCL-GNE decreases to zero; in some circumstances Algorithm 6.1 may require several iterations to converge.

6.6 Case Study

Direct current (DC) microgrids have increased their influence in modern electrical systems due to their high efficiency and natural interface to many types of *renewable energy sources* (RESs) and *energy storage systems* (ESSs).

One of the critical issues in DC microgrids – inherited from the operation of power systems – is the well-known *optimal power flow* (OPF) problem, which determines the best operating point regarding power losses or energy production costs. The OPF relies on the power flow model, which in DC microgrids corresponds to a set of nonlinear nonconvex algebraic equations that cannot be solved analytically [46]. When the OPF is addressed by a centralized approach, a central unit must have access to all system parameters. However, several independent parties are nowadays progressively involved in the control and optimization of power grids, strongly affecting their dynamics. The cooperation of such independent entities is challenging: on the one hand, they act selfishly;

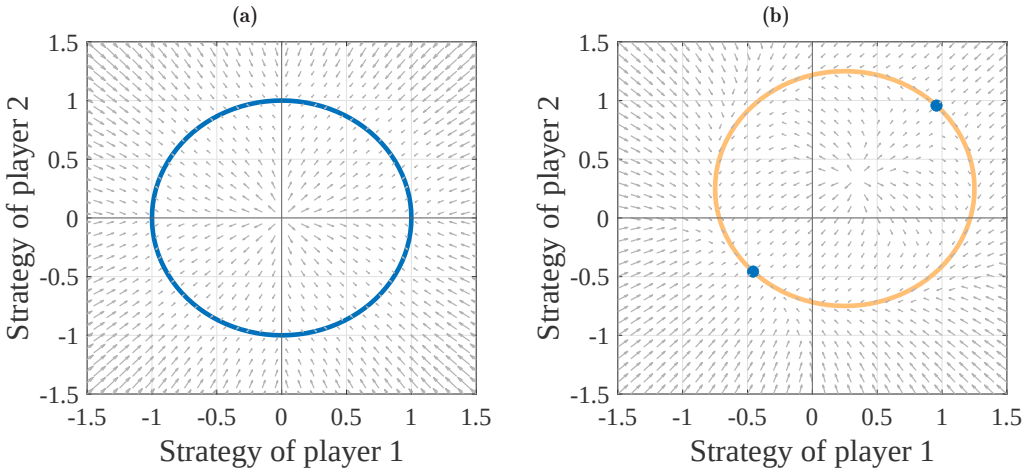

Figure 6.3: Pseudo phase plane plots for Example 1 (a) and Example 2 (b), where we indicate the vCL-GNE in blue.

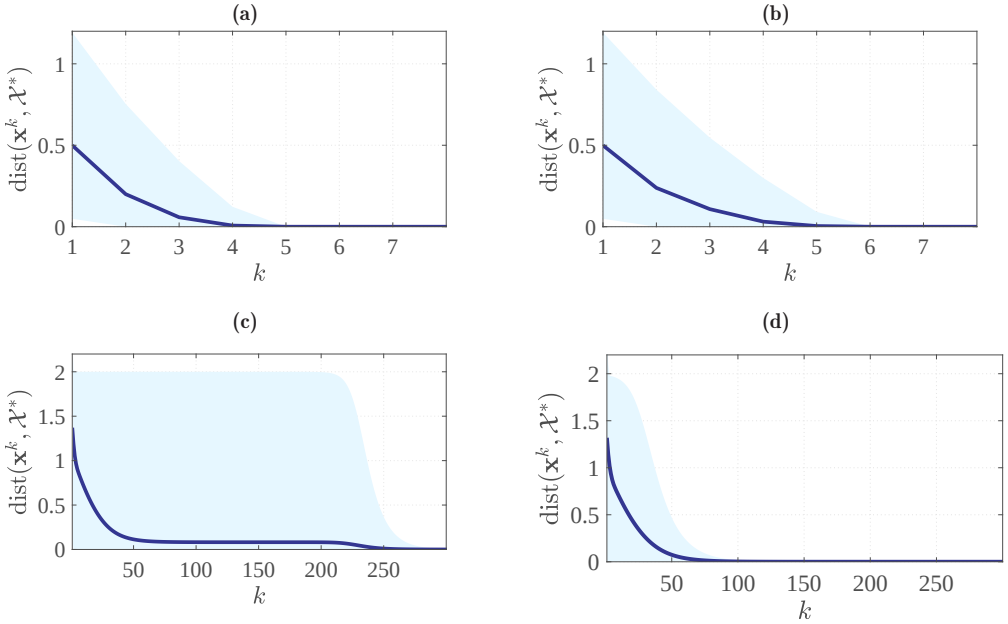

Figure 6.4: Distance to a vCL-GNE with respect to the iteration (line corresponds to the mean, while the shaded area represents the boundaries): Algorithm 6.1 with Example 1 (a), Algorithm 6.2 with Example 1 (b), Algorithm 6.1 with Example 2 (c), and Algorithm 6.2 with Example 2 (d).

on the other hand, since they are physically interconnected through power lines, they must cooperate to ensure safe and secure grid operations. In this context, several game-theoretic methods have been proposed for distributed generation and storage control in power grids. Nevertheless, most of these works focus on the economic dispatch only [47]–[49]; indeed, their main focus is on the game perspective, while physical constraints are partially disregarded.

Therefore, here we propose a novel noncooperative approach for the management of DC microgrids including the full power flow equations leading to a noncooperative game with shared nonconvex constraints.

6.6.1 OPF as a Noncooperative Game

Let us consider a DC microgrid model composed of several interconnected buses and connected to the AC distribution grid through the so-called slack bus. We suppose that the grid is controlled over a control horizon denoted as $\mathcal{H} := \{1, ..., h, ..., H\}$, with H discrete time slots with equal length Δh, where h is a generic time slot.

The microgrid is described by a graph $\mathcal{G} = (\mathcal{N}, \mathcal{E})$, where $\mathcal{N}$ is the set of nodes with cardinality N, whilst $\mathcal{E} \in \mathcal{N} \times \mathcal{N}$ is the set of pairs of distinct nodes called edges with cardinality E. The nodes $i \in \mathcal{N}$ of the graph represent the buses and the edges $(i, r) \in \mathcal{E}$ represent the lines between these buses. Each bus $i \in \mathcal{N}$ is connected with several non-controllable loads and RESs whose aggregated per-slot power profile over the control horizon $\mathcal{H}$ is $\mathbf{P}_i := (P_i(1), ..., P_i(h), ..., P_i(H))^\top \in \mathbb{R}^H$.

We assume that the variables related to each bus are controlled by an active user $i \in \mathcal{N}$ that can modify the energy scheduling profile of the bus aiming at decreasing its total cost, while providing flexibility to the overall microgrid. In particular, each user schedules over the control horizon both the voltage magnitude of the bus $\mathbf{V}_i := (V_i(1), ..., V_i(h), ..., V_i(H))^\top \in \mathbb{R}^H_{\geq 0}$ and the power injected in the bus $\mathbf{g}_i := (g_i(1), ..., g_i(h), ..., g_i(H))^\top \in \mathbb{R}^H_{\geq 0}$. Hence, let us define for each active agent $i \in \mathcal{N}$ its strategy by $\mathbf{x}_i = \text{col}(\mathbf{V}_i, \mathbf{g}_i) \in \mathbb{R}^{2H}_{\geq 0}$.

We further assume that user $i = 1$, i.e., the slack bus, can only buy energy from the main grid with a linear function $W_1(\mathbf{g}_1) = \Delta\text{h}\, \eta_1 \mathbf{1}_H^\top \mathbf{g}_1$, where η_1 is the energy price coefficient. Conversely, we assume that users $i \in \mathcal{N} \setminus \{1\}$ are equipped with dispatchable energy generation devices and are subject to variable production costs in accordance with a linear cost function $W_i(\mathbf{g}_i) = \Delta\text{h}\, \eta_i \mathbf{1}_H^\top \mathbf{g}_i$, where η_i is the generation cost of user i. As commonly done in power distribution grids, we include a constraint for the slack bus whose voltage magnitude must be fixed:

$$\mathbf{V}_1 = V_{\text{ref}} \mathbf{1}_H \tag{6.28}$$

where V_{ref} is the reference voltage magnitude. Moreover, we impose a minimum and a maximum voltage magnitude for the remaining buses:

$$V_i^{\min} \mathbf{1}_H \leq \mathbf{V}_i \leq V_i^{\max} \mathbf{1}_H, \quad \forall i \in \mathcal{N} \setminus \{1\}. \tag{6.29}$$

Due to technological limitations, the generation profile is bounded by a minimum and a maximum per-slot energy generation capacity:

$$g_i^{\min} \mathbf{1}_H \leq \mathbf{g}_i \leq g_i^{\max} \mathbf{1}_H, \quad \forall i \in \mathcal{N} \setminus \{1\}. \tag{6.30}$$

In addition, the power flow equations must be satisfied; disregarding the power losses, these equations can be formulated for DC grids as:

$$\sum_{r \in \mathcal{N}} V_i(h)(V_i(h) - V_r(h)) Y_{i,r} = P_i(h) + g_i(h),\ \forall i \in \mathcal{N},\ \forall h \in \mathcal{H} \tag{6.31}$$

where $Y_{i,r}$ is the element (i, r) of the conductance matrix, defined as:

$$Y_{i,r} = \begin{cases} \sum_{h \neq r} Y_{n,h} & \text{if } i = r \\ -Y_{i,r} & \text{if } i \neq r \end{cases}, \quad \forall (i, r) \in \mathcal{E} \tag{6.32}$$

and $Y_{i,r} = Y_{r,i}$ is the line conductance between buses i and r. Summing up, all users are subject to a global nonconvex feasible set defined as:

$$\mathcal{X} = \left\{ \mathbf{x} \in \mathbb{R}^{2HN} \,|\, (6.28) - (6.31) \text{ hold} \right\}. \tag{6.33}$$

As regards cost functions, we assume that the control objective of the noncooperative game is to increase the microgrid predictability through a liberalized market where the cost of energy is proportional to the microgrid's energy mismatch. Hence, the cost function

Table 6.1: Parameters of the different generators

i	$g_i^{\min}$(p.u.)	$g_i^{\max}$(p.u.)	η_i (financial units)
2	0	3.50	0.35
3	0	1.30	0.60
4	0	2.00	0.55
5	0	2.00	0.50
6	0	2.00	0.70
7	0	2.00	0.35
8	0	2.00	0.70
9	0	1.00	0.41
10	0	4.50	0.45

of each independent active user comprehends the cost of energy, which is proportional to the microgrid's power mismatch, and generation costs as follows:

$$f_i\left(\mathbf{x}_i, \mathbf{x}_{-i}\right) = \sum_{h \in \mathcal{H}\Delta \mathrm{h}} \left(\kappa_i \sum_{j \in \mathcal{N}\setminus\{1\}} \left(\mathbf{g}_j(h) - \mathbf{P}_j(h)\right) \mathbf{g}_i(h) + \eta_i \mathbf{g}_i(h) \right), \forall i \in \mathcal{N} \quad (6.34)$$

where $\kappa_i > 0$ are the pricing coefficients. Note that for the slack bus we have $\kappa_1 = 0$ since we assumed that in the slack bus we can only inject power from the main grid.

The aforementioned game, defined by the cost functions f_i in (6.34) and by the shared feasible set $\mathcal{X}$ in (6.33), straightforwardly verifies Assumptions 6.2.1 and 6.2.2. Hence, if we can prove that the set (6.33) is proximally smooth we can compute a vCL-GNE employing Algorithm 6.1 or Algorithm 6.2.

Proposition 6.6.1

The (nonconvex) set defined in 6.33 is proximally smooth. □

Proof 6.6.1

The set in (6.33)*, is defined by a set of finitely many equality and inequalities* $m \in \mathcal{M}$ *that are continuous differentiable. Hence, when considered individually, they are proximally smooth with constant* r_m *[36]. It is easy to verify that the intersection of these different constraints is metrically calm with constant* $\zeta > 1$ *as in [38]. Therefore, by defining* $\bar{r}_m = \min_{m \in \mathcal{M}} r_m$*, we can verify the proximal smoothness of* (6.33) *with constant* $r = \bar{r}_m / \zeta_M$ *(See Proposition 7.4 in [38]).*

■

6.6.2 Case Study

In this section, we show the performance of Algorithm 6.1 on the noncooperative power flow. For the case study we employ a test microgrid depicted in Fig. 6.5. The microgrid is composed of 10 buses, which are connected through 9 branches in a radial topological distribution, as commonly occurs in low voltage distribution networks.

We consider a control horizon including H =24 time slots of Δh =1 hour and we assume for all buses, except the slack bus $i = 1$, a net power profile randomly generated. The slack bus can buy energy from the main grid and inject it in the microgrid with a price coefficient $\eta_1 = 1$ financial units. In the remaining nine buses, the distribution grid has diesel generators whose parameters are indicated in Table 6.1. As for the voltage magnitude, we set $V_{\text{ref}} = 1$p.u., $V_i^{\min} = 0$p.u. and $V_i^{\max} = 2$p.u..

The step coefficient for Algorithm 6.1 is $\gamma = 0.01$. All software simulations are conducted in the MATLAB 2020a environment on a laptop with a 1.3 GHz Intel Core(TM)i7 CPU with 8-GB RAM memory.

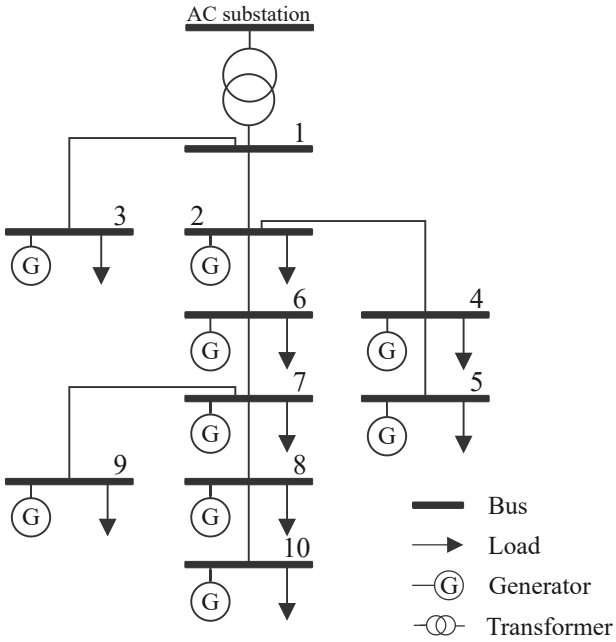

Figure 6.5: Scheme of the simulated DC microgrid.

In the rest of this section, we firstly evaluate the algorithm performance by analyzing the impact of the initial state. Consequently, the results of the noncooperative approach are compared with those obtained by a standard version of the OPF.

6.6.2.1 Impact of the Initial State

The solution of the resulting problem depends on the agents' initial state; hence, we can compute, as for the standard OPF, the regions of convergence for Algorithm 6.1 that in our case correspond to the basin of attraction of the different vCL-GNEs. To this aim, we perform a set of simulations changing each time the initial voltage magnitude V_i^0 and the power injection in each bus g_i^0 sampling them over the interval $[0, 2]$. However, for the sake of showing the convergence results in a two-dimensional plot, in each simulation we set an equal voltage magnitude and power injection for all buses. The results of these simulations are presented in Fig. 6.6, where we plot the region of convergence with different initial states. As it can be seen, there are two different regions of convergence corresponding to the same number of different vCL-GNEs, i.e., the white and orange areas.

Let us now analyze in detail these two equilibria reported in Fig. 6.7a and Fig. 6.7b, where we plot for each bus $i \in \mathcal{N}$ the voltage magnitude and the power injection, respectively.

It should be noted that the white region of convergence corresponds to the solution with high voltage magnitudes in all buses and balanced power injections for all generators, while the orange region converges to the low voltage solution. The latter solution corresponds to the case where there is a high power injection from the slack bus and consequently, in order to make feasible this power transfer, a low voltage magnitude in the remote buses of the microgrid. As for the standard OPF, this low voltage solution should be avoided since it is less interesting in terms of power quality requirements. Nevertheless, as for the classical OPF, we can employ the so-called flat start approach setting all voltage magnitudes equal to 1p.u. and all power injections equal to zero [50]. In Fig. 6.8a and Fig. 6.8b, we show respectively the convergence of the voltage magnitudes and the power injections of each bus when this standard approach is used.

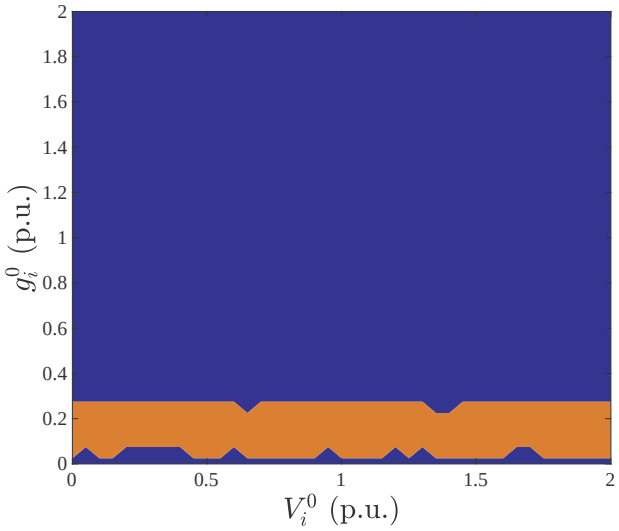

Figure 6.6: Convergence regions with respect to the initial voltage magnitude and power injection (both equal for all buses). The white and the orange regions correspond to the two equilibria of the noncooperative game.

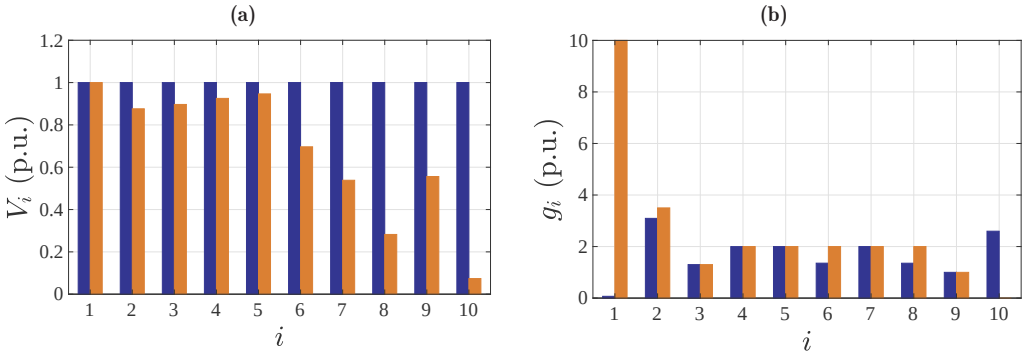

Figure 6.7: Results of Algorithm 6.1 achieved by different initial conditions: voltage magnitudes (a) and power injections (b). The blue and the orange stems represent the two equilibria of the noncooperative game, corresponding to the white and orange area of Fig. 6.6, respectively.

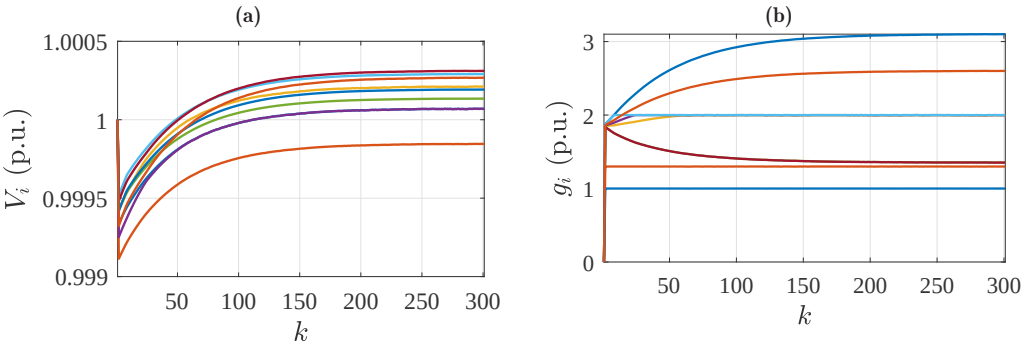

Figure 6.8: Convergence of Algorithm 6.1 with the flat-start approach: voltage magnitudes (a) and power injections (b).

6.6.2.2 Comparison with the Standard OPF

Having computed the region of convergence for the proposed test microgrid, let us now compare the proposed approach with the standard OPF with the same control goal, i.e., reducing the power gap at the slack bus and thus increasing predictability. The standard

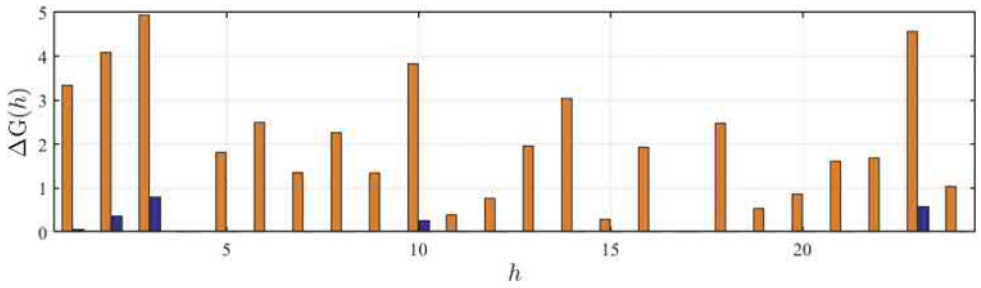

Figure 6.9: Power mismatch $\Delta G(h)$ of the microgrid over the control horizon achieved by the standard OPF (orange bars) and the noncooperative approach (blue bars).

OPF presents several disadvantages inherited by the centralized architecture that leads to the minimization of the overall microgrid cost, possibly penalizing some users. In fact, to overcome these drawbacks, in our non-cooperative framework several coupled optimization problems are simultaneously solved by all users.

From the results illustrated in Fig. 6.9, we see that the noncooperative approach is able to reduce the power mismatch $\Delta G(h) = \sum_{j\in\mathcal{N}\setminus\{1\}} (-\mathbf{P}_j(h) + \mathbf{g}_j(h))$ of the microgrid under 1 p.u.. However, as regards the total energy costs of the microgrid, the standard OPF has a total cost of 2872 financial units while the noncooperative approach of 3342 financial units. Therefore, the total cost of the noncooperative approach is 15% higher than the centralized one. In the centralized scheme, the goal is to minimize the overall gap by ignoring any possible inequalities between different users; on the other hand, in the noncooperative case, each user aims at optimizing its objective thus leading to a more fair yet higher cost summation.

6.7 Conclusion

In this work, we have addressed the problem of solving a class of games with nonconvex coupling constraints. We have defined a local equilibrium concept presenting the conditions for optimality, existence and local uniqueness. Our technical contributions allow us, under certain conditions, to define two iterative schemes with global convergence guarantee toward this novel equilibrium concept.

This work can be extended in several directions, including addressing stochasticity in constraints and cost functions and proposing fully distributed algorithms to steer the strategies of agents in a distributed fashion.

Appendix 6.A Preliminaries on Cones

In the related literature, several different definitions of cones have been proposed, hence, for the sake of clarity, let us here recall some concepts related to tangent cones following the convention used in [25] and [51].

Definition 6.A.1 (*Clarke's tangent vector*)

Let us consider a nonempty subset $\mathcal{X} \subseteq \mathbb{R}^n$, and a point $\mathbf{x} \in cl(\mathcal{X})$. If there is a sequence of elements $(\mathbf{x}_n)_{n\in\mathbb{N}} \in \mathcal{X}$, a sequence $(t_n)_{n\in\mathbb{N}}$ of positive real numbers and a sequence $(h_n)_{n\in\mathbb{N}} \in \mathbb{R}^n$ of vectors such that:

$$\mathbf{x} = \lim_{n\to\infty} \mathbf{x}_n \tag{6.35}$$

$$\lim_{n\to\infty} t_n = 0 \tag{6.36}$$

$$\mathbf{d} = \lim_{n\to\infty} d_n \tag{6.37}$$

and:

$$\mathbf{x}_n + t_n d_n \in \mathcal{X} \tag{6.38}$$

then the vector $\mathbf{d} \in \mathbb{R}^n$ *is called a Clarke's tangent vector to* $\mathcal{X}$ *at* $\mathbf{x}$. □

Definition 6.A.2 (*Clarke's tangent cone*)

Let us consider a nonempty subset $\mathcal{X} \subseteq \mathbb{R}^n$. *The set of all Clarke's tangent vectors to* $\mathcal{X}$ *at* $\mathbf{x}$ *is called the Clarke's tangent cone of the subset* $\mathcal{X}$ *at* $\mathbf{x}$ *and is defined as* $T_{cl}(\mathcal{X}, \mathbf{x})$. □

Note that, due to its definition, Clarke's tangent cone is always convex even if $\mathcal{X}$ is nonconvex. Moreover, Clarke's tangent cone is always a subset of the so-called *Bouligand tangent cone* (and coincides with it if $\mathcal{X}$ is convex). To better show the difference between these two cones, we show an example with a generic nonconvex set $\mathcal{X}$ in Fig. 6.10 (a).

Let us define the so-called *linearized cone*. Firstly, let us assume that the feasible set is composed of a set of equality and inequality constraints:

$$\mathcal{X} = \left\{ \mathbf{x} \in \mathbb{R}^n \;\middle|\; \begin{array}{l} g_m(\mathbf{x}) = 0,\ m \in \mathcal{E} \\ g_m(\mathbf{x}) \leq 0,\ m \in \mathcal{I} \end{array} \right. \tag{6.39}$$

hence, we define the active set $A(\mathbf{x})$ as the set comprehending all indices $m \in \mathcal{E} \cup \mathcal{I}$ with $g_m(\mathbf{x}) = 0$.

Definition 6.A.3 (*Linearised feasible directions set*)

We define the set of Linearised feasible directions $\mathcal{F}(\mathcal{X}, \mathbf{x})$ *as the set comprehending all vectors* $\mathbf{y} \in \mathbb{R}^n$ *such that:*

$$\begin{array}{c} \nabla g_m(\mathbf{x})^\top \mathbf{y} = 0,\ \forall\, m \in \mathcal{E}, \\ \nabla g_m(\mathbf{x})^\top \mathbf{y} \leq 0,\ \forall\, m \in \mathcal{I} \cap A(\mathbf{x}). \end{array} \tag{6.40}$$

□

It is easy to see that this is a closed convex nonempty cone and a linear approximation of the feasible set at a generic point $\mathbf{x}$. Moreover, it can be shown that Clarke's tangent cone is a subset of the linearized cone $T_{\text{cl}}(\mathcal{X}, \mathbf{x}) \subset \mathcal{F}(\mathcal{X}, \mathbf{x})$, however, when a quasiregularity constraint qualification holds (e.g., Mangasarian-Fromovitz) these two cones are equal, i.e., $T_{\text{cl}}(\mathcal{X}, \mathbf{x}) = \mathcal{F}(\mathcal{X}, \mathbf{x})$ [52].

Lastly, let us define the *Clarke's normal cone* and *proximal normal cone* as follows.

Definition 6.A.4 (*Clarke's normal cone*)

Let us consider a nonempty subset $\mathcal{X} \subseteq \mathbb{R}^n$. *The Clarke's normal cone of* $\mathcal{X}$ *in a generic point* $\mathbf{x} \in cl(\mathcal{X})$ *is defined as the polar cone of Clarke's tangent cone to* $\mathcal{X}$ *in* $\mathbf{x}$, *that is:*

$$\begin{aligned} N_{cl}(\mathcal{X}, \mathbf{x}) := T_{cl}(\mathcal{X}, \mathbf{x})^\circ = \\ = \{\mathbf{y} \in \mathbb{R}^n \mid \mathbf{y}^\top \mathbf{d} \leq 0,\ \forall \mathbf{d} \in T_{cl}(\mathcal{X}, \mathbf{x})\} \end{aligned} \tag{6.41}$$

□

In Fig. 6.10 (b) we show three examples of Clarke's normal cone defined in three different points of a generic set $\mathcal{X}$. Note that for point $\mathbf{x}_2$ the relative Clarke's normal cone is $N_{\text{cl}}(\mathcal{X}, \mathbf{x}_2) = \{0\}$.

Definition 6.A.5 (*Proximal normal cone*)

Let us consider a nonempty subset $\mathcal{X} \subseteq \mathbb{R}^n$. *The proximal normal cone of* $\mathcal{X}$ *in a generic point* $\mathbf{x} \in cl(\mathcal{X})$ *is given by:*

$$N_{px}(\mathcal{X}, \mathbf{x}) := \{\mathbf{y} \in \mathbb{R}^n \mid \mathbf{x} \in \text{proj}_{\mathcal{X}}(\mathbf{x} + \alpha \mathbf{y})\} \tag{6.42}$$

where $\alpha > 0$ *is a constant.* □

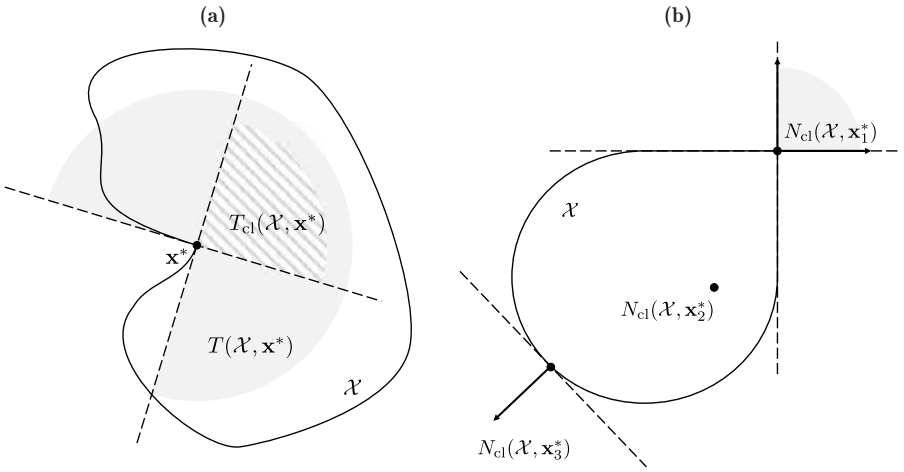

Figure 6.10: Example of a nonconvex set $\mathcal{X}$ with its Bouligand $T(\mathcal{X},\mathbf{x})$ and Clarke's tangent cone $T_{\rm cl}(\mathcal{X},\mathbf{x})$ in a generic point $\mathbf{x}$ (a). Example of a set $\mathcal{X}$ with three different Clarke's normal cones. (b).

Note that $N_{\rm cl}(\mathcal{X},\mathbf{x})$ is always a closed and convex cone while $N_{\rm px}(\mathcal{X},\mathbf{x})$ is convex but may not be closed. In general $N_{\rm px}(\mathcal{X},\mathbf{x}) \subset N_{\rm cl}(\mathcal{X},\mathbf{x})$, however for proximally smooth sets $N_{\rm px}(\mathcal{X},\mathbf{x})$ is closed and $N_{\rm px}(\mathcal{X},\mathbf{x}) = N_{\rm cl}(\mathcal{X},\mathbf{x})$ [53].

References

[1] Nash, J. F. *et al.*, "Equilibrium points in n-person games," *Proceedings of the national academy of sciences*, vol. 36, no. 1, pp. 48–49, 1950.

[2] Lu, Q., Lü, S., and Leng, Y., "A Nash-Stackelberg game approach in regional energy market considering users' integrated demand response," *Energy*, vol. 175, pp. 456–470, 2019.

[3] Jošilo, S. and Dán, G., "Selfish decentralized computation offloading for mobile cloud computing in dense wireless networks," *IEEE Transactions on Mobile Computing*, vol. 18, no. 1, pp. 207–220, 2018.

[4] Pavel, L., "Distributed GNE seeking under partial-decision information over networks via a doubly-augmented operator splitting approach," *IEEE Transactions on Automatic Control*, vol. 65, no. 4, pp. 1584–1597, 2019.

[5] Li, S., Zhang, W., Lian, J., and Kalsi, K., "Market-based coordination of thermostatically controlled loads—Part I: A mechanism design formulation," *IEEE Transactions on Power Systems*, vol. 31, no. 2, pp. 1170–1178, 2015.

[6] Han, L., Zhou, M., Jia, W., Dalil, Z., and Xu, X., "Intrusion detection model of wireless sensor networks based on game theory and an autoregressive model," *Information sciences*, vol. 476, pp. 491–504, 2019.

[7] Deng, R., Yang, Z., Chen, J., Asr, N. R., and Chow, M.-Y., "Residential energy consumption scheduling: A coupled-constraint game approach," *IEEE Transactions on Smart Grid*, vol. 5, no. 3, pp. 1340–1350, 2014.

[8] Li, Y., Tee, K. P., Yan, R., Chan, W. L., and Wu, Y., "A framework of human–robot coordination based on game theory and policy iteration," *IEEE Transactions on Robotics*, vol. 32, no. 6, pp. 1408–1418, 2016.

[9] Kulkarni, A. A. and Shanbhag, U. V., "On the variational equilibrium as a refinement of the generalized Nash equilibrium," *Automatica*, vol. 48, no. 1, pp. 45–55, 2012.

[10] Belgioioso, G. and Grammatico, S., "Semi-decentralized generalized Nash equilibrium seeking in monotone aggregative games," *IEEE Transactions on Automatic Control*, 2021.

[11] Facchinei, F., Fischer, A., and Piccialli, V., "On generalized nash games and variational inequalities," *Operations Research Letters*, vol. 35, no. 2, pp. 159–164, 2007.

[12] Baye, M. R., Tian, G., and Zhou, J., "Characterizations of the existence of equilibria in games with discontinuous and non-quasiconcave payoffs," *The Review of Economic Studies*, vol. 60, no. 4, pp. 935–948, 1993.

[13] Pang, J.-S. and Scutari, G., "Nonconvex games with side constraints," *SIAM Journal on Optimization*, vol. 21, no. 4, pp. 1491–1522, 2011.

[14] Grammatico, S., "Dynamic control of agents playing aggregative games with coupling constraints," *IEEE Transactions on Automatic Control*, vol. 62, no. 9, pp. 4537–4548, 2017.

[15] Farzaneh, H., Shokri, M., Kebriaei, H., and Aminifar, F., "Robust energy management of residential nanogrids via decentralized mean field control," *IEEE Transactions on Sustainable Energy*, vol. 11, no. 3, pp. 1995–2002, 2019.

[16] Gadjov, D. and Pavel, L., "Single-timescale distributed GNE seeking for aggregative games over networks via forward–backward operator splitting," *IEEE Transactions on Automatic Control*, vol. 66, no. 7, pp. 3259–3266, 2020.

[17] Biasi, C., Monis, T. F. M., *et al.*, "Weak local Nash equilibrium," *Topological Methods in Nonlinear Analysis*, vol. 41, no. 2, pp. 409–419, 2013.

[18] Alós-Ferrer, C. and Ania, A. B., "Local equilibria in economic games," *Economics Letters*, vol. 70, no. 2, pp. 165–173, 2001.

[19] Cornet, B. and Czarnecki, M.-O., "Existence of generalized equilibria," *Nonlinear Analysis: Theory, Methods & Applications*, vol. 44, no. 5, pp. 555–574, 2001.

[20] Pang, J.-S. and Scutari, G., "Joint sensing and power allocation in nonconvex cognitive radio games: Quasi-Nash equilibria," *IEEE Transactions on Signal Processing*, vol. 61, no. 9, pp. 2366–2382, 2013.

[21] Huang, X., Beferull-Lozano, B., and Botella, C., "Quasi-nash equilibria for non-convex distributed power allocation games in cognitive radios," *IEEE Transactions on Wireless Communications*, vol. 12, no. 7, pp. 3326–3337, 2013.

[22] Ratliff, L. J., Burden, S. A., and Sastry, S. S., "On the characterization of local Nash equilibria in continuous games," *IEEE Transactions on Automatic Control*, vol. 61, no. 8, pp. 2301–2307, 2016.

[23] Belgioioso, G., Ananduta, W., Grammatico, S., and Ocampo-Martinez, C., "Operationally-safe peer-to-peer energy trading in distribution grids: A game-theoretic market-clearing mechanism," *IEEE Transactions on Smart Grid*, 2022.

[24] Facchinei, F. and Sagratella, S., "On the computation of all solutions of jointly convex generalized Nash equilibrium problems," *Optimization Letters*, vol. 5, no. 3, pp. 531–547, 2011.

[25] Miettinen, K. and Mäkelä, M. M., *Tangent and normal cones in nonconvex multiobjective optimization*. Springer, 2000, pp. 114–124.

[26] Franci, B. and Grammatico, S., "Stochastic generalized Nash equilibrium seeking in merely monotone games," *IEEE Transactions on Automatic Control*, pp. 1–1, 2021. DOI: 10.1109/TAC.2021.3108496.

[27] Rosen, J. B., "Existence and uniqueness of equilibrium points for concave n-person games," *Econometrica: Journal of the Econometric Society*, pp. 520–534, 1965.

[28] Pang, J.-S. and Fukushima, M., "Quasi-variational inequalities, generalized Nash equilibria, and multi-leader-follower games," *Computational Management Science*, vol. 2, no. 1, pp. 21–56, 2005.

[29] Federer, H., "Curvature measures," *Transactions of the American Mathematical Society*, vol. 93, no. 3, pp. 418–491, 1959.

[30] Adly, S., Nacry, F., and Thibault, L., "New metric properties for prox-regular sets," *Mathematical Programming*, vol. 189, no. 1, pp. 7–36, 2021.

[31] Clarke, F. H., Stern, R., and Wolenski, P., "Proximal smoothness and the lower-c2 property," *J. Convex Anal*, vol. 2, no. 1-2, pp. 117–144, 1995.

[32] Canino, A., "On p-convex sets and geodesics," *Journal of differential equations*, vol. 75, no. 1, pp. 118–157, 1988.

[33] Shapiro, A., "Existence and differentiability of metric projections in Hilbert spaces," *SIAM Journal on Optimization*, vol. 4, no. 1, pp. 130–141, 1994.

[34] Vial, J.-P., "Strong and weak convexity of sets and functions," *Mathematics of Operations Research*, vol. 8, no. 2, pp. 231–259, 1983.

[35] Poliquin, R., Rockafellar, R., and Thibault, L., "Local differentiability of distance functions," *Transactions of the American mathematical Society*, vol. 352, no. 11, pp. 5231–5249, 2000.

[36] Adly, S., Nacry, F., and Thibault, L., "Preservation of prox-regularity of sets with applications to constrained optimization," *SIAM Journal on Optimization*, vol. 26, no. 1, pp. 448–473, 2016.

[37] Adly, S., Nacry, F., and Thibault, L., "Prox-regularity approach to generalized equations and image projection," *ESAIM: Control, Optimisation and Calculus of Variations*, vol. 24, no. 2, pp. 677–708, 2018.

[38] Bernard, F., Thibault, L., and Zlateva, N., "Prox-regular sets and epigraphs in uniformly convex banach spaces: Various regularities and other properties," *Transactions of the American Mathematical Society*, vol. 363, no. 4, pp. 2211–2247, 2011.

[39] Lefschetz, S., "Intersections and transformations of complexes and manifolds," *Transactions of the American Mathematical Society*, vol. 28, no. 1, pp. 1–49, 1926.

[40] Brown, R., "On a homotopy converse to the Lefschetz fixed point theorem," *Pacific Journal of Mathematics*, vol. 17, no. 3, pp. 407–411, 1966.

[41] Palomar, D. P. and Eldar, Y. C., *Convex optimization in signal processing and communications*. Cambridge university press, 2010.

[42] Glendinning, P., *Stability, instability and chaos: an introduction to the theory of nonlinear differential equations*. Cambridge university press, 1994.

[43] Korpelevich, G. M., "The extragradient method for finding saddle points and other problems," *Ekonomie i Mathematik Metody*, vol. 12, pp. 747–756, 1976, [English translation: Matecon 13 (1977) 35–49.]

[44] Monderer, D. and Shapley, L. S., "Potential games," *Games and economic behavior*, vol. 14, no. 1, pp. 124–143, 1996.

[45] Bramoullé, Y., Kranton, R., and D'amours, M., "Strategic interaction and networks," *American Economic Review*, vol. 104, no. 3, pp. 898–930, 2014.

[46] Scarabaggio, P., Carli, R., and Dotoli, M., "A game-theoretic control approach for the optimal energy storage under power flow constraints in distribution networks," in *2020 IEEE 16th International Conference on Automation Science and Engineering (CASE)*, 2020, pp. 1281–1286. DOI: 10.1109/CASE48305.2020.9216800.

[47] Atzeni, I., Ordóñez, L. G., Scutari, G., Palomar, D. P., and Fonollosa, J. R., "Demand-side management via distributed energy generation and storage optimization," *IEEE Trans. Smart Grid*, vol. 4, no. 2, pp. 866–876, 2012.

[48] Kargarian, A., Mohammadi, J., Guo, J., *et al.*, "Toward distributed/decentralized dc optimal power flow implementation in future electric power systems," *IEEE Trans. Smart Grid*, vol. 9, no. 4, pp. 2574–2594, 2016.

[49] Yang, L., Luo, J., Xu, Y., Zhang, Z., and Dong, Z., "A distributed dual consensus admm based on partition for dc-dopf with carbon emission trading," *IEEE Trans. Ind. Informat.*, 2019.

[50] Vinkovic, A. and Mihalic, R., "A current-based model of an ipfc for newton–raphson power flow," *Electric Power Systems Research*, vol. 79, no. 8, pp. 1247–1254, 2009.

[51] Jahn, J., *Tangent cones*. Springer, 2020, pp. 79–106.

[52] Nocedal, J. and Wright, S., *Numerical optimization*. Springer Science & Business Media, 2006.

[53] Clarke, F. H., Ledyaev, Y. S., Stern, R. J., and Wolenski, P. R., *Nonsmooth analysis and control theory*. Springer Science & Business Media, 2008, vol. 178.

Chapter 7

Noncooperative Control for Energy Scheduling Under Nonconvex Physical and Quality Constraints

VII

Abstract

Power distribution grids are commonly controlled through centralized approaches, such as the optimal power flow. However, the current pervasive deployment of distributed renewable energy sources and the increasing growth of active players, providing ancillary services to the grid, have made these centralized frameworks no longer appropriate. In this context, we propose a novel noncooperative control mechanism for optimally regulating the operation of power distribution networks equipped with traditional loads, distributed generation, and active users. The latter, also known as prosumers, contribute to the grid optimization process by leveraging their flexible demand, dispatchable generation capability, and/or energy storage potential. Active users participate in a noncooperative liberalized market designed to increase the penetration of renewable generation and improve the predictability of power injection from the high voltage grid. The novelty of our game-theoretical approach consists in incorporating economic factors as well as physical constraints and grid stability aspects. Lastly, by integrating the proposed framework into a rolling-horizon approach, we show its effectiveness and resiliency through numerical experiments.

Contents

7.1 Introduction

Power grids around the world are acquiring an increasingly distributed feature in the last few years. Indeed, several independent players are now typically involved in the control and optimization of power grids, strongly affecting their dynamics [1]. The integration in the grid of these active users —also known as prosumers-– is strictly related to the so-called *demand-side management*, which is recognized as a very effective solution for the planning and optimization of power grid operations. This new paradigm is widely used to tackle the complexity issues and uncertainties of modern power grids, which are mainly caused by the extensive diffusion of non-controllable *renewable energy sources* (RESs) at different levels of energy distribution systems [2]. Moreover, *distributed generation* (DG) and *distributed storage* (DS), are currently used in power systems aiming at suitably supporting the grid operations and providing ancillary services, such as frequency regulation and voltage control. Currently, most of these new elements are mainly integrated into the *medium voltage* (MV) and *low voltage* (LV) power distribution networks that are characterized by

a high R/X ratio (i.e., resistance to reactance ratio). Moreover, while these grids were traditionally designed for monodirectional, radial and weakly meshed power flows, they are now massively stressed by an incessant swap in direction and magnitude of power flows, caused by the continuous integration of unpredictable RESs [3].

The integration in the grid of new proactive players, responsible for the control of various parts of power grids, can considerably reduce these issues. On the one hand, the cooperation of such independent entities is challenging. These entities act selfishly aiming at their profit; in addition, the control of a large number of independent entities can be computationally demanding, ill scalable, limitedly fault-tolerant, and poorly respectful of privacy. On the other hand, since they are physically interconnected through power lines, they must be effectively coordinated to ensure safe and secure grid operations [4].

One of the critical problems in power systems is the well-known *optimal power flow* (OPF) problem, which consists in optimally scheduling the committed generators based on the results of the day-ahead economic dispatch problem [5]. More in detail, the OPF problem has the objective of calculating the optimal operating point for each generator, resulting in the least cost required to supply a given power demand, while fulfilling the power system and equipment constraints. In case this computation is performed in a centralized approach, the so-called Independent System Operator must have access to all the generators' cost functions and system parameters.

However, in the presence of selfish players operating in power grids, as well as flexible loads, DG, and DS, some issues discourage the use of this centralized decision-making structure. In fact, this is usually computationally demanding, ill scalable, limitedly fault-tolerant, and poorly respectful of privacy [4]. In order to improve the drawbacks of such an architecture, several distributed/decentralized OPF and economic dispatch frameworks have been recently proposed [6], [7]. Most of these works either focus on the economic dispatch problem only or address the *direct current optimal power flow* (DCOPF) system, thus ignoring a reliable model of the power network dynamics. In addition, most works deal with the *high voltage* (HV) transmission network only, which is modeled more straightforwardly than MV/LV networks. Specifically, several economic dispatch and linearized OPF models (e.g., the DCOPF) are largely implemented in a decentralized architecture [8], [9]. However, these models are not applicable to MV/LV distribution networks, where different physical assumptions must be made, and they cannot fully capture the behavior of independent elements in the grid. Only very few distributed approaches such as [10] employ convexified models for distribution networks, for instance based on conic relaxation. Nevertheless, this model may includes some error and inexactness.

All these strategies focus on the control of cooperative integrated elements: in fact, the final goal of these approaches is to optimize the global welfare rather than the single players' revenues. Conversely, to cope with the situation where several noncooperative agents are involved in the optimization of power grids, game-theoretic methods have been proposed for the generation and storage control in power grids. These control approaches are based on centralized architectures or on distributed ones that have the advantage of requiring only a little sharing of private information [11], [12]. In detail, several works focus their effort on defining efficient noncooperative decentralized control policies that rely on effective models of power distribution components. For instance, the authors in [13], [14] propose a noncooperative approach for distributed generation in power systems, considering economic and power flow constraints. However, the common weakness of these works is the inadequate representation of the underlying power system. Indeed, their main focus is on the game perspective, while physical constraints are partially disregarded. Several studies (e.g., [15]), include a constraint barely on the mismatch between the generated and the requested power. Nevertheless, this assumption is sufficient only during the economic dispatch phase, while it is not adequate for real-time control of the grid.

Summing up, in the case of HV power grids, certain simplifying assumptions hold, and thus several approximated convex models ensure a reliable solution of the control problem using game-theoretical techniques. On the contrary, in distribution grids these hypotheses become inappropriate; hence, the classical AC power flow must be used. In

particular, in case the underlying models are nonconvex and in general nonlinear, few game-theoretical approaches are available in the literature, while their application to power systems is to the best of our knowledge almost absent.

The above reported literature review shows that little attention has been devoted to game theory based frameworks able to satisfy the AC power flow constraints. Therefore, in this chapter we propose a reliable distribution grid model that comprehends several buses connected with noncontrollable loads and RESs as well as active users. The distribution grid is connected with the *high voltage* (HV) transmission grid through a slack bus from which power is injected. The *distribution system operator* (DSO) schedules this injection over a control horizon, to satisfy the load demand and taking into account the RESs' production. However, due to the uncertainties in both demand and production, this schedule may be not accurate. For the sake of increasing the predictability of the distribution grid, from the HV grid's perspective, the DSO encourages by means of economical rewards noncooperative active users to modify their energy scheduling. In particular, these users have some flexible loads, with an elastic energy demand, or own either a traditional energy generator or a storage system.

The contributions of this work with respect to the related literature can be summarized as follows.

1) We model the system not only in a decentralized or distributed fashion, such as in works [8], [9], but we consider multiple agents with a noncooperative behavior for a better representation of the market. This representation aims at increasing the predictability and flexibility of the power grid, while allowing each user to preserve its privacy. In addition, differently from [10], where the offered flexibility is indeed not properly valued at the individual level but only shared among all members, we provide users with an incentivizing control goal. Moreover, differently from other game-theoretical approaches presented for instance in [13]–[15], in addition to mere economical aspects, we take into account the nonlinear AC power flow equations, and consequently the power quality constraints.

2) We extensively improve our previous work [16], where we preliminarily introduce a noncooperative framework of energy storage providers participating in the grid optimization under power flow constraints. In particular, in this work we significantly enhance the grid model by integrating flexible loads and dispatchable generators, while additionally including power quality constraints.

3) Due to the nonconvexity of the power flow constraints, we define a weaker game-theoretical equilibrium concept showing the condition required for the existence and uniqueness. Moreover, we propose a novel decentralized algorithm that iteratively leads the single profit strategies to converge to a local variational equilibrium, if this exists. We implement this algorithm in a rolling-horizon approach and we assess its effectiveness over a set of numerical experiments based on two IEEE test bus systems.

7.1.1 Basic Notation

Let us introduce some basic notation. $\mathbb{R}$, $\mathbb{R}_{>0}$ and $\mathbb{R}_{\geq 0}$ denote the set of real, positive real, and non-negative real numbers, respectively. Moreover, $\mathbb{R}^n$, $\mathbb{R}^n_{>0}$ and $\mathbb{R}^n_{\geq 0}$ denote the set of real, positive real, and non-negative real n-dimensional vectors, respectively. $A^\top$ denotes the transpose of A. $\|A\|$ is the square norm of A. $A \otimes B$ and $A \circ B$ indicate the Kronecker and the Hadamard product between matrices A and B. $\mathbf{0}_n$ and $\mathbf{1}_n$ indicate the column vectors with n entries all equal to 0 and to 1, respectively, e.g., $\mathbf{0}_n = (0, ..., 0)^\top \in \mathbb{R}^n$. We define the $n \times n$ identity matrix as $I_n = \text{diag}(1, 1, \ldots, 1)$. Moreover, $\mathbf{x} = \text{col}(x_1, ..., x_n)$ is equal to $\mathbf{x} = (x_1^\top, ..., x_n^\top)^\top$. We define the mapping $\Pi_{\mathcal{X}} : \mathbb{R}^n \to \mathcal{X}$ as the projection into the generic closed non-empty set $\mathcal{X} \subseteq \mathbb{R}^n$, i.e., $\Pi_{\mathcal{X}}(\mathbf{y}) = \text{argmin}_{\mathbf{x} \in \mathcal{X}} \|\mathbf{x} - \mathbf{y}\|$. The set-valued mapping $N_{\mathcal{X}} : \mathbb{R}^n \to \mathbb{R}^n$ denotes the normal cone operator for the the set $\mathcal{X} \subseteq \mathbb{R}^n$, i.e., $N_{\mathcal{X}}(\mathbf{y}) := \varnothing$ if $\mathbf{y} \in \mathcal{X}$, $N_{\mathcal{X}}(\mathbf{y}) := \left\{\mathbf{x} \in \mathbb{R}^n \mid \sup_{\mathbf{z} \in \mathbb{R}^n} \mathbf{x}^\top (\mathbf{z} - \mathbf{y}) \leq 0\right\}$ otherwise. The mapping $F(\mathbf{x}) : \mathbb{R}^n \to \mathbb{R}^n$ is strongly monotone with a constant $s \in \mathbb{R}_{>0}$ if $(F(\mathbf{x}) - F(\mathbf{y}))^\top (\mathbf{x} - \mathbf{y})) \geq s \|\mathbf{x} - \mathbf{y}\|^2$, $\forall \mathbf{x}, \mathbf{y} \in \mathbb{R}^n$.

For a fixed sampling interval ΔH, the value of a variable x at the h-th sampling time $h\,\Delta$H is denoted by $x(h)$, where $h = 1, 2, ... \in \mathbb{N}$ is the discrete-time index. We indicate a real number with x and a complex number with $\bar{x}$. For $\bar{x} \in \mathbb{C}$, we indicate its modulus by $|\bar{x}|$ and its conjugate by $\bar{x}^*$.

7.2 System Model

In this section, we introduce the model of the smart energy systems and of the MV distribution grid. The grid is composed by several interconnected buses and is connected with the HV transmission network through a slack bus, from which the DSO injects power into the MV distribution grid. We suppose that the grid is controlled through a predictive approach characterized by a control and prediction horizon with fixed length H. The control horizon at time step t is denoted as $\mathcal{H}_t = \{t, ..., h, ..., t + H - 1\}$, where $h > t$ is a generic time slot of the moving horizon.

We employ a graph $\mathcal{G} = (\mathcal{B}, \mathcal{E})$ to model the power distribution grid elements and interconnections (i.e., buses and transmission lines), where $\mathcal{B}$ is the set of nodes with cardinality B, whilst $\mathcal{E} \in \mathcal{B} \times \mathcal{B}$ is the set of pairs of distinct nodes called edges with cardinality E. The nodes $b \in \mathcal{B}$ of the graph represent the buses of the power system and the edges $(b, r) \in \mathcal{E}$ represent the transmission lines among these buses. We assume that each bus $b \in \mathcal{B}$ is connected with several non-controllable loads whose aggregated per-slot active and reactive power demand scheduling vectors over the control horizon $\mathcal{H}_t$ are $\mathbf{P}_b^{\mathrm{c}} := (P_b^{\mathrm{c}}(t), ..., P_b^{\mathrm{c}}(h), ..., P_b^{\mathrm{c}}(t + H - 1))^\top \in \mathbb{R}_{\geq 0}^H$ and $\mathbf{Q}_b^{\mathrm{c}} := (Q_b^{\mathrm{c}}(t), ..., Q_b^{\mathrm{c}}(h), ..., Q_b^{\mathrm{c}}(t + H - 1))^\top \in \mathbb{R}_{\geq 0}^H$, respectively. Moreover, we assume that the RESs (i.e., non-dispatchable generators) connected with the bus b have an aggregated active and reactive power production scheduling vectors over the control horizon $\mathcal{H}_t$ equal to $\mathbf{P}_b^{\mathrm{w}} := (P_b^{\mathrm{w}}(t), ..., P_b^{\mathrm{w}}(h), ..., P_b^{\mathrm{w}}(t + H - 1))^\top \in \mathbb{R}_{\geq 0}^H$ and $\mathbf{Q}_b^{\mathrm{w}} := (Q_b^{\mathrm{w}}(t), ..., Q_b^{\mathrm{w}}(h), ..., Q_b^{\mathrm{w}}(t + H - 1))^\top \in \mathbb{R}_{\geq 0}^H$, respectively. For the sake of clarity, let us define the net active and reactive power associated to bus b as $\mathbf{P}_b = \mathbf{P}_b^{\mathrm{w}} - \mathbf{P}_b^{\mathrm{c}} \in \mathbb{R}^H$ and $\mathbf{Q}_b = \mathbf{Q}_b^{\mathrm{w}} - \mathbf{Q}_b^{\mathrm{c}} \in \mathbb{R}^H$, respectively.

Moreover, we assume that the power distribution grid includes a set $\mathcal{N}$ of N active users that modify their energy scheduling profile aiming at decreasing their total cost, while providing flexibility services to the grid. In particular, users $i \in \mathcal{N}$ are classified into the three categories $\mathcal{N}_c$, $\mathcal{N}_g$, and $\mathcal{N}_s$, denoting respectively the sets of users that can dynamically modify the profile of their controllable energy consumption, their dispatchable energy generation, and their energy charging/discharging strategy.

7.2.1 Flexible Loads

Users $i \in \mathcal{N}_c$ have a controllable energy consumption profile $\mathbf{c}_i := (c_i(t), ..., c_i(h), ..., c_i(t + H - 1))^\top \in \mathbb{R}_{\geq 0}^H$ that can be modified in accordance with the market conditions. First, we assume that the controllable energy consumption is bounded by lower (i.e., $c_i^{\min}$) and upper (i.e., $c_i^{\max}$) limits:

$$c_i^{\min} \mathbf{1}_H \leq \mathbf{c}_i \leq c_i^{\max} \mathbf{1}_H, \quad \forall i \in \mathcal{N}_c\,. \tag{7.1}$$

Moreover, we assume that a given amount of controllable energy demand (i.e., $\xi_{t,i}$) must be satisfied over the control horizon $\mathcal{H}_t$:

$$\mathbf{1}_H^\top \mathbf{c}_i = \xi_{t,i}, \quad \forall i \in \mathcal{N}_c. \tag{7.2}$$

For the sake of compactness, let us define for each user $i \in \mathcal{N}_c$ a set of feasible strategies as follows:

$$\Omega_{c_i} = \left\{ \boldsymbol{c}_i \in \mathbb{R}_{\geq 0}^H \mid (7.1), (7.2) \text{ hold} \right\}, \quad \forall i \in \mathcal{N}_c. \tag{7.3}$$

7.2.2 Dispatchable Generators

The group of users $i \in \mathcal{N}_g$ are equipped with dispatchable energy devices that aim at producing a generation profile $\mathbf{g}_i := (g_i(t), ..., g_i(h), ..., g_i(t+H-1))^\top \in \mathbb{R}^H_{\geq 0}$. We assume that energy producers are subject to variable production costs in accordance with a linear cost function $W_i(\mathbf{g}_i) = \eta_i \mathbf{1}_H^\top \mathbf{g}_i$, where η_i is the generation cost per time slot [12]. The non-negative generation profile is upper bounded by the maximum per-slot energy generation capacity:

$$\mathbf{0}_H \leq \mathbf{g}_i \leq g_i^{\max} \mathbf{1}_H, \quad \forall i \in \mathcal{N}_g \,. \tag{7.4}$$

For the sake of compactness, let us define for each producer $i \in \mathcal{N}_g$ a set of feasible strategies as follows:

$$\Omega_{\mathbf{g}_i} = \left\{ \mathbf{g}_i \in \mathbb{R}^H_{\geq 0} \mid (7.4) \text{ hold} \right\}, \quad \forall i \in \mathcal{N}_g. \tag{7.5}$$

7.2.3 Energy Storage Systems

Users $i \in \mathcal{N}_s$ are equipped with an ESS whose energy storage profile is denoted as $\mathbf{s}_i = \text{col}(\mathbf{s}_{c,i}, \mathbf{s}_{d,i}) \in \mathbb{R}^{2H}_{\geq 0}$, where $\mathbf{s}_{c,i} := (s_{c,i}(t), ..., s_{c,i}(h), ..., s_{c,i}(t+H-1))^\top \in \mathbb{R}^H_{\geq 0}$ is the charging profile and $\mathbf{s}_{d,i} := (s_{d,i}(t), ..., s_{d,i}(h), ..., s_{d,i}(t+H-1))^\top \in \mathbb{R}^H_{\geq 0}$ the discharging profile. Neglecting the ESS technology specificity, for each user $i \in \mathcal{N}_s$ we characterize the corresponding ESS with its storage capacity $\text{SoC}_i^{\max}$, maximum charging/discharging rate $s_i^{\max}$, charging and discharging efficiency $0 < \beta_{c,i} \leq 1$ and $\beta_{d,i} \geq 1$, and leakage rate $0 < \alpha_i \leq 1$. The reactive power does not affect the ESSs state of charge [17]: indeed, ESSs are mainly used for active power support; as a consequence, we neglect the reactive power in the storage model.

In particular, the ESS state of charge at a given time step is equal to the value at the previous time step, decreased by the leakage rate and incremented or reduced by the energy storage profile $s_i(h) = (s_{c,i}(h), s_{d,i}(h))^\top$ altered through the charging and discharging efficiency $\beta_i = (\beta_{c,i}, -\beta_{d,i})^\top$ [12]:

$$\text{SoC}_i(h) = \alpha_i \text{SoC}_i(h-1) + \beta_i^\top s_i(h), \quad \forall i \in \mathcal{N}_s. \tag{7.6}$$

The charging and discharging profile is respectively limited by the available state of charge and the storage capacity:

$$-\text{SoC}_i(h-1) \leq \beta_i^\top s_i(h) \leq \text{SoC}_i^{\max} - \text{SoC}_i(h-1), \forall i \in \mathcal{N}_s \,. \tag{7.7}$$

The maximum charging/discharging rate must be respected:

$$-s_i^{\max} \mathbf{1}_{2H} \leq \boldsymbol{\beta}_i^\top \mathbf{s}_i \leq s_i^{\max} \mathbf{1}_{2H}, \quad \forall i \in \mathcal{N}_s \tag{7.8}$$

where $\boldsymbol{\beta}_i := \text{col}(\beta_{c,i} \mathbf{1}_H, -\beta_{d,i} \mathbf{1}_H)$.

All the various ESS technologies suffer from degradation in terms of capacity decreasing and resistance increase. For the sake of simplicity, we introduce a simple quadratic cost function $C_i(\mathbf{s}_i) = \zeta_i \mathbf{s}_i^\top \mathbf{s}_i$ where ζ_i is the known degradation coefficient [18].

Finally, for the sake of compactness, for each user $i \in \mathcal{N}_s$ we define the set of feasible strategies as:

$$\Omega_{s_i} = \left\{ \mathbf{s}_i \in \mathbb{R}^{2H}_{\geq 0} \mid (7.6) - (7.8) \text{ hold} \right\}, \quad \forall i \in \mathcal{N}_s. \tag{7.9}$$

7.3 Preliminaries on Power Flow

In this section, we recall some basic concepts on the network power flow analysis, which aims at determining the steady-state condition of electric power systems. Specifically, the final goal is the computation of the voltage magnitude and phase angle in each bus of the network, given a power injection profile in each bus as input data [19].

Remark 7.3.1

In this work, we employ a simplified version of the AC OPF problem, as we disregard

power losses and consider each bus as a PQ bus. The latter assumption is reasonable since generators can be modeled as PQ buses when a frequency droop control approach is not used [20]. However, we remark that the proposed approach can be easily improved including PV buses and considering power losses or it can be extended including other techniques to more accurately model the power flow in distribution systems (e.g., employing current injection models to represent unbalanced networks) [21]–[23]. □

For the sake of keeping the notation light, in this section we refer to the value of variables at time h avoiding the time-dependency (h) in the symbols. Using the classical π-model for the power grid, and disregarding the power losses, the relation between the current injection $\bar{I}_b$ at bus b and the voltage in a network of B nodes can be defined as:

$$\bar{I}_b = \sum_{r \in \mathcal{B}} \bar{Y}_{br} \bar{V}_r, \ \forall b \in \mathcal{B} \tag{7.10}$$

where $\bar{Y}_{br}$ is the element (b, r) of the admittance matrix, defined as:

$$\bar{Y}_{br} = \begin{cases} \bar{y}_{bb} + \sum_{h \neq r} \bar{y}_{nh} & \text{if } b = r \\ -\bar{y}_{br} & \text{if } b \neq r \end{cases}, \ \forall (b, r) \in \mathcal{E} \tag{7.11}$$

where $\bar{y}_{bb}$ is the admittance to the ground at bus b and $\bar{y}_{br} = \bar{y}_{rb}$ is the line admittance between buses b and r. It is apparent that $\bar{y}_{br} = \bar{y}_{rb} = 0$ holds if there is no link between bus b and r. The complex power at bus b is given by:

$$\bar{S}_b = \bar{V}_b \sum_{r \in \mathcal{B}} \bar{Y}^*_{br} \bar{V}^*_r, \ \forall b \in \mathcal{B}. \tag{7.12}$$

By representing the variables in a polar form, it is worthwhile to define $\bar{V}_b = |V_b| \angle \theta_b$, $\bar{V}^*_b = |V_b| \angle (-\theta_b)$ and $\bar{Y}_{br} = |Y_{br}| \angle \theta_{br}$, where θ_b is the phase angle at bus b while θ_{br} is the phase difference between bus b and bus r. Consequently, by splitting the complex power into its active and reactive part we obtain:

$$|V_b| \sum_{r \in \mathcal{B}} |V_r||Y_{br}| \cos(\theta_{br} + \theta_r - \theta_b) - P_b = 0, \ \forall b \in \mathcal{B} \tag{7.13}$$

$$-|V_b| \sum_{r \in \mathcal{B}} |V_r||Y_{br}| \sin(\theta_{br} + \theta_r - \theta_b) - Q_b = 0, \ \forall b \in \mathcal{B}. \tag{7.14}$$

The set of nonlinear equations (7.13)-(7.14) –also known as power flow equations– can be solved in several ways; however, the most common approach in the literature is the Newton–Raphson approach [24]. The Newton-Raphson approach works iteratively, employing an initial guess for the value of parameters, most of the time with the so-called flat start. The results of this procedure correspond to the steady-state solution of the network; however, this may not be feasible due to some constraints violations. Indeed, in real-world applications, several quality constraints are applied to the power system, the most critical ones concerning the lower and upper bounding of the voltage magnitude and the maximum active power transfer:

$$V_b^{\min} \leq |V_b| \leq V_b^{\max}, \forall b \in \mathcal{B} \tag{7.15}$$

$$-P_{br}^{\max} \leq P_{br} \leq P_{br}^{\max}, \forall (b, r) \in \mathcal{E} \tag{7.16}$$

where the active power P_{br} transmitted between two interconnected buses b and r is calculated by:

$$P_{br} = |V_b|^2 |y_{br}| \cos(\theta_{br}) - |V_b||V_r||y_{br}| \cos(\theta_n - \theta_r - \theta_{br}), \forall (b, r) \in \mathcal{E}. \tag{7.17}$$

7.4 Game Model

The goal of this section is to illustrate the overall optimization problem for the proposed distribution network model. We preliminarily remark that, on the one hand, in traditional power systems, distribution grids are modeled in an approximated way as highly predictable time-constant loads. As a consequence, from the viewpoint of the HV network, which is connected to the MV network through the slack bus, the distribution infrastructure is merely considered passive and it is accordingly sized on the specific demand. On the other hand, the current pervasive integration of distributed renewable sources and flexible loads at the distribution level may affect the predictability of modern MV grids. Therefore, our goal is to design an intelligent mechanism that allows the DSO to increase the distribution network predictability with respect to the active power injected through the slack bus. To this aim, we introduce the reference signal $\mathbf{P}_{\mathrm{r}} := (P_{\mathrm{r}}(t), ..., P_{\mathrm{r}}(h), ..., P_{\mathrm{r}}(t+H-1))^{\top} \in \mathbb{R}^{H}$ as the planned active power that the DSO intends to inject into the distribution network. Then, we define the mismatch as:

$$\boldsymbol{\Delta} = \mathbf{P}_{\mathrm{r}} - \mathbf{P}\,\mathbf{1}_{B} \tag{7.18}$$

where $\mathbf{P} := (\mathbf{P}_1, ..., \mathbf{P}_b, ..., \mathbf{P}_B)^{\top} \in \mathbb{R}^{H \times B}$ collects the active power demands actually forecasted in all the buses over the whole control horizon.

We now suppose that the deviation between the planned and the forecasted power demand is dynamically regulated by leveraging on the optimal control of the independent active users. In particular, we assume the existence of two different electricity markets. The passive users connected to the distribution grid participate in a traditional electricity market employing a standard pricing mechanism (e.g., with time tariff based on a liberalized market). On the other side, the DSO coordinates a market where the prosumers participate to offer ancillary services in the distribution network. The DSO encourages active users to minimize the above-defined mismatch through a pricing mechanism based on such a deviation. At the same time, each prosumer tries to maximize its own profit over the given time horizon, while fully satisfying the power grid topology and physical limits. A natural framework to capture such a competitive and decentralized decision-making process relies on game theory. In particular, in the sequel, we propose a novel noncooperative game model to drive the individual decisions of active users towards a feasible solution.

A *noncooperative game* is usually defined by a set of players (here corresponding to the active users), a strategy of each player, a cost or payoff function for each player and a set of feasible strategies for each player. Each player behaves selfishly to optimize its own welfare, quantified through a net cost function. However, the main difference between a game with N players and N single independent optimization problems relies on the assumption that the net cost function for each player depends not only on its strategy but also on the strategies of the other players. More in detail, let us define for each active player $i \in \mathcal{N}$ its strategy by $\mathbf{x}_i = \mathrm{col}(\mathbf{c}_i, \mathbf{g}_i, \mathbf{s}_i) \in \mathbb{R}^{4H}_{\geq 0}$, that collects the controllable consumption, dispatchable generation and ESS charging/discharging profile. Moreover, $\mathbf{x}_{-i} := \mathrm{col}\,(\mathbf{x}_1, ..., \mathbf{x}_{i-1}, \mathbf{x}_{i+1}, ..., \mathbf{x}_N) \in \mathbb{R}^{4H(N-1)}$ collects the strategies of all the active users different from i, while $\mathbf{x} := \mathrm{col}\,(\mathbf{x}_1, ..., \mathbf{x}_i, ..., \mathbf{x}_N) \in \mathbb{R}^{4HN}$ collects the strategies of all the players. Each player can choose a strategy from its local feasible set defined as:

$$\Omega_{\mathbf{x}_i} = \left\{ \mathbf{x}_i \in \mathbb{R}^{4H}_{\geq 0} \,|\, \mathbf{c}_i \in \Omega_{\mathbf{c}_i}, \mathbf{g}_i \in \Omega_{\mathbf{g}_i}, \mathbf{s}_i \in \Omega_{\mathbf{s}_i} \right\}, \forall i \in \mathcal{N}. \tag{7.19}$$

Note that $\mathbf{x}$ must belong to the intersection of the local feasible set $\boldsymbol{\Omega} = \prod_{i=1}^{N} \boldsymbol{\Omega}_{\mathbf{x}_i}$.

As mentioned above, the net cost for the prosumers is based on the mismatch in (7.18). In particular, we assume that the net cost function of each independent active user equals the operating costs (degradation and generation) minus the monetary exchange with the DSO over the control horizon $\mathcal{H}$ as:

$$f_i\,(\mathbf{x}_i, \mathbf{x}_{-i}) = \eta_i \delta_g^{\top} \mathbf{x}_i + \zeta_i (\delta_s \circ \mathbf{x}_i)^{\top} (\delta_s \circ \mathbf{x}_i)$$

$$-\kappa_i\Big(\boldsymbol{\Delta}-\boldsymbol{\delta}^\top\mathbf{x}_{-i}-\delta^\top\mathbf{x}_i\Big)^\top\left(\delta^\top\mathbf{x}_i\right),\forall i\in\mathcal{N} \quad (7.20)$$

where we define the vectors $\delta_g = \text{col}(\mathbf{0}_H,\mathbf{1}_H,\mathbf{0}_H,\mathbf{0}_H)$, $\delta_s = \text{col}(\mathbf{0}_H,\mathbf{0}_H,\mathbf{1}_H,\mathbf{1}_H)$, $\delta=(I_H,-I_H,-I_H,I_H)^\top$ and $\boldsymbol{\delta}:=\mathbf{1}_{N-1}\otimes\delta$. Moreover, $\kappa_i\in\mathbb{R}_{>0}$ are pricing coefficients that rely on the different agreements between active players and the energy retailer. In the game, each player $i\in\mathcal{N}$ tries to minimize its cost function $f_i\left(\mathbf{x}_i,\mathbf{x}_{-i}\right):\mathbb{R}^{4H}\to\mathbb{R}$, by choosing a strategy in its local feasible set $\mathbf{x}_i\in\Omega_{\mathbf{x}_i}$. Note that we explicitly underline the dependence of the net cost function of the other players' strategies.

However, in our model, the interaction between the players occurs also at the feasible set level, since the power systems constraints must be respected. For each time slot $h\in\mathcal{H}$, the two power flow equations in (7.13) and (7.14) must be respected for each bus $b\in\mathcal{B}$. Hence, $L=2BH$ equality constraints must hold. In particular, we define the mapping $\varphi(\mathbf{x}):\mathbb{R}^{4HN}\to\mathbb{R}^L$ by collecting the L mappings $\varphi_l(\mathbf{x})$ that represent the constraints (7.13) and (7.14):

$$\varphi_l(\mathbf{x})=0,\quad \forall l=1,...,L. \quad (7.21)$$

Moreover, for each time slot $h\in\mathcal{H}$, the two power quality constraints in (7.15) and the two constraints (7.16) must be respected for each bus $b\in\mathcal{B}$ and for each line $(b,r)\in\mathcal{E}$, respectively. Hence, $M=2H(E+B)$ inequality constraints must hold. First, let us define the vector of power transfer between two buses $(b,r)\in\mathcal{E}$ over the control horizon as $\mathbf{P}_{br}:=(P_{br}(t),...,P_{br}(h),...,P_{br}(t+H-1))^\top\in\mathbb{R}^H$: this is dependent on the strategies of all active users in the grid and is computed by (7.17). Consequently, we define $\mathbf{P}_f(\mathbf{x})=\text{col}(\mathbf{P}_{11},...,\mathbf{P}_{br},...,\mathbf{P}_{BB})\in\mathbb{R}^{HB}$ as the vector collecting all power transfers in the network and we assume that the maximum transfer values are constant over time and are defined as $\mathbf{P}_f^{\max}=\text{col}(P_{11}^{\max}\mathbf{1}_H,..,P_{br}^{\max}\mathbf{1}_H,...,P_{BB}^{\max}\mathbf{1}_H)\in\mathbb{R}^{HB}$. Thus, the following relations must hold:

$$-\mathbf{P}_f(\mathbf{x})-\mathbf{P}_f^{\max}\le\mathbf{0}_{HB},\quad \mathbf{P}_f(\mathbf{x})-\mathbf{P}_f^{\max}\le\mathbf{0}_{HB}. \quad (7.22)$$

Similarly, let us denote the voltage magnitude for each bus $b\in\mathcal{B}$ over the control horizon as $\mathbf{V}_b:=(|V_1|(t),...,|V_b|(h),...,|V_B|(t+H-1))^\top\in\mathbb{R}^H$. Then, we define $\mathbf{V}_v(\mathbf{x})=\text{col}(\mathbf{V}_1,...,\mathbf{V}_b,...,\mathbf{V}_B)\in\mathbb{R}^{HE}$ as the vector collecting all the voltage magnitudes in the network and we assume that the maximum (minimum) voltage magnitude is constant over time and defined as $\mathbf{V}_v^{\max}=\text{col}(V_1^{\max}\mathbf{1}_H,..,V_b^{\max}\mathbf{1}_H,...,V_B^{\max}\mathbf{1}_H)\in\mathbb{R}^{HE}$ and $\mathbf{V}_v^{\min}=\text{col}(V_1^{\min}\mathbf{1}_H,..,V_b^{\min}\mathbf{1}_H,...,V_B^{\min}\mathbf{1}_H)\in\mathbb{R}^{HE}$. Thus, the following relations must hold:

$$-\mathbf{V}_v(\mathbf{x})+\mathbf{V}_v^{\min}\le\mathbf{0}_{HE},\quad \mathbf{V}_v(\mathbf{x})-\mathbf{V}_v^{\max}\le\mathbf{0}_{HE}. \quad (7.23)$$

We now define the mapping $\phi(\mathbf{x}):\mathbb{R}^{4HN}\to\mathbb{R}^M$ as $\phi(\mathbf{x})=\text{col}(-\mathbf{P}_f(\mathbf{x})-\mathbf{P}_f^{\max},\mathbf{P}_f(\mathbf{x})-\mathbf{P}_f^{\max},-\mathbf{V}_v(\mathbf{x})+\mathbf{V}_v^{\min},\mathbf{V}_v(\mathbf{x})-\mathbf{V}_v^{\max})\in\mathbb{R}^M$, i.e., by collecting the $M=2H(E+B)$ mappings $\phi_m(\mathbf{x})$ that represent the constraints (7.22) and (7.23):

$$\phi_m(\mathbf{x})\le 0,\quad \forall m=1,...,M. \quad (7.24)$$

Hence, we finally define the overall feasible set $\mathcal{X}$ as the coupling constraint set by:

$$\mathcal{X}=\boldsymbol{\Omega}\cap\left\{\mathbf{x}\in\mathbb{R}^{4HN}_{\ge 0}\mid (7.21),(7.24)\text{ hold}\right\} \quad (7.25)$$

Having introduced all the game elements, let us formalize the overall problem as a *generalized Nash equilibrium problem* (GNEP), whose solution is the *generalized Nash equilibrium* (GNE), defined as the set of the inter-dependent optimization problems as follows:

$$\min_{\mathbf{x}_i} f_i(\mathbf{x}_i,\mathbf{x}_{-i}),\quad \text{s.t. }(\mathbf{x}_i,\mathbf{x}_{-i})\in\mathcal{X},\ \forall i\in\mathcal{N}. \quad (7.26)$$

In the formulated problem (7.26) the feasible set $\mathcal{X}$ may be nonconvex and, in general, the coupling constraints are nonlinear. In this context, the existence of a GNE cannot be proven and, as for the optimal power flow problem, its seeking is challenging [25].

In order to overcome these issues, let us employ the novel concept of *Clarke's local generalized Nash equilibrium problem* (CL-GNEP) defined in Chapter 6 and let us search for its possible solutions, i.e., the *Clarke's local generalized Nash equilibrium* (CL-GNE). A CL-GNE is a collective strategy profile with the property that no single agent can benefit by unilaterally changing its strategy with another feasible one contained in Clarke's tangent cone.

In the related literature [26], JC games are usually solved by finding a solution to the associated *variational inequality problem* (VIP), since the resulting *variational generalized Nash equilibrium* (vGNE) not only exists but is also unique whenever the cost functions are strongly monotone [27]. By relaxing the convexity condition on the coupling feasible set $\mathcal{X}$, we can no longer rely on the existence and uniqueness of a vGNE. However, we can still consider the following *quasi-variational inequalities* (QVI) associated with the CL-GNEP, and thus employ the *variational Clarke's local generalized Nash equilibrium* (vCL-GNE) defined in Chapter 6. For a given vCL-GNE, we have that, in a in a local subset of $\mathcal{X}$, each user unilaterally maximizes its own function, while keeping the rivals' strategies fixed at the optimal value. Moreover, if at this point the common optimal multiplier associated with the individual constraints are the same for all the players $\boldsymbol{\lambda}^* = \boldsymbol{\lambda}_i$, $\forall i \in \mathcal{N}$, then the point is a vLGNE, and thus a locally "fair" equilibrium point [28].

7.5 Decentralized Convergence to Equilibrium

In this work, the goal is to reach an equilibrium which is nontrivial due to presence of the nonlinear and possibly nonconvex coupling constraints. Hence, let us propose an approach based on the coupling constraints reformulation and the CL-GNEP definition to find a possible equilibrium.

7.5.1 Coupling Constraints Reformulation

In our model, satisfying the power quality constraints requires the variation of the power injection in some buses. Hence, given a power injection profile for the overall network, the DSO must identify which bus injection causes the constraint violation and calculate the corresponding violation level. Moreover, we need to linearize the constraints to compute the linearized set of coupling constraints.

Therefore, let us employ the so-called sensitivity factors (SFs), i.e., the first order derivatives at the points corresponding to the Newton-Raphson solutions. Note that, for the sake of keeping the notation light, in this subsection we refer to the value of variables at time h avoiding indicating the time-dependency (h) in the corresponding symbols.

The SF for the voltage magnitude can be directly calculated from the inverse of the Jacobian matrix of the last Newton-Raphson iteration. More formally, for bus $b \in \mathcal{B}$, the voltage SF with respect to a power injection change in the generic bus $i \in \mathcal{B}$ is defined as $\partial|V|_b/\partial P_i$, then we arrange it in a compact form for all the control horizon as $\mathrm{SF}^v_{i,b} = (\partial|V|_b/\partial P_i(t), ..., \partial|V|_b/\partial P_i(h), ..., \partial|V|_b/\partial P_i(t+H-1))^\top \in \mathbb{R}^H$. Therefore, we define it for all the buses in the grid as $\mathbf{SF}^v_i := \mathrm{col}(\mathrm{SF}^v_{i,1}, ..., \mathrm{SF}^v_{i,b}, ..., \mathrm{SF}^v_{i,B}) \in \mathbb{R}^{BH}$.

The power transfer SF cannot be directly calculated. However, by differentiating (7.17), we calculate the power transfer SF with respect to phase angle and the voltage magnitude as follows:

$$\frac{\partial P_{br}}{\partial \theta_h} = \begin{cases} 0 & \text{if } h \neq r, h \neq b \\ |V_n||V_r||y_{br}|\sin(\theta_n - \theta_r - \theta_{br}) & \text{if } h = b \\ -|V_n||V_r||y_{br}|\sin(\theta_n - \theta_r - \theta_{br}) & \text{if } h = r \end{cases} \tag{7.27}$$

$$\frac{\partial P_{br}}{\partial |V_h|} = \begin{cases} 0 & \text{if } h \neq r, h \neq b \\ 2\,|V_n||y_{br}|\cos(\theta_{br}) & \\ \quad -|V_r||y_{br}|\cos(\theta_n - \theta_r - \theta_{br}) & \text{if } h = b \\ -|V_n||y_{br}|\cos(\theta_n - \theta_r - \theta_{br}) & \text{if } h = r. \end{cases} \tag{7.28}$$

Subsequently, we link the above calculated SFs to the power transfer SFs with respect to the active and reactive power injection at each bus by using the Jacobian matrix J [24]. More formally, for each branch between buses b and r, $(b,r) \in \mathcal{E}$ we get:

$$\begin{bmatrix} \partial P_{br}/\partial P_1 \\ \vdots \\ \partial P_{br}/\partial P_N \\ \partial P_{br}/\partial Q_1 \\ \vdots \\ \partial P_{br}/\partial Q_N \end{bmatrix} = (J^\top)^{-1} \begin{bmatrix} \partial P_{br}/\partial \theta_1 \\ \vdots \\ \partial P_{br}/\partial \theta_N \\ \partial P_{br}/\partial |V_1| \\ \vdots \\ \partial P_{br}/\partial |V_N| \end{bmatrix}, \forall (b,r) \in \mathcal{E} \tag{7.29}$$

Hence, let us define the power transfer variation in branch $(b,r) \in \mathcal{E}$ for a power injection in bus $i \in \mathcal{B}$ as $\partial P_{br}/\partial P_i$ and let us collects these for all the control horizon as $\mathrm{SF}^f_{i,br} := (\partial P_{br}/\partial P_i(t), ..., \partial P_{br}/\partial P_i(h), ..., \partial P_{br}/\partial P_i(t+H-1))^\top \in \mathbb{R}^H$ and for all branches as $\mathbf{SF}^f_i := \mathrm{col}(\mathrm{SF}^f_{i,11}, ..., \mathrm{SF}^f_{i,br}, ..., \mathrm{SF}^f_{i,BB}) \in \mathbb{R}^{EH}$.

Finally, we define the linearized coupling constraints in a point $\mathbf{y}$, with respect to the variation of the strategy of user i, as:

$$\tilde{\phi}_{\mathbf{y}}(\mathbf{x}_i, \mathbf{y}_{-i}) = \phi(\mathbf{y}) + \left(\boldsymbol{\delta}_g^\top (\mathbf{x}_i - \mathbf{y}_i)\right) \circ \mathbf{SF}_i(\mathbf{y}) \tag{7.30}$$

where $\boldsymbol{\delta}_g := (I_{BE} \otimes \delta^\top)^\top$ is an auxiliary matrix and $\mathbf{SF}_i := \mathrm{col}(\mathbf{SF}^f_i, -\mathbf{SF}^f_i, \mathbf{SF}^v_i, -\mathbf{SF}^v_i) \in \mathbb{R}^M$.

7.5.2 Decentralized Control Algorithm

Let us now present a decentralized control architecture to reach an equilibrium: each agent computes its control action, while a central coordinator attempts to satisfy the shared constraints possibly forcing the agents' strategies. It should be noted that in this approach only a limited information exchange occurs between agents; in particular, when the shared constraints are satisfied without the intervention of the central coordinator, this approach becomes distributed.

Several decentralized penalty approaches have been proposed to solve the GNEP leveraging on the definition of a *penalized Nash equilibrium problem* (PNEP) of the original problem. Therefore, let us propose an algorithm based on the penalized reformulation of the original generalized game. The core idea of the proposed control algorithm is to solve at each step a penalized problem defined employing the coupling constraint reformulation around the current solution. In particular, by modifying the approach in [29] substituting the original constraints with their corresponding linear reformulation, we can rewrite the CL-GNEP as a penalized game:

$$\mathrm{P}(\mathbf{y}, \boldsymbol{\rho}_i) = \underset{\mathbf{x}_i \in \boldsymbol{\Omega}_{\mathbf{x}_i}}{\operatorname{argmin}} \; f_i(\mathbf{x}_i, \mathbf{x}_{-i}) + \boldsymbol{\rho}_i^\top \left| \tilde{\phi}_{\mathbf{y}}(\mathbf{x}_i, \mathbf{y}_{-i}) \right|_+ \tag{7.31}$$

where $|\cdot|_+$ is the projection onto the positive orthant and $\boldsymbol{\rho}_i = \mathrm{col}(\rho_{i,1}, ..., \rho_{i,M}, ..., \rho_{i,M}) \in \mathbb{R}^M_{\geq 0}$ is the vector collecting the penalizing factors for the player $i \in \mathcal{N}$. Note that the reformulated problem $\mathrm{P}(\mathbf{y}, \boldsymbol{\rho}_i)$ is a convex NEP and thus a solution always exists and is unique. Moreover, for sufficiently large and finite penalizing factors $\boldsymbol{\rho}_i$, all players will be forced to satisfy the constraints until a feasible point is reached. However, the correct value of the penalty parameters is not known in advance and therefore a strategy must be selected that allows to update the values of the penalty parameters so that eventually the correct values are reached. In order to reach a vCL-GNEP the penalizing factors associated with an individual constraint should be the same for all the players, thus we assume an equal update rule for all the players.

We now propose the novel decentralized procedure to reach a vCL-GNEP formally defined in Algorithm 1. In the first phase, players initialize their starting strategies $\mathbf{x}^0$ and the coordinator defines the initial penalty factors $\boldsymbol{\rho}^0$. The proposed algorithm works

Algorithm 7.1 Decentralized Convergence to vCL-GNEP

Inputs: γ, $\mathbf{x}^0$, $\boldsymbol{\rho}^0$

1: $k = 0$
2: **while** A termination criterion is reached **do**
3: Coordinator computes $\mathbf{SF}_b(\mathbf{x}^k)$, $\forall b \in \mathcal{B}$
4: Coordinator broadcasts $\boldsymbol{\rho}^k$ and $\mathbf{SF}_b(\mathbf{x}^k)$
5: **for** $i = 1, ..., N$ **do**
6: User i computes $\mathbf{x}_i^{k+1} = \gamma \mathrm{P}(\mathbf{x}^k, \boldsymbol{\rho}^k) + (1-\gamma)\mathbf{x}_i^k$
7: User i sends $\mathbf{x}_i^{k+1}$ back to Coordinator
8: **end for**
9: Coordinator solves the power flow eqs. (7.13)-(7.14)
10: Coordinator computes $\phi(\mathbf{x}^{k+1})$
11: **for** $m = 1, ..., M$ **do**
12: **if** $\phi_m(\mathbf{x}^{k+1}) \leq 0$ **then**
13: Coordinator updates $\rho_m^{k+1} = \rho_m^k$
14: **else**
15: Coordinator updates $\rho_m^{k+1} = \rho_m^k + \Delta_\rho$
16: **end if**
17: **end for**
18: $k = k + 1$
19: **end while**

Outputs: $\mathbf{x}^*$

iteratively (lines 1-2, 18-19). At each iteration, given the overall players' strategies, the coordinator computes the sensitivity factor to connect the overall outage to a specific bus power injection for the prediction horizon (line 3). Then, the coordinator broadcasts the penalty factors and the sensitivity factors to all active players. Note that the coordinator computes the sensitivity factor for each bus of the grid $b \in \mathcal{B}$; however, it broadcasts to the generic active user $i \in \mathcal{N}$ only the factors related to its position (line 4).

After this phase, each player updates its strategy based on its previous step by solving the penalized problem (7.31) defined with the coupling constraints linearized around the current solution $\mathbf{x}^k$. However, the next strategy is selected employing a standard regularization approach with coefficient γ, in order to improve convergence (lines 5-6).

Moreover, the coordinator collects all the computed strategies (line 7) and solves the power flow for all the time steps of the prediction horizon (line 9). Then it evaluates each constraint (line 10), and checks if it is satisfied. When a constraint is not satisfied, the coordinator updates the respective penalty factor by a fixed value Δ_ρ (lines 11-17).

Finally, the coordinator terminates the iterative process when an adequate termination criterion is reached.

Remark 7.5.1

It should be noted that, due to the decentralized scheme of Algorithm 1, any untruthful report or behavior of a player may lead to a higher individual outcome. Consequently, as usually done in related works, let us assume the presence of a surveillance mechanism that acts to prevent such an issue [30], [31]. □

Remark 7.5.2

Note that in Algorithm 1 (lines 10-17) we do not consider (7.13) *and* (7.14) *that defining the feasible set $\mathcal{X}$. In fact, we assume that any solution computed with the Newton-Raphson approach (line 9) –that is feasible for* (7.22) *and* (7.23)*– is also feasible for* (7.13) *and* (7.14)*.* □

We finally note that the vCL-GNEPs are quasi-variational equilibria that –differently from the well-known variational equilibrium in jointly convex games– may not be unique. In fact, starting from different initial players' strategies, a different equilibrium may be

reached. Nevertheless, as commonly done in the AC OPF, we initialize all the strategies to a standard value; hence, all players begin from the same situation. In this way, we guarantee to always reach the same quasi-variational equilibrium for the same scenario.

7.6 Case Study

In this section we show the performance of the proposed algorithm through several numerical experiments, by analyzing distribution systems under a high power flow variation due to a large penetration of distributed generation and active users. In particular, we refer to two standard test bus system widely used by researchers as a benchmark for evaluating the performance of control solutions proposed in the power systems field: the IEEE 33-bus system [32] composed of 33 buses, which are connected through 37 branches in accordance with the radial topology typically employed in power distribution networks, and the IEEE 118-bus system [33], which includes 118 buses and 177 lines and has a meshed structure with several radial branches.

In the Newton Raphson-method, we use the so-called flat start [34] as a starting point for the unknown variables, i.e., all the angle phases are equal to zero, and all the voltage magnitudes are set to 1 in p.u. system. Note that this is extremely important for a fast power flow convergence and, therefore, for the overall algorithm's performance.

We consider a control horizon of 24 hours and we assume for the PQ buses $b \neq 1$ (i.e., in all buses except the slack bus $b = 1$) a net power profile randomly generated with an average active and reactive power equal to 0.15 MW and 0.5 MVAr, respectively. The controllable loads have a randomly generated profile with an average active power equal to 0.02 MW. All data are updated at each time step to simulate the variability of their values in a rolling horizon framework. For the sake of simplicity, we assume that the minimum and maximum voltage magnitudes (i.e., $V_b^{\min}$ and $V_b^{\max}$) at each bus are 0.95 and 1.05 p.u., respectively. Moreover, the maximum power transfer of each line (i.e., $P_{br}^{\max}$) is set equal to 200% of the average power transfer in the merely passive case (i.e., Scenario 1 described in the sequel).

For the sake of simplicity, we assume that the energy price coefficients of active users κ_i are all equal to 0.1. Each active user owns a lithium-ion battery and a small diesel generator. The values of ESS parameters are defined as follows: leakage rate $\alpha_i = 0.90$, charging and discharging inefficiencies $\beta_{c,i} = 0.99$ and $\beta_{d,i} = 1.01$, battery capacity $\mathrm{SoC}_i^{\max} = 0.3\mathrm{MW}$, maximum charging rate $s_i^{\max} = 0.25\mathrm{SoC}_i^{\max}$, and initial charge $\mathrm{SoC}(0) = 0.25\mathrm{SoC}_i^{\max}$. Moreover, the maximum hourly dispatchable generation is $g_i^{\max} = 0.1\mathrm{MWh}$ while $\eta_i = 0.4$. Computations for all users are done in parallel. The step coefficient for Algorithm 1 is $\gamma = 0.3$.

To assess the proposed framework, we perform several experiments both on the IEEE-33 and IEEE-118 bus systems addressing the three scenarios defined as follows:

- Scenario 1. The distribution system comprehends only non-controllable loads, without distributed renewable generation and active users.
- Scenario 2. The system comprises non-controllable loads and RESs as well as noncooperative active users, even though the latter neglects the coupling constraints on the maximum power transfer and voltage magnitude (i.e., users play a traditional Nash game rather than a generalized one).
- Scenario 3. The system comprises all the elements as in the previous case; in addition, active users address the power quality coupling constraints.

As for the first set of experiments, we employ the IEEE-33 bus system with seven active users, namely in buses 2, 3, 6, 19, 13, 14, and 15. In Fig. 7.1, we show a colormap graph representing the network state in a time step computed with the Newton-Raphson method. In particular, for each line the percentage loading level normalized with respect to the maximum value by employing different colors and line weights, i.e., hot colors indicate congestion in the line.

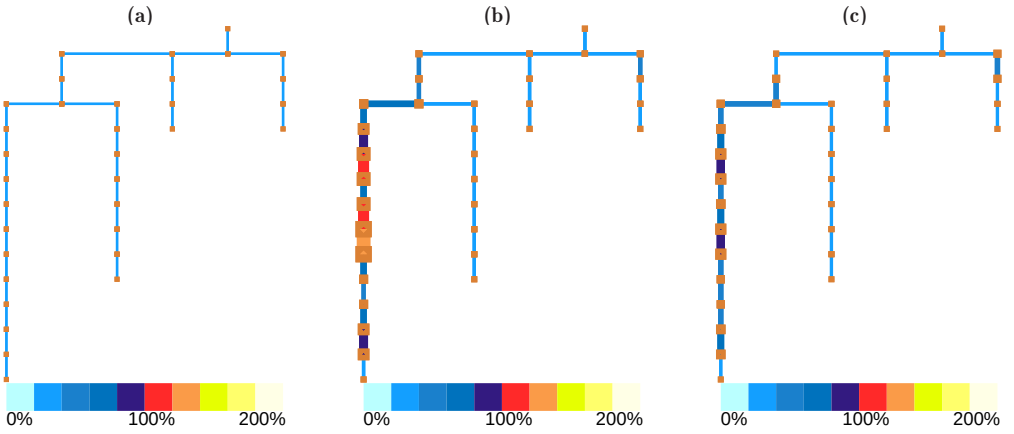

Figure 7.1: Percentage loading level normalized with respect to the maximum value over all the distribution lines in the IEEE bus-system - Scenario 1: loads only (a); Scenario 2: loads, RESs, and active users without coupling constraints (b); Scenario 3: loads, RESs, and active users subject to coupling constraints (c).

In the first scenario, presented in Fig. 7.1(a), it is evident that the grid is merely a passive system; therefore, this case represents the current state of traditional distribution systems around the world. Note that the power flow constraints are satisfied in a passive way because the capacity of the distribution system was correctly sized in the design phase, suitably taking into account the power demand on each bus.

In Fig. 7.1(b) we show the results related to Scenario 2, where the system comprehends the same non-controllable loads profile in addition to several unpredictable RESs. Additionally, active users participate in the grid optimization to increase their profit. In particular, the active users modify their own strategies without any power flow restriction, i.e., active users' strategies are coupled only via the cost function. As a consequence, in such a scenario, the increased power production, together with lower power demand and the uncoordinated active users participation, may cause a high instability in the grid (represented by all the hot colors) causing an outage in the grid.

In order to show the effectiveness of our algorithm, in Fig. 7.1(c) we show the results related to Scenario 3: the distribution system is equipped with loads, RESs, and active users but the proposed noncooperative coordination scheme is applied. The algorithm is able to steer active users' strategies to a global equilibrium while satisfying the power flow constraints.

Moreover, we show the convergence properties of the proposed algorithm for Scenarios 2 and 3. In particular, we reduce the maximum allowable power transfer for all the branches linked with active users to 80% of the power transfer in the passive case (i.e., Scenario 1). We remark that, even though this setup may correspond to unrealistic data, it allows testing the proposed approach under extremely severe conditions, which could make also the passive scenario without active users infeasible. In particular, in Fig. 7.2 we show the convergence of the overall power exchange of each player with the main grid. Since the players have the same characteristic coefficients and initial conditions, it is evident that in Scenario 2, shown in Fig. 7.2(a), the only possible equilibrium corresponds to bringing all players to have the same strategy. Conversely, in Scenario 3, convergence is reached with different strategies as shown in Fig. 7.2(b). This is caused by the different displacements of active users in the distribution grid and therefore of their impact on the power quality constraints. In fact, we notably reduced the maximum admissible power transfer by forcing the active users responsible for the power outages to work against the market to satisfy the constraints.

As for the second set of experiments, we consider the IEEE-118 bus system including 30 active users randomly displaced in the power grid. First, in Fig. 7.3 we show the mismatch between the active power injected into the slack bus and the reference value

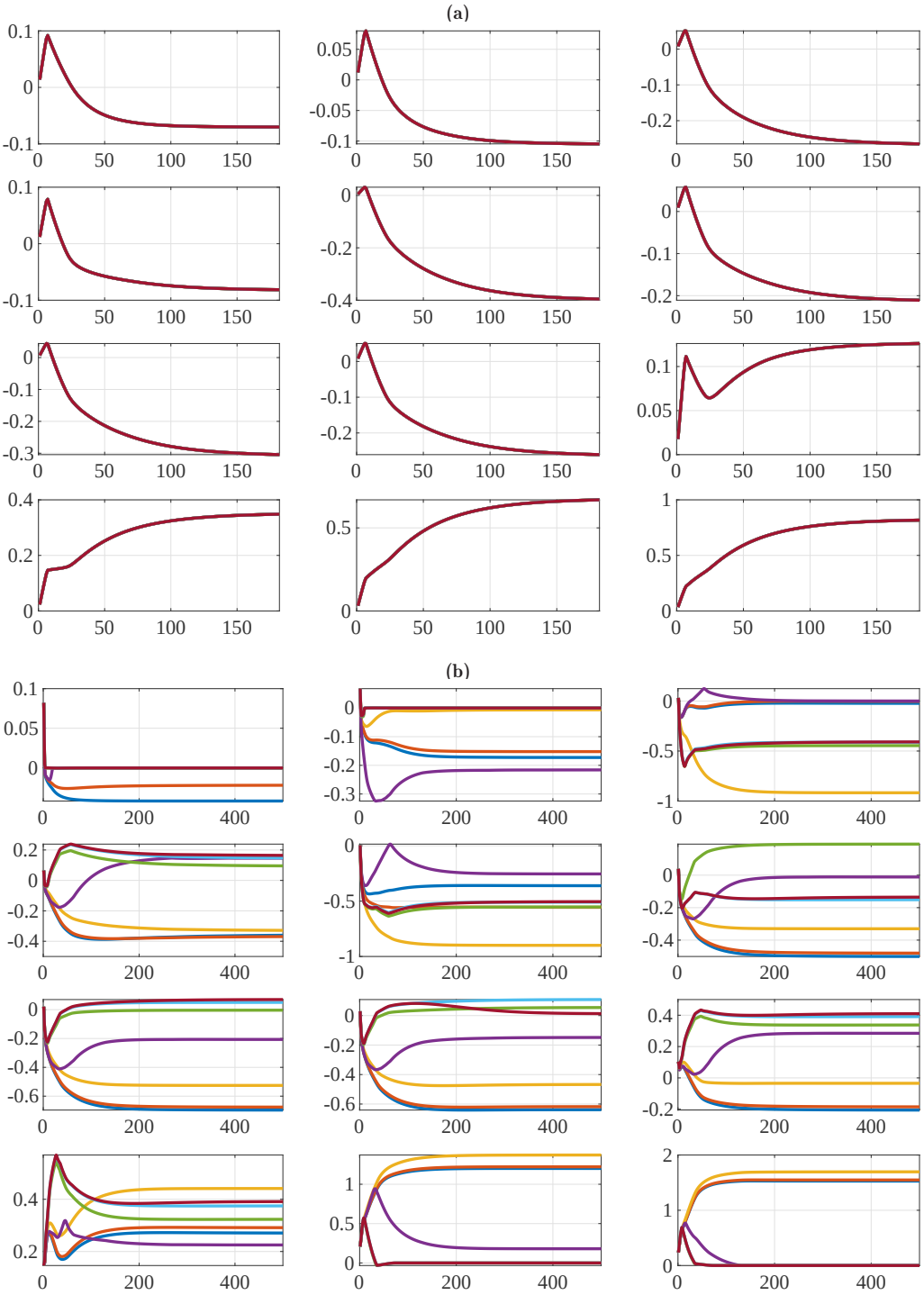

Figure 7.2: Convergence of Algorithm 1: Scenario 2 (a) and Scenario 3 (b).

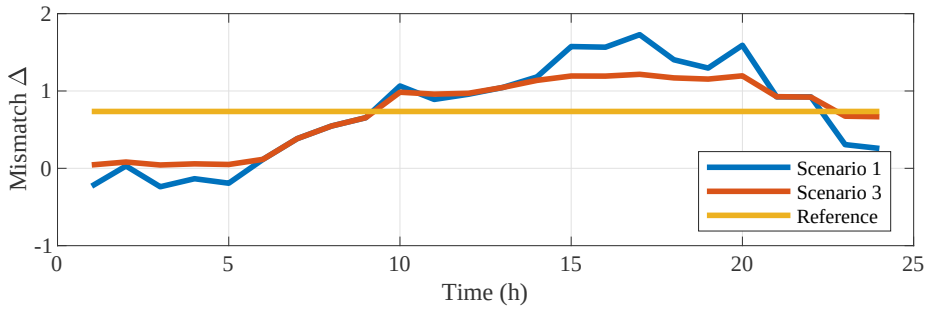

Figure 7.3: Mismatch between the active power injected into the slack bus of the IEEE-118 bus system and the reference value.

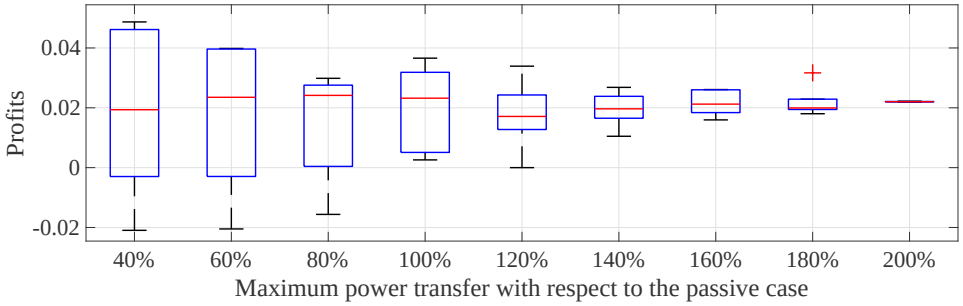

Figure 7.4: Boxplot of the players' net costs with different maximum power transfer.

over the time window, in the case the proposed approach is deployed (Scenario 3) or not (Scenario 1). From Fig. 7.3 it is evident that the injected power profile is flatter in Scenario 3 than in Scenario 1, thus proving that the proposed framework increases the predictability and the power stability.

Lastly, we analyze the impact of the coupling constraints on the payoff functions of the different players. In fact, if the power quality constraints are tight, the prosumers in the grid may be forced to work against the market. For instance, in a situation where it is profitable to charge a battery, a prosumer may be forced instead to discharge it in order to satisfy the constraints. In this experiment, we aim at exacerbating this situation by extremely varying the maximum power transfer. In particular, we modify the maximum power transfer of each line from 40% up to 200% of the average power transfer in the passive case (i.e., Scenario 1), and then computing the players' net cost. The results are shown in Fig. 7.4, where it is clear that in the case of a lower maximum power transfer the net cost spread over the users is very large, while when the maximum power transfer increases the net cost tends to be equal for all users. It should be noted that, as the active players are equipped with equal resources, in the case of no power quality constraints, the net costs should be equal; conversely, if the power quality constraints are included, the users net costs are different due to their diverse displacement in the power grid.

7.7 Conclusion

In this chapter we employ a novel game-theoretic control mechanism for optimally regulating the operation of power distribution networks including active users with demand flexibility, dispatchable generation capability, and/or energy storage potential. Differently from the existing literature, this work investigates a decentralized model aimed at efficiently enhancing the penetration of distributed generation in medium voltage networks, as well as the predictability of the power injection from the transmission grid, while fulfilling the power system physical constraints. In addition, the conducted numerical experiments show that the proposed optimal control of active users is effective in increasing the predictability and power stability of the distribution networks. Future

research will addres: demonstrating the optimality and the convergence properties of the proposed algorithm, and extending the proposed approach to different control goals (e.g., by replacing the cost functions with terms that take the reactive power mismatch into account) and different power flow models possibly including power losses. Moreover, it should be noted that the proposed framework can be modified to directly take into account uncertainty.

References

[1] Fang, X., Misra, S., Xue, G., and Yang, D., "Smart grid — the new and improved power grid: A survey," *IEEE Commun. Surveys Tuts.*, vol. 14, no. 4, pp. 944–980, 2011.

[2] Hosseini, S. M., Carli, R., and Dotoli, M., "Robust optimal energy management of a residential microgrid under uncertainties on demand and renewable power generation," *IEEE Trans. Autom. Sci. Eng.*, vol. 18, no. 2, pp. 618–637, 2021.

[3] Bahrami, S., Amini, M. H., Shafie-Khah, M., and Catalao, J. P., "A decentralized renewable generation management and demand response in power distribution networks," *IEEE Trans. Sustain. Energy*, vol. 9, no. 4, pp. 1783–1797, 2018.

[4] Saad, W., Han, Z., Poor, H. V., and Basar, T., "Game-theoretic methods for the smart grid: An overview of microgrid systems, demand-side management, and smart grid communications," *IEEE Signal Process. Mag.*, vol. 29, no. 5, pp. 86–105, 2012.

[5] Yao, M., Molzahn, D. K., and Mathieu, J. L., "An optimal power-flow approach to improve power system voltage stability using demand response," *IEEE Trans. Control of Netw. Syst.*, vol. 6, no. 3, pp. 1015–1025, 2019.

[6] Magnússon, S., Weeraddana, P. C., and Fischione, C., "A distributed approach for the optimal power-flow problem based on admm and sequential convex approximations," *IEEE Trans. Control of Netw. Syst.*, vol. 2, no. 3, pp. 238–253, 2015.

[7] Hübner, N., Rink, Y., Suriyah, M., and Leibfried, T., "Distributed ac-dc optimal power flow in the european transmission grid with admm," *arXiv preprint arXiv:1912.03942*, 2019.

[8] Kargarian, A., Mohammadi, J., Guo, J., *et al.*, "Toward distributed/decentralized dc optimal power flow implementation in future electric power systems," *IEEE Trans. Smart Grid*, vol. 9, no. 4, pp. 2574–2594, 2016.

[9] Yang, L., Luo, J., Xu, Y., Zhang, Z., and Dong, Z., "A distributed dual consensus admm based on partition for dc-dopf with carbon emission trading," *IEEE Trans. Ind. Informat.*, 2019.

[10] Hupez, M., Toubeau, J.-F., De Grève, Z., and Vallée, F., "A new cooperative framework for a fair and cost-optimal allocation of resources within a low voltage electricity community," *IEEE Transactions on Smart Grid*, vol. 12, no. 3, pp. 2201–2211, 2020.

[11] Börgens, E. and Kanzow, C., "A distributed regularized Jacobi-type ADMM-method for generalized Nash equilibrium problems in Hilbert spaces," *Numerical Functional Analysis and Optimization*, vol. 39, no. 12, pp. 1316–1349, 2018.

[12] Atzeni, I., Ordóñez, L. G., Scutari, G., Palomar, D. P., and Fonollosa, J. R., "Demand-side management via distributed energy generation and storage optimization," *IEEE Trans. Smart Grid*, vol. 4, no. 2, pp. 866–876, 2012.

[13] Zhu, Q., Zhang, J., Sauer, P., Dominguez-Garcia, A., and Basar, T., "A game-theoretic framework for distributed generation of renewable energies in smart grids," in *Amer. Control Conf. (ACC)*, 2012, pp. 3623–3628.

[14] Chen, J. and Zhu, Q., "A game-theoretic framework for resilient and distributed generation control of renewable energies in microgrids," *IEEE Trans. Smart Grid*, vol. 8, no. 1, pp. 285–295, 2016.

[15] Carli, R., Dotoli, M., and Palmisano, V., "A distributed control approach based on game theory for the optimal energy scheduling of a residential microgrid with shared generation and storage," in *15th Int. Conf. on Automation Science and Engineering (CASE)*, IEEE, 2019, pp. 960–965.

[16] Scarabaggio, P., Carli, R., and Dotoli, M., "A game-theoretic control approach for the optimal energy storage under power flow constraints in distribution networks," in *2020 IEEE 16th International Conference on Automation Science and Engineering (CASE)*, 2020, pp. 1281–1286. DOI: 10.1109/CASE48305.2020.9216800.

[17] Kisacikoglu, M. C., Kesler, M., and Tolbert, L. M., "Single-phase on-board bidirectional pev charger for v2g reactive power operation," *IEEE Trans. Smart Grid*, vol. 6, no. 2, pp. 767–775, 2014.

[18] Tan, X., Qu, G., Sun, B., Li, N., and Tsang, D. H., "Optimal scheduling of battery charging station serving electric vehicles based on battery swapping," *IEEE Transactions on Smart Grid*, vol. 10, no. 2, pp. 1372–1384, 2017.

[19] Garces, A., "Uniqueness of the power flow solutions in low voltage direct current grids," *Electric Power Systems Research*, vol. 151, pp. 149–153, 2017.

[20] Adhikari, S., Li, F., and Li, H., "Pq and pv control of photovoltaic generators in distribution systems," *IEEE Transactions on Smart Grid*, vol. 6, no. 6, pp. 2929–2941, 2015.

[21] Jha, B. K., Kumar, A., Dheer, D. K., Singh, D., and Misra, R. K., "A modified current injection load flow method under different load model of ev for distribution system," *International Transactions on Electrical Energy Systems*, vol. 30, no. 4, e12284, 2020.

[22] Adepoju, G. and Komolafe, O., "Analysis and modelling of static synchronous compensator (statcom): A comparison of power injection and current injection models in power flow study," *International Journal of Advanced Science and Technology*, vol. 36, no. 2, pp. 65–76, 2011.

[23] Hwang, P.-I., Moon, S.-I., and Ahn, S.-J., "A vector-controlled distributed generator model for a power flow based on a three-phase current injection method," *Energies*, vol. 6, no. 8, pp. 4269–4287, 2013.

[24] Maskar, M. B., Thorat, A., and Korachgaon, I., "A review on optimal power flow problem and solution methodologies," in *Int. Conf. on Data Management, Analytics and Innovation (ICDMAI)*, IEEE, 2017, pp. 64–70.

[25] Bukhsh, W. A., Grothey, A., McKinnon, K. I., and Trodden, P. A., "Local solutions of the optimal power flow problem," *IEEE Trans.Power Syst.*, vol. 28, no. 4, pp. 4780–4788, 2013.

[26] Franci, B. and Grammatico, S., "Stochastic generalized Nash equilibrium seeking in merely monotone games," *IEEE Transactions on Automatic Control*, pp. 1–1, 2021. DOI: 10.1109/TAC.2021.3108496.

[27] Rosen, J. B., "Existence and uniqueness of equilibrium points for concave n-person games," *Econometrica: Journal of the Econometric Society*, pp. 520–534, 1965.

[28] Belgioioso, G. and Grammatico, S., "Semi-decentralized generalized Nash equilibrium seeking in monotone aggregative games," *IEEE Transactions on Automatic Control*, 2021.

[29] Fukushima, M., "Restricted generalized nash equilibria and controlled penalty algorithm," *Computational Management Science*, vol. 8, no. 3, pp. 201–218, 2011.

[30] MacKenzie, A. B. and Wicker, S. B., "Game theory in communications: Motivation, explanation, and application to power control," in *GLOBECOM'01. IEEE Global Telecommunications Conference (Cat. No. 01CH37270)*, IEEE, vol. 2, 2001, pp. 821–826.

[31] Ghorbanian, M., Dolatabadi, S. H., and Siano, P., "Game theory-based energy-management method considering autonomous demand response and distributed generation interactions in smart distribution systems," *IEEE Systems Journal*, vol. 15, no. 1, pp. 905–914, 2020.

[32] Baran, M. E. and Wu, F. F., "Network reconfiguration in distribution systems for loss reduction and load balancing," *IEEE Power Eng. Rev.*, vol. 9, no. 4, pp. 101–102, 1989.

[33] Pena, I., Martinez-Anido, C. B., and Hodge, B.-M., "An extended ieee 118-bus test system with high renewable penetration," *IEEE Transactions on Power Systems*, vol. 33, no. 1, pp. 281–289, 2017.

[34] Vinkovic, A. and Mihalic, R., "A current-based model of an ipfc for newton–raphson power flow," *Electric Power Systems Research*, vol. 79, no. 8, pp. 1247–1254, 2009.

Chapter 8

Conclusions

Energy systems are increasingly complicated by the proliferation of clean energy technologies such as solar, wind, storage and electric vehicles. Therefore, future energy systems will require secure, autonomous, and reliable communications, control, and interoperability among millions of distributed generation points and billions of buildings, vehicles, and more. To enable effective control of these distributed devices and extensive metering, the concept of *autonomous power grids* (APGs) has been developed and several key challenges have been identified in this area.

In this thesis, two main research directions related to the implementation of game-theoretic control approaches for APGs have been presented.

In the first part we describe a series of control techniques aimed at reducing the gap between the variable distributed generation and the adjustable load demand. On the one hand, we provide several novel game-theoretical control schemes to coordinate multiple autonomous entities with adjustable load demand; on the other hand, we provide a set of new methodologies to specifically deal with the uncertain nature of renewable energy sources. The specific contributions of each chapter are reported hereafter.

- The decentralized and distributed control frameworks presented in Chapter 2 allow the autonomous trade of energy between independent entities in large-scale autonomous grids while keeping a high level of privacy. Numerical simulations show that the designed architectures are extremely scalable reducing the computational effort with respect to a traditional centralized approach.
- The noncooperative energy market for electric vehicles presented in Chapter 3 is able to increase the predictability of the aggregate load from the distribution grid point of view while minimizing the degradation wearing costs of batteries.
- The stochastic model predictive control approach presented in Chapter 4 can effectively determine the robust cost-optimal energy scheduling of a grid-connected smart energy system with the goal of reducing costs or increasing the penetration of renewable energy.
- The game-theoretic energy scheduling approach presented in Chapter 5 can be used in the control of large-scale autonomous power grids to increase the share of highly uncertain renewable energy sources. The approach copes with the uncertain generation by boosting the flexibility of the grid through a game-theoretic demand side management scheme and a stochastic programming technique.

The research problems presented in the first part of this thesis have left open problems and paved the way for novel research directions.

- The main limitation of the presented control frameworks is the absence of strategies to include modeling errors and non-idealities (e.g., latency, faults, etc.).
- Future work should also focus on including other devices, such as different kinds of controllable loads or individually owned energy sources, and integrating additional objective functions of autonomous players (e.g., wider sustainability payoffs beyond economic benefits) and technical constraints affecting the operations of system components.

In the second part of the thesis we further focus on coordinating selfish entities under game-theoretical control frameworks in autonomous power grids. In particular, besides the usual economic aspects, we include the quality and physical constraints of power

distribution (e.g., the well-known power flow equations) coupling the actions of these autonomous agents. These constraints are typically nonconvex, and thus neglected in the related literature due to the absence of adequate mathematical tools. To cope this gap, we provide an innovative mathematical theory for multi-agent systems with nonconvex coupling constraints and we apply it to the control of autonomous power grids. The two specific contributions are described hereafter.

- In Chapter 6, we address the problem of solving a class of games with nonconvex coupling constraints. We define a local equilibrium concept presenting the conditions for optimality, existence and local uniqueness. Our technical contributions allow us, under certain conditions, to define two iterative schemes with global convergence guarantee toward this novel equilibrium concept.
- The approach in Chapter 7 is the first to our knowledge to propose a novel game-theoretic control mechanism for optimally regulating the operation of power distribution networks including active users with demand flexibility, dispatchable generation capability, and/or energy storage potential, while fulfilling the power system physical and quality constraints.

The research problems presented in the second part of this thesis have left open problems and paved the way for novel research directions.

- The main open problem of the proposed control theory is proposing fully distributed algorithms to steer the strategies of agents in a distributed fashion.
- Future research will also address extending the proposed approach to different control goals and different power flow models, possibly including power losses or addressing stochasticity in constraints and cost functions.

Appendices

Appendix A

Preliminaries

The goal of this section is to give a brief overview on the theoretical preliminaries required by this thesis and, specifically, about game theory concepts and tools.

A.1 Convexity

We begin recalling a few fundamental definitions related to convexity.

A.1.1 Convex Sets

Let S be a vector space or an affine space over the real numbers. This includes Euclidean spaces, which are affine spaces. A subset K of S is *convex* if, for all $\mathbf{x}$ and $\mathbf{y}$ in K, the line segment connecting $\mathbf{x}$ and $\mathbf{y}$ is included in K. More formally, a set $K \subset \mathbb{R}^n$ is convex if for any two points $\mathbf{x}, \mathbf{y} \in K$ if:

$$\alpha\mathbf{x} + (1-\alpha)\mathbf{y} \in K, \quad \forall \mathbf{x}, \mathbf{y} \text{ and } \alpha \in [0,1] \tag{A.1}$$

This implies that convexity (the property of being convex) is invariant under affine transformations. This implies also that a convex set in a real or complex topological vector space is path-connected, thus connected. We recall that the intersection of convex sets is a convex set (while the union of convex sets is not, in general).

A set K is *strictly convex* if every point on the line segment connecting $\mathbf{x}$ and $\mathbf{y}$ other than the endpoints is inside the interior of K. More formally, a set $K \subset \mathbb{R}^n$ is strictly convex if for any two points $\mathbf{x}, \mathbf{y} \in K$, such that $\mathbf{x} \neq \mathbf{y}$, if:

$$\alpha\mathbf{x} + (1-\alpha)\mathbf{y} \in K, \quad \forall \mathbf{x}, \mathbf{y}, \mathbf{x} \neq \mathbf{y} \text{ and } \alpha \in (0,1) \tag{A.2}$$

A.1.2 Convex Functions

Let us consider a convex set $K \subset \mathbb{R}^n$ and a function $f(\mathbf{x}) : K \to \mathbb{R}$. The function f is

- *convex* on K if, $\forall \mathbf{x}, \mathbf{y} \in K$ and $\alpha \in (0,1)$,

$$f(\alpha\mathbf{x} + (1-\alpha)\mathbf{y}) \leq \alpha f(\mathbf{x}) + (1-\alpha) f(\mathbf{y}) \tag{A.3}$$

- *strictly convex* on K if the previous inequality is strict
- *strongly convex* on K if, $\forall \mathbf{x}, \mathbf{y} \in K$ and $\alpha \in (0,1)$ it exists a constant $c > 0$ such that

$$f(\alpha\mathbf{x} + (1-\alpha)\mathbf{y}) \leq \alpha f(\mathbf{x}) + (1-\alpha) f(\mathbf{y}) - \frac{c}{2}\alpha(1-\alpha)\left\|\mathbf{x}-\mathbf{y}\right\|^2 \tag{A.4}$$

Hence, the following holds

$$\text{strong convexity} \implies \text{strict convexity} \implies \text{convexity} \tag{A.5}$$

while the reversed implications are, in general, not true.

The function f is said to be concave (resp. strictly concave if $-f$ (f multiplied by -1) is convex (resp. strictly convex).

Convexity can also be interpreted geometrically. Consider the function in Fig. A.1(a) and the segment $\mathcal{S}$ joining the points $(x, f(x))$ and $(y, f(y))$. Saying that f is convex means that the graph of f doesn't lie above the segment $\mathcal{S}$. Strict convexity means that

the graph of f lies below the segment $\mathcal{S}$, as in Figure A.1(b), while strong convexity requires the function f to lie sufficiently below the segment $\mathcal{S}$, as in Fig. A.1(c). Many operations on functions preserve convexity, e.g. summing convex functions, multiplying them by a non-negative scalar and taking their point-wise maximum gives rise to convex functions. Other composition rules that preserve the convexity can be found in [1], [2].

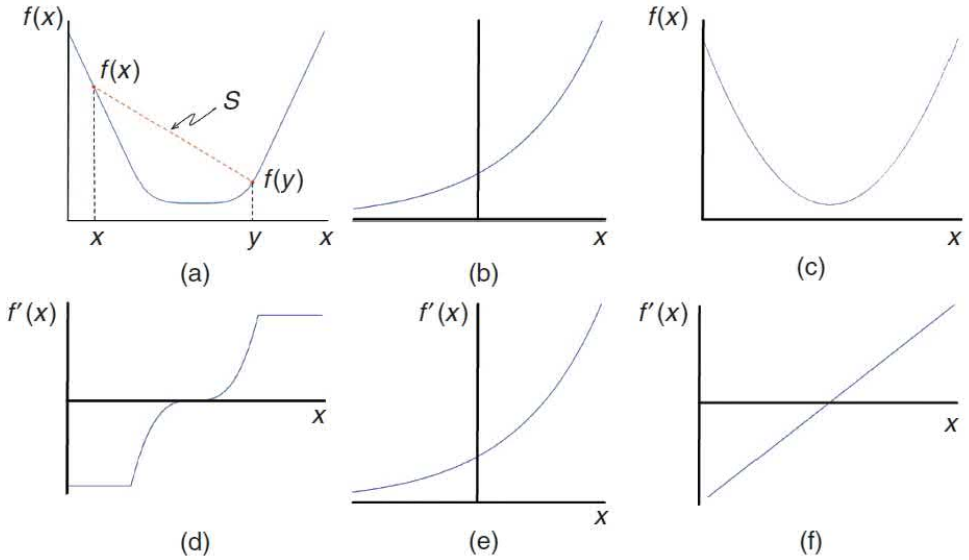

Figure A.1: Examples of convex and monotone functions: (a) convex function; (b) strictly convex function; (c) strongly convex function; (d) monotone function; (e) strictly monotone function; (f) strongly monotone function. (Source [3])

A.1.3 Convex Optimization

Convex optimization is a subfield of mathematical optimization that studies the problem of minimizing convex functions over convex sets (or, equivalently, maximizing concave functions over convex sets). A convex optimization problem is the problem of finding some $\mathbf{x}^* \in K$ attaining: $\inf\{f(\mathbf{x}) : \mathbf{x} \in K\}$, where the objective function $f : K \subseteq \mathbb{R}^n \to \mathbb{R}$ is convex, as is the feasible set K. If such a point exists, it is referred to as an *optimal point* or *solution*; the set of all optimal points is called the *optimal set*. If f is unbounded over K or the infimum is not attained, then the optimization problem is said to be *unbounded*. Otherwise, if K is the empty set, then the problem is said to be *infeasible*. A convex optimization problem is in *standard form* if it is written as:

$$\underset{\mathbf{x}}{\text{minimize}} \quad f(\mathbf{x}) \tag{A.6a}$$

$$\text{subject to} \quad g_i(\mathbf{x}) \leq 0, \quad i = 1, \ldots, m \tag{A.6b}$$

$$h_i(\mathbf{x}) = 0, \quad i = 1, \ldots, p, \tag{A.6c}$$

where:

- $\mathbf{x} \in \mathbb{R}^n$ is the optimization variable;
- The objective function $f : K \subseteq \mathbb{R}^n \to \mathbb{R}$ in (A.6a) is a convex function;
- The inequality constraint functions $g_i : \mathbb{R}^n \to \mathbb{R}$, $i = 1, \ldots, m$ in (A.6b), are convex functions;
- The equality constraint functions $h_i : \mathbb{R}^n \to \mathbb{R}$, $i = 1, \ldots, p$ in (A.6c), are affine transformations, that is, of the form: $h_i(\mathbf{x}) = \mathbf{a_i} \cdot \mathbf{x} - b_i$, where $\mathbf{a_i}$ s a vector and b_i s a scalar.

This notation describes the problem of finding $\mathbf{x} \in \mathbb{R}^n$ that minimizes $f(\mathbf{x})$ among all $\mathbf{x}$ satisfying $g_i(\mathbf{x}) \leq 0$, $i = 1, \ldots, m$ and $h_i(\mathbf{x}) = 0$, $i = 1, \ldots, p$. The function f is

the objective function of the problem, and the functions g_i and h_i are the constraint functions.

The fundamental optimality condition for convex optimization problems is called the *minimum principle*, which is defined as follows

Theorem A.1.1 (*Minimum principle*)

A point $\mathbf{x}^* \in K$ is a solution of (A.6) if and only if

$$(\mathbf{y} - \mathbf{x}^*)^\top \nabla f(\mathbf{x}^*) \geq 0, \quad \forall \mathbf{y} \in K \tag{A.7}$$

□

The minimum principle states that if we consider the convex optimization problem (A.6) and a feasible point $\mathbf{x}^*$, then, if $\mathbf{x}^*$ is optimal, the feasible region must not lie in the half-space where the function decreases. It can be proved that convexity makes this condition also sufficient for optimality. Figure A.2 depicts the principle: Fig.A.2 (a) represents surfaces of equal cost $\mathbf{x}$ with the gradient at $\mathbf{x}$ (orthogonal to one of these surfaces) that divides the space into three regions, one in which $f(\mathbf{x})$ increases locally, one in which $f(\mathbf{x})$ decreases locally, and one in which we cannot make a sound guess. Fig.A.2 (b) denotes the feasible point $\mathbf{x}^*$ that satisfies the minimum principle, $\nabla f(\mathbf{x}^*)$ forms a non-obtuse angle with all feasible vectors $\boldsymbol{d}$ originating from $\mathbf{x}^*$ while in Fig.A.2 (c) a feasible point $\mathbf{x}$ that does not satisfy the minimum principle. There are other feasible points $\mathbf{y} \neq \mathbf{x}$ such that $f(\mathbf{y}) < f(\mathbf{x})$.

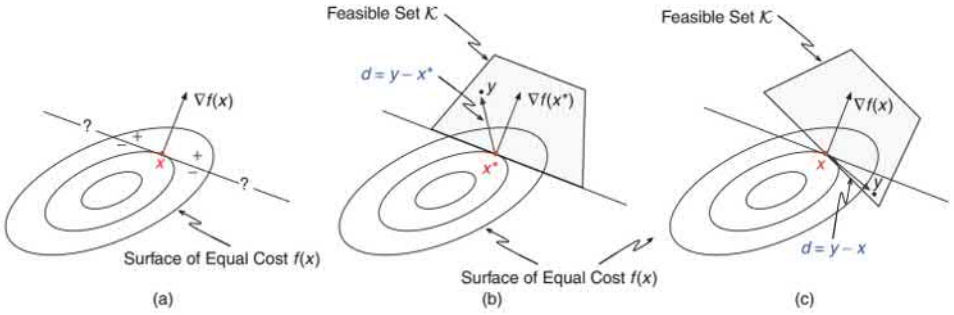

Figure A.2: Geometrical interpretation of the minimum principle. (Source [3])

A.2 Variational Inequality

Variational inequality (VI) problems constitute a broad class of problems encompassing convex optimization and bearing strong connections to game theory. The simplest example of a VI is the classical problem of solving a system of nonlinear equations. Indeed, as we see shortly, this problem can be thought of as a VI without constraints. A VI problem can be considered as a generalization of the *minimum principle* in (A.1.1), substituting the gradient $\nabla f(\mathbf{x})$ with a generic vector function F. In its general form, a variational inequality is formally defined below.

Definition A.2.1 (*Variational Inequality problem*)

Given a closed and convex set $K \subseteq \mathbb{R}^n$ and a map $F : K \to \mathbb{R}^n$, the VI problem, indicated with VI(K, F) consists in finding a vector $\mathbf{x}^* \in K$ such that:

$$(\mathbf{y} - \mathbf{x}^*)^\top F(\mathbf{x}^*) \geq 0, \quad \forall \mathbf{y} \in K \tag{A.8}$$

□

In the sequel, for the sake of simplicity, we shall always assume that F is continuously differentiable on the interior of K and that K is closed and convex. From Theorem (A.1.1) and Definition (A.2.1) we have that if $F = \nabla f$ for some objective function f,

then the optimization problem in (A.6) coincides to solving the (variational) problem VI($K, \nabla f$). Instead, if f cannot be expressed as the gradient of some function, the VI is not comparable to an optimization problem. Indeed, a known result states that $F = \nabla f$, for some f, if the Jacobian of F is symmetric. This is the difference between convex optimization problems and VI, which also underlines the reason why VIs provide the mathematical background for dealing with a larger class of optimization problems.

Some aspects of the characterization of the solution for VIs will be provided here, focusing on the reformulation of the VI problem as a classical fixed-point problem. This allows the development of iterative algorithms. Reformulating the VI as a fixed-point problem means studying the Euclidean projection of a vector onto a closed and convex set. The Euclidean projection of a vector $\mathbf{x}$, denotes as $\text{proj}_K(\mathbf{x})$, is the unique vector in K that is closest to $\mathbf{x}$. Hence, we obtain the following result.

Theorem A.2.1

The vector $\mathbf{x}^*$ is a solution to VI(K, F) if and only if

$$\mathbf{x}^* = proj_K(\mathbf{x}^* - F(\mathbf{x})^*) \tag{A.9}$$

□

The most basic results on the existence of a solution of the VI is by assuming that the set K is convex and compact (closed and bounded) and that the map F is continuous. In this case, we have that the set of solutions is nonempty and compact.

The boundedness assumption of set K might be too restrictive. Existence can still be established if we trade the boundedness assumption of the set K with certain additional properties of the function F. To this end, we recall some basic *monotonicity* properties of vector functions that are naturally satisfied by the gradient maps of convex functions. Indeed, monotonicity plays in the VI field a role similar to that of convexity in optimization. Given a convex set K, a mapping $F : K \to \mathbb{R}^n$ is said to be

- *monotone* on K if

$$(F(\mathbf{x}) - F(\mathbf{y}))^\top (\mathbf{x} - \mathbf{y}) \geq 0, \quad \forall \mathbf{x}, \mathbf{y} \in K. \tag{A.10}$$

- *strictly monotone* on K if

$$(F(\mathbf{x}) - F(\mathbf{y}))^\top (\mathbf{x} - \mathbf{y}) > 0, \quad \forall \mathbf{x}, \mathbf{y} \in K. \tag{A.11}$$

- *strongly monotone* on K if there exists a constant $c > 0$ such that

$$(F(\mathbf{x}) - F(\mathbf{y}))^\top (\mathbf{x} - \mathbf{y}) > \alpha ||\mathbf{x} - \mathbf{y}||, \quad \forall \mathbf{x}, \mathbf{y} \in K. \tag{A.12}$$

Finally, observe that if the vector function F is the gradient of a scalar function f, the above monotonicity properties can be related to the convexity properties of the function f discussed in the previous subsection.

- If f is convex $\Leftrightarrow$ F is monotone
- If f is strictly convex $\Leftrightarrow$ F is strictly monotone
- If f is strongly convex $\Leftrightarrow$ F is strongly monotone

Using the above monotonicity properties, we can now state a few results on the solutions of the VI without requiring the boundedness of the closed and convex set K.

- F monotone: the solution set of VI($\mathcal{X}, F(x)$), is closed and convex.
- F strictly monotone: the solution set of VI($\mathcal{X}, F(x)$), admits at most one solution.
- F strongly monotone: the solution set of VI($\mathcal{X}, F(x)$), admits a unique solution.

A.3 Noncooperative Game Theory

Game theory is a branch of mathematics that enables the modeling and analysis of the interactions between several decision-makers (called players) who can have conflicting or common objectives. A game is a situation in which the benefit or cost achieved by each player from an interactive situation depends, not only on its own decisions but also on those taken by the other players.

Non-cooperative game theory deals with resolving conflictual interactions among decision-makers, each behaving selfishly in order to optimize their own well-being, usually quantified through an objective function. It provides useful models for applications where the interaction among agents is not negligible and centralized approaches are not suitable. In this appendix, we consider two classes of problems. The first is the class of *Nash equilibrium problem* (NEP) [4] (NEPs), named after mathematician John Nash, where the interactions among players take place only at the level of objective functions. The second is the class of generalized *generalized Nash equilibrium problem* (GNEP) where in addition we have that the choices available to each player also depend on the actions taken by his rivals. While NEPs are by far better studied and approachable, GNEPs have a wider range of applicability but sparser available results.

A.3.1 Nash Equilibrium Problem

A noncooperative game is usually defined by four components:

- a set of players $i \in \mathcal{N} := \{1, ..., N\} \subseteq \mathbb{N}$;
- a strategy for each player $\mathbf{x}_i \in \mathbb{R}^n$;
- a set of feasible strategies for each player $\mathbf{x}_i \in \Omega_i \subseteq \mathbb{R}^n$;
- a cost (or profit) function for each player $f_i(\mathbf{x}_i, \mathbf{x}_{-i}) : \mathbb{R}^n \times \mathbb{R}^{(N-1)n} \to \mathbb{R}$;

where $\mathbf{x}_{-i} := \text{col}(\mathbf{x}_1, ..., \mathbf{x}_{i-1}, \mathbf{x}_{i+1}, ..., \mathbf{x}_N) \in \mathbb{R}^{(N-1)n}$ and $\mathbf{x} := \text{col}(\mathbf{x}_1, ..., \mathbf{x}_i, ..., \mathbf{x}_N) \in \mathbb{R}^{Nn}$ collecting the strategies of all the players different from i and the strategies of all the players, respectively.

The scope of each player $i \in \mathcal{N}$ is to minimize their own objective function $f_i(\mathbf{x}_i, \mathbf{x}_{-i})$, by choosing a strategy in its local feasible set Ω_i, given the choices of all the other players $\mathbf{x}_{-i}$. Note that we explicitly underline the dependence of the cost function of the other players' strategies to better show the dependency of the strategies. In addition, we remark that $\mathbf{x}$ must belongs to the intersection of the local feasible set $\mathbf{\Omega} = \prod_{i=1}^{N} \mathbf{\Omega}_i$.

The most studied problem with noncooperative games is the so-called *Nash equilibrium problem* (NEP), defined with the inter-dependent optimization problems as follows:

$$\forall i \in \mathcal{N} : \quad \begin{cases} \min\limits_{\mathbf{x}_i} & f_i(\mathbf{x}_i, \mathbf{x}_{-i}) \\ \text{subject to} & \mathbf{x}_i \in \Omega_i \end{cases} \tag{A.13}$$

Roughly speaking, a NEP is a set of coupled optimization problems. We make the blanket assumption that the objective functions are continuously differentiable and, as a function of $\mathbf{x}_i$ alone, convex, while the sets Ω_i are all closed and convex. The main difference between a game with N players and a N single independent optimization problem relies on the assumption that the cost (profit) function for each player depends not only on its strategy but also on the strategies of the other players.

Solving the NEP means computing a *Nash equilibrium* (NE), which is a collective strategy profile such that no single player can benefit from a unilateral deviation if all the other players act according to the NE. More formally it is possible to define a NE as follows.

Definition A.3.1 (*Nash equilibrium*)

Solving the NEP means computing a NE, which is a collective strategy profile $\mathbf{x}^* \in \mathbf{\Omega}$

with the property that no single player $i \in \mathcal{N}$ can benefit from a unilateral deviation from $\mathbf{x}_i^*$ if all the other players act according to the NE. More formally:

$$f_i(\mathbf{x}_i^*, \mathbf{x}_{-i}^*) \leq \inf \left\{ f_i(\mathbf{x}_i, \mathbf{x}_{-i}^*) \mid \mathbf{x}_i \in \mathbf{\Omega}_i \right\}, \quad \forall i \in \mathcal{N}. \tag{A.14}$$

□

In general, the existence of an NE is not guaranteed; neither is the uniqueness nor the convergence to an equilibrium. Without the existence of an equilibrium, little can be said regarding the likely outcome of the game. If there are multiple equilibria, then it is not clear which one will be the outcome. Indeed, it is possible the outcome is not even an equilibrium because the players may choose strategies from different equilibria. Approaches to address this issue mainly rely on fixed-point theory [5], [6] and *ad hoc* methods, such as *potential* [7] and *supermodular* [8] games. A common approach to address this problem focuses on reducing the NEP to a *variational inequality* (VI) problem. This approach is described in detail in [9] and, given the well-developed VI theory, has the advantage of permitting an easy derivation of results about the existence, uniqueness, and stability of the solutions. But its main benefit is probably that of leading quite naturally to the derivation of implementable algorithms, along with their convergence properties [3].

Nevertheless, the simplest (and the most widely used) technique for demonstrating the existence of an NE is through verifying the convexity of the players' payoffs, which implies continuous best response functions.

Theorem A.3.1

Suppose that for each player the strategy space is compact and convex and the payoff function is continuous and quasi-convex with respect to each player's own strategy. Then there exists at least one pure strategy NE in the game. □

A.3.2 Generalized Nash Equilibrium Problem

The *generalized Nash equilibrium problem* (GNEP) extends the NEP by assuming that the interaction between the players may take place (also) at the feasible set level. Hence, assuming that each player's strategy set can depend on the rival player's strategies [10]. Let us consider a finite number of constraints $m \in \mathcal{P} := \{1, ..., M\} \subseteq \mathbb{N}$, each denoted as $g_m(\mathbf{x}) \leq 0$, defining the coupled feasible set as:

$$\mathcal{X} = \mathbf{\Omega} \cap \left\{ \mathbf{x} \in \mathbb{R}^{Nn} \mid g(\mathbf{x}) \leq \mathbf{0}_M \right\} \tag{A.15}$$

where $g(\mathbf{x}) := ((g_m(\mathbf{x}))_{m \in \mathcal{P}})$. By defining the set-valued mapping $\mathcal{X}_i(\mathbf{x}_{-i}) = \{\mathbf{y}_i \in \mathbb{R}^n \mid (\mathbf{y}_i, \mathbf{x}_{-i}) \in \mathcal{X}\}$ one can define the N interdependent optimization problems as follows:

$$\forall i \in \mathcal{N}: \quad \begin{cases} \min\limits_{\mathbf{x}_i} & f_i(\mathbf{x}_i, \mathbf{x}_{-i}) \\ \text{s.t.} & \mathbf{x}_i \in \mathcal{X}_i(\mathbf{x}_{-i}). \end{cases} \tag{A.16}$$

The latter problem is a GNEP whose solution is the *generalized Nash equilibrium* (GNE), formally defined as follows.

Definition A.3.2 (*Generalized Nash equilibrium*)

Solving the generalized GNEP means computing a GNE, which is a collective strategy profile $\mathbf{x}^* \in \mathcal{X}$ with the property that no single player $i \in \mathcal{N}$ can benefit from a unilateral deviation from $\mathbf{x}_i^*$ if all the other players act according to the NE. More formally:

$$f_i(\mathbf{x}_i^*, \mathbf{x}_{-i}^*) \leq \inf \left\{ f_i(\mathbf{x}_i, \mathbf{x}_{-i}^*) \mid \mathbf{x}_i \in \mathcal{X}_i(\mathbf{x}_{-i}^*) \right\}. \tag{A.17}$$

□

In other words, a GNE is a collective strategy profile $\mathbf{x}^* = \text{col}(\mathbf{x}_1^*, , ..., , \mathbf{x}_i^*, , ..., , \mathbf{x}_N^*) \in \mathcal{X}$ with the property that no single player $i \in \mathcal{N}$ can improve its objective function function by unilaterally changing its strategy with another feasible one.

Proprieties such as stability, uniqueness, and optimality of the GNE have been studied under different standing assumptions. Due to the variability of the feasible sets, the GNEP is a much harder problem than an ordinary NEP. Indeed in its full generality, the GNEP problem is almost intractable.

In its full generality, the GNEP problem is almost intractable, except for particular cases. Hence, let us focus on the case where both the cost functions of the players and the coupled feasible set is convex, i.e., the so-called jointly convex games. In the related literature [3], jointly convex games are usually solved by finding a solution to the associated VI problem [11].

Therefore, we can define the VI associated with the GNEP (A.16) as $\text{VI}(\mathcal{X}, F(\mathbf{x}))$, where $F(\mathbf{x}) = \text{col}\left(\nabla_{\mathbf{x}_1} f_1(\mathbf{x}_1, \mathbf{x}_{-1}), ..., \nabla_{\mathbf{x}_N} f_i(\mathbf{x}_N, \mathbf{x}_{-N})\right)$. The VI is much more tractable than the original GNEP: in fact, a very substantial set of results is available. The resulting solution, the so-called *variational equilibrium*, is also a solution of the associated GNEP and is thus called *variational generalized Nash equilibrium* (vGNE). It should be noted that not all the solutions of the GNEP are solutions of the VI but all the solutions of the VI are solutions for the respective GNEP.

The GNEP solutions achieved through the VI are exactly those for which all players' *Karush–Kuhn–Tucker* (KKT) conditions have the same Lagrangian multipliers for the respective constraints, i.e., $\boldsymbol{\lambda}^* = \boldsymbol{\lambda}_i$, $\forall i \in \mathcal{N}$, where $\boldsymbol{\lambda}_i = \text{col}(\lambda_i^1, ..., \lambda_i^M) \in \mathbb{R}^M$ is the vector collecting the Lagrangian multipliers for all the coupling constraints (we refer to [12] for a more formal definition). The equivalence of the Lagrangian multipliers (acting as penalizing coefficients) imposes the vGNE a fair behavior between all the possible GNE.

References

[1] Bertsekas, D., Nedić, A., and Ozdaglar, A., *Convex Analysis and Optimization* (Athena Scientific optimization and computation series). Athena Scientific, 2003.

[2] Boyd, S. and Vandenberghe, L., *Convex Optimization*. Cambridge University Press, 2004.

[3] Scutari, G., Palomar, D. P., Facchinei, F., and Pang, J.-s., "Convex optimization, game theory, and variational inequality theory," *IEEE Signal Process. Mag.*, vol. 27, no. 3, pp. 35–49, 2010.

[4] Nash, J., "Non-cooperative games," *Annals of Mathematics*, vol. 54, no. 2, pp. 286–295, 1951.

[5] Glicksberg, I. L., "A further generalization of the kakutani fixed point theorem, with application to nash equilibrium points," *Proceedings of the American Mathematical Society*, vol. 3, no. 1, pp. 170–174, 1952.

[6] Daskalakis, C., Goldberg, P. W., and Papadimitriou, C. H., "The complexity of computing a nash equilibrium," in *Proceedings of the Thirty-Eighth Annual ACM Symposium on Theory of Computing*, ser. STOC '06, Seattle, WA, USA: Association for Computing Machinery, 2006, pp. 71–78. DOI: 10.1145/1132516.1132527.

[7] Monderer, D. and Shapley, L. S., "Potential games," *Games and economic behavior*, vol. 14, no. 1, pp. 124–143, 1996.

[8] Amir, R., "Supermodularity and complementarity in economics: An elementary survey," *Southern Economic Journal*, pp. 636–660, 2005.

[9] Facchinei, F. and Pang, J.-S., "Nash equilibria: The variational approach," in *Convex Optimization in Signal Processing and Communications*, Palomar, D. P. and Eldar, Y. C., Eds. Cambridge University Press, 2009, pp. 443–493. DOI: 10.1017/CBO9780511804458.013.

[10] Facchinei, F. and Kanzow, C., "Generalized nash equilibrium problems," *Annals of Operations Research*, vol. 175, no. 1, pp. 177–211, 2010. DOI: https://10.1007/s10479-009-0653-x.

[11] Rosen, J. B., "Existence and uniqueness of equilibrium points for concave n-person games," *Econometrica: Journal of the Econometric Society*, pp. 520–534, 1965.

[12] Facchinei, F., Fischer, A., and Piccialli, V., "On generalized nash games and variational inequalities," *Operations Research Letters*, vol. 35, no. 2, pp. 159–164, 2007.